Synthesis and Reaction Chemistry of Various N,N,C- and O,N,C- Palladium Pincer Complexes

Thesis submitted for the degree of Doctor of Philosophy at the University of Leicester

2016

Rena Simayi

Department of Chemistry

University of Leicester

Synthesis and reaction chemistry of various *N,N,C* and *O,N,C* palladium pincer complexes

Rena Simayi

Abstract

In this thesis, the synthesis, characterisation and complexation chemistry of a series of related *NNC* and *ONC* pyridine based pincer ligands, together with some reaction chemistry of the metal complexes is described. The pro-ligands and the metal complexes have been characterised by a combination of multinuclear NMR spectroscopic techniques, IR spectroscopy, mass spectrometry and, for selected examples, by single crystal X-ray crystallography; remarkable spectroscopic and structural data are discussed.

In Chapter 2, the synthesis and characterization of thirteen *NNC* and *ONC* pyridine based pincer ligands is described, including nine novel pincer ligands and four pyridine based pincers which have been previously reported. In Chapter 3, the palladium/platinum chemistry of NNC_{aryl} and ONC_{aryl} pyridine based pincer ligands is explored. Variation on the donor atoms has allowed an investigation of donor property influences on C-H activation, by giving peri-activated palladium pincer complexes for the ketimine-, aldimine-, amine- and biyridine-armed ligands and generating ortho-activated *ONC* palladium pincer complexes in the case of the alcohol-armed pro-ligand. Use of different palladium salts also led to different regioselective C-H activations. With the ketimine-armed naphthyl ligand (H**L1**$_{ket\text{-}nap}$) as the example, the interconversion chemistry between the ortho- and peri-C-H activated products is also explored.

In Chapter 4, sp^3 C-H activation of the Et-armed ligand H**L4**$_{Et}$ with both palladium acetate and palladium chlorides has been unsuccessful, giving the *N,N*-coordinated bidentate species. The reaction of palladium acetate with the ^{i}Pr-armed pro-ligand H**L4**$_{iPr}$ has resulted in minor amounts of C-H activated vinyl species with the major product being the non-activated palladium diacetate complex. Noticeably, upon reaction with Na_2PdCl_4, a mixture of the non-activated bis-chloride palladium complex and the sp^3 C-H activated NNC-tridentate palladium species has been obtained, in a ratio of 1:1.5. Moreover, the sp^3 C-H activation and the isolation of a rare sp^3 C-H activated palladium complex have been achieved by reacting the ^{t}Bu-armed pro-ligand H**L4**$_{tBu}$ with palladium acetate. The reaction of this ligand with Na_2PdCl_4 also resulted in the successful C-H activation of the ^{t}Bu-arm to give a palladium pincer complex with a yield of 95%. Other than the NMR and FABMS analyses, the solid state X-ray structure of the latter complex confirmed the formation of the material as a rare sp^3 C-H activated palladium complex.

The stoichiometric reactivity of the (*NNC/ONC*)PdCl species towards $AgBF_4$/$AgPF_6$, and the subsequent ligand exchange reactions are disclosed in Chapter 5, together with the application of twelve palladium complexes as a series of promising catalysts in the allylic arylation of various allylic acetates with sodium tetraphenylborate.

Acknowledgements

I feel that I have been blessed to receive so much help and support from so many people during this PhD. Firstly, I would like to take this opportunity to thank my Supervisor – Professor Eric Hope. Without you, it would have not been possible for me to finish this PhD. You have always been my mentor, not just in study, but also in my life. The past couple of years have been the most difficult times of my life, but with your help and my family's support, I made it. So thank you, for your guidance, support, help and patience; thank you for being my supervisor. I would also like to thank Dr. Solan, for his dedicated supervision on my research project/projects in the last four years. Your inspiring advice and feedback guided me through a lot of difficult problems. Thank you for being so patient with me all the time. I must also thank Kuldip Singh, Mick Lee and Gerry Griffith for their continuous support with the X-ray crystallography, mass spectrometry and NMR spectroscopy, respectively.

I cannot forget to thank my grandparents, who are no longer with us anymore, for bringing me up into this vulnerable-looking person yet with a strong mind. I wish you could have been here to see your grand-daughter completing her PhD, although I can always feel that you have never left, you are always by my side.

I want to thank my parents for their continuous support, financially, emotionally and in any other possible ways. I know I have not always been a good daughter, and I have sometimes ignored your feelings over my grandparents'. But I have always wanted to say, and have never been able to say it out loud that, I love you, and I feel so grateful for having parents like you, I have always been proud of you. I hope you can be proud of me now.

I also want to thank all the very dear friends I made in the last five years here – Martyna, Jingting, Rusul, Mona, Amina, Meshari, Ahmed and Jinglei. Because of you, the most tiring lab hours have been a breeze. Because of you, the write-up always felt like a 'second home'. Thank you, you guys.

Finally, I want to thank my husband, Mustafa, without who it would have been impossible for me to even be here. I can't imagine how much courage it took for you to leave everything behind – to leave your job, your friends and your family – and come with me to this foreign country, just for me to fullfil MY dreams. You have never complained, in fact, I have been the one always complaining, about my failed experiments, never ending literature readings, and the overly-stressed writing up. You have been being my (mental health) consultant, my careers advisor, my stress manager, my family, and, my best friend. Thank you for believing in me so much, thank you for supporting me in every possible way, and thank you for always making me happy.

Contents

Abbreviations

°	degrees
Å	angstrom (0.1 nm)
app.	apparent
Ar	aryl fragment
ASAP	atmospheric solids analysis probe
ca.	circa
CMD	concerted metalation/deprotonation
Cp	cyclopentadienyl
d	doublet
DCM	dichloromethane
dd	doublet of doublets
ddd	doublet of doublet of doublets
dipp	diisopropylphenyl
Eq	equivalents
ESI	electrospray ionisation
FAB	fast atom bombardment
g	grams
h	hours
HOAc	acetic acid
HR	high resolution
i	iso
IR	infra red
J	joules
M	molar concentration
m	multiplet
m/z	mass/charge ratio

MAO	methylaluminoxane
Me	methyl fragment
MeCN	acetonitrile
MHz	mega hertz
m.p.	melting point
MS	mass spectrometry
NMR	nuclear magnetic resonance
OAc	acetate
OTf	triflate
ppm	parts per million
ppb	parts per billion
Pr	propyl fragment
Py	pyridyl fragment
R	alkyl fragment
s	singlet
sept.	septet
tBu	t-butyl fragment
td	triplet of doublets
THF	tetrahydrofuran
TMA	trimethylaluminium
v/v	volume/volume
δ	chemical shift

Chapter One

Introduction

1.1 Pincer ligands

1.1.1 Pincer ligands in general

The development of cost-effective, multi-step, one-pot reactions with a minimum amount of salt waste and solvent usage are becoming the current trends in homogenous catalysis. However, these are challenging processes because of their reliance on catalyst stability, substrate and solvent compatibility. Organometallic complexes supported by pincer ligands are powerful tools that can be used to achieve many of these objectives. Thus, extensive research has been conducted in the synthesis and modification of such pincer ligands in the organometallic chemistry.

A pincer ligand is usually defined as a chelating agent that coordinates three neighbouring coplanar sites (donors), normally with a transition metal atom in the centre. The electron density around the central metal and the binding of the metal to potential substrates can be controlled by the chelating donor atoms and their substituents. This allows potential fine tuning of the reactivity of the complex. Highly stable metal complexes could be afforded by using these rigidly coordinated pincer ligands, enabling a great increase in the lifetime of the catalysts and their resistance under harsh reaction conditions.

The control of the properties of metal centres by a well-defined ligand system is an ultimate goal in the fields of inorganic and organometallic chemistry. Chelation, the binding of a ligand to a metal through two or more bonds, is a versatile method to realize this. In organometallic complexes containing a direct (transition) metal-carbon bond, chelation leads to the formation of metallacycles, which provide additional stabilization of the M-C bond.[1] The first organometallic complexes containing tridentate monoanionic ligands were reported in the late 1970s.[2] These 'pincer'[3] ligands comprise a potentially E,C,E tridentate coordinating, mono-anionic array, with the general formula [2,6-$(ECH_2)_2C_6H_3]^-$ (ECE). E represents a neutral two-electron donor such as $N(R_2)$, $P(R_2)$, OR, or SR, while C is the anionic aryl carbon atom of the 2,6-disubstituted phenyl ring (**Scheme 1.1**).[4] The formation of two five-membered metallacycles affords a metal complex $[MX_n(ECE)L_m]$ by the complexation of the metal with pincer ligands. A two-carbon linkage between the aryl-carbon and the E-donor atoms results in the formation of five-membered metallacycles.[5]

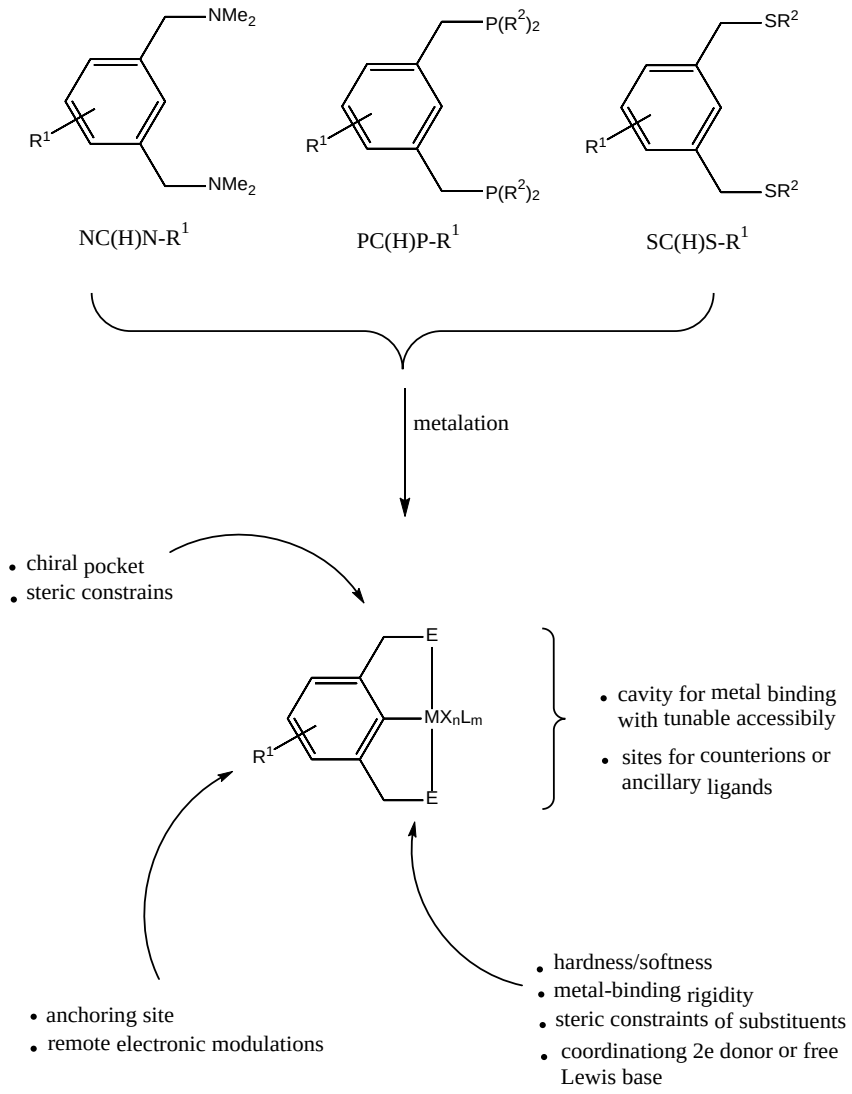

Scheme 1.1 | Potential modification sites in pincer ligands and their effects on the properties of the metal centre.

The application of the pincer ligands in coordination with several types of metals, such as Ti, Zr, Hf, Ni, Pd, Pt, Rh, and Ir, have been reported, highlighting their application as active catalysts for the addition of O-H, N-H, or Si-H bonds to alkynes.[6,7,8] There are many types of pincer ligands, categorized according to the geometry of the structure, electronic properties of the molecule or the donor atoms on the coordination sites.

Figure 1.1 lists examples of symmetric and unsymmetric pincer ligands. Other than the symmetry, pincer ligands could also be classified as neutral or anionic. However, the most rational and common way to categorize them can be according to the types of donor atoms on the coordination sites as this is essential to the properties and applications of these ligands. It determines which metal could be suitable for this pincer ligand to coordinate

to, and the electronic properties of the donor atom determine the binding strength of the ligand to the metal.

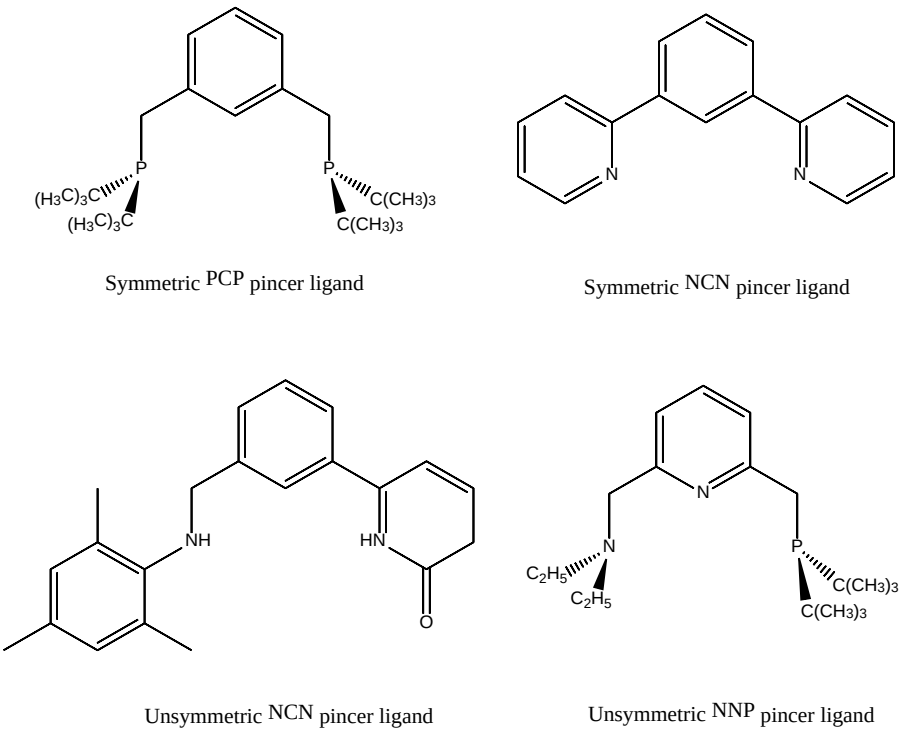

Symmetric PCP pincer ligand

Symmetric NCN pincer ligand

Unsymmetric NCN pincer ligand

Unsymmetric NNP pincer ligand

Figure 1.1 | Examples of symmetric and unsymmetric pincer ligands

Due to the existence of numerous different types of pincer ligands, it is beyond the scope of any literature review to examine the synthesis of every pincer ligand system. Therefore, in this introduction, the scope has focused on the most commonly used pincer systems, carbon-based pincers – PCP and NCN pincer ligands, and the widely used pyridine-based pincer ligands.

1.1.2 PCP pincer ligands

Anionic ligands with a carbanion at the centre and two phosphines on each side, which are known as PCP pincers, were early examples of pincer ligands. PCP pincers were the most popular pincer ligands until even a few years ago. A rapid expansion in studies on conventional ligand systems has enabled the discovery of more variable and flexible

donor sets. Thioethers and tertiary amines have been used as alternatives for the phosphines. In the recent years, nitrogen has been increasingly used as the most popular donor atom altogether with carbon and oxygen.[9]

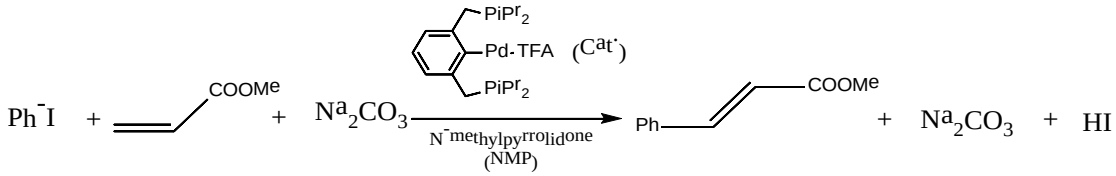

Figure 1.2 | PCP type palladium pincer complexes as active catalyst for Heck reactions

Over the past decade, many chemical transformations have been shown to be achieved using transition metal complexes supported by PCP pincer ligands as effective catalysts.[10] Therefore, a considerable amount of research has been dedicated to their application in both stoichiometric and catalytic reactions, such as C−C coupling reactions (**Figure 1.2**),[11] dehydrogenations (**Figure 1.3**),[12] and the activation of small molecules (**Figure 1.4**).[13]

The chelating effect could easily be enhanced using auxiliary ligands attached on the backbone,[14] or the reactivity of the vacant coordination site could be increased because of the trans effect of the carbanionic ligand.[15] Although the most common examples are the symmetric ECE type of ligands, studies on unsymmetric pincer ligands bearing one soft phosphorus donor and one hard oxygen or nitrogen donor, which are derived from the PCP pincer system, have also been reported.

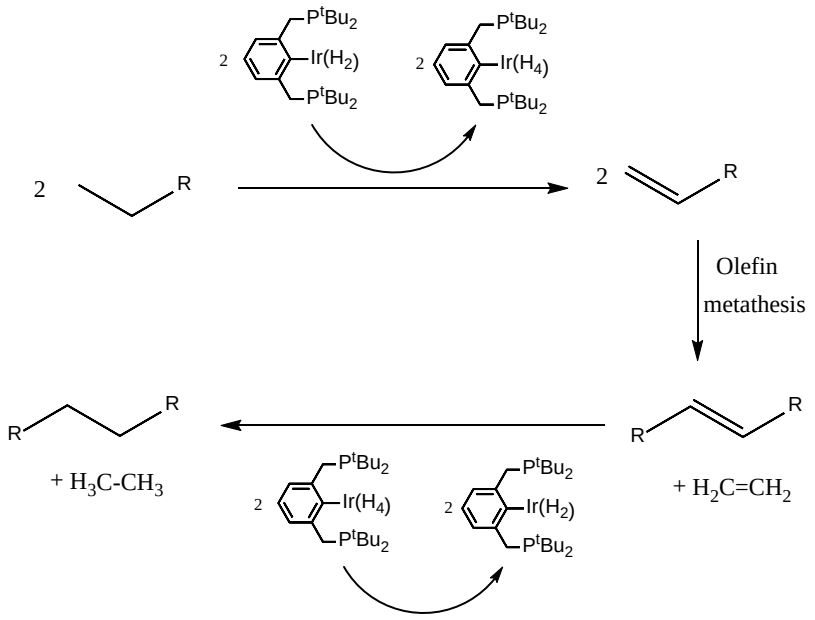

Figure 1.3 | Transition metal pincer complex used as versatile catalyst for dehydrogenation reactions[12]

Whilst PCN-type pincer ligands are the most common examples, many cases of PCO,[16] PSiN,[17] and PNN[18] also exist. The hemilabile nature of the ligands in these complexes gives the opportunity for more coordination sites to be created, hence, leading to more interesting reaction chemistry.

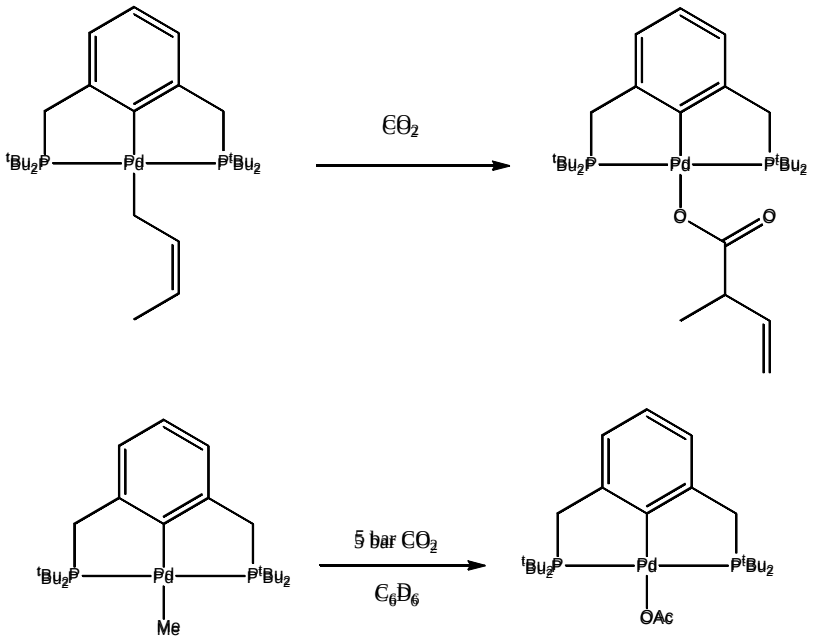

Figure 1.4 | The activation of small molecules using palladium pincer complexes[13]

1.1.3 NCN type pincer ligands

Another type of commonly used pincer ligand, which contains a carbon atom or simply a phenyl ring as the central donor, has attracted great interest in the most recent studies on transition metal pincer complexes. Transition metal complexes supported by NCN- pincer ligands have been reported for their many applications for catalyst immobilization, supermolecular assembly and sensor materials.[19]

Many studies have revealed that the reaction speed could be greatly increased when the ligand can exhibit a dynamic hemilabile binding to the metal centre.[20] The metal complex could better adjust itself to the steric and electronic changes of the reaction if there is a transient dissociation of a coordination group without disturbing the formally chelated structure of the coordination system. Several catalytic reactions demonstrating such hemilabile coordination have been reported in which the catalyst is a metal complex supported by an NCN pincer ligand.[21]

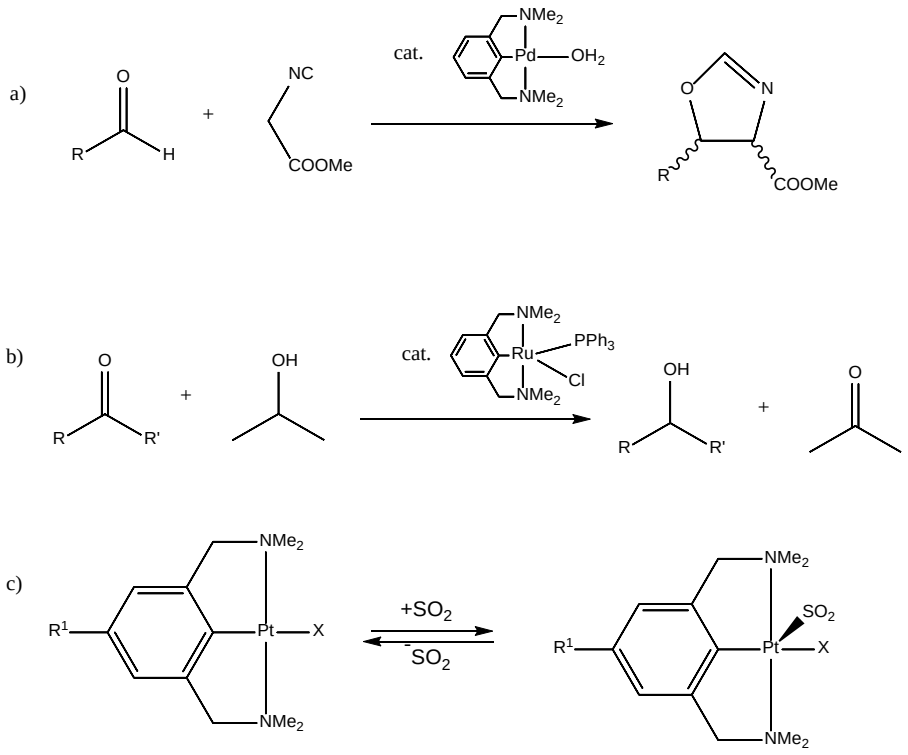

Figure 1.5 | a. Palladium complexes of the NCN pincer ligand used for the Aldol condensation; b. Hydrogen transfer reactions with pincer-aryl ruthenium(II) complexes; c. Reversible binding of SO_2 to NCN-platinum complexes with formation of five-coordinate adducts.

According to the work reported by Milstein and co-workers, hemilabile pincer ligand coordination is necessary in the coupling of alcohols and amines catalyzed by Ru(II)[22] and C-H/C-C bond cleavage reactions at Rh(III).[23] Although it is still a difficult task to map out pincer ligand systems with adjustable hemilabile properties, especially with the NCN donor set, the application of these pincer ligands has drawn a great deal of interest lately. **Figure 1.5** summarizes some of the useful application which has been reported in the recent years, with examples of active metal complexes of palladium, ruthenium and platinum supported by NCN pincers.[24]

1.1.4 Pyridine-based pincer ligands

Another widely used, and extensively studied, family of pincer ligands are known, generally, as the pyridine-based pincer ligands, in which a 2,6-substituted pyridine ring serves as the central donor, with two symmetrical or unsymmetrical donors form the two pincer arms. This family of pincer ligands include a considerably wide range of pincers, with the same feature that the central atom is defined by a pyridine nitrogen, systems such as PNP, PNN, NNN, NNO, NNC and ONC, are all included in the scope of pyridine-based pincer chemistry.

Pincers with PNP ligating moieties are commonly known in affording neutral complexes, allowing different oxidation states to be accessed. The central group being an 2,6-pyridine linker gives a ligand that does not necessarily require any C–H activation upon ligation. Nishibayashi and co-workers have reported a series of dinitrogen-bridged dimolybdenum−dinitrogen complexes bearing a variety of 4-substituted PNP-pincer ligands, which have been proved to be effective catalysts for formation of ammonia from molecular dinitrogen (**Figure 1.6**).[25] The best results, where 52 equiv of ammonia are produced based on the catalyst, were obtained when the substituent on the central pyridine is a methoxy group.

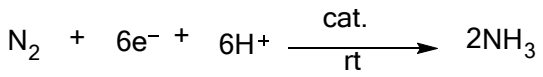

Catalyst:

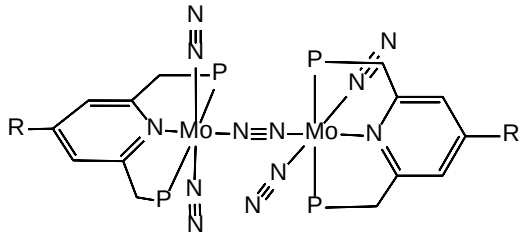

R= Ph, Me_3Si, ^tBu, Me, MeO

Figure 1.6 | Molybdenum complexes bearing PNP-pincer ligands as effective catalysts toward the catalytic formation of ammonia from molecular dinitrogen

Palladium (II) complexes of *NNN*-pincer ligands and nickel (II) complexes adopting *NNO*-chelating systems have been reported, by Zhang and co-workers, to exhibit high catalytic activities for olefin polymerization (**Figure 1.7**).[26] In the presence of MAO, moderate activity for norbornene polymerization by all the palladium complexes was observed; whilst the nickel complexes were reported to exhibit high activity for ethylene dimerization, with activation by $AlEt_2Cl$, up to 83.4×10^5 $gmol_{Ni}^{-1}$ h^{-1}, indicating the viability of these complexes as promising catalysts for ethylene dimerization.

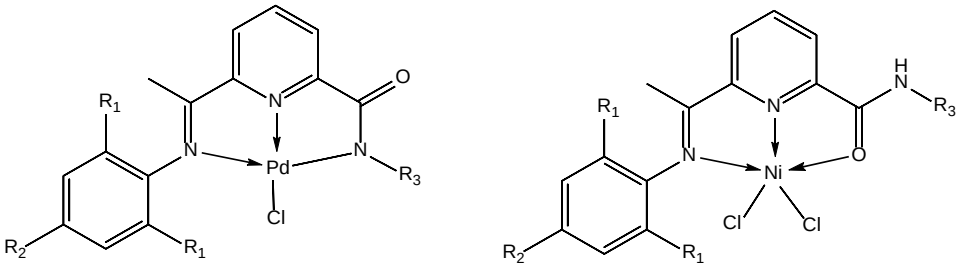

Figure 1.7 | Palladium and nickel complexes of NNN- and NNO-pincers

Furthermore, pyridine-based pincer ligands have also been reported to be active in a new mode of bond activation by metal-ligand cooperation based on aromatization–dearomatization of the pyridine ring.[27] The process involves the deprotonation of a pyridylic proton of a pyridine-based pincer complex, leading to dearomatization;

followed by the activation of a chemical bond (X–Y) by the dearomatized complex via cooperation between the metal and the ligand, thereby regaining aromatization (**Figure 1.8**). The overall process does not involve a change in the metal oxidation state.

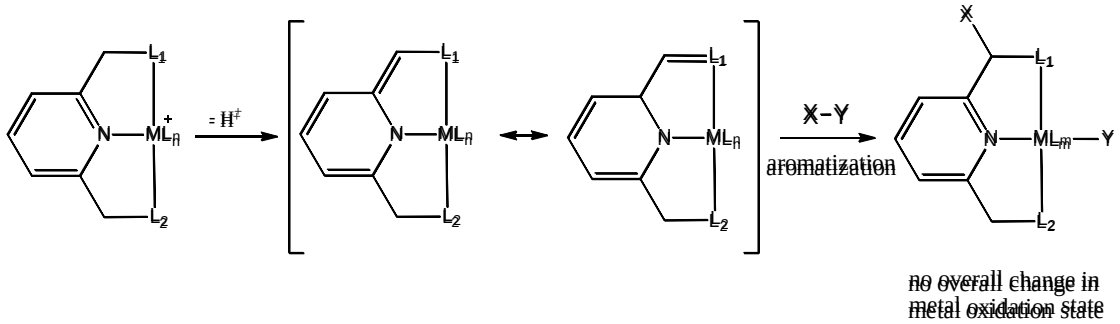

Figure 1.8 | Bond activation via metal-ligand cooperation by pyridine-based pincer complexes

The activation of H_2 and C–H bonds by PNP Ir complexes has been demonstrated by this type of metal–ligand cooperation.[28] This process has also been found to play a key role in the recently discovered environmentally benign reactions of alcohols, catalyzed by PNP and PNN pincer complexes of ruthenium, including dehydrogenation of secondary alcohols to ketones,[29] dehydrogenative coupling of primary alcohols to form esters and H_2,[30] hydrogenation of esters to alcohols under mild conditions[31] and unprecedented amide synthesis: catalytic coupling of amines with alcohols, with liberation of H_2.[32] Moreover, the exceptional synthesis of imines with H_2 liberation has been achieved by simple ligand modification in the latter reaction. The high efficiency and mild conditions of these reactions, and the fact that they produce no waste (the only by-product being H_2, valuable by itself) allow them to emerge as an attractive, "green" route to the synthesis of amides.

Overall, pincer ligands are increasingly gaining interest and use as one of the favoured ligands in fields such as organometallic chemistry, homogeneous catalysis and materials science.[33] Their simple design and the possibilities to build and vary, through ligand modification, their molecular features to the effect that the desired properties of the bound metal site can be induced and their stability (thermal, and low reactivity to electrophiles or nucleophiles) contribute to the versatility and applicability of pincer-metal units as building blocks.

1.2 C-H activation

The catalysts for the activation of C-H bonds play an important role in the world of chemistry. The carbon-hydrogen bond was considered as relatively inert. So a process that can make the C-H bond active would certainly open a new door to the reactivity of organic compounds. Therefore, the world of chemistry could be changed dramatically by carbon-hydrogen bond activation reactions. Some low-cost materials, such as hydrocarbons, cannot be used as synthetically useful reagents because the conversion from these raw materials to synthetic ingredients is quite difficult. But, C-H activation processes are now making it possible. Methanol could now be obtained via the C-H activation of methane which is a starting material widely available. Besides, the process converts a cheap, readily available and difficult to be transported substance into a valuable chemical solvent and synthetic starting material (**eq. 1.1**).

$$CH_4 + 1/2\ O_2 \rightleftharpoons CH_3OH \qquad \text{(eq.1.1)}$$

Carbon-hydrogen bond activation reactions could also provide greener ways to products, especially in the pharmaceutical sector, because the activation of hindered reaction sites can be facilitated and the number of steps needed to obtain the desired product can be reduced.

Many materials, such as plastics which are present in most of the products in our daily life, are carbon chain based organic molecules. Due to the better performance in use, ease of synthesis and recyclable properties of these organic molecules, they are replacing traditional inorganic materials like metals and ceramics. However, the types and numbers of hydrocarbons which can be used to synthesize these useful organic materials are very limited. This is probably the main reason why C-H activation has been a great focus of interest in the past decades – it converts the unreactive hydrocarbons into reactive ones.

There are two main types of hydrocarbons, the first one being saturated hydrocarbons and the second one is unsaturated hydrocarbons. The saturated nature of the hydrocarbons which only consist of single bonds results in inert chemical properties while the unsaturated hydrocarbons which contain multiple bonds in their molecules can be quite reactive. This means only half of the hydrocarbon feed stocks are chemically reactive.

Hence the main challenge here is to activate saturated hydrocarbons so that they can react with other chemicals.

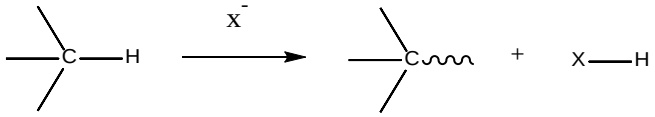

Figure 1.9 | C-H activation by simply removing the hydrogen.[34]

By 'activating the un-reactive carbon- hydrogen bond' we mean the cleavage of the C-H bond and the formation of a C-X bond, X being any other atom besides hydrogen. There are several ways to view this process. The most straightforward way would be simply removing the hydrogen then filling the site with a different atom in the subsequent reaction step (**Figure 1.9**). Although the reaction looks simple enough, it often requires very harsh reaction conditions such as strong acids, bases or the need for the generation of active free radicals.

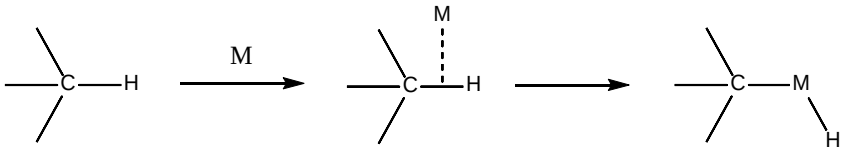

Figure 1.10 | C-H activation by oxidative addition (M=metal).

The oxidative addition, which happens usually with the help of a soluble metal salt or complex, is another approach of achieving C-H activation. As illustrated in **Figure 1.10**, the first step in this oxidative addition process is the weak coordination of the metal to the C-H bond to form an intermediate species. This intermediate subsequently yields a product that contains both a carbon-metal bond and metal-hydrogen bond. The earliest examples of C-H activation by oxidative addition have been observed in 1960s and 1970s (**Figure 1.11**).[34] **Figure 1.11** (a) demonstrates the reaction in which organometallic compounds were found to be supportive to the C-H activation process for the very first time resulting in the coordination of the metal to a cyclopentadienyl ligand. The C-H activation reaction of a cyclohexane molecule by an iridium complex is shown in **Figure**

1.11 (b). Both examples together illustrate the C-H activation reactions via oxidative addition which greatly promoted the development of this field.

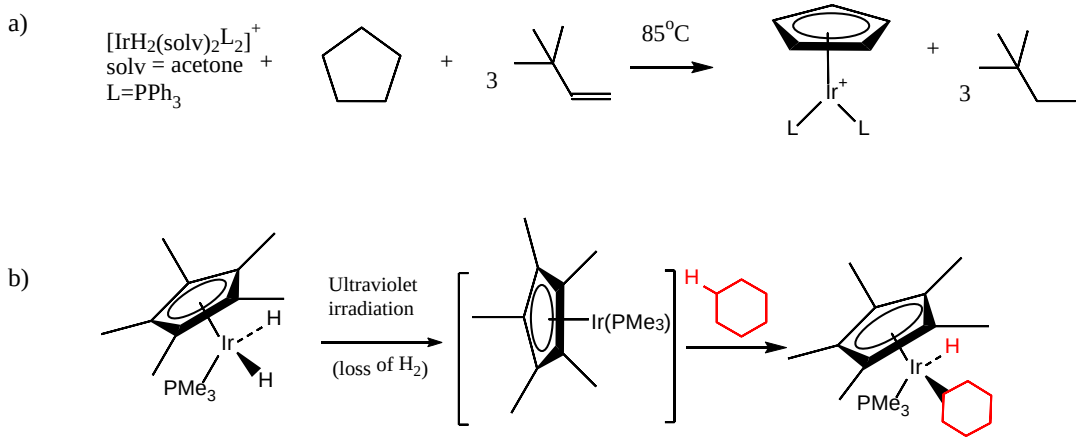

Figure 1.11 | (a) Reaction of organometallic compounds with alkanes; (b) First direct observation of oxidative addition in C-H activation[34]

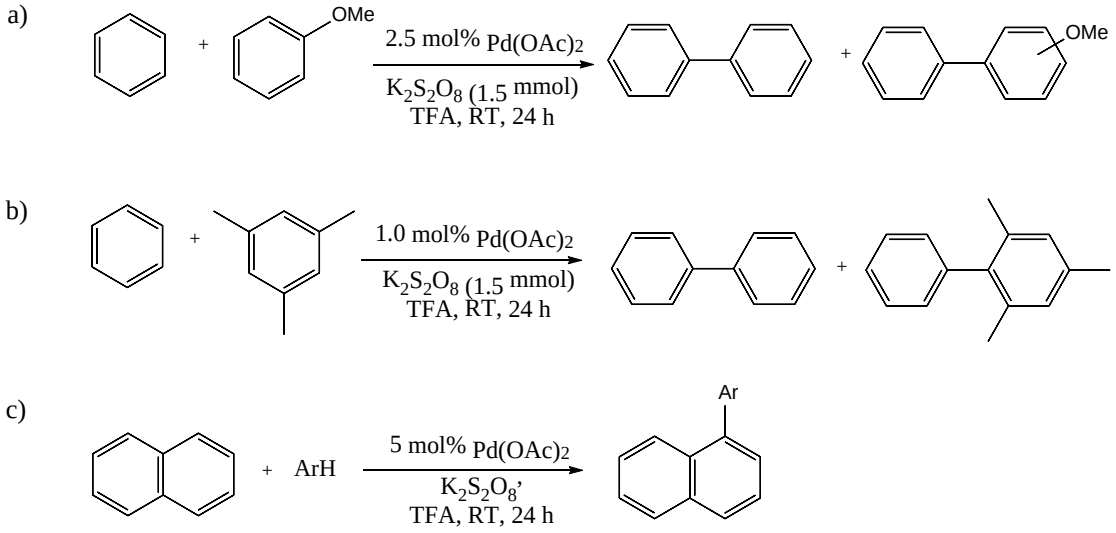

Figure 1.12 | Pd(II)-Catalyzed Oxidative Cross-Coupling of: (a, b) Benzene with Anisole or Mesitylene; (c) Naphthalene with Various Arenes[36]

However, these reactions might be impractical because the total cost of the reactants is much higher than the product since stoichiometric amounts of the metal and the hydrocarbon were used. This has raised the new question: Could small amounts of the metal complexes facilitate the same transformations? In other words, this moved the focus of the research interest to exploring catalytic C-H activation processes which uses only catalytic amounts of complexes. Numerous studies have been carried out regarding the C-H activation with transition metal catalysts including useful chemical transformations, such as alkane functionalization,[35] intermolecular cross-coupling of arenes (**Figure 1.12**),[36] C-H fluorination (**Figure 1.13**),[37] Heck reactions, Suzuki couplings etc.

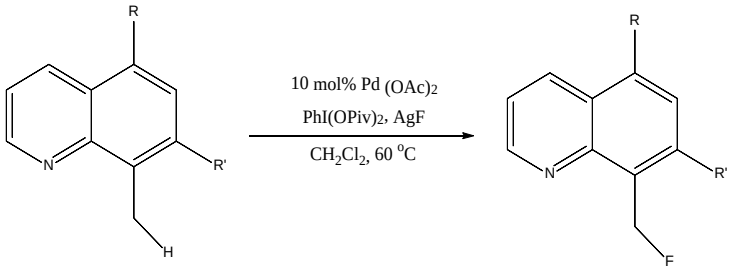

Figure 1.13 | The palladium-catalyzed C-H fluorination of 8-methylquinoline derivatives

Other than these examples, transition metal-catalyzed C-H activation has also been reported to be useful in material science, pharmaceuticals and polymer sciences.[38] Unlike the traditional cross-coupling reactions, these processes do not require the pre-activation of the C-H bond to convert this inert bond into other active ones as a first step. Hence, catalytic C-H activation is a more efficient and atom economic way of synthesizing organic molecules. Yet improving the reactivity of the inert C-H bonds and manipulating the regioselectivity of the reaction remain as the two main challenges in this area. Research has revealed that breaking of the C-H bond could be promoted by the binding of the transition metal to the substrate then move on to the subsequent M-C bond forming step. Then, the metal-carbon bond has been proven to be reactive in a wide range of chemical processes.[39]

However, controlling the regioselectivity of the C-H activation process seems to be a more difficult thing to achieve. In the practical applications of sp^2 C-H activation reaction of an arene substrate, it is essential to control the selective activation of the substrate as

the outcomes of C-H activation often gives a mixture of the ortho, meta, and para activated products. Therefore, the initial steps in these C-H activation reactions, focusing mainly on the elements which are controlling the selectivity, have attracted a great deal of research attention. In general, four types of transition metal catalysed C-H activation mechanisms are known including oxidative addition, traditional electrophilic aromatic substitution, concerted metalation/deprotonation mechanism and a σ-bond metathesis mechanism (**Scheme 1.2**).

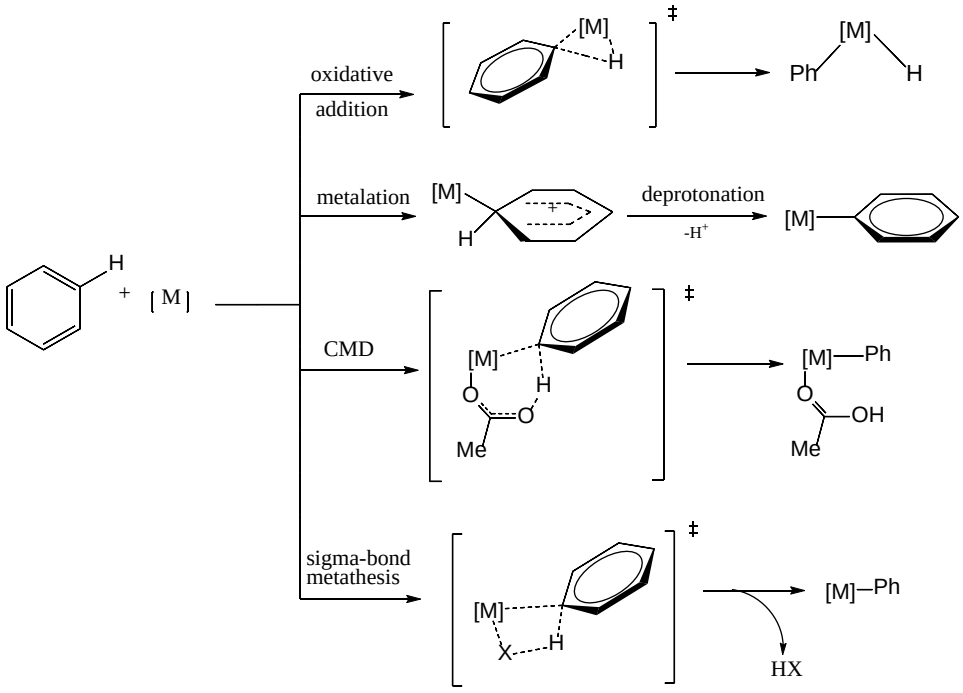

Scheme 1.2 | Proposed C-H activation mechanisms in transition metal catalysis

As illustrated in **Scheme 1.2**, the C-H activation process via oxidative addition involves the oxidative addition of the substrate to the transition metal and the subsequent generation of a metal hydride intermediate. Such metal hydrides are not formed in cases of the electrophilic aromatic substitution and concerted metalation/deprotonation (CMD) pathways. Instead, the hydrogen is taken away from the carbon atom as a proton to allow the metal-carbon bond to form.

However, a rate-limiting metalation process is present in the electrophilic aromatic substitution mechanism together with the subsequent rapid deprotonation to form a transition metal-aryl species while a smooth breaking of the C-H bond and the generation

of a metal-carbon bond happens in the process of concerted metalation/deprotonation (CMD). As to the last kind of transition metal-mediated C-H activation mechanism – σ-bond metathesis – the reaction pathway goes through a four-membered intermediate species which includes both the metal-X and carbon-hydrogen bonds breaking.

1.3 Palladium chemistry

Palladium is used in combination with a broad variety of ligands for highly selective chemical transformations. A large number of carbon-carbon bond or carbon-heteroatom bond forming reactions in organic chemistry are made possible with the help of catalysis containing palladium compounds. The wide ligand system tolerance and binding mode of Pd(II) have made it a very hot research topic over the past decades.

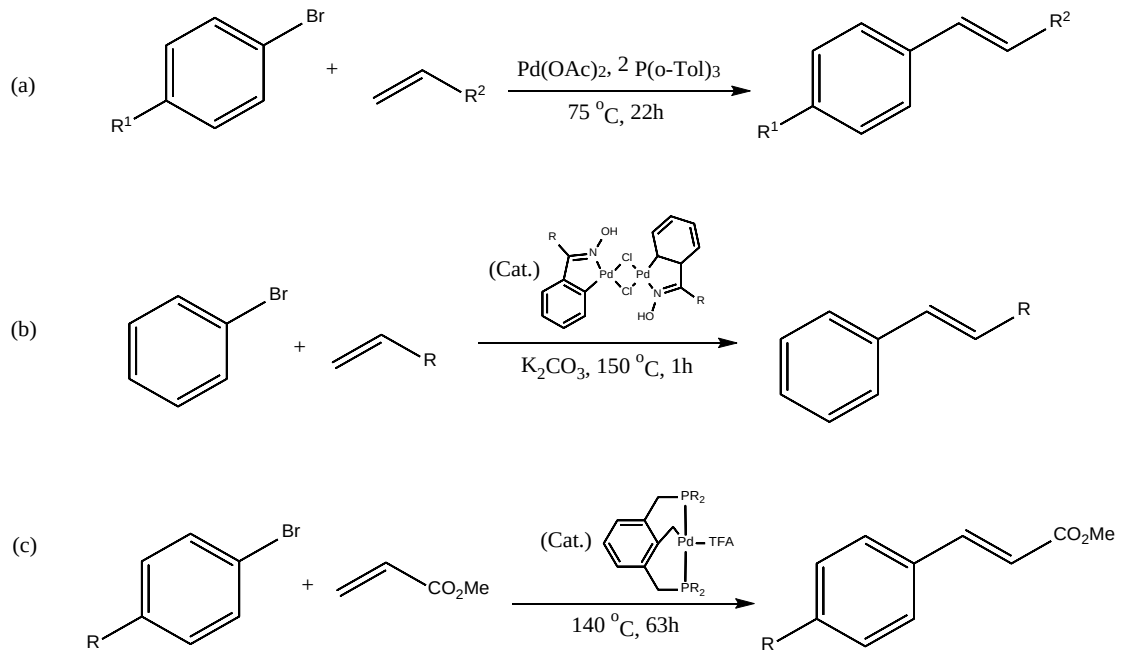

Figure 1.14 | (a) Heck reactions of aryl bromides using monodentate phosphine ligands; (b) Heck reactions of aryl bromides using bidentate ligands; (c) Heck reactions of aryl bromides using tridentate ligands

The Heck and Suzuki coupling reactions in particular are significant examples of palladium catalysts being used in carbon-carbon bond forming reactions. A wide range of substituted olefins, dienes, and monomers for conjugated polymerization have been reported to be synthesizable using palladium-catalyzed Heck reactions.[40] Heck reactions are widely useful in synthesizing pharmaceuticals,[41] agrochemicals,[42] and natural products.[43,44] Various palladium catalysts with mono-, bi- or tri-dentate ligands have been reported for their application in Heck type reactions (**Figure 1.14**).

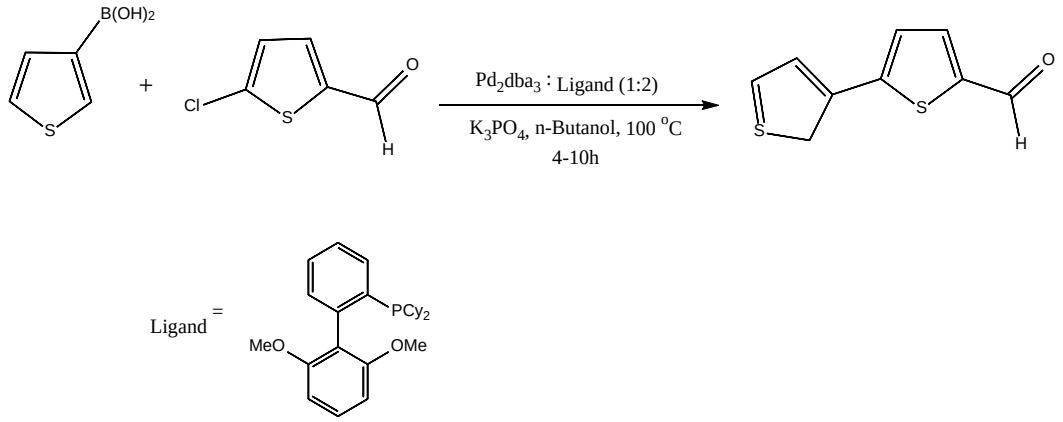

Figure 1.15 | Suzuki cross-coupling reactions using phosphine ligands

Another important use of palladium catalysts lies in Suzuki coupling reactions; the cross-coupling of aryl halides with arylboronic acids is a most efficient, convenient, and versatile approach.[53] Extensive research has revealed that the synthesis of various organic compounds could be realized with the help of this dependable method for C-C bond forming reactions. Among the wide range of ligands that have been used for Suzuki coupling reactions, phosphine ligands used to be the most favoured ones (**Figure 1.15**). Yet their toxicity, sensitivity to moisture and air, and most importantly, their high price have inhibited their wide application, especially in the chemical industry.[45]

Therefore, the application of other inexpensive, more stable and tolerable systems, such as those with N,N,O-, N,N,N-, N,C,O-, N,S-, and N,N- ligands, which are 'phosphine-free', have attracted many researchers and great progress has been achieved in this field. **Figure 1.16** summarizes some of the examples of the ligand systems that have been utilized in Suzuki cross-coupling reactions in combination with palladium.

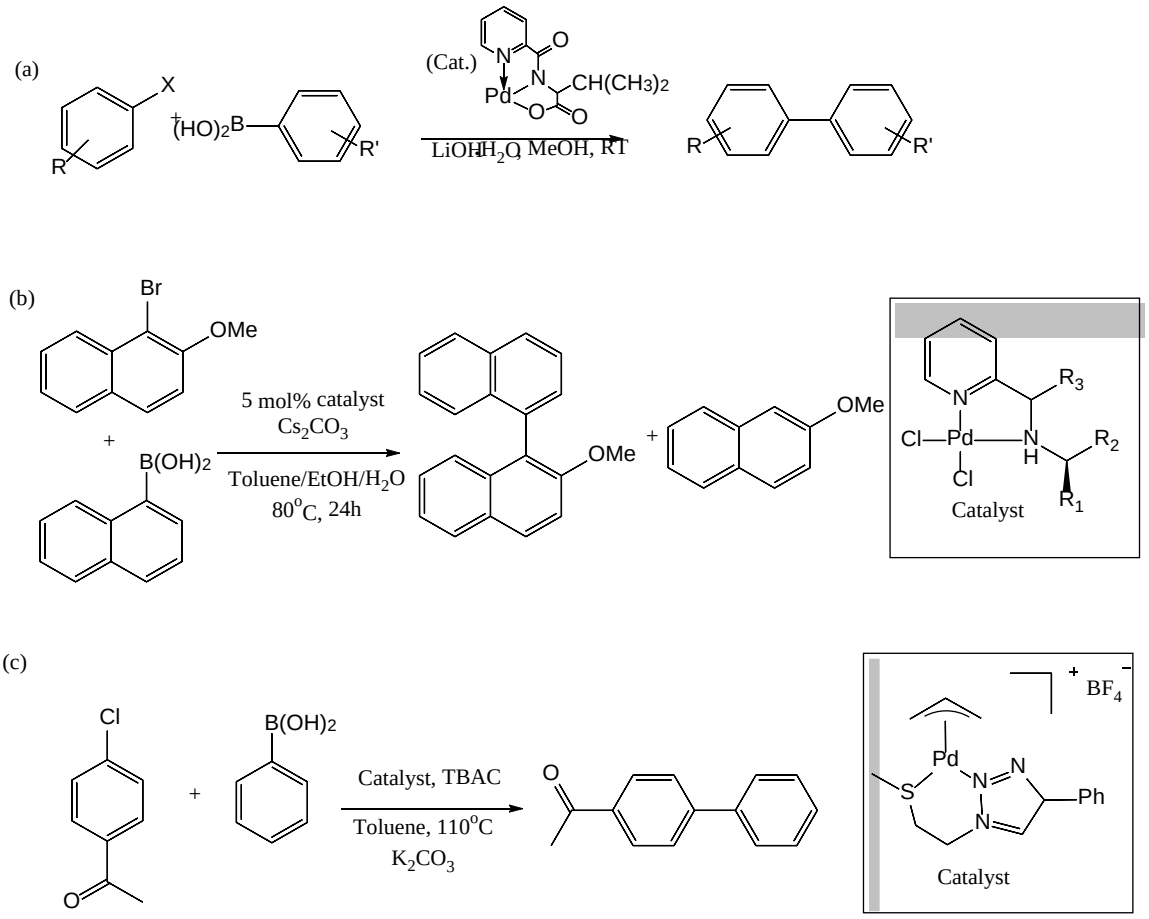

Figure 1.16 | Examples of various ligand systems used in Suzuki coupling reactions: a. NNO-tridentate; b. N,N-bidentate; c. N,S-bidentate.

The utilization of Pd(II) catalysis for the direct coupling of alkenes and arenes together in the late 1960s by Fujiwara and Moritani[46,47] heralded a breakthrough in C–H activation. With the use of directing groups or ligands, which help to control the selectivity, such C–H activation reactions have been impressively enhanced in recent works. Carboxylic acid derivatives[48–50] along with *N*-heterocycles are the most widely used directing groups in Pd(II)-catalyzed C–H activations. There are two main catalytic cycles in such palladium catalyzed C-H activation reactions：

a. The Pd^{II}/Pd^{0} catalytic cycle. During the last decade, arene-arene coupling reactions have attracted great attention. Studies on the palladium(II) catalyzed coupling

reactions between two different arenes have mainly focused on the elimination of the less desirable arene-arene homocoupling product.

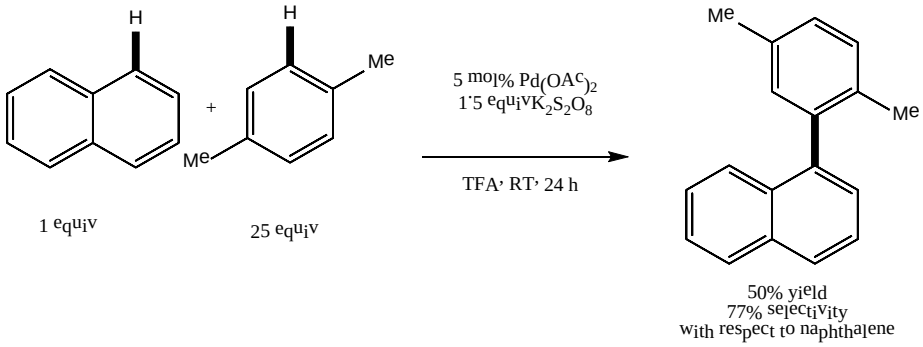

Figure 1.17 | Example of arene-arene coupling.

Lu and co-workers have made remarkable progress towards this goal (**Figure 1.17**).[36] The commonly accepted catalytic cycle for a Pd^{II}/Pd^{0} catalyzed arylation is illustrated in **Scheme 1.3.**[36]

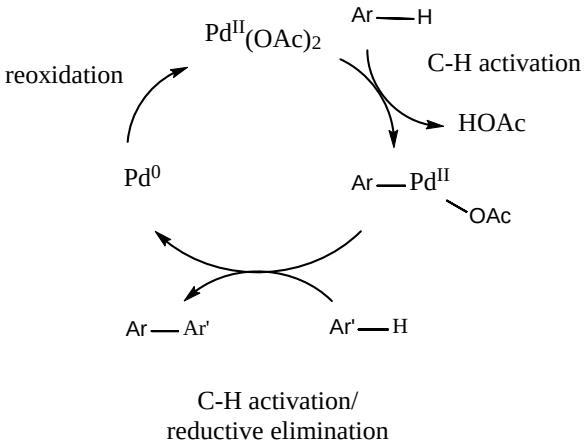

Scheme 1.3 | Pd^{0}/Pd^{II} catalytic cycle

b. The Pd^{II}/Pd^{IV} catalytic cycle. The first plausible example of a Pd^{II}/Pd^{IV} mechanism was reported by Tremont and Rhaman who presented the intriguing methylation of ortho C-H bonds in anilide (**Scheme 1.4**).[37]

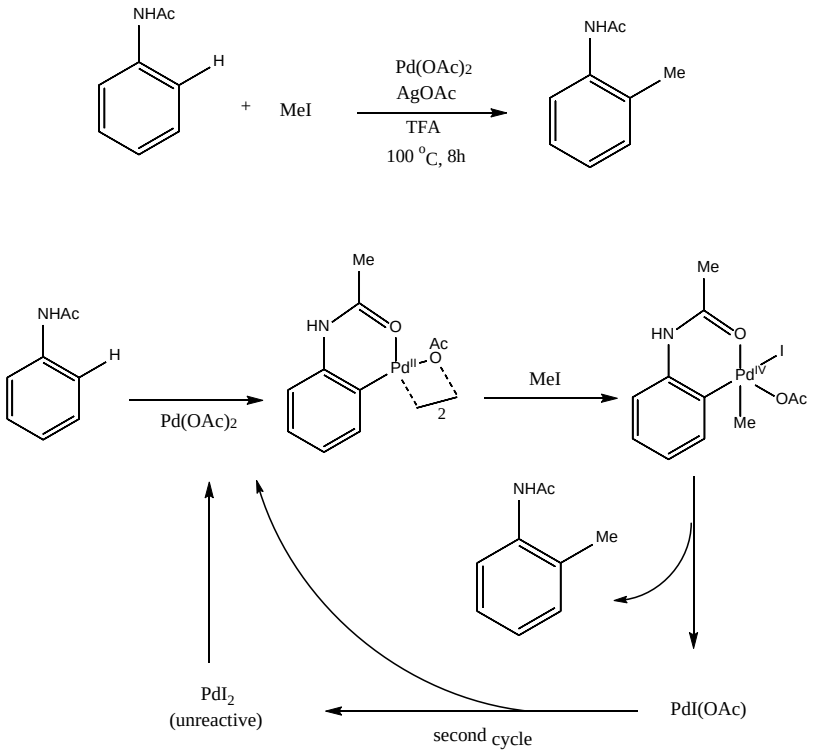

Scheme 1.4 | Pd^{II}/Pd^{IV} catalytic cycle

In 2005, Sanford and co-workers developed a more general process using Pd^{II}/Pd^{IV} catalysis and $[Ph_2I]PF_6$ for the arylation of C-H bonds.[51] Here, the oxidation role of MeI in the catalytic cycle in **Scheme 1.4** is replaced by $[Ph_2I]PF_6$. Furthermore, Sanford has been able to expand the scope of this chemistry to milder reaction conditions and other substrates.[52]

1.4 This work

This thesis is concerned with the development of pyridine-based, unsymmetrical, monoanionic CNN and CNO pincer ligands, and the reaction chemistry of the tridentate pincer complexes formed by reaction of these pincer ligands with palladium and platinum salts. A range of pyridine-based pincer ligands have been targeted with the general structure 2-{2-[(aldimine/ketimine/amine)-(2,6-$^{i}Pr_2C_6H_3$)]/bipyridine/alcohol}-6-(Aryl/Naphthyl/Alkyl)-C_5H_3N (**Figure 1.18**). With a pyridine unit forming the common central donor and the 6-position containing a hydrocarbyl group that will be available for C-H activation in all cases, the 2-position varied from a ketimine moiety to an aldimine, amine and pyridine moiety, to examine the influence of the 2-substituted nitrogen donors on the C-H activation chemistry. In addition, two 2-substituted tertiary alcohol ligands

have been targeted as examples of relatively rare pyridine based ONC pincers, which allows a comparison between the nitrogen and oxygen donors in C-H activation chemistry. Moreover, variation at the 6-position from aryl to naphthyl was targeted to investigate regioselectivity effects where two accessible C-H sites are present. To extend the scope of C-H activation, three pro-ligands with alkyl groups at the 6-position were also targeted to investigate the potential for sp^3 C-H activations. The design, synthesis and full characterization of these 13 pro-ligands will be discussed in Chapter 2.

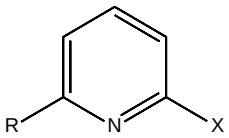

R = tolyl
2,6-dimethylphenyl
2,4,6-trimethylphenyl
naphthyl
Et
^{i}Pr
^{t}Bu

X = C(N)H-dipp
C(N)Me-dipp
C(NH)Me_2-dipp
Py
C(OH)Me_2

Figure 1.18 | General structure for targeted pro-ligands

Chapter 3 describes the 10 'aryl/naphthyl-armed ligands', which all facilitate sp^2 C-H activations upon reaction with palladium and platinum salts. It contains an investigation on the influence of different donor properties on C-H activation, as well as the exploration of ortho-/peri-selectivity on the naphthyl ring. Chapter 3 comprises the main chapter on the discussion of the synthesis, characterization and interconversion chemistry of the palladium/platinum pincer complexes supported by pyridine based pincer ligands in this thesis.

In Chapter 4, the reactions of three 'alkyl-armed' pro-ligands with palladium acetate and palladium chloride salts will be described, with the example of rare palladium pincer complexes obtained by sp^3 C-H activation of an alkyl arm.

In Chapter 5, the reactivity of these well-defined palladium complexes with bidentate or tridentate ligands, in terms of both stoichiometric and catalytic transformations, will be explored. As examples of stoichiometric chemistry, the salt exchange reactions with $AgBF_4$/$AgPF_6$, which generate a series of cationic palladium-NCMe and palladium-Py

complexes, will be investigated; whilst the catalytic allylic arylation reactions will also be reported as an example of the application of the palladium complexes synthesized in this work.

References

1 (a) G. W. Parshall, *Acc. Chem. Res*., 1970, **3**, 139; (b) J. Dehand and M. Pfeffer, *Coord. Chem. Rev*., 1976, **18**, 327; (c) M. I. Bruce, *Angew. Chem*., 1977, **89**, 75; *Angew. Chem. Int. Ed. Engl*., 1977, **16**, 73; (d) I. Omae, *Chem. Rev*., 1979, **79**, 287; (e) I. Omae, *Coord. Chem. Rev*., 1979, **28**, 37; (f) G. R. Newkome, W. E. Puckett, V. K. Gupta and G. E. Kiefer, *Chem. Rev.,* 1986, **86**, 451; (g) A. E. Shilov and G. B. Shul'pin, *Chem. Rev*., 1997, **97**, 2897.

2 (a) J. G. Noltes, *J. Organomet. Chem.*, 1978, **148**, 233; (b) C. S. Creaser and W. C. Kaska, *Inorg. Chim. Acta*., 1978, **30**, L325.

3 G. van Koten, *Pure Appl. Chem*., 1989, **61**, 1681.

4 (a) G. W. V. Cave, F. P. Fanizzi, R. J. Deeth, W. Errington and J. P. Rourke, *Organometallics*, 2000, **19**, 1355; (b) W. Lu, C. W. Chan, K.-K. Cheung and C.-M. Che, *Organometallics*, 2001, **20**, 2477; (c) A. Vigalok and D. Milstein, *Organometallics*, 2000, **19**, 2061.

5 M. Albrecht and G. van Koten, *Angew. Chem., Int. Ed.*, 2001, **40**, 3750.

6 (a) J. Cho, T. K. Hollis, E. J. Valente and J. M. J. Trate, *Organomet. Chem*. 2011, **696**, 373−377. (b) T. R. Helgert, T. K. Hollis and E. J. Valente, *Organometallics*, 2012, **31**, 3002.

7 C. Sui-Seng, A. Castonguay, Y. F. Chen, D. Gareau, L. F. Groux and D. Zargarian, *Top. Catal.*, 2006, **37**, 81. (b) A. Castonguay, D. M. Spasyuk, N. Madern, A. L. Beauchamp, and D. Zargarian, *Organometallics*, 2009, **28**, 2134.

8 (a) G. T. S. Andavan, E. B. Bauer, C. S. Letko, T. K. Hollis, and F. S. J. Tham, *Organomet. Chem*., 2005, **690**, 5938. (b) R.-Y. Lai, K. Surekha, A. Hayashi, F. Ozawa, Y.-H. Liu, S. M. Peng, and S.-T. Liu, *Organometallics*, 2007, **26**, 1062.

9 I. P. Beletskaya and A. V. Cheprakov, *Chem. Rev.*, 2000**, 100**, 3009..

10 (a) D. Morales-Morales and C. M. Jensen (Eds.), The Chemistry of Pincer Compounds; Elsevier: Amsterdam, The Netherlands, 2007. (b) G. van Koten and D. Milstein (Eds.), Organometallic Pincer Chemistry; Topics in Organometallic Chemistry; Springer-Verlag: Berlin−Heidelberg, 2013, Vol. 40.

11 M. Ohff, A. Ohff, M. E. van der Boom and D. Milstein, *J. Am.Chem. Soc*., 1997, **119**, 11687.

12 (a) C. M. Jensen, *Chem. Commun*., 1999, 2443. (b) K. Krogh-Jespersen, M. Czerw, K. M. Zhu, B. Singh, M. Kanzelberger, N. Darji, P. D. Achord, K. B. Renkema and

A. S. Goldman, *J. Am. Chem.Soc*., 2002, **124**, 10797. (c) A. S. Goldman, A. H. Roy, Z. Huang, R. Ahuja, W. Schinski and M. Brookhart, *Science*, 2006, **312**, 257.

13 M. T. Johnson and O. F. Wendt, *J. Organomet. Chem*., 2014, **751**, 213.

14 M. Weck and C. W. Jones, *Inorg. Chem*., 2007, **46**, 1865.

15 R. Johansson, M. Jarenmark and O. F. Wendt, *Organometallics*, 2005, **24**, 4500.

16 G. R. Fulmer, W. Kaminsky, R. A. Kemp and K. I. Goldberg, *Organometallics*, 2011, **30**, 1627.

17 A. J. Ruddy, S. J. Mitton, R. McDonald and L. Turculet, *Chem. Commun*., 2012, **48**, 1159.

18 J. Zhang, G. Leitus, Y. Ben-David and D. Milstein, *Angew. Chem., Int. Ed.*, 2006, **45**, 1113.

19 (a) B. Rybtchinski and D. Milstein, *Angew. Chem. Int. Ed.*, 1999, **111**, 918; (*b*) P. Steenwinkel, R. A. Gossage and G. van Koten, *Chem. Eur. J.*, 1998, **4**, 759.

20 (a) J. F. Remenar and D. B. Collum, *J. Am. Chem. Soc*., 1997, **119**, 5573. (b) P. Braunstein and F. Naud, *Angew. Chem., Int. Ed*., 2001, **40**, 680. (c) Z.; Weng, S. Teo and T. S. A. Hor, *Acc. Chem. Res*., 2007, **40**, 676.

21 (a) P.-Y. Shi, Y.-H. Liu, S.-M. Peng and S.-T. Liu, *Organometallics*, 2002, **21**, 3203. (b) M. Bassetti, A. Capone, M. Salamone, *Organometallics*, 2004, **23**, 247.

22 J. Zhang, G. Leitus, Y. Ben-David and D. Milstein, *J. Am. Chem. Soc*., 2005, **127**, 10840.

23 M. Gandelman, A. Vigalok, L. J. W. Shimon and D. Milstein, *Organometallics*, 1997, **16**, 3981.

24 A. F. M. J. van der Ploeg, G. van Koten and C. Brevard, *Inorg. Chem*., 1982, **21**, 2878.

25 S. Kuriyama, K. Arashiba, K. Nakajima, H. Tanaka, N. Kamaru, K. Yoshizawa, and Y. Nishibayashi, *J. Am. Chem. Soc*., 2014, **136,** 9719.

26 W. Zhang, Y. Wang, J. Yu, C. Redshaw, X. Hao and W. Sun, *Dalton Trans*., 2011, **40**, 12856.

27 D. Milstein, *Top Catal*., 2010, **53**, 915.

28 E. Ben-Ari, G. Leitus, L. J. W. Shimon and D. Milstein, *J. Am. Chem. Soc*., 2006, **128**, 15390.

29 J. Zhang, M. Gandelman, L. J. W. Shimon, H. Rozenberg and D. Milstein, *Organometallics*, 2004, **23**, 4026.

30 J. Zhang, G. Leitus, Y. Ben-David and D. Milstein, *J. Am. Chem. Soc*., 2005, **127**, 12429.

31 J. Zhang, G. Leitus, Y. Ben-David and D. Milstein, *Angew. Chem. Int. Ed*., 2006, **45**, 1113.

32 C. Gunanathan, Y. Ben-David and D. Milstein, *Science*, 2007, **317**, 790.

33 For recent reviews; (a) Contributions by G. van Koten, E. Poverenov, D. Milstein, D. M. Roddick, G.R. Freeman, J. A. G. Williams, D. Zargarian, A. Castonguay, D.M. Spasyuk, R. Jambor, L. Dostál, K. J. Szabo, J.-I. Ito, H. Nishiyama, A. St. John, K. I. Goldberg, D. M. Heinekey, in: G. van Koten, D. Milstein (Eds.), Organometallic Pincer Chemistry, *Top. Organometal. Chem*., 2013, 40, Springer, Heidelberg, 1-352; (b) Special issue, in: G. van Koten, R. J. M. Klein Gebbink (Eds.), *Dalton Trans*., 2011, **40**, 8731.

34 R. G. Bergman, *Nature*, 2007, **446**, 391.

35 R. H. Crabtree, *J. Chem. Soc., Dalton Trans.*, 2001, 2437.

36 R. Li, L. Jiang and W. Lu, *Organometallics*, 2006, **25**, 5973.

37 S. J. Tremont and H. U. Rahman, *J. Am. Chem. Soc*., 1984, **106**, 5760.

38 (a) X. Chen, K. M. Engle, D. H. Wang and J. Q. Yu, *Angew. Chem., Int. Ed*., 2009, **48**, 5094; (b) O. Daugulis, H.-Q. Do and D. Shabashov, *Acc. Chem. Res.*, 2009, **42**, 1074; (c) L. Ackermann, R. Vicente and A. R. Kapdi, *Angew. Chem., Int. Ed*. 2009, **48**, 9792.

39 (a) D. Alberico, M. E. Scott and M. Lautens, *Chem. Rev*., 2007, **107**, 174; (b) T. W. Lyons and M. S. Sanford, *Chem. Rev.*, 2010, **110**, 1147.

40 (a) N. J. Whitcombe, K. K. Hii and S. E. Gibson, *Tetrahedron*, 2001, **57**, 7449. (b) G. T. Crisp, *Chem. Soc. Rev*., 1998, **27**, 427.

41 I. Shinkai, A. O. King and R. D. Larsen, *Pure Appl. Chem*., 1994, **66**, 1551.

42 J. G. D. Vries, *Can. J. Chem.*, 2001, **79**, 1086.

43 L. E. Overman, D. J. Ricca and V. D. Tran, *J. Am. Chem. Soc*., 1993, **115**, 2042.

44 G. Ren, X. Cui, E. Yang, F. Yang and Y. Wu, *Tetrahedron*, 2010, **66**, 4022.

45 K. Billingsley and S.L. Buchwald, *J. Am. Chem. Soc*., 2007, **129**, 3358.

46 (a) I. Moritani and Y. Fujiwara, *Tetrahedron Lett*., 1967, **8**, 1119; (b) Y. Fujiwara, I. Moritani, S. Danno, R. Asano and S. Teranishi, *J. Am. Chem. Soc.*, 1969, **91**, 7166; (c) C. Jia, T. Kitamura and Y. Fujiwara, *Acc. Chem. Res.*, 2001, **34**, 633.

47 (a) R. Heck, *Acc. Chem. Res.*, 1979, **12**, 146; (b) R. Heck, *Org. React.*, 1982, **27**, 345; (c) I. Beletskaya and A. V. Cheprakov, *Chem. Rev.*, 2000, **100**, 3009; (d) A. Dounay and L. Overman, *Chem. Rev.*, 2003, **103**, 2945.

48 (a) D. Wang, K. Engle, B. Shi and J. Yu, *Science*, 2010, **327**, 315; (b) K. Engle, D. Wang and J. Yu, *Angew. Chem., Int. Ed*., 2010, **49**, 6169; (c) K. Engle, D. Wang and J. Yu, *J. Am. Chem. Soc*., 2010, **132**, 14137.

49 (a) Y. Ano, M. Tobisu and N. Chatani, *Org. Lett*., 2012, **14**, 354; (b) Y. Ano, M. Tobisu and N. Chatani, *J. Am. Chem. Soc*., 2011, **133**, 12984; (c) S. Rakshit, C. Grohmann, T. Besset and F. Glorius, *J. Am. Chem. Soc*., 2011, **133**, 2350.

50 (a) T. Gong, B. Xiao, Z. Liu, J. Wan, J. Xu, D. Luo, Y. Fu and L. Liu, *Org. Lett*., 2011, **13**, 3235; (b) C. Feng and T. Loh, *Chem. Commun*., 2011, **47**, 10458; (c) X. Zhao, C. Yeung and V. Dong, *J. Am. Chem. Soc*., 2010, **132**, 5837.

51 D. Kalyani, N. Deprez and M. Sanford, *J. Am. Chem. Soc.*, 2005, **127**, 7330.

52 N. Deprez, L. Desai and M. Sanford, *J. Am. Chem. Soc*., 2006, **128**, 4927.

53 N. Selander and K. J. Szabo, *Chem. Rev*., 2011, **111**, 2048.

Chapter Two

Pro-ligand Synthesis

2.1 Introduction

2.1.1 Pincer ligands

The 'traditional' pincer ligands have a symmetrical geometry with a central donor and two symmetrical donors on each side. The symmetrical nature of these ligands enables the simplification of the synthesis while allowing the electronic and steric environments to be modified easily. Anionic ligands with a carbanion at the centre and two phosphines on each side, which are known as PCP pincers, were the earliest examples of symmetric pincer ligands,[1] and PCP pincers have been widely popular tridentate ligands. Further research has enabled the discovery of more variable and flexible donor sets. For example, thioether and tertiary amines are used as alternatives for the phosphines.

Despite the slight difficulties in synthesis, a variety of non-symmetric pincer ligands, obtained by either changing one of the donor atoms or by adding different substituents to the backbone of the pincer ligand, have been reported and widely used in organometallic chemistry in the recent years. An enormous amount of potential ligands could be produced using any of the two modification techniques mentioned above. Additionally, the unsymmetrical nature of these ligands can generate chiral centres at various positions in the molecules. Due to their versatile application in catalytic systems, sometimes more powerful than their symmetric counterparts, there has been a huge rise in the synthesis and application of unsymmetrical pincer ligands over the last decade,[2-4] and nitrogen has been increasingly used as the 'most popular donor atom' in these ligands.[5] Pincer ligands in which a neutral pyridine is the central donor are known as pyridine-based pincer ligands.

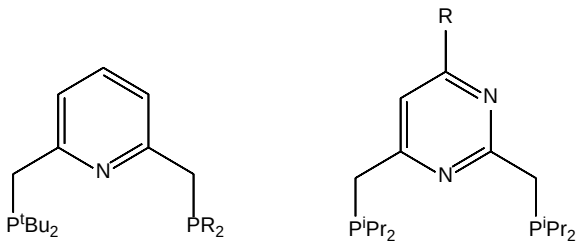

Figure 2.1 | PNP pincer ligands

This type of ligands do not require C-H activation on the central position and often has no charge, enabling access to different oxidation states than those observed for PCP pincer ligands. A typical example of this ligand system is the PNP pincers (**Figure 2.1**).[6,7] The organometallic chemistry associated with these ligands is mainly focused on molybdenum, tungsten and iridium while the amine linkers exhibit rich chemistry with their benefits as protic cooperative ligands.[8]

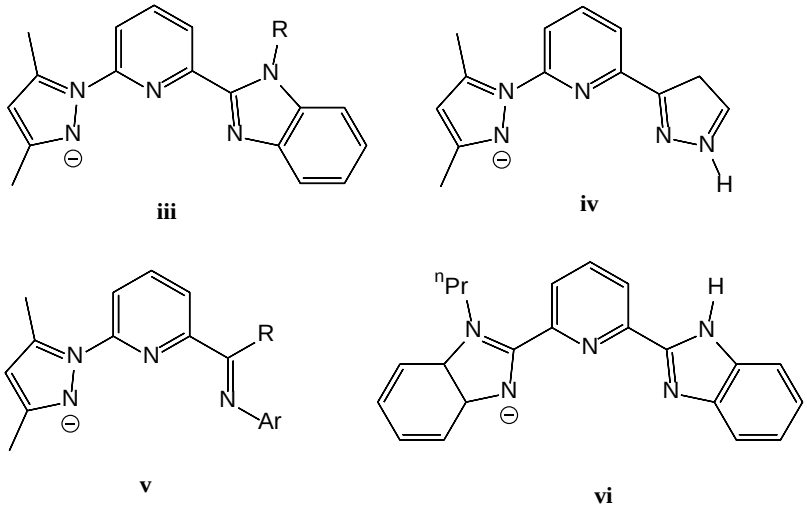

Figure 2.2 | Non-symmetric NNN pincer ligands

A common modification on these ligands is to add a variety of nitrogen-based donors to the central pyridine ring, for instance, to form a class of N,N,N pincer ligands (**Figure 2.2**).[9-12] The advantage of these ligands is their potential for supporting cooperative interactions between the metal and the ligand. In the case of ligand **v** (**Figure 2.2**), pincer complexes with restricted lability on one arm (amido) and hemilability on the other arm (imine) are generated.

Pyridine-based ligands with different donors on each side have incredible potential in collaborative metal-ligand reactivity, due to the *trans* arrangement of their different donor ligands. Examples of only the PNN and CNN systems are to be given in this introduction. However, the potential diversity of these pyridine-based non-symmetric donor systems is myriad. The first example of a PNN ligand system was reported by Milstein and co-workers in 2005 (**Figure 2.3**).[13]

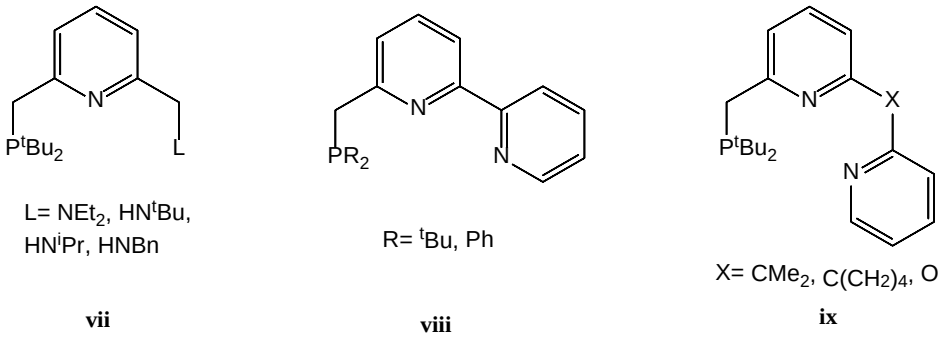

Figure 2.3 | Examples of PNN ligands

Replacing one phosphine with the more labile amine enhances the reactivity of the metal centre due to the potential of the amine to dissociate. There are also examples of ligand systems in which the amine is substituted with a pyridine (**Figure 2.3,** ligand **viii**).[14] PNN ligands with a carbon or oxygen linker between two pyridine groups have also been synthesized by Milstein and co-workers (**Figure 2.3,** ligand **ix**).[15]

Another typical class of these pyridine-based non-symmetrical pincer systems is ligands with a 2,6-disubstituted pyridine as a central unit and an amino moiety as one arm while an aryl group being the other (**Figure 2.4,** ligand **x**).[16] This CNN ligand system facilitates C-H activation of the aryl group upon coordination to the metal centre thus introducing rich chemistry into the study of pyridine-based pincers. One of the most common examples of CNN ligands is ligand **x** in **Figure 2.4** with subsequent modifications such as methylating the amine or adding alkyl groups (Me/tBu) to the methylene linker.[17, 18]

Herein, we explore the generation and characterization of *CNN* ligand systems and their 'derivative' *CNO* pincer pro-ligands, with their subsequent application in the formation of catalytically active transition metal complexes in the next two chapters.

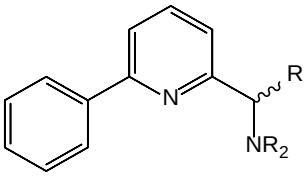

Figure 2.4 | Example of CNN ligands

2.1.2 Aims and objectives

This chapter describes and discusses the synthesis and characterization of the 13 pyridine-based pro-ligands that will be used in this thesis. The ligands are grouped into categories according to their donor atom types (see **Figure 2.5**) with a pyridine unit forming the common central donor in all cases. At the 2-position, the donor unit is either nitrogen- or oxygen-based while the 6^{th} position contains a hydrocarbyl group that will be available for C-H activation (Chapter 3). In designing the ligands targeted in the project, the 2,6-diisopropyl aniline was chosen, as an N-aryl group is common to all the ligands for two reasons: (a) recrystallization of the metal complexes would be expected to be more straightforward with the diisopropyl aryl group; (b) the septet signal of the diisopropyl group in the ^{1}H NMR spectrum offers a straightforward, easy-to-spot resonance for tracking the progress of reactions for the large molecules and complexes to be generated.

To examine the influence of the 2-substituted nitrogen donors on the C-H activation chemistry, ketimine, aldimine, amine and pyridine derivatives have been prepared as selected examples of nitrogen donors. In addition, two 2-substituted tertiary alcohol ligands have been targeted as relatively rare potential ONC pincer pro-ligands to allow a comparison between the nitrogen and oxygen donors in C-H activation chemistry. Moreover, to explore the scope of C-H activation, the nature of the 6-substituted hydrocarbyl group has been varied to include aryl, naphthyl and alkyl groups. It is envisaged that this range of hydrocarbyl groups will allow an investigation of both sp^2- and sp^3-C-H activation chemistry along with regioselectivity effects where two accessible C-H sites are present.

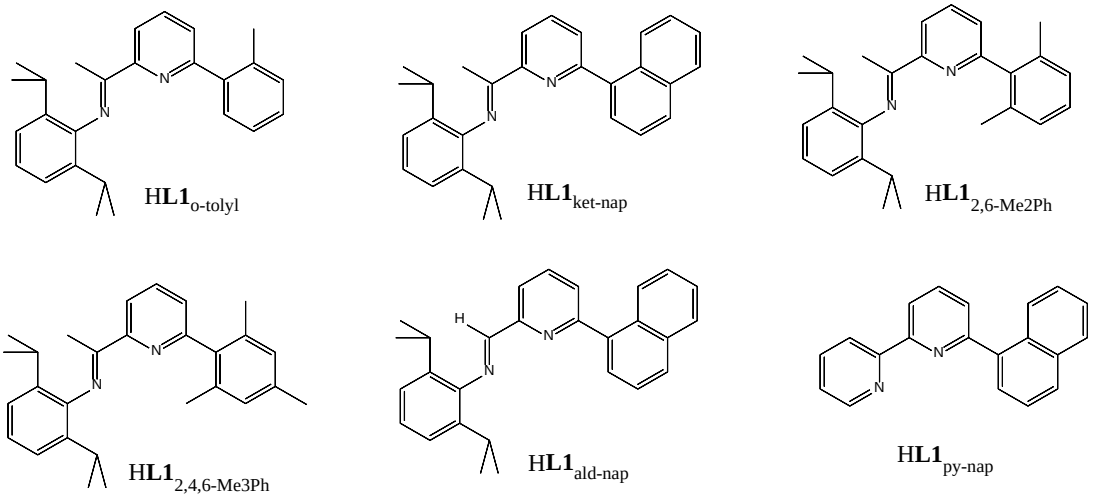

Aryl-containing pyridyl-imines (HL1)

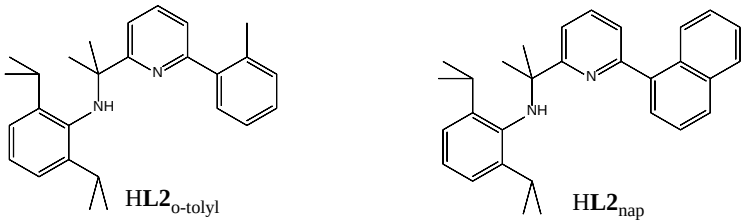

Aryl-containing pyridyl-amines (HL2)

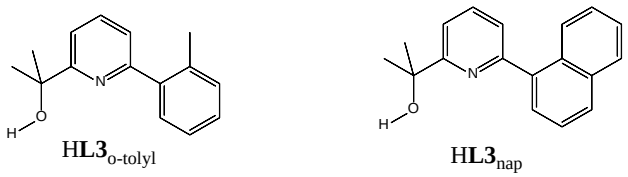

Aryl-containing pyridyl-alcohols (HL3)

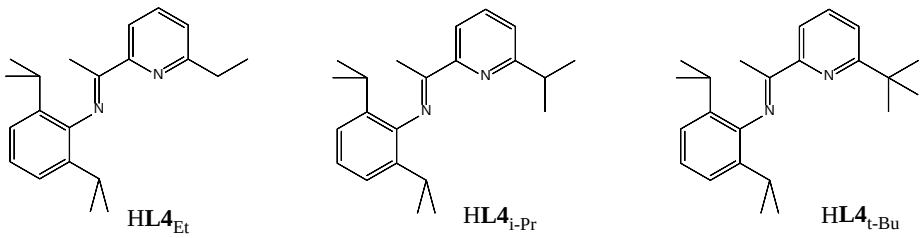

Alkyl-containng pyridyl-imines (HL4)

Figure 2.5| The target pro-ligands

2.1.3 Retro synthetic analysis

Illustrated in **Figure 2.6** is the retro synthetic analysis for the preparation of the aryl-containing pyridyl-imine/amine/alcohol pro-ligands. H**L1**$_{py\text{-}nap}$ required an alternative approach (**Figure 2.7**). The alkyl-containing ligands (H**L4**) were targeted via a third approach (**Figure 2.8**).

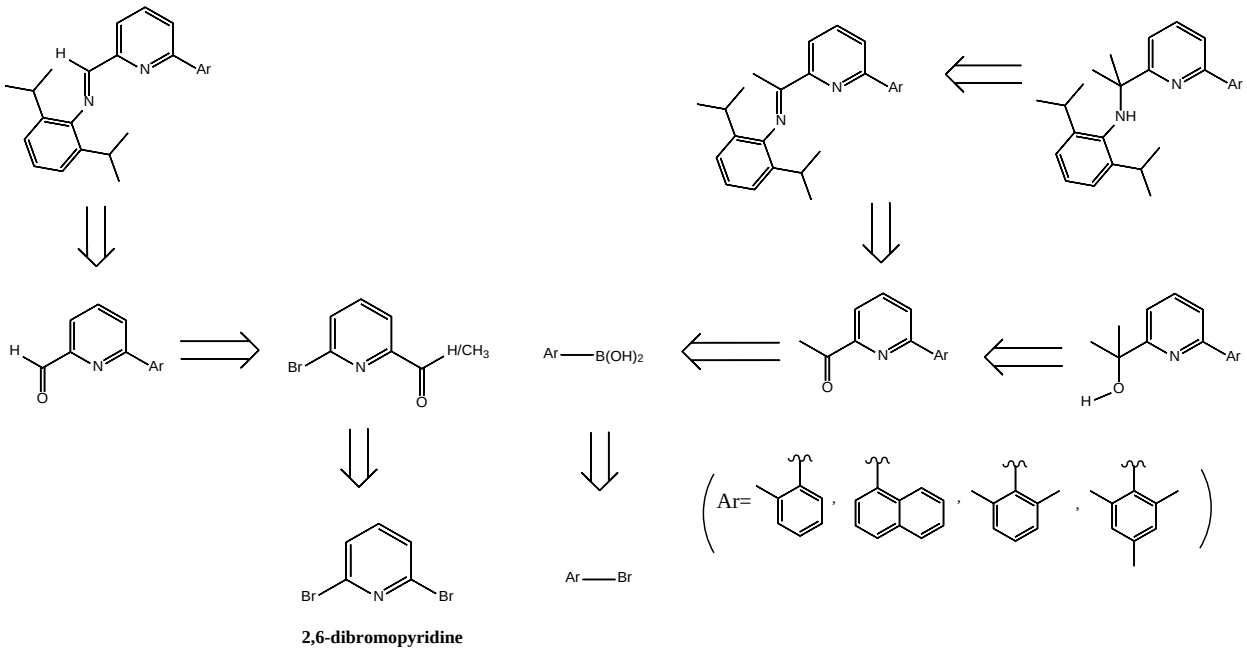

Figure 2.6 | Retro synthesis for the aryl-containing pyridyl-imines/amines/alcohols

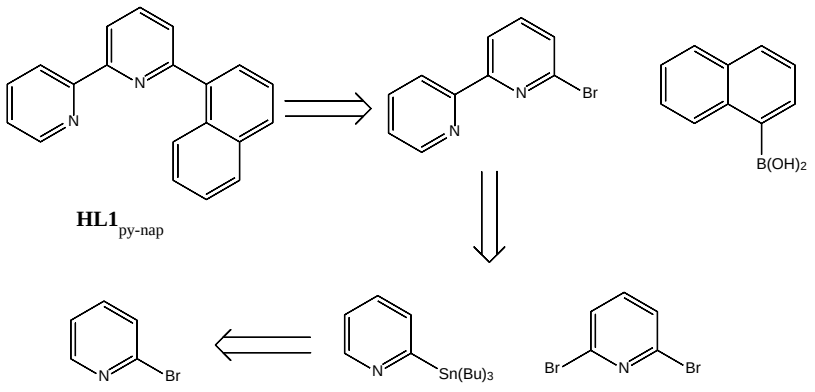

Figure 2.7 | Retro synthesis for H**L1**$_{py\text{-}nap}$

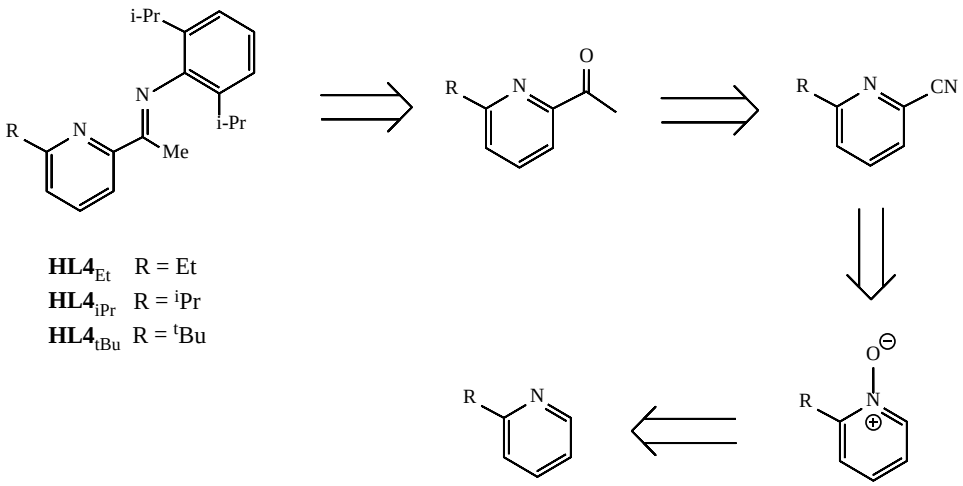

HL4$_{Et}$ R = Et
HL4$_{iPr}$ R = ^{i}Pr
HL4$_{tBu}$ R = ^{t}Bu

Figure 2.8 | Retro synthesis for the alkyl-containing ligands (H**L4**)

2.2 Synthesis of the aryl-containing pyridyl-imines/amines/alcohols

2.2.1 Synthesis of the intermediates

2.2.1.1 Synthesis of 2-bromo-6-acetylpyridine

Based on the retro synthetic analysis, the preparation of the starting materials was undertaken prior to the synthesis of the pro-ligands. The synthesis of 2-bromo-6-acetylpyridine was carried out according to a protocol refined by our group and based on a literature preparation and could be achieved in 60% yield (**Figure 2.9**).[19] Spectroscopic data for the product are consistent with those in the literature.

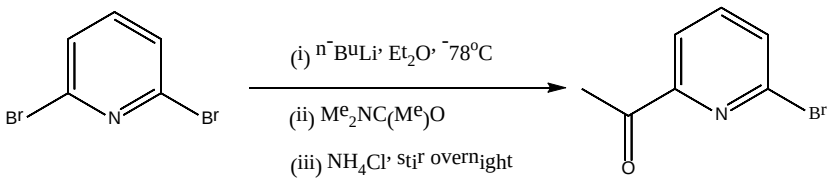

Figure 2.9 | Synthesis of 2-bromo-6-acetyl pyridine

2.2.1.2 Synthesis of 2-bromo-6-formylpyridine

The 2-bromo-6-formylpyridine was prepared via a lithium-halogen exchange/DMF sequence, based on the literature procedure (**Figure 2.10**).[28] The pure product was

obtained in 85% yield, with characterization data that is consistent with those reported in the literature.

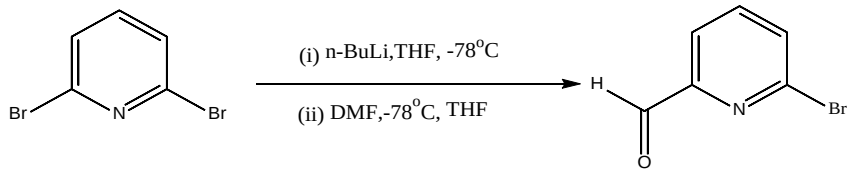

Figure 2.10 | Synthesis of 2-bromo-6-formylpyridine

2.2.1.3 Synthesis of 2-Methylphenyl boronic acid

2-Methylphenyl boronic acid could be readily prepared from 2-bromotoluene (**Figure 2.11**) using a protocol detailed elsewhere and the data is consistent with those reported in the literature.[29]

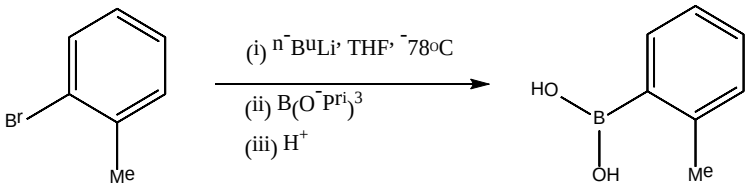

Figure 2.11 | Synthesis of 2-methylphenyl boronic acid

2.2.1.4 Synthesis of 1-naphthalene boronic acid (**1d**)

The 1-naphthalene boronic acid was prepared using the same synthetic approach (**Figure 2.12**). The ^{1}H NMR spectrum of the product is consistent with that in the literature.[20] The material was used in the subsequent Suzuki coupling reaction without any further purification.

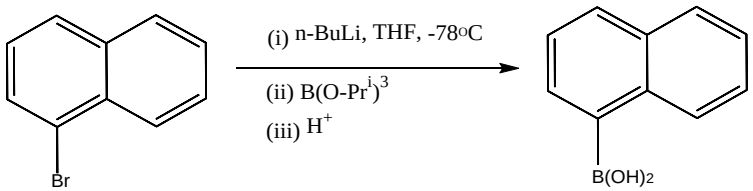

Figure 2.12 | Synthesis of 1-naphthalene boronic acid

2.2.1.5 Synthesis of 2,6-dimethyl phenyl boronic acid

The 'general' n-BuLi route for the synthesis of the previously described boronic acids (2-methylphenyl boronic acid and 1-naphthalene boronic acid) did not work very well for the preparation of 2,6-dimethyl phenyl boronic acid (less than 20% yield). Therefore, the alternative Grignard reaction was tried instead. The synthetic approach is illustrated in **Figure 2.13**.[30]

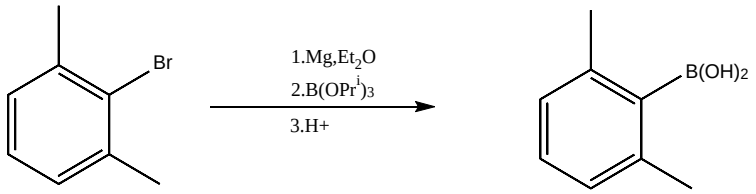

Figure 2.13 | Synthesis of 2,6-dimethyl phenyl boronic acid

Using this method, the boronic acid was obtained in very high purity and with a yield of 71%. In the ^{1}H NMR spectrum, the broad singlet at δ 4.80 for two protons is assigned to the $B(OH)_2$ signal. The product was used in the following Suzuki coupling reaction without further purification.

2.2.1.6 Synthesis of 2,4,6-trimethyl phenyl boronic acid

The synthesis of the 2,4,6-trimethyl phenyl boronic acid was achieved via the same synthetic approach as that used for the synthesis of 2,6-dimethyl phenyl boronic acid in a 68% yield. The data is consistent with those reported in the literature.[30]

2.2.1.7 Synthesis of 2-tolyl-6-acetylpyridine

The two reagents, 2-bromo-6-acetylpyridine and 2-methylphenyl boronic acid, were then employed in a Suzuki coupling reaction to give the ketone product, 2-tolyl-6-acetylpyridine (**Figure 2.14**).

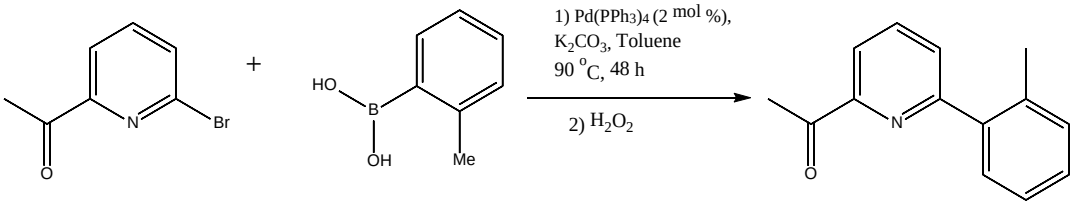

Figure 2.14 | Synthesis of the 2-tolyl-6-acetylpyridine

2-Tolyl-6-acetylpyridine has been fully characterized by several analytical methods. The infrared spectrum of the product shows peaks at 1581 cm^{-1} and 1696 cm^{-1} which correspond to vibrations of the $(C\text{-}N)_{pyridine}$ and $(C\text{-}O)_{ketone}$ bonds, respectively. The ^{1}H NMR spectrum for the product shows two singlets at 2.37 ppm and 2.65 ppm assigned to the aryl methyl and the carbonyl methyl protons respectively. The signals appearing as a 3H multiplet at 7.16-7.26 ppm and a 1H doublet at 7.34 ppm correspond to the protons on the aryl ring. Furthermore, two 1H doublets at 7.48 ppm and 7.91 ppm are due to the meta protons of the pyridine moiety while the signal at 7.76 ppm belongs to the para proton on the pyridine unit. The $^{13}C\{^{1}H\}$ NMR spectrum of this compound showed a peak at 200.5 ppm which is assigned to the C(=O) in the molecule. ESMS data of this compound gave two peaks at 212 ($[M+H]^{+}$), 234 ($[M+Na]^{+}$) which agree with the calculated molecular mass of the desired product. High resolution mass spectrometry (HRMS) revealed a peak at 212.1075; the calculated molecular mass for $C_{14}H_{14}NO$ ($[M+H]^{+}$) is 212.1036.

2.2.1.8 Synthesis of 2-naphthyl-6-acetylpyridine

2-naphthyl-6-acetylpyridine was obtained in a moderate yield and with excellent purity using a similar Suzuki-based synthetic approach to that described for the synthesis of 2-tolyl-6-acetylpyridine (**Figure 2.15**).

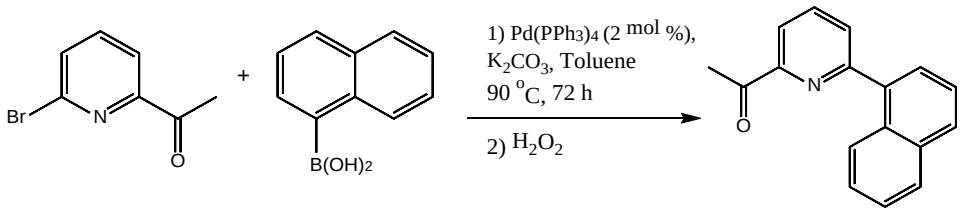

Figure 2.15 | Synthesis of 2-naphthyl-6-acetylpyridine

The ^{1}H NMR spectrum for 2-naphthyl-6-acetylpyridine shows a singlet at 2.69 ppm

corresponding to the carbonyl methyl protons and reveals six other signals (10H) in the aromatic region assigned to be the protons on the pyridyl and naphthalene rings. The $^{13}C\{^{1}H\}$ NMR spectrum of this compound shows a peak at 200.6 ppm which is assigned to the C(=O) in the molecule. ESMS data of this compound gave two peaks at 248 ($[M+H]^+$), 270 ($[M+Na]^+$) which agrees with the calculated molecular mass of the desired product. The infrared spectrum of the product shows peaks at 1584 cm^{-1} and 1695 cm^{-1} which correspond to vibrations of the $(C\text{-}N)_{pyridine}$ and $(C\text{-}O)_{ketone}$ bonds, respectively.

2.2.1.9 Synthesis of 2-naphthyl-6-formylpyridine

Similarly to the synthesis of 2-naphthyl-6-acetylpyridine, the 2-naphthyl-6-formylpyridine was also obtained via a Suzuki coupling between 1-naphthalene boronic acid and 2-bromo-6-formylpyridine (**Figure 2.16**).

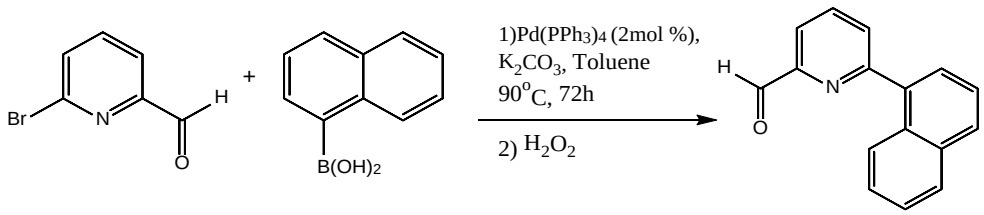

Figure 2.16 | Synthesis of aldehyde

The ^{1}H NMR spectrum of the product was consistent with that reported in the literature.[21] The spectrum revealed a 1H singlet at 10.19 ppm, which is indicative of an aldehyde proton, and five other signals in the aromatic region assigned to be the protons on the pyridyl and naphthalene rings. The ESMS showed a peak at *m/z* 234 confirming the product to be the desired aldehyde product.

2.2.1.10 Synthesis of 2-(2,6-dimethylphenyl)-6-acetylpyridine and 2-(2,4,6-trimethyl phenyl)-6-acetylpyridine

Synthesis of these two ketones was also achieved through a Suzuki coupling of 2-bromo-6-acetylpyridine and the corresponding boronic acids (**Figure 2.17**).

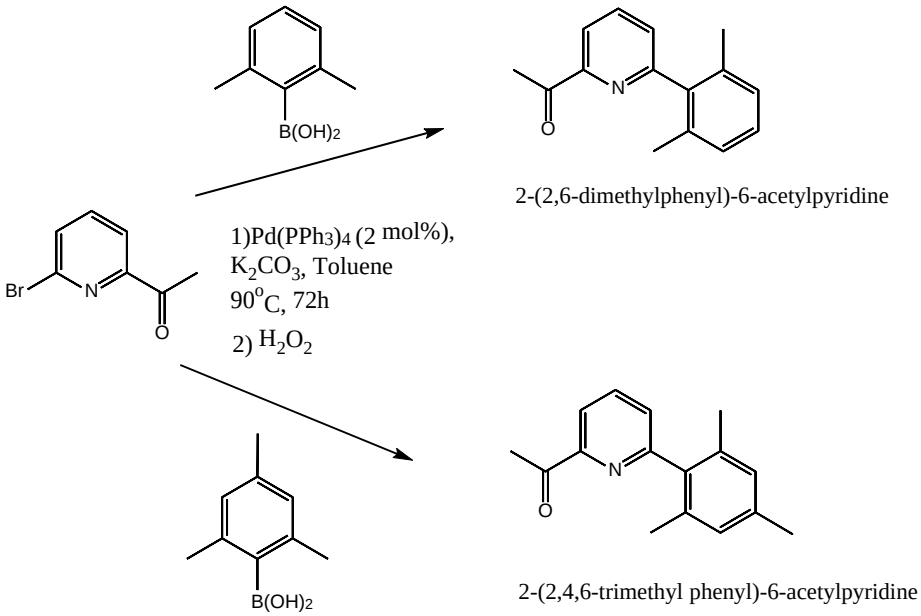

Figure 2.17 | Synthesis of 2-(2,6-dimethylphenyl)-6-acetylpyridine and 2-(2,4,6-trimethyl phenyl)-6-acetylpyridine

The ^{1}H NMR spectrum for 2-(2,6-dimethylphenyl)-6-acetylpyridine shows a 6H singlet at 2.00 ppm and a 3H singlet at 2.61 ppm assigned to the aryl methyls and the carbonyl methyl respectively. The signals appearing as a 2H doublet at 7.06 ppm and a 1H triplet at 7.15 ppm correspond to the protons on the aryl ring. Furthermore, two 1H doublets at 7.31 ppm and 7.92 ppm are due to the meta protons of the pyridyl moiety while the triplet at 7.80 ppm can be assigned to the para proton on the pyridine ring. The $^{13}C\{^{1}H\}$ NMR spectrum of this compound shows a peak at 200.7 ppm which is assigned to the C(=O) in the molecule. ESMS data of this compound gave two peaks at 226 ($[M+H]^+$), 248 ($[M+Na]^+$) which agree with the calculated molecular mass of the desired product. The infrared spectrum of the product shows a peak at 1694 cm^{-1} which corresponds to vibrations of the $(C\text{-}O)_{ketone}$ bond. High resolution mass spectrometry (FAB) revealed a peak at 226.2119 while the calculated molecular mass for $C_{15}H_{15}NO$ $[M+H]^+$ is 226.2124. 2-(2,4,6-trimethyl phenyl)-6-acetylpyridine was also characterized by proton and carbon NMR spectroscopies. The ^{1}H NMR spectrum for 2-(2,4,6-trimethylphenyl)-6-acetylpyridine shows a 6H singlet at 2.10 ppm and a 3H singlet at 2.61 ppm assigned to the ortho- and para-aryl methyls respectively. The signal appearing as a 2H singlet at 7.00 ppm corresponds to the two protons on the aryl ring. The fact that this signal does not show any splitting, indicates the symmetry of the 2,4,6-trimethylpenyl moiety regardless

of the unsymmetrical structure of the pyridine and ketone units on the other side of the molecule. The $^{13}C\{^{1}H\}$ NMR spectrum of this compound shows a peak at 198.9 ppm which is assigned to the C(=O) in the molecule. ESMS data of this compound gave two peaks at 240 ($[M+H]^+$), 262 ($[M+Na]^+$) which agree with the calculated molecular mass of the desired product. The infrared spectrum of the product shows a peak at 1699 cm^{-1} which corresponds to vibrations of the $(C\text{-}O)_{ketone}$ bond.

2.2.2 Synthesis of the imine/amine/alcohol-pyridine-aryl pro-ligands:

2.2.2.1 Synthesis of H**L1**$_{o\text{-}tolyl}$

The target compound H**L1**$_{o\text{-}tolyl}$ was then obtained via a condensation reaction of 2-tolyl-6-acetylpyridne with 2,6-diisopropyl aniline (**Figure 2.18**). The reaction was carried out in ethanol heated to reflux with a catalytic amount of formic acid. The reason for using two equivalents of aniline is to force the reaction towards the formation of H**L1**$_{o\text{-}tolyl}$.

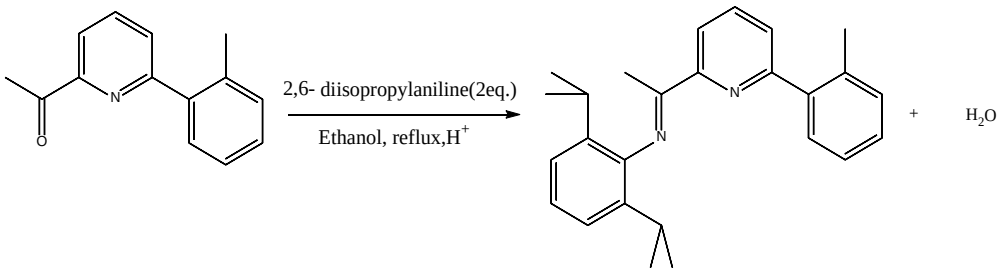

Figure 2.18 | Synthesis of H**L1**$_{o\text{-}tolyl}$

Upon comparing the results of three synthetic attempts, the use of two equivalents of aniline proved to be the most effective one. The formation of a stoichiometric amount of water during the reaction is noteworthy since it could prevent the reaction going towards the formation of the ligand as the reaction continues. Adding some more aniline during the process and thereby pushing the equilibrium to the ligand's side could be an approach to solving this problem. Another thing to notice during the work up of this reaction is to keep the filtrate after filtering and washing with cold ethanol, as the product can be further crystallized out from the filtrate. Using the above conditions, the pro-ligand H**L1**$_{o\text{-}tolyl}$ was produced in high purity in fairly good yields. There was no sign of any impurities in either the ^{1}H or $^{13}C\{^{1}H\}$ NMR spectra of the product. The proton NMR spectrum shows a 2H septet at 2.71 ppm and two 6H doublets at 1.08 and 1.10 ppm, while the ^{13}C NMR

spectrum reveals two different methyl signals for the iPr groups, indicating that the imine methyl blocks the rotation of the N=C bond thus making the methyl groups on the iPr moiety inequivalent. IR data of the ligand shows peaks at 1587 cm^{-1} and 1645 cm^{-1} which are indicative of the C-N pyridine and C=N imine bonds, respectively. ESMS and HRMS spectrometric analysis have also confirmed the compound to be the correct product. Crystals suitable for single crystal X-ray diffraction were grown from the slow evaporation of a methanol solution of the ligand. The molecular structure of H**L1**$_{o\text{-tolyl}}$ reveals the expected 2,6-substituted pyridine with the imine unit adopting a trans configuration with respect to the pyridine (**Figure 2.19** and **Table 2.1**).

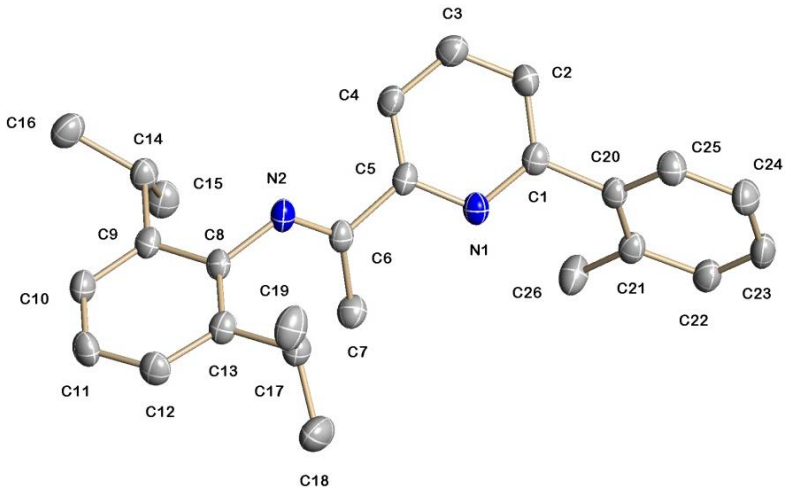

Figure 2.19 | Molecular structure of H**L1**$_{o\text{-tolyl}}$

Table 2.1: Selected bond lengths (Å) and angles (º) for H**L1**$_{o\text{-tolyl}}$

	Bond length		Bond angle
N(2)-C(6)	1.265(3)	N(2)-C(6)-C(5)	116.1(2)
C(5)-C(6)	1.481(3)	C(6)-N(2)-C(8)	122.2(2)
		N(1)-C(1)-C(20)	116.7(2)
		N(1)-C(5)-C(6)	115.3(2)

2.2.2.2 Synthesis of H**L1**$_{ket\text{-}nap}$

The reason for targeting pro-ligand H**L1**$_{ket\text{-}nap}$ was to probe the site of C-H activation on the aromatic moiety. The ketone precursor 2-naphthyl-6-acetylpyridine was employed in a condensation reaction with 2,6-diisopropyl aniline to give the new pro-ligand H**L1**$_{ket\text{-}nap}$ in high purity and very good yield (**Figure 2.20**).

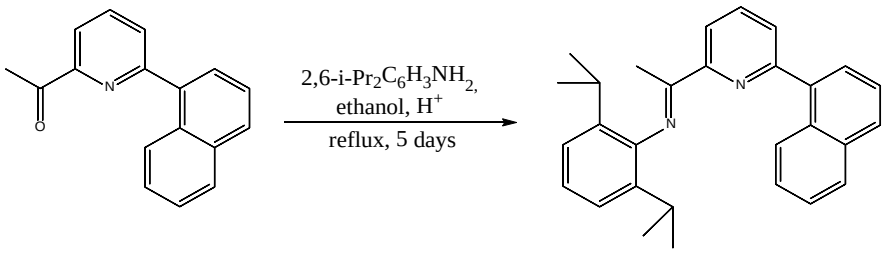

Figure 2.20 | Preparation of H**L1**$_{ket\text{-}nap}$

Interestingly, in the ^{1}H NMR spectrum of the ligand, there is an apparent triplet at 1.09 ppm which corresponds to 12 protons that belong to the methyl groups on the C2 and C3 carbon atoms (**Figure 2.21**). This apparent triplet is actually two overlapping doublets rather than a triplet. Whilst the isopropyl carbons C2 and C3 are equivalent, the methyl carbon atoms C4 and C4' are not equivalent thus resulting in two 6H methyl doublets. This was confirmed by the 1D and 2D ^{13}C{^{1}H} NMR spectra of this compound. There are two inequivalent carbon atoms found at 22.9 ppm and 23.3 ppm in the 1D carbon NMR spectrum which are correlated to these 12 protons in the HMQC spectrum.

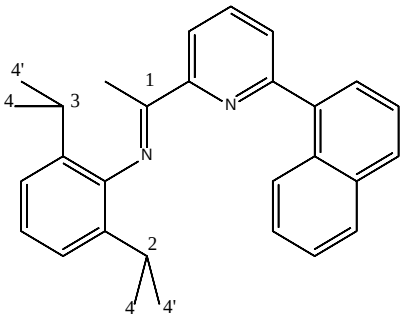

Figure 2.21 | H**L1**$_{ket\text{-}nap}$

2.2.2.3 Synthesis of **HL1**$_{2,6\text{-Me2Ph}}$

The reason for targeting this ligand was to block the ortho C-H activation site on the aryl ring and to subsequently investigate whether C-H activation could still occur (possibily on the pyridyl ring). The synthetic approach employed the 2-(2,6-dimethylphenyl)-6-acetylpyridne in a condensation reaction with 2,6-diisopropyl aniline (**Figure 2.22**). The reaction was monitored by proton NMR spectroscopy. After five days of reaction, the target pro-ligand was obtained in excellent purity and characterized by proton and carbon NMR spectroscopies. The ^{1}H NMR spectrum for H**L1**$_{2,6\text{-Me2Ph}}$ shows a 12H apparent triplet at 1.09 ppm which corresponds to the four methyl groups on the 2,6-diisopropyl phenyl ring. The 12H resonance appearing as two doublets merged together is further evidence of the inequivalency of the two methyl groups on each isopropyl moiety due to the lack of symmetry of the molecule.

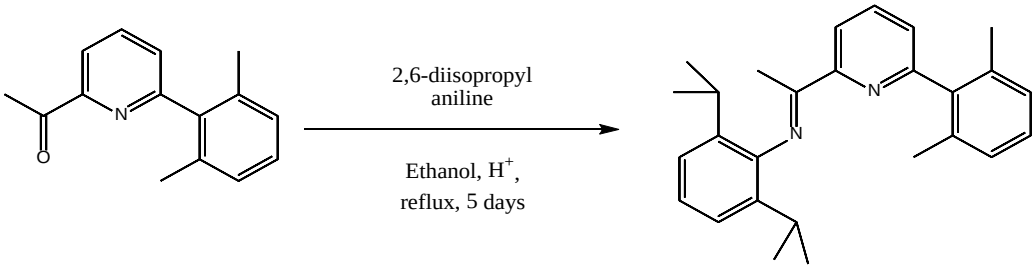

Figure 2.22 | Preparation of H**L1**$_{2,6\text{-Me2Ph}}$

The signals appearing as two multiplets at 7.01-7.09 ppm and 7.11-7.17 ppm correspond to the six protons on the aryl rings. Furthermore, the two 1H doublets at 7.27 ppm and 8.25 ppm are due to the meta protons of the pyridyl moiety while the triplet at 7.81 ppm belongs to the para proton on the pyridine ring. The $^{13}C\{^{1}H\}$ NMR spectrum of the ligand shows a peak at 166.7 ppm, which is assigned to the imine carbon atom. IR data of the ligand shows peaks at 1566 cm^{-1} and 1641 cm^{-1} which are indicative of the C-N pyridine and C=N imine bonds, respectively. ESMS data of this compound gave two peaks at 385 ($[M+H]^+$), 407 ($[M+Na]^+$) which agree with the calculated molecular mass of the desired product. High resolution mass spectrometry (FAB) revealed a peak at 385.1095 while the calculated molecular mass for $C_{27}H_{32}N_2$ $[M+H]^+$ is 385.1088.

2.2.2.4 Synthesis of H**L1**$_{2,4,6\text{-Me3Ph}}$

The H**L1**$_{2,4,6\text{-Me3Ph}}$ pro-ligand was targeted similarly. The pure product was obtained by a condensation reaction with 2,6-diisopropyl aniline and the corresponding ketone precursor (**Figure 2.23**). For H**L1**$_{2,4,6\text{-Me3Ph}}$, the signals for the isopropyl methyl protons happen to be coincident, a 12H doublet at 1.07 ppm.

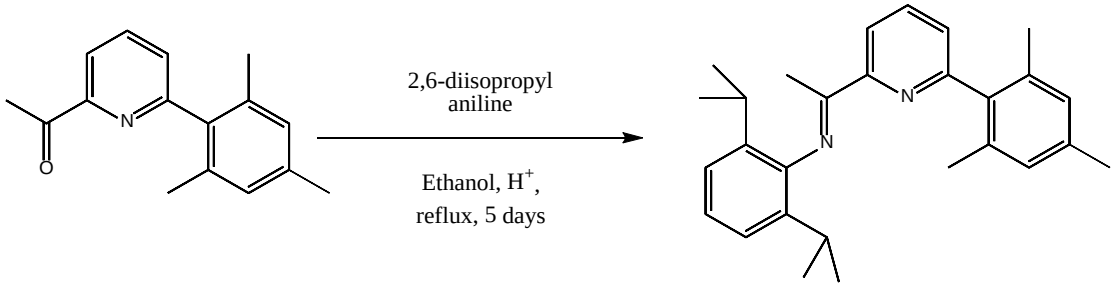

Figure 2.23 | Synthesis of pro-ligand H**L1**$_{2,4,6\text{-Me3Ph}}$

Moreover, the signals of the two protons on the mesityl moiety appear as one singlet at 6.89 ppm. The $^{13}C\{^{1}H\}$ NMR spectrum of the ligand shows a peak at 166.5 ppm, which is assigned to the imine carbon atom. IR data of the ligand shows peaks at 1581 cm^{-1} and 1640 cm^{-1} which are indicative of the C-N pyridine and C=N imine bonds, respectively. ESMS data of this compound gave a peak at 399 ($[M+H]^+$) which agrees with the calculated molecular mass of the desired product. High resolution mass spectrometry (FAB) revealed a peak at 399.2813 while the calculated molecular mass for $C_{27}H_{32}N_2$ $[M+H]^+$ is 399.2800. An X-ray crystal structure analysis unambiguously confirmed the molecular structure of the pro-ligand (**Figure 2.24** and **Table 2.2**).

Table 2.2: Selected bond lengths (Å) and angles (º) for H**L1**$_{2,4,6\text{-Me3Ph}}$

	Bond length		Bond angle
N(1)-C(7)	1.2789(18)	N(1)-C(7)-C(9)	116.93(13)
C(1)-C(6)	1.401(2)	C(7)-N(1)-C(1)	121.68(13)
		N(2)-C(13)-C(14)	116.24(13)
		N(2)-C(9)-C(7)	115.52(13)

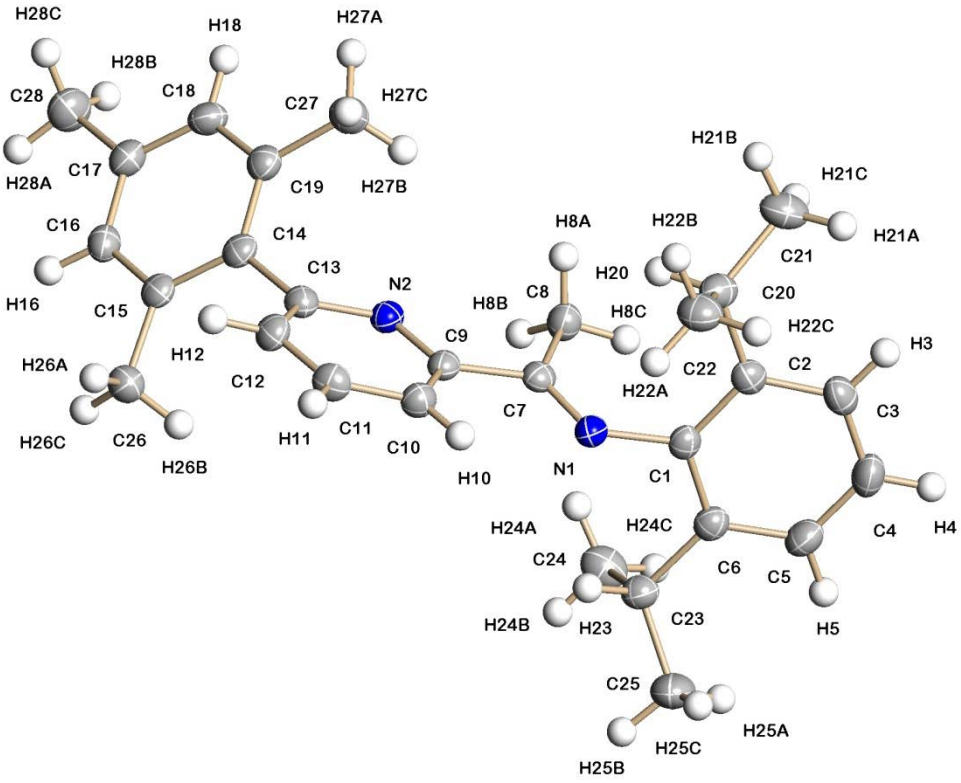

Figure 2.24 | Molecular structure of H**L1**$_{2,4,6\text{-}Me3Ph}$

2.2.2.5 Synthesis of H**L1**$_{ald\text{-}nap}$

This pro-ligand is the aldimine analogue of HL1$_{ket\text{-}nap}$. The purpose of making this ligand was to examine the influence of the imine substituents upon C-H activation. The synthesis was very similar to that for the ketimine analogue. Following the Suzuki coupling, the pro-ligand H**L1**$_{ald\text{-}nap}$ was obtained via a condensation reaction of the aldehyde precursor and 2,6-diisopropyl aniline (**Figure 2.25**). Unlike the previous condensation reactions, this reaction was carried out at 40 ^{o}C rather than at reflux due to the potential self-polymerization of the aldehyde when heated to more than 40 ^{o}C.

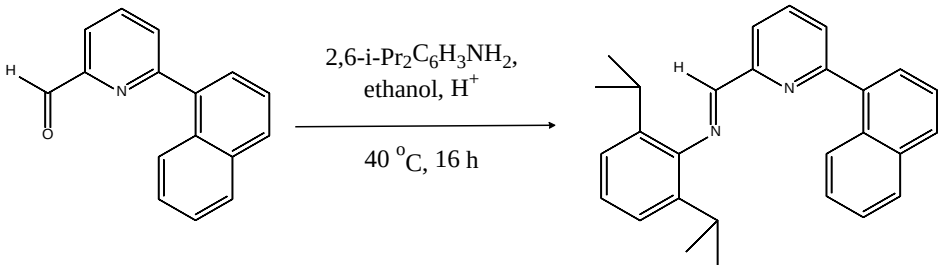

Figure 2.25 | Synthesis of H**L1**$_{ald\text{-}nap}$

The 1H singlet at 8.42 ppm in the proton NMR spectrum of the ligand was assigned to the aldimine proton, and the corresponding carbon atom of the aldimine moiety was found at 163.4 ppm in the carbon NMR spectrum. The IR spectrum revealed a peak at 1637 cm^{-1} which is diagnostic of the $(C=N)_{imine}$ stretching vibration. A protonated molecular ion peak of m/z 393 was found in the ESMS further confirming the formation of the desired product. The FAB analysis of the product revealed a molecular ion peak at 393.2334, while the calculated value for $C_{28}H_{28}N_2$ $[M+H]^+$ is 393.2331. The structure of $HL1_{ald\text{-}nap}$ was further confirmed in the form of a single crystal X-ray diffraction study (**Figure 2.26** and **Table 2.3**). The structure consists of a central pyridine unit substituted at its 6-position by the 1-naphthyl group and at its 2-position by the aldimine-containing CHN(2,6-*i*$Pr_2C_6H_3$) fragment. The 1-naphthyl moiety shows an angle of 55.4(10) ^{o} to the pyridine plane. The $C(6)_{Py}$–$C(7)_{alk}$ bond length is in the typical (sp^2)–(sp^3) range of values.[22]

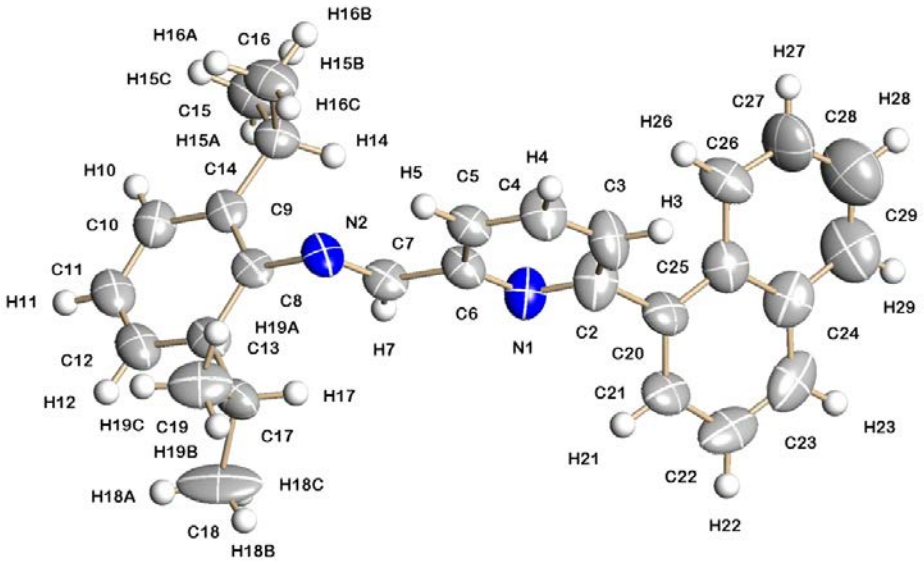

Figure 2.26 | Molecular structure of H**L1**$_{ald\text{-}nap}$

Table 2.3: Selected bond lengths (Å) and angles (^{o}) for H**L1**$_{ald\text{-}nap}$

	Bond length/ angle		Bond angle
N(2)-C(7)	1.243(7)	N(2)-C(7)-C(6)	123.9(6)
C(6)-C(7)	1.477(9)	C(7)-N(2)-C(8)	117.4(5)
N(1)-C(2)-C(20)-C(21)	55.4(10)	N(1)-C(2)-C(20)	115.4(6)
		N(1)-C(6)-C(7)	116.3(6)

2.2.2.6 Synthesis of H**L2**$_{o\text{-tolyl}}$

The preparation of the amine containing ligands was achieved by the reduction of their imine analogues. The reduction of the imine H**L1**$_{o\text{-tolyl}}$ to the amine H**L2**$_{o\text{-tolyl}}$ was carried out via a trimethylaluminium-induced methylation and subsequent hydrolysis (**Figure 2.27**). According to a protocol developed in the group, seven equivalents of TMA (trimethylaluminium) are required for this type of methylation reaction. However, after testing different amounts of TMA, three equivalents was found to be the most suitable for this specific reaction (**Table 2.3**). There is a remarkable colour change for the reaction mixture while adding the TMA into the reaction flask.

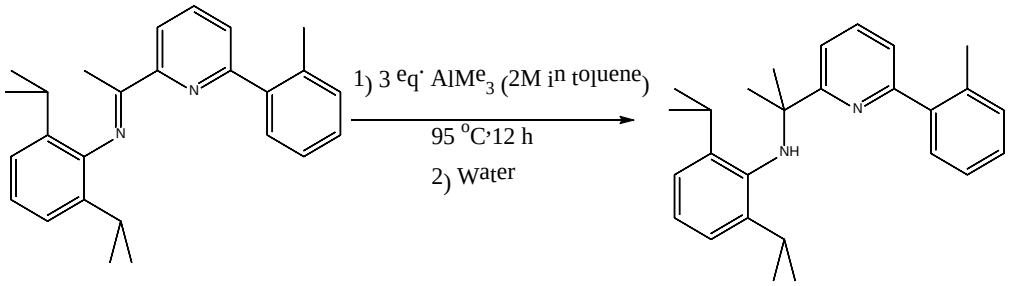

Figure 2.27 | Synthesis of amine H**L2**$_{o\text{-tolyl}}$

During the process, the solution turns into a deep yellow colour at first and then turns back to the original green colour. This phenomenon is a reflection of the formation of an intermediate aluminium complex and has been seen in other methylation reactions with TMA.[31]

Table 2.3: Test reactions with different amount of TMA.

Equivalence of TMA (eq.)	Solvent (toluene, ml)	Reaction yield (%)
7	30 ml	85%
4.5	30 ml	91%
3	30 ml	96%

After the isolation of the product, a yellow oil was obtained in excellent purity which turned into a yellow solid on prolonged standing at ambient temperature. Feathery crystals were obtained by recrystallisation from ethanol heated at reflux. Single crystals

suitable for analysis by X-ray diffraction could be obtained by recrystallisation from dichloromethane.

On comparing the IR data for H**L1**$_{o\text{-tolyl}}$ and H**L2**$_{o\text{-tolyl}}$, the peak at 1645 cm^{-1} which corresponds to a $(C=N)_{imine}$ bond does not appear in the spectrum of the amine ligand (H**L2**$_{o\text{-tolyl}}$). Further, it presents a peak at 3351 cm^{-1} which is indicative of an $(N\text{-}H)_{amine}$ bond. Therefore, the amine pro-ligand was considered to be formed. The ^{1}H NMR spectrum of this compound shows a singlet with six protons at 1.42 ppm corresponding to the two methyl groups on C6 (**Figure 2.28**). More importantly, there is a broad singlet with one proton at 4.17 ppm which correlated to none of the carbons on HMQC spectrum. In consideration of the high chemical shift and the fact that it is not coupled to any carbon atoms, this hydrogen is identified to be the amine proton on N2.

It is interesting to note that, the two pairs of methyl groups on C14 and C17 appear to be equivalent as they present a 12H doublet at 0.97 ppm and also the four carbon atoms come out as one strong signal at 24.11 ppm in the $^{13}C\{^{1}H\}$NMR spectrum. This is quite different from the proton and carbon NMR spectra of the imine HL1$_{o\text{-tolyl}}$ which indicates inequivalency of the two carbon atoms (C14 and C17) on the isopropyl groups. These results suggest the more flexible nature of the amine N-C single bond in comparison to the imine N=C double bond. ESMS of this compound shows a peak at m/z 387 in line with the protonated molecular ion peak. The calculated mass for $C_{27}H_{35}N_2$ $[M+H]^+$ is 387.2747, HRMS (TOF) revealed an extremely close value of 387.2796. Fast Atom Bombardment (FAB) data further confirmed the compound to be the desired new amine ligand by presenting a peak of 387 for $[M+H]^+$.

Further confirmation of the structure of H**L2**$_{o\text{-tolyl}}$ was obtained from the X-ray crystal structure (see **Figure 2.28** and **Table 2.4**). The structure consists of a central pyridine unit substituted at its 6-position by the aryl group and at its 2-position by the amine-containing $C(Me)_2NH(2,6\text{-}i\text{Pr}_2C_6H_3)$ fragment.

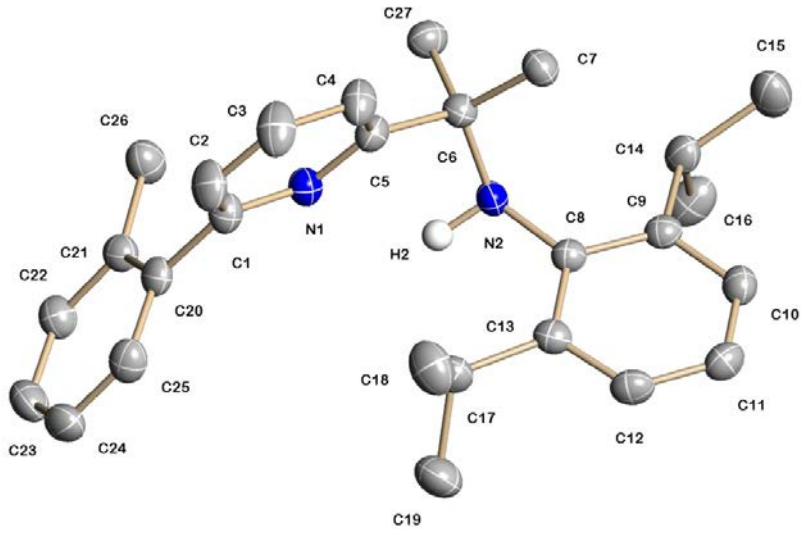

Figure 2.28 | Molecular structure of H**L2**$_{o\text{-tolyl}}$**.** Figure shows a 50% displacement ellipsoids. The hydrogen atoms (exception N-H) have been omitted from the diagrams.

Table 2.4: Selected bond lengths (Å) and angles (°) for H**L2**$_{o\text{-tolyl}}$

	Bond length/ angle		Bond angle
N(2)-C(6)	1.491(2)	N(2)-C(6)-C(5)	109.77(14)
C(5)-C(6)	1.540 (3)	C(6)-N(2)-C(8)	120.39(14)
N(1)-C(5)-C(6)	113.37(15)	N(1)-C(1)-C(20)	116.89(16)
N(1)-C(1)-C(20)-C(21)	-52.9 (3)	N(1)-C(5)-C(6)-N(2)	45.1(2)

The aryl moiety shows an angle of -52.9 (3)° to the pyridine plane which is consistent with the opinion that the more sterically demanding the aryl unit, the more orthogonal it is to the pyridine plane.[23] The $C(5)_{Py}$–$C(6)_{alk}$ bond length is in the typical (sp^2)–(sp^3) range of values.[22] The C(6)–N(2) vector is rotated closer to the pyridine plane, whereas the N(1)–C(5)– C(6)–N(2) torsion angle brings the N(2)H hydrogen atom into a position in which it is able to form a hydrogen bond to the neighbouring pyridine nitrogen atom, with a bond length of 2.248 Å.

2.2.2.7 Synthesis of H**L2**$_{nap}$

As with the synthesis of H**L2**$_{o\text{-}tolyl}$, H**L2**$_{nap}$ was prepared via a reduction from its imine analogue (H**L1**$_{ket\text{-}nap}$). Identical reaction conditions were used and the product was obtained as a yellow oil in excellent purity which turned into a yellow solid on prolonged standing at ambient temperature (**Figure 2.29**).

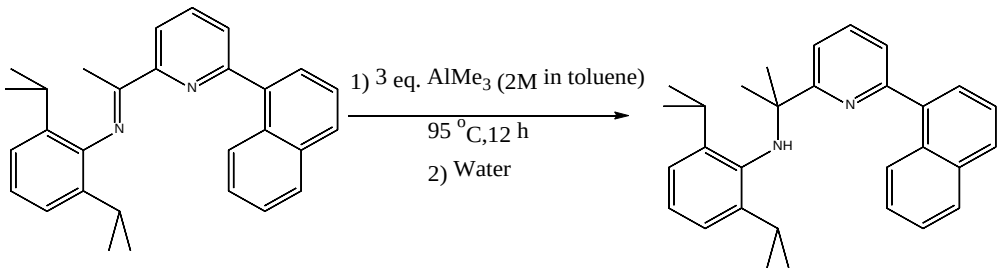

Figure 2.29 | Synthesis of amine H**L2**$_{nap}$

The absence of the (C=N) band in the IR spectrum of H**L2**$_{nap}$ and a peak appearing at 3054 cm^{-1}, which is the indicative of an (N-H) bond, suggests that this new amine pro-ligand has been obtained. The broad singlet at 4.27 ppm in the proton NMR spectrum suggests the presence of an N-H proton. And the ^{13}C NMR spectrum shows one more alkyl proton signal comparing to the starting material, further confirming the formation of the amine pro-ligand. Moreover, the ESMS reveals a peak at m/z 423 in line with the protonated molecular ion peak. The calculated mass for $C_{30}H_{34}N_2$ $[M+H]^+$ is 423.2788, HRMS (TOF) shows a very close value of 423.2792.

2.2.2.8 Synthesis of H**L3**$_{o\text{-}tolyl}$

The aim of synthesizing the two novel ligands to be described in this section and section 2.2.2.9 is to see how a weaker donor, i.e. oxygen, will bind with the metal centre in the subsequent complexation process. The reduction with TMA is also suitable for preparing alcohol bearing ligands from ketones.[24] The same reaction conditions used in the synthesis of the amine pro-ligands were used in the preparation of H**L3**$_{o\text{-}tolyl}$ from its ketone precursor (**Figure 2.30**).

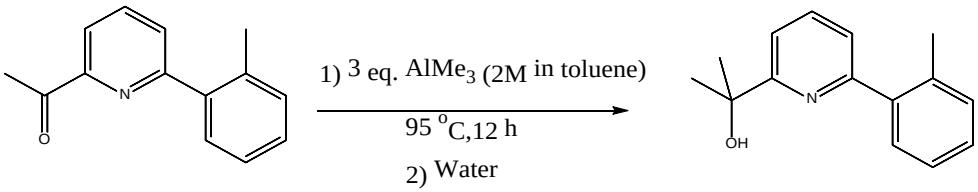

Figure 2.30 | Synthesis of the alcohol pro-ligand H**L3**$_{o\text{-tolyl}}$

The product was obtained in high purity and excellent yield as a pale yellow oil which crystallized into a white solid upon standing at room temperature overnight. The ^{1}H NMR spectrum of the product reveals a broad singlet at 5.18 ppm. Considering the high chemical shift and broadness of the signal, this peak is assigned to be the proton on the O-H moiety. The 3H singlet at 2.65 ppm which corresponds to the ketone methyl in the proton NMR spectroscopy of the starting material is no longer present in the product, and there is a new 6H singlet at 1.49 ppm assigned to the two alcohol methyl groups. The IR spectrum shows a peak at 3398 cm^{-1} which confirmed the formation of an alcohol product since the peak is indicative of an O-H bond in the molecule. A protonated molecular ion peak at m/z 216 was observed on the ESMS and the FAB results show a close value of 216.2914 while the calculated value for $C_{14}H_{17}NO$ $[M+H]^+$ is 216.2911. Thus all the characterization data agrees with the formation of the new alcohol pro-ligand H**L3**$_{o\text{-tolyl}}$.

2.2.2.9 Synthesis of H**L3**$_{nap}$

The synthesis of H**L3**$_{nap}$ was achieved using the same approach as that used for the synthesis of H**L3**$_{o\text{-tolyl}}$ (**Figure 2.31**). After the hydrolysis and aqueous work up, the product was obtained in a high purity with a yield of 98%.

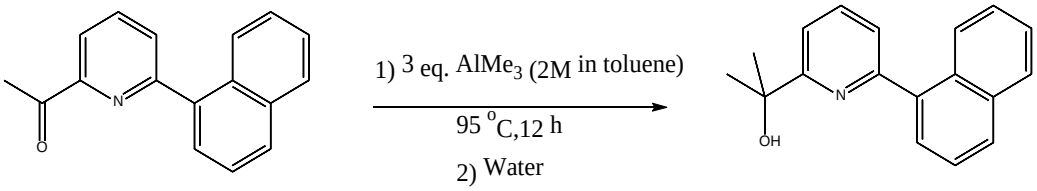

Figure 2.31 | Synthesis of the alcohol pro-ligand (H**L3**$_{nap}$)

A 1H broad singlet at 5.16 ppm in its proton NMR spectrum and a stretching vibration at 3409 cm^{-1} in its IR spectrum both suggest the formation of the alcohol product. The 3H singlet at 2.69 ppm which corresponds to the ketone methyl in the proton NMR

spectroscopy of the starting material is no longer present in the product, and there is a new 6H singlet at 1.47 ppm assigned to the two alcohol methyl groups. In addition, in the carbon NMR spectrum of the product, the *C*=O carbon signal around 200 ppm is no longer present, suggesting the methylation of the ketone precursor has been successful. This is further confirmed by a protonated molecular ion peak of m/z 264 in the ESMS and an accurate mass of 264.1380 $[M+H]^+$ on FAB while the calculated value for this molecule is 264.1372.

2.2.3 Synthesis of the bi-pyridine-aryl ligand H**L1**$_{py\text{-}nap}$

Previously we have systematically changed the imine arm of our starting pro-ligands (H**L1**) into amine or alcohol arms to allow a subsequent investigation of the influence of different donor atoms upon the process of C-H activation (to be discussed in Chapter 3). The reason for synthesizing this ligand was the same. Only the naphthyl-derivatised pro-ligand has been targeted since it has more than one activation site on the aromatic ring and thus will invite more interesting chemistry into the project.

The synthetic approach to this ligand starts from the preparation of 2-tributylstannyl pyridine followed by a Stille coupling and a Suzuki coupling to give the desired ligand (H**L1**$_{py\text{-}nap}$) (**Figure 2.32**). The synthetic intermediates 2-tributylstannyl pyridine and 6-bromo-2,2'-bipyridine were characterized by proton NMR spectroscopy and the data are consistent with those reported in the literature.[25]

The proton NMR spectrum of H**L1**$_{py\text{-}nap}$ revealed 12 signals all in the aromatic region accounting for the 14 protons on the bipyridine and naphthyl moeities. The ^{13}C NMR spectrum also showed no other impurities. A deprotonated molecular ion peak at m/z 281 was observed on the ESMS and the FAB results show a close value of 283.1224 while the calculated value for $C_{20}H_{14}N_2$ $[M+H]^+$is 283.1235.

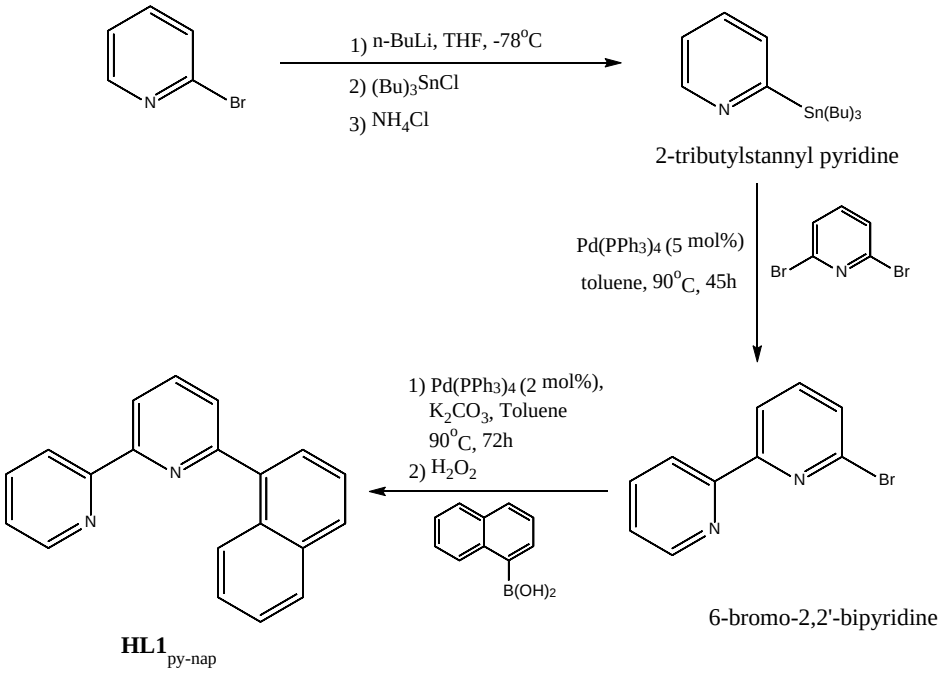

Figure 2.32 | Synthesis of H**L1**$_{py\text{-}nap}$

Crystals suitable for single crystal X-ray diffraction were grown by slow evaporation of a methanol solution of the pro-ligand. The X-ray structure confirms the product to be the H**L1**$_{py\text{-}nap}$ (**Figure 2.33** and **Table 2.5**) with a pyridine ring substituted at its 2- and 6-positions by a pyridine and 1-naphthyl group. As with the pyridyl imines developed in this work the two pyridine moieties are mutually trans.

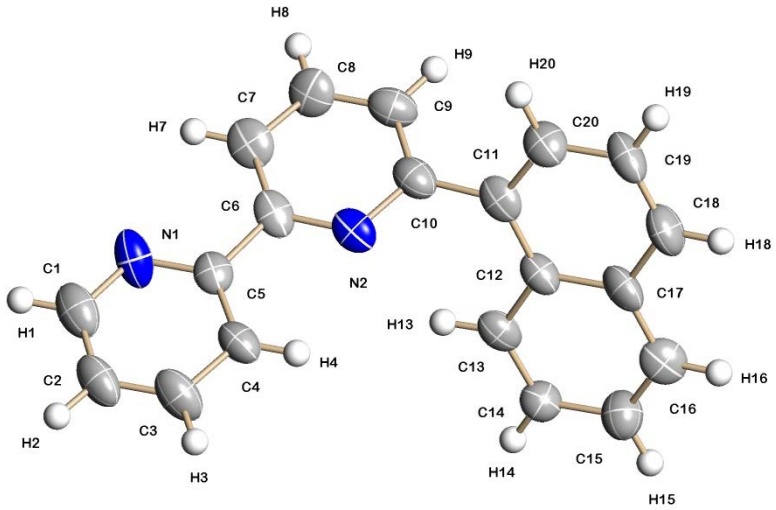

Figure 2.33 | Molecular structure of H**L1**$_{py\text{-}nap}$

Table 2.5: Selected bond lengths (Å) and angles (°) for H**L1**$_{py\text{-}nap}$

	Bond length (Å)		Bond angle (°)
N(1)-C(5)	1.324(9)	N(2)-C(6)-C(5)	115.1(8)
N(2)-C(6)	1.348(8)	N(2)-C(10)-C(11)	116.6(8)
C(5)-C(6)	1.467(9)	C(11)-C(12)-C(13)	121.8(9)
C(10)-C(11)	1.471(10)	N(1)-C(5)-C(6)	117.2(8)

2.2.4 Synthesis of the imine-pyridine-alkyl ligands H**L4**

After conducting a synthetic programme to develop pyridine-based ligands substituted at the 2-position by a N/O donor unit and aryl group at the 6-position we decided to keep the imine donor constant at the 2-position and introduce an alkyl group at the 6-position. It was envisoned that this would allow a subsequent investigation of the more challenging sp^3-CH activation (see Chapter 4).

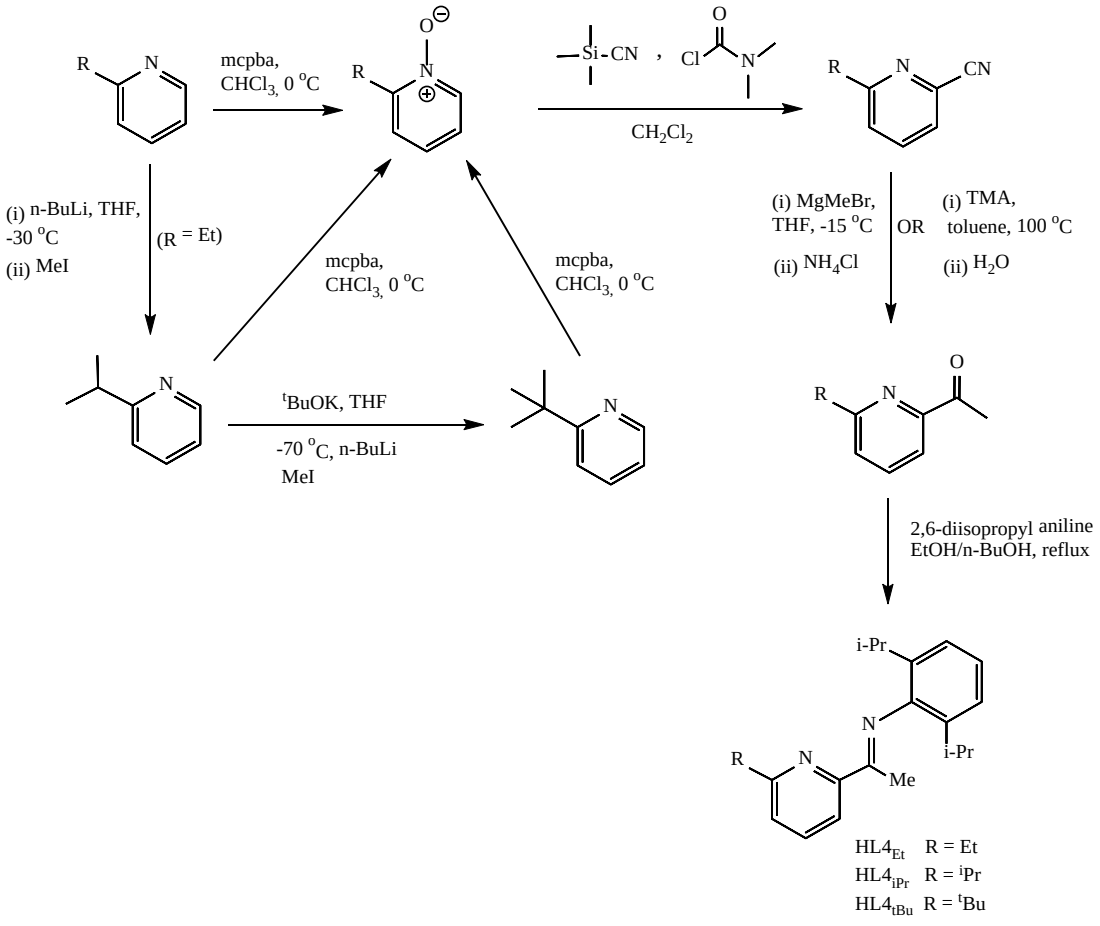

Figure 2.34 | Synthesis of ligands H**L4**

At first, the synthesis of these alkyl-armed ligands was attempted to be obtained by the same synthetic approach as ligands H**L1**. Unfortunately, the route did not work for these ligands. Thus an alternative route from the commercially available 2-ethyl pyridine was designed (**Figure 2.34**).

The 2-cyano substituent was introduced by a modified Reissert–Henze reaction.[27] For that purpose, the '2-alkyl pyridines' were first converted into their respective pyridine *N*-oxides by treatment with m-chloroperbenzoic acid in chloroform at 0 °C. The selective CN introduction was achieved by treatment of the pyridine *N*-oxides with Me_3SiCN in the presence of dimethylcarbamoyl chloride in chloroform at ambient temperature. The ketone products were then obtained by either a Grignard reaction or a TMA route. The pro-ligands (H**L4**) were then formed via a condensation reaction of the ketone precursors and 2,6-diisopropyl aniline. All the synthetic intermediates were characterized by proton NMR spectroscopy and the data are consistent with those reported in the literature.[26] The three pro-ligands H$\mathbf{L4}_{Et/iPr/tBu}$ were fully characterized by IR, proton and carbon NMR spectroscopies as well as by ESMS and FAB mass spectrometry.

The ^{1}H NMR spectrum of H$\mathbf{L4}_{Et}$ shows a 12H doublet at 1.15 ppm coupling with the 2H septet at 2.76 ppm, assigned to the isopropyl moiety. However, the ^{13}C NMR spectrum shows two different methyl signals for ^{i}Pr, indicating the inequivalency of the ^{i}Pr methyls. Thus, it can be deduced that, the two 6H doublets happen to overlap and be present as one 12H doublet on the proton NMR spectrum. The 3H triplet at 1.36 ppm in the ^{1}H NMR spectrum shows coupling to the 2H quartet at 2.78 ppm. Hence these protons belong to the ethyl moiety, whilst the 3H singlet at 2.00 ppm is indicative of the methyl protons on the imine moiety. There are four sets of signals in the aromatic region which in total account for 6 protons on the pyridine and aromatic rings. IR data of the ligand shows peaks at 1585 cm^{-1} and 1644 cm^{-1} which are indicative of the C-N pyridine and C=N imine bonds, respectively. ESMS data of this compound gives a peak at m/z 310 which agrees with the value for the protonated molecular ion peak of the desired product. The FAB results further confirm the product to be the pro-ligand H$\mathbf{L4}_{Et}$ by showing a value of 310.2324 for [M+H] while the calculated value for $C_{21}H_{28}N_2$ $[M+H]^+$ is 310. 2337.

The isopropyl armed pro-ligand (H$\mathbf{L4}_{i\text{-}Pr}$) was obtained in high purity with a yield of 65% using the protocol illustrated in Figure **2.34**. There are two septets apparent in the proton NMR spectrum. The 1H septet at 3.05 ppm belongs to the isopropyl group on the pyridine

unit while the other septet signal with two protons comes from the two isopropyl groups on the aromatic ring. Accordingly, there is a 6H doublet at 1.29 ppm coupling to the 1H septet, which is assigned to the two methyl groups on the pyridyl-isopropyl group, and another 12H doublet at 1.08 ppm corresponding to the six methyl protons on the aromatic-isopropyl. This 12H doublet appears like a 'doublet of doublets', in line with the inequivalency of the two methyl groups on the aromatic-isopropyl units. IR data of the compound shows peaks at 1577 cm^{-1} and 1642 cm^{-1} which are indicative of the C-N pyridine and C=N imine bonds, respectively. ESMS data of this compound reveals two peaks at m/z 323 and 345 which agrees with the value for protonated molecular ion peak and [M+Na] peak of the desired product.

The synthesis of the tert-butyl armed ligand H**L4**$_{t\text{-}Bu}$ was slightly more difficult than those for the other two ligands in this section. Firstly, the synthesis of the 2-tert-butyl pyridine from 2-isopropyl pyridine was tried with the n-BuLi/MeI route (as used in the synthesis of 2-isopropyl pyridine) (**Figure 2.35**). However, the reaction returned mostly unreacted starting material, which was likely to be because deprotonation of the tertiary proton is more difficult than that for the secondary analogue. Thus, a much stronger base, potassium diisopropylamide (generated *in situ* from diisopropylamine, KO^{t}Bu and nBuLi), was used instead (**Figure 2.35**). Following quenching with MeI at -75 ^oC and purification with column chromatography, the 2-tert-butyl pyridine was obtained in excellent purity in a good yield. The absence of a septet, which is the indicative of the isopropyl moiety, and the emergence of a 9H singlet at 1.36 ppm in the proton NMR spectrum, suggests the formation of the desired product.

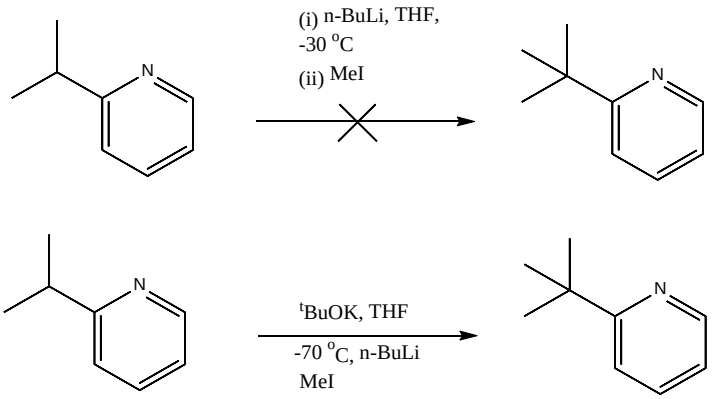

Figure 2.35 | The failed and succeeded synthetic routes to 2-tert-butyl pyridine

After the formation of the 2-tert-butyl pyridine N-oxide and the subsequent introduction of the 2-cyano substituent, the Grignard reaction, which had been used to form the 2-ethyl- and 2-isopropyl-6-acetyl pyridines in fairly good yields, gave almost zero yield for the 2-tertbutyl-6-acetyl pyridine. Thus, the TMA route was applied. After hydrolysis and aqueous work up, the desired product (2-tert-butyl-6-acetyl pyridine) was obtained. Subsequent treatment of 2-tert-butyl-6-acetyl pyridine with 2,6-diisopropyl aniline in ethanol showed no conversion of the starting materials to the product, thus a higher boiling point solvent, n-butanol, was used. After heating at reflux for 3 days, the product was obtained as a yellow powder. The proton NMR spectrum shows a strong singlet with 9 protons at 1.34 ppm indicating the presence of the t-butyl moiety. The mutually coupled doublet and septet at 1.07 and 2.69 ppm are indicative of the isopropyl groups on the aromatic ring. The 1H doublets at 8.07 and 7.32 ppm and the 1H triplet at 7.63 ppm are assigned to the pyridine protons, while the two multiplets at 7.00 and 7.08 ppm, with one and two protons respectively, are assigned to the protons on the aromatic ring. The ESMS spectrum reveals a peak at m/z 337 in line with the protonated molecular ion peak. The FAB results confirmed the product to be the pro-ligand ($HL4_{t\text{-}Bu}$) by giving a close value of 336.2617 for $[M+H]^+$ while calculated for $C_{23}H_{33}N_2$ is 336.2623.

2.3 Summary and conclusions

The synthesis and characterization of thirteen pyridine-based pincer ligands is described in detail in this chapter. The ketimine/aldimine-pyridine-aryl ligands were prepared by the Suzuki couplings of the 2-bromo-6-acetyl/formyl-pyridine and the corresponding boronic acids; followed by a condensation with 2,6-diisopropylaniline. Other than the aldimine-armed ligand H$\mathbf{L1}_{ald\text{-}nap}$, all the ligands were obtained in good to excellent yields. The slightly lower yield of H$\mathbf{L1}_{ald\text{-}nap}$ at the condensation step of the synthesis is due to the self-polymerization of the aldehyde at temperatures higher than 40 ^oC.

The amine-armed ligands H$\mathbf{L2}_{o\text{-}tolyl}$ and H$\mathbf{L2}_{nap}$ were prepared via a reduction with TMA from their imine-pyridine-aryl analogues while the synthesis of the *O,N,C*-pincers H$\mathbf{L3}_{o\text{-}tolyl}$ and H$\mathbf{L3}_{nap}$ was achieved by reducing their ketone precursors with TMA. Both types of ligands were obtained in very good yields with excellent purity.

The synthetic approach to the bi-pyridine-aryl ligand H**L1**$_{py\text{-}nap}$ started from the preparation of 2-tributylstannyl pyridine followed by a Stille coupling and a Suzuki coupling to give the desired product.

Since the 'general' Suzuki coupling route was not applicable for the synthesis of the imine-pyridine-alkyl ligands, they were prepared from 2-alkyl-pyridines via protection of the pyridine, cyanation of the 6-position, reduction to the ketone, and condensation with 2,6-diisopropylaniline.

The synthesis of all the targeted ligands to be used in this thesis has been achieved and the products fully characterized by proton/carbon NMR spectroscopy, IR spectroscopy, ESMS spectroscopy and for H**L1**$_{o\text{-}tolyl}$, H**L1**$_{2,6\text{-}Me3Ph}$, H**L1**$_{ald\text{-}nap}$, H**L2**$_{o\text{-}tolyl}$ and H**L1**$_{py\text{-}nap}$ by single crystal X-Ray diffraction. The complexation of the aryl-containing pyridyl-imines (H**L1**), aryl-containing pyridyl-amines (H**L2**) and aryl-containing pyridyl-alcohols (H**L3**) with palladium and platinum salts will be discussed in the next chapter, whilst the sp^3 C-H activation of the alkyl-containng pyridyl-imines (H**L4**) are to be described in Chapter 4.

References

1 Moulton, C. J.; Shaw, B. L. *J. Chem. Soc., Dalton Trans*., 1976, **11**, 1020.

2 W. Baratta, G. Bossi, E. Putignano and P. Rigo, *Chem. – Eur. J*., 2011, **17**, 3474.

3 M. van der Boom and D. Milstein, *Chem. Rev.*, 2003, **103**, 1759.

4 C. Gunanathan and D. Milstein, *Chem. Rev*., 2014, **114**, 12024.

5 I. P. Beletskaya and A. V. Cheprakov, *Chem. Rev.*, 2000**, 100**, 3009.

6 E. Kinoshita, K. Arashiba, S. Kuriyama, Y. Miyake, R. Shimazaki, H. Nakanishi and Y. Nishibayashi, *Organometallics*, 2012, **31**, 8437.

7 D. Benito-Garagorri, L. G. Alves, M. Puchberger, K. Mereiter, L. F. Veiros, M. J. Calhorda, M. D. Carvalho, L. P. Ferreira, M. Godinho and K. Kirchner, *Organometallics*, 2009, **28**, 6902.

8 Y.-H. Chang, Y. Nakajima, H. Tanaka, K. Yoshizawa and F. Ozawa, *J. Am. Chem. Soc.*, 2013, **135**, 11791.

9 M. A. Halcrow, *Coord. Chem. Rev*., 2005, **249**, 2880.

10 F. Zeng and Z. Yu, *Organometallics*, 2008, **27**, 2898.

11 (a) W. Jin, L. Wang and Z. Yu, *Organometallics*, 2012, **31**, 5664; (b) M. Zhao, Z. Yu, S. Yan and Y. Li, J. *Organomet. Chem*., 2009, **694**, 3068.

12 W. Ye, M. Zhao, W. Du, Q. Jiang, K. Wu, P. Wu and Z. Yu, *Chem. – Eur. J.*, 2011, **17**, 4737.

13 J. Zhang, G. Leitus, Y. Ben-David and D. Milstein, *J. Am. Chem. Soc.*, 2005, **127**, 10840.

14 E. Balaraman, B. Gnanaprakasam, L. J. W. Shimon and D. Milstein, *J. Am. Chem. Soc.*, 2010, **132**, 16756.

15 R. Barrios-Francisco, E. Balaraman, Y. Diskin-Posner, G. Leitus, L. J. W. Shimon and D. Milstein, *Organometallics*, 2013, **32**, 2973.

16 W. Baratta, G. Chelucci, S. Gladiali, K. Siega, M. Toniutti, M. Zanette, E. Zangrando and P. Rigo, *Angew. Chem., Int. Ed*., 2005, **44**, 6214.

17 W. Baratta, M. Bosco, G. Chelucci, A. Del Zotto, K. Siega, M. Toniutti, E. Zangrando and P. Rigo, *Organometallics*, 2006, **25**, 4611.

18 W. Baratta, G. Chelucci, S. Magnolia, K. Siega and P. Rigo, *Chem. – Eur. J.*, 2009, **15**, 726.

19 J. Parks, B. Wagner and R. Holm, J. Organomet. Chem., 1973, **56**, 53.

20 Y.-H. Lin, MSc project report 2012, University of Leicester.

21 T. Wang, X.–Q. Hao, J.–J. Huang, K. Wang and M.–P. Song, *Organometallics*, 2014, **33**, 194.

22 F. H. Allen, O. Kennard and D. G. Watson, *J. Chem. Soc., Perkin Trans.*, 1987, S1.

23 L. Luconi, C. Bianchini, A. Rossin, G. Giambastiani, D. Lyubov, G. Fukin, A. Cherkasov, A. Shavyrin, A. Trifonov and C. Faggi, *Eur. J. Inorg.Chem.*, 2010**,** **4**, 608 .

24 S. Sano, H. Shimizu and Y. Nagao, *Tetrahedron Lett.*, 2005, ***46***, 2887.

25 T. N. Y Hoang, M. Humbert-Droz, T. Dutronc, L. Guénée, C. Besnard and C. Piguet, *Inorg. Chem.* 2013, **52**, 5570.

26 K. Nienkemper, V. V. Kotov, G. Kehr, G. Erker and R. Fröhlic, *Eur. J. Inorg. Chem.*, 2006, 366.

27 W. K. Fife, *J. Org. Chem.*, 1983, **48**, 1375.

28 R. Hicks, B. Koivisto, and M. Lemaire, *Org. Lett*., 2004, **6**, 1887.

29 S. Bruns, V. Sinnwell and J. Voss, *Magn. Reson. Chem*., 2003, **41**, 269.

30 T. Leermann, F. Leroux, and F. Colobert, *Org. Lett*., 2011, **13**, 4479.

31 V. Gibson, C. Redshaw and G. A. Solan, *Chem. Rev.*, 2007, **107**, 1745.

Chapter Three

Palladium and Platinum Chemistry of N,N,C_{aryl}- and O,N,C_{aryl}-pincer Ligands

3.1 Introduction

3.1.1 Pincer complexes of palladium and platinum

Due to their contributions in reducing the amount of toxic or expensive transition metals, the development of novel and highly active transition metal catalysts has been a keen interest in organic synthesis. Transition metal pincer complexes have become an important topic in synthetic and coordination chemistry in the recent years, because of their versatile catalytic applications in highly selective chemical transformations.[1-4] Particular interest has been given to the studies on the pincer complexes of palladium[5,6,7] and platinum[8] as active catalysts. For example, low loadings (molar ppm levels) of palladium pincer complexes efficiently catalyze allylic arylation reactions. (**Figure 3.1**).[9]

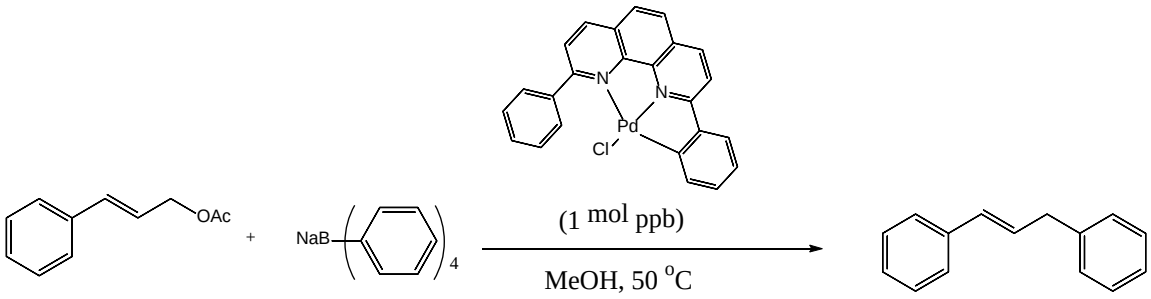

Figure 3.1 | A palladium NNC-pincer complex as an efficient catalyst for allylic arylation at parts per billion levels

The myriad of advantages of the tridentate ligand scaffold, such as producing complexes that are more stable than their monodentate counterparts, enables these complexes to be applied as catalysts in high temperature/pressure reactions without catalyst decomposition. Moreover, the reactivity of the complex can be enhanced due to the constrained geometry, and the large scope of available pincer ligands enables modifications of the geometries and electronic properties of the catalyst. [10]

However, due to the difficulties in the synthesis of pincer complexes, their application in catalysis is sometimes limited. The ligand precursors for these pincer complexes are sometimes commercially available, but most of the time they need to be synthesized. Furthermore, to study the catalytic activity of pincer complexes, pincer ligands with

broadly different substituents in the side arms are often required. Hence, in this chapter the synthesis and characterization of novel palladium and platinum pincer complexes via the C-H activation of a wide scope of *N,N,C*- and *O,N,C*-pincer pre-ligands are explored.

3.1.2 Mechanism of C-H activation using palladium(II) acetate

The importance of C-H activation is not only highlighted by its essential research significance but also by its promising application for generating functionalized hydrocarbons.[11-16] Many examples of ruthenium- or rhodium-catalyzed reactions employing functionalized aromatic compounds, in which the C-H activation is considered to have proceeded as a cyclometalation via oxidative addition, have been reported.[17-20] A great number of electrophilic transition metals have been studied as illustrations for arene C-H activation.[21-23] In recent years, catalytic sp^2 and sp^3 C-H activations have been achieved by the cyclometalation at a Pd^{2+} centre and subsequent oxidation (**Figure 3.2**).[24-27]

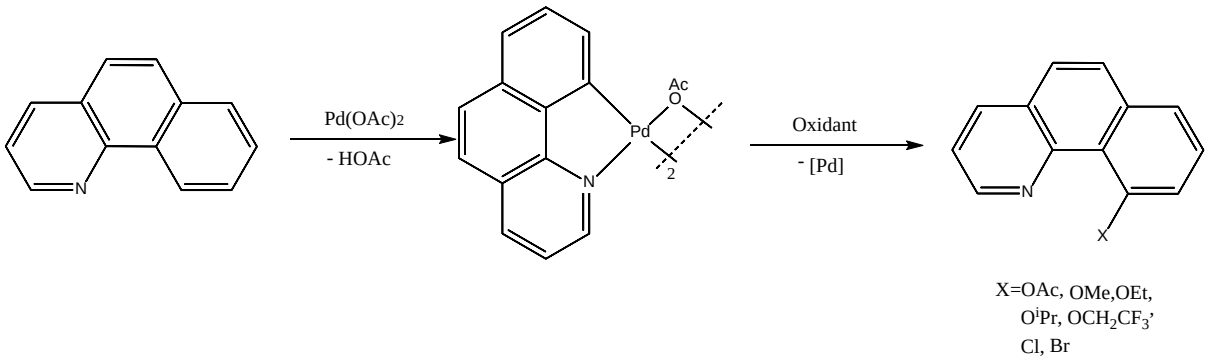

Figure 3.2 | Pd(II)-catalyzed oxidation of benzo[h]quinoline.

The mechanisms of C-H activation have been widely studied and three broad classes have been recognized: oxidative addition, σ-bond metathesis, and electrophilic activation. Due to the difficulties in unambiguously distinguishing between these pathways by experimental methods, the computational approach has emerged as a practical way for probing the mechanisms of C-H activation. Goddard's proposal of "oxidative hydrogen migration" is a typical example for the application of computational studies not only in

gaining insights into C-H activation mechanisms but also for identifying undiscovered pathways for the process.[28]

C-H activation using palladium has received considerable attention due to the application of cyclopalladated compounds in organic synthesis, catalysis, photochemistry, metallomesogen chemistry and resolution of racemic ligands.[29] Efficient C-C and C-heteroatom bond formation can be achieved following the cyclopalladation of an aryl ring. Thus, this topic has become an attractive research topic in the recent years in organometallic chemistry.[30] A cyclopalladation process usually occurs via the metallation directed by a strong N-donor ligand connected to the arene group and the subsequent assistance of a basic coordinating ligand. Intensive research involving detailed computational studies has also been undertaken in probing the exact role of the intramolecular base in cyclopalladation.[31-39]

Ryabov and co-workers reported the mechanism of palladium-promoted cyclometalation of dimethylbenzylamine (DMBA-H) in the 1980s and put forward a mechanism in which the C-H activation happens via a Wheland intermediate (**Figure 3.3**).[16,31]

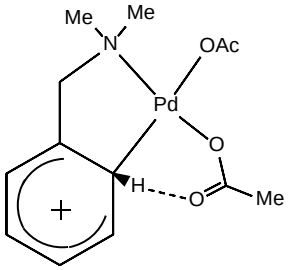

Figure 3.3 | Wheland intermediate

According to their proposal, a highly ordered six-membered transition state is present, through which the metal arenium intermediate transfers a proton to the bound acetate. And the intramolecular base- the acetate- provides the electrophilic activation of the arene moiety.

However, computational studies by Davies and co-workers in 2005 showed evidence for an acetate-coordinated proton transfer process involving a six-membered transition state being the most achievable pathway, in which the C-H activation proceeds via an agostic C-H intermediate (**Figure 3.4**) rather than the previously assumed arenium structure (Wheland intermediate).[40] They proposed that the electrophilic activation of the C-H bond and the subsequent deprotonation both rely on the ambiphilic palladium acetate. Later, in

2009, they reported the 'ambiphilic metal ligand activation' (AMLA) mechanism in detail for the cyclometalation of dimethylbenzylamine (DMBA-H) using $[IrCl_2Cp^*]_2$.[41]

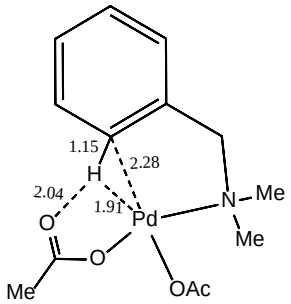

Figure 3.4 | The agostic intermediate

Recently, the electrophilic metallation of a naphthalene ring has recieved a great interest,[42-51] due to the potential of the naphthyl ring for more than one C-H activation site, which leads to interesting chemistry involving regioselectivity. Herein, we explore the regioselective C-H activation of the naphthyl ring using different chelating ligands as well as various metal salts.

3.1.3 Aims and objectives

The reactions of the aryl-containing N,N or N,O pro-ligands, **HL1**, **HL2** and **HL3**, with palladium(II) and, in selected cases, platinum(II) salts will be discussed in this chapter. C-H activation on the aromatic moiety in **HL1** – **HL3** is targeted on complexation with the metal salts: $Pd(OAc)_2$, Na_2PdCl_4, $PdCl_2(NCMe)_2$ and K_2PtCl_4. Isolation of pre-activation intermediate complexes will also be described. Where there is potential for activation at inequivalent C-H sites, the regioselectivity will be examined as will the potential for interconversions between sites. In addition, aryl groups that have their *ortho*-aryl C-H sites blocked will be probed in order to explore the potential for alternative C-H activation pathways. Taking advantage of the broad ligand scope, the influence of different donor atoms (*i.e.* imine *vs.* amine *vs.* alcohol) on the C-H activation process will be investigated. For each complex, key identification is given. All the products have been characterized by MS, IR and NMR spectroscopies. For some of the complexes, ^{13}C NMR was not applicable because of the insolubility of the complexes in NMR solvents. In

addition, single crystal X-Ray structures have been obtained for the majority of the complexes.

3.2 Reaction chemistry of the o-tolyl substituted ligands H**L1**$_{o\text{-tolyl}}$, H**L2**$_{o\text{-tolyl}}$, H**L3**$_{o\text{-tolyl}}$

3.2.1 Reactions of ligands with $Pd(OAc)_2$

Complexation of the pro-ligand H**L1**$_{o\text{-tolyl}}$ with palladium has been achieved using $Pd(OAc)_2$ (**Figure 3.5**). Initially, the reaction was attempted on a small scale (0.23 mmol). After 48 hours of stirring at 60 ^{o}C, the ^{1}H NMR spectrum of the crude product still showed 27% of starting material remaining. Further stirring for up to 72 hours did improve the yield of the reaction. By the third attempt (0.81 mmol scale), the percentage of the unreacted starting material was reduced to 7%.

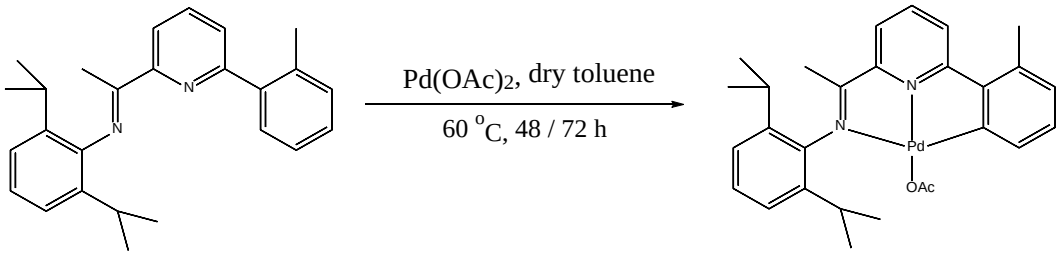

HL1$_{o\text{-tolyl}}$ **L1**$_{o\text{-tolyl}}$PdOAc

Figure 3.5 | Synthesis of (**L1**$_{o\text{-tolyl}}$)PdOAc.

Since the reaction did not go to 100% conversion, purification of the crude product became necessary. Several methods were tried to remove the unreacted starting material in the product. Among them, crystallization from dichloromethane/hexane was found to be the most effective. The product (**L1**$_{o\text{-tolyl}}$)PdOAc, after the recrystallization, was obtained in excellent purity. In addition, this crystallization process afforded crystals suitable for a single crystal X-Ray diffraction study.

The spectroscopic data collected for (**L1**$_{o\text{-tolyl}}$)PdOAc suggests that coordination of the ligand to palladium had been successful. One indication of this is the shift of the C=N stretching vibration to lower wavenumber in comparison to that for the pro-ligand. Specifically, the infra-red stretching frequency of the bonded imine has shifted from 1645

cm^{-1} (pro-ligand) to 1604 cm^{-1} in (**L1**$_{o\text{-tolyl}}$)PdOAc due to the effect of back bonding.[52] The two peaks at 1382 cm^{-1} and 1558 cm^{-1} in IR spectrum refer to the symmetric and asymmetric ν(COO) vibrations of the acetate ligand, respectively. These numbers are in agreement with those reported in the literature for this type of metal complex.[53]

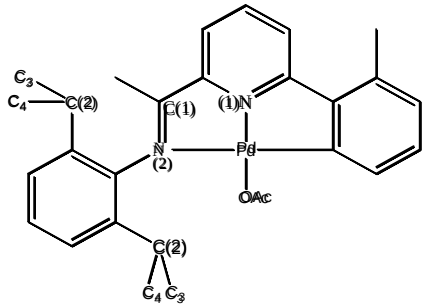

Figure 3.6 | (**L1**$_{o\text{-tolyl}}$)PdOAc.

In the ^{1}H NMR spectrum of (**L1**$_{o\text{-tolyl}}$)PdOAc, there are two 6H doulets for the ^{i}Pr methyl groups, and one 2H septet for the CH protons on the diisopropyl moiety. This indicates the symmetry of the diisopropyl phenyl group along the N-dipp bond and the inequivalency of carbon atoms C3 and C4 due to the lack of symmetry (**Figure 3.6**). In line with the proton NMR spectrum, the signals for the C3 and C4 carbon atoms also appear as two separate signals in the ^{13}C{^{1}H} NMR spectrum while only 15 carbon signals are present in the aromatic region. This is in agreement with the deduction that the two isopropyl moieties are symmetrical along the 'N-dipp axes'. Moreover, the absence of a proton signal on the tolyl moiety indicates C-H activation on the aromatic ring. The ESMS rendered a peak at m/z 475 assigned to $[M\text{-}OAc]^{+}$ fragment of the complex as the acetate group could easily be detached from the palladium centre during the ESMS analysis. The X-Ray structure of the complex unambiguously revealed its structure as the expected product (**Figure 3.7** and **Table 3.1**). In line with all the structures in this chapter, there is the expected virtually square planar arrangement around palladium.

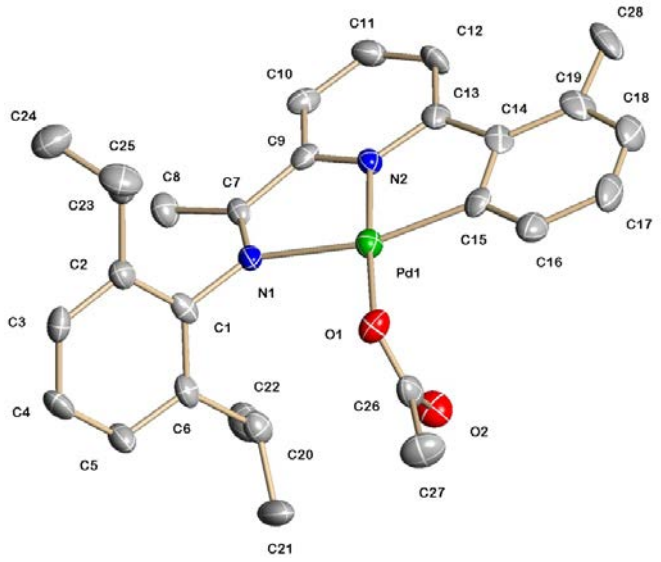

Figure 3.7 | Molecular structure of (**L1**$_{o\text{-tolyl}}$)PdOAc

Table 3.1: Selected bond lengths (Å) and angles (°) for (**L1**$_{o\text{-tolyl}}$)PdOAc

	Bond length (Å)		Bond angles (°)
Pd(1)-N(1)	2.171(5)	N(2)-Pd(1)-C(15)	81.7(2)
Pd(1)-N(2)	1.958(5)	N(2)-Pd(1)-N(1)	78.8(2)
Pd(1)-C(15)	1.960(7)	C(15)-Pd(1)-O(1)	160.5(2)
Pd(1)-O(1)	2.034(4)	N(1)-Pd(1)-O(1)	104.28(19)

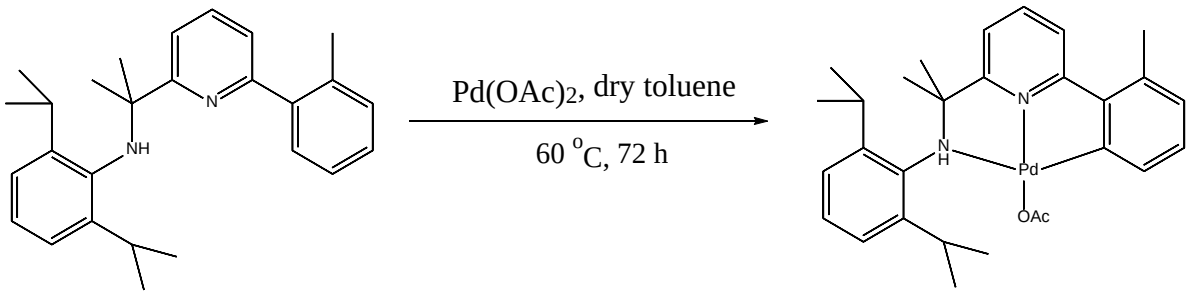

HL2$_{o\text{-tolyl}}$ **L2**$_{o\text{-tolyl}}$PdOAc

Figure 3.8 | Synthesis of **L2**$_{o\text{-tolyl}}$PdOAc

The synthetic approach to obtain the C-H activated product of H**L2**$_{o\text{-tolyl}}$ is similar to the previous C-H activation reaction. Upon treatment with $Pd(OAc)_2$ at 60 °C, H**L2**$_{o\text{-}}$

$_{tolyl}$PdOAc was obtained in an excellent yield after 72 h (**Figure 3.8**). The ^{1}H NMR spectrum of (**L2**$_{o\text{-}tolyl}$)PdOAc shows two split septets at 3.26 ppm and 3.38 ppm assigned to the two protons on C21 and C24 (**Figure 3.10**) while in the proton NMR spectrum of the free ligand, these hydrogen signals appear as one septet. This is a clear indication of the formation of the palladium complex for the amine pro-ligand. The changes of the carbon environments of these two carbon atoms are due to the loss of symmetry, as a result of the bonding of the amine nitrogen to palladium which makes N a chiral centre. Another concern upon the complexation of this free ligand with palladium was that palladium might deprotonate the amine rather than the tolyl group. Hence, locating the amine proton on the proton NMR became a priority. The amine proton apprears at 4.17 ppm in the proton NMR spectrum of the free ligand. However, no similar peaks were seen in the same region in the proton NMR of (**L1**$_{o\text{-}tolyl}$)PdOAc. Hence, 2D NMR (COSY and HMQC) were taken to analyze the proton-proton and proton-carbon correlations. A singlet with one proton was found at 6.9 ppm which does not show any correlations to the other protons on the COSY spectrum and to any of the carbons on the HMQC. However, an amine proton usually appears in 4-6 ppm region in the proton NMR. The apparent downfield shift of this proton is not consistent with a normal amine proton. Nevertheless, if there is hydrogen bonding between this amine proton and the acetate group, the proton signal could be shifted downfield (**Figure 3.9**).

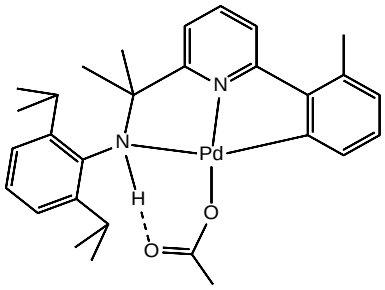

Figure 3.9 | The hydrogen bonding in (**L2**$_{o\text{-}tolyl}$)PdOAc

In the solid state, X-Ray crystallographic results strongly supported this assumption by showing the presence of a hydrogen bond, with a distance of 2.251 Å between the N-H proton and the oxygen on the acetate moiety (**Figure 3.10** and **Table 3.2)**. The solid-state structure of the complex indicates that the ortho-palladation of the free ligand H**L2**$_{o\text{-}tolyl}$ has occurred on the 2-methyl-phenyl ring. The Pd-C, Pd-N$_{Pyridine}$ and Pd-N$_{amine}$ bond lengths are consistent with similar Pd-X bond lengths reported in the literature. [54]

The HRMS (ESI) of **L2**$_{o\text{-tolyl}}$PdOAc showed clusters of peaks whose patterns were in agreement with $[M\text{-}OAc]^+$. The ESI (Electrospray Ionization) also revealed peaks at m/z 532, 491 and 550 assigned to $[(M\text{-}OAc)+MeCN]^+$, $[M\text{-}OAc]^+$, $[M]^+$ fragments respectively. The IR spectrum of the complex shows peaks at 1590 $cm^{-1}$and 3230 cm^{-1} which is in line with the N-H amine bending and stretching frequencies.

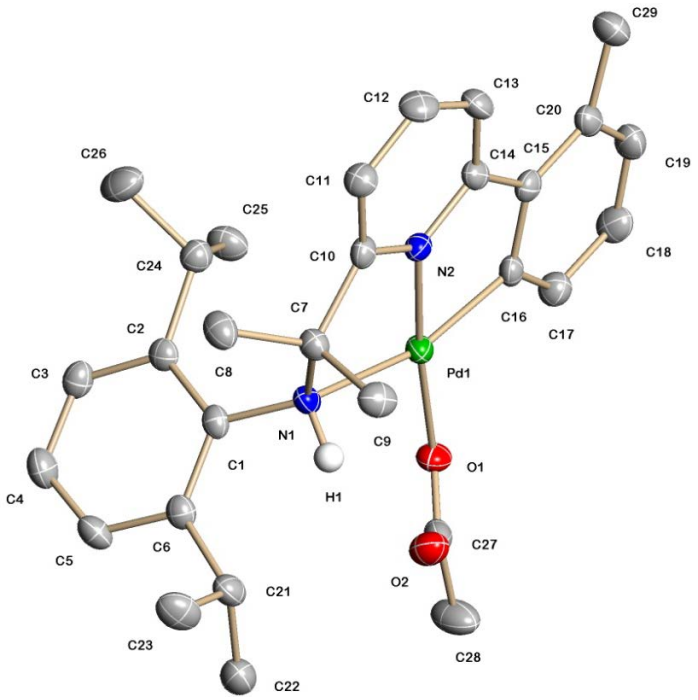

Figure 3.10 | Molecular Structure of (**L2**$_{o\text{-tolyl}}$)Pd(OAc)

Table 3.2: Selected bond lengths (Å) and angles (°) for (**L2**$_{o\text{-tolyl}}$)Pd(OAc)

	Bond length (Å)		Bond angles (°)
Pd(1)-N(1)	2.221(2)	N(2)-Pd(1)-C(16)	81.78(11)
Pd(1)-N(2)	1.956(2)	N(2)-Pd(1)-N(1)	81.84(10)
Pd(1)-C(16)	1.960(3)	C(16)-Pd(1)-O(1)	95.19(11)
Pd(1)-O(1)	2.056(2)	N(1)-Pd(1)-O(1)	101.47(9)
		N(2)-Pd(1)-O(1)	174.68(9)

The IR spectrum also revealed two peaks at 1373cm^{-1} and 1566 cm^{-1} which are assigned to the symmetric and asymmetric vibrations of the COO group, respectively. These data are in agreement with those described in the literature for this type of complex.[53]

Similarly, the C-H activation of H**L3**$_{o\text{-tol}}$ was achieved by reaction with $Pd(OAc)_2$ in toluene at 60 ^oC (**Figure 3.11**). The conversion of the starting material to the product was no more than 60%, even if the reaction time was prolonged (to 96 h) and the temperature was raised (to 80 ^oC). The reaction mixture gave signs of decomposition, such as the generation of palladium black, after 72 h, or when the reaction temperature was higher than 75 ^oC. These results suggest the slight difficulty of the C-H activation of these alcohol-armed ligands in comparison to that of their imine and amine analogues.

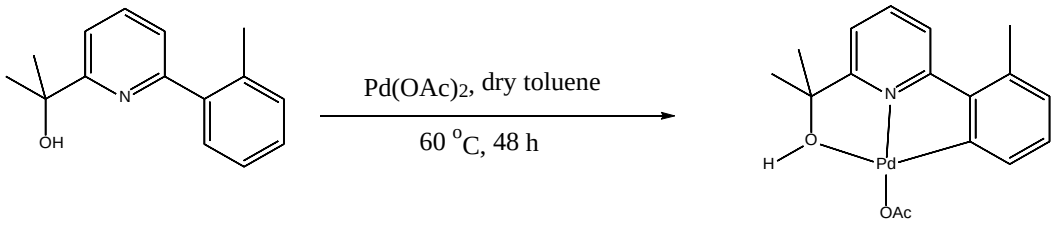

HL3$_{o\text{-tolyl}}$ **L3**$_{o\text{-tolyl}}$PdOAc

Figure 3.11 | C-H activation of H**L3**$_{o\text{-tolyl}}$

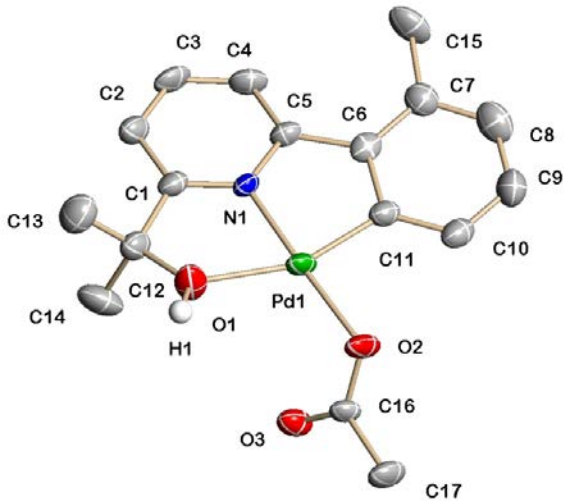

Figure 3.12 | Molecular Structure of **L3**$_{o\text{-tolyl}}$ PdOAc

Table 3.3: Selected bond lengths (Å) and angles (^{o}) for **L3**$_{o\text{-tolyl}}$ PdOAc

	Bond length (Å)		Bond angles (^{o})
Pd(1)-N(1)	1.948(4)	N(1)-Pd(1)-C(11)	83.0(2)

Pd(1)-O(1)	2.174(4)	N(1)-Pd(1)-O(1)	77.80(18)
Pd(1)-O(2)	2.042(4)	C(11)-Pd(1)-O(2)	94.4(2)
Pd(1)-C(11)	1.938(6)	O(1)-Pd(1)-O(2)	104.83(17)

The X-Ray crystallographic results confirmed the C-H activated structure of the complex **L3**$_{o\text{-tolyl}}$PdOAc (**Figure 3.12** and **Table 3.3**). The hydroxyl group has not been deprotonated and the hydroxyl proton shows an intramolecular hydrogen bond to the oxygen O(3) on the acetate moiety. The palladium complex adopts a square planar geometry with two five membered palladacycles on each side.

3.2.2 Reactions of **L**Pd(OAc) with NaCl (**L**=H**L1-3**$_{o\text{-tolyl}}$)

Following the achievement of the C-H activation of the o-tolyl substituted ligands with $Pd(OAc)_2$, the exchange of the –OAc ligand with –Cl was achieved by the reaction of the palladium-acetate complexes with saturated sodium chloride solution. The reaction of (**L1**$_{o\text{-tolyl}}$)PdOAc and saturated sodium chloride solution at room temperature yielded (**L1**$_{o\text{-tolyl}}$)PdCl in a quantitative yield with excellent purity (**Figure 3.13**). The complex was fully characterized by ^{1}H, ^{13}C{^{1}H} NMR and IR spectroscopies, ESMS and FAB spectrometries. Noticeably, the 3H singlet at 1.63 ppm, assigned to the methyl on acetate group in the proton NMR of (**L1**$_{o\text{-tolyl}}$)PdOAc, had disappeared in the ^{1}H NMR spectrum of (**L1**$_{o\text{-tolyl}}$)PdCl. Furthermore, the carbon signals which belong to the acetate carbons were not detected in the ^{13}C NMR spectrum of this complex. Based on these data, the (**L1**$_{o\text{-tolyl}}$)PdCl is considered to be obtained in excellent purity since there is no trace of any impurities in the NMR spectra. The HRMS revealed the accurate mass for the compound is 510.1151, while that calculated for $C_{26}H_{29}N_2Cl^{35}Pd^{106}$ $[M]^+$ is 510.1131.

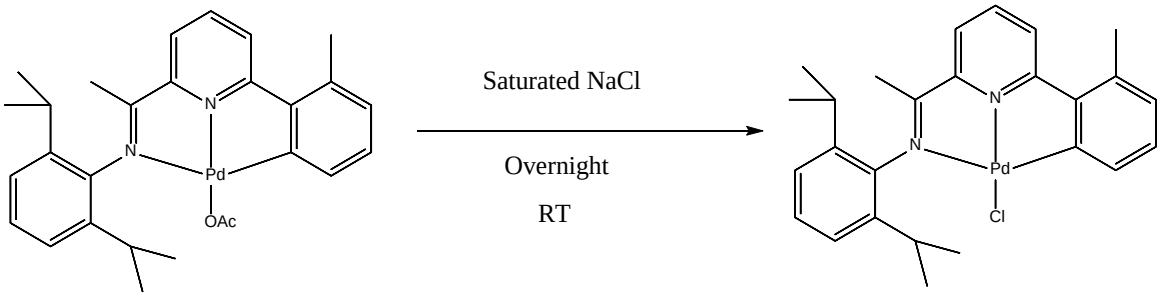

(**L1**$_{o\text{-tolyl}}$)PdOAc (**L1**$_{o\text{-tolyl}}$)PdCl

Figure 3.13 | Synthesis of (**L1**$_{o\text{-tolyl}}$)PdCl

The solubility of this palladium complex is extremely poor. Hence, a very small amount of crystals suitable for single crystal X-Ray diffraction were obtained using dichloromethane, as the compound is only slightly soluble in dichloromethane. The X-Ray crystal structure confirmed the product as the desired palladium chloride complex of H**L1**$_{o\text{-tolyl}}$ (**Figure 3.14** and **Table 3.4**).

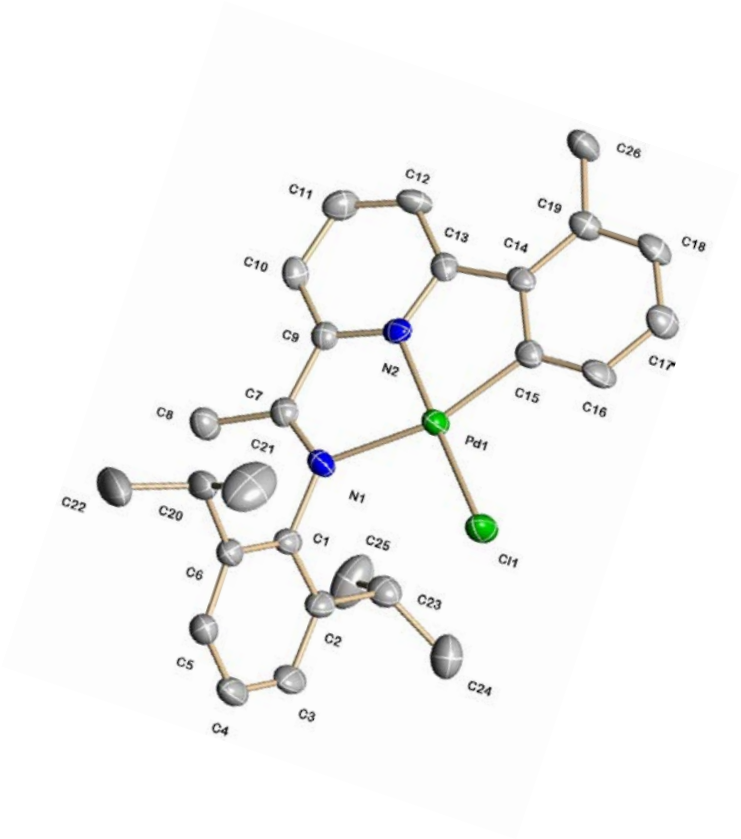

Figure 3.14 | Molecular structure of (**L1**$_{o\text{-tolyl}}$)PdCl

Table 3.4 Selected bond lengths (Å) and angles (°) for (**L1**$_{o\text{-tolyl}}$)PdCl

	Bond length (Å)		Bond angles (°)
Pd(1)-N(1)	2.161(4)	N(2)-Pd(1)-C(15)	81.24(19)
Pd(1)-N(2)	1.952(4)	N(2)-Pd(1)-N(1)	78.58(16)
Pd(1)-C(15)	1.977(5)	C(15)-Pd(1)-Cl(1)	97.78(16)
Pd(1)-Cl(1)	2.3167(14)	N(1)-Pd(1)-Cl(1)	102.45(11)

The same reaction conditions as for previous acetate-chloride exchange reaction were employed in the preparation of **L2**$_{o\text{-tolyl}}$PdCl from **L2**$_{o\text{-tolyl}}$PdOAc (**Figure 3.15**). The reaction gave 100% conversion to the chlorinated complex.

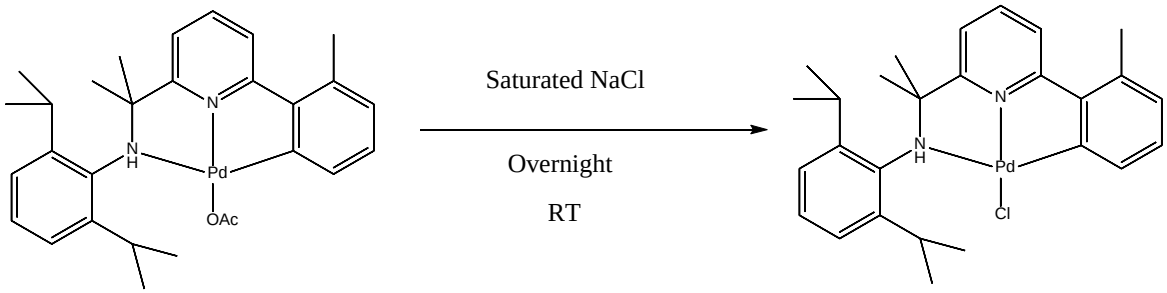

L2$_{o\text{-tolyl}}$PdOAc **L2**$_{o\text{-tolyl}}$PdCl

Figure 3.15 | Synthesis of **L2**$_{o\text{-tolyl}}$PdCl

The absence of the hydrogen and carbon signals belonging to the acetate group in the proton and ^{13}C NMR spectra both strongly indicated that formation of **L2**$_{o\text{-tolyl}}$PdCl had been achieved. Further confirmation comes from the mass spectrum of **L2**$_{o\text{-tolyl}}$PdCl. The ESMS revealed a fragment peak of m/z 526 which is in line with the calculated molecular weight of the complex. The FAB-MS showed clusters of peaks whose isotopic patterns were in agreement with $[M]^+$ and $[M\text{-}Cl]^+$ fragments. Crystals suitable for single crystal X-Ray diffraction studies were grown by layering the dichloromethane solution of the complex with hexane. The solid state X-Ray crystal structure and selected bond lengths and angles are given in **Figure 3.16** and **Table 3.5**.

Table 3.5: Selected bond lengths (Å) and angles (°) for **L2**$_{o\text{-tolyl}}$PdCl

	Bond length (Å)		Bond Angle (°)
Pd(1)-N(1)	2.205(3)	N(2)-Pd(1)-C(16)	81.60(15)
Pd(1)-N(2)	1.964(3)	C(16)-Pd(1)-Cl(1)	98.56(12)
Pd(1)-C(16)	1.970(4)	N(1)-Pd(1)-Cl(1)	97.93(9)
Pd(1)-Cl(1)	2.313(10)	N(2)-Pd(1)-N(1)	81.88(12)
		N(2)-Pd(1)-Cl(1)	179.05(9)

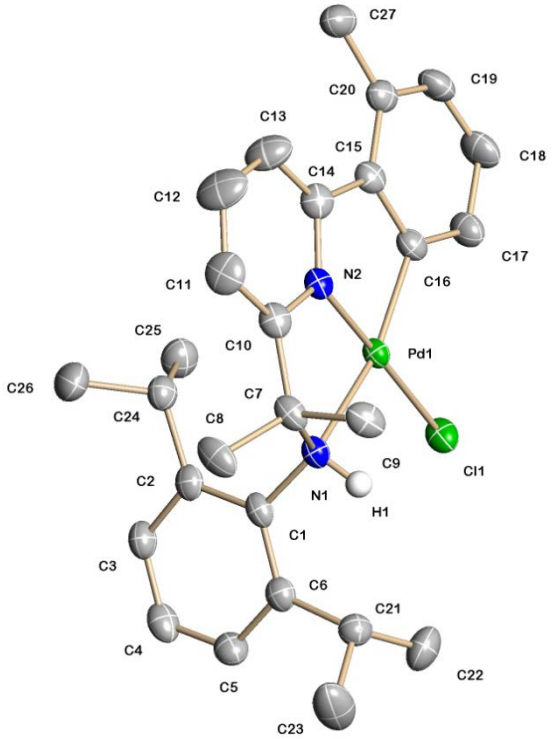

Figure 3.16 | Molecular Structure of **L2**$_{o\text{-tolyl}}$PdCl

The exchange of acetate group for chloride was also achieved for **L3**$_{o\text{-tolyl}}$PdOAc similarly (**Figure 3.17**). The absence of the acetate methyl signals in the proton and carbon NMR spectrum of the complex suggested that the exchange of the acetate with chloride has been successful. The X-Ray molecular structure of the compound confirmed the complex obtained to be the desired chlorinated analogue (**Figure 3.18** and **Table 3.6**).

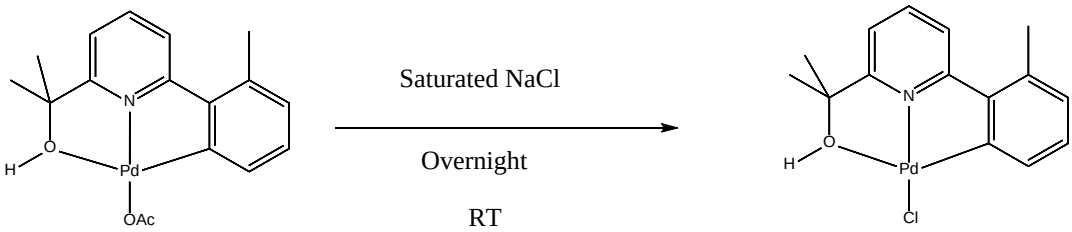

L3$_{o\text{-tolyl}}$PdOAc **L3**$_{o\text{-tolyl}}$PdCl

Figure 3.17 | Synthesis of **L3**$_{o\text{-tolyl}}$PdCl

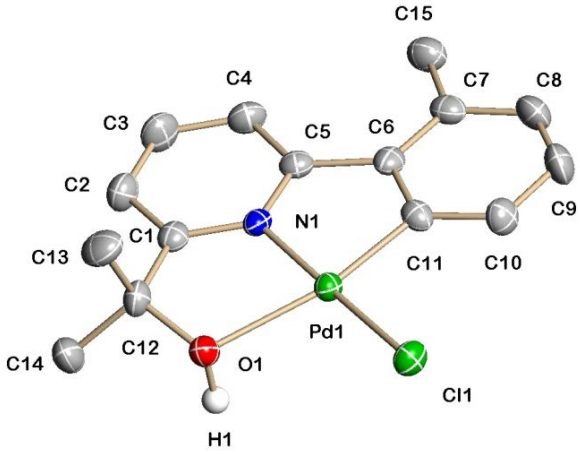

Figure 3.18 | Molecular Structure of **L3**$_{o\text{-tolyl}}$PdCl

Table 3.6: Selected bond lengths (Å) and angles (°) for **L3**$_{o\text{-tolyl}}$PdCl

	Bond length (Å)		Bond angles (°)
Pd(1)-N(1)	1.966(3)	N(1)-Pd(1)-C(11)	81.96(15)
Pd(1)-O(1)	2.211(3)	N(1)-Pd(1)-O(1)	79.48(12)
Pd(1)-Cl(1)	2.3335(11)	C(11)-Pd(1)-Cl(1)	98.43(12)
Pd(1)-C(11)	1.948(4)	O(1)-Pd(1)-Cl(1)	100.34(8)

3.3 Reaction chemistry of the 'site-blocked' ligands H**L1**$_{2,6\text{-Me2Ph}}$ and H**L1**$_{2,4,6\text{-Me3Ph}}$

Having achieved the C-H activation on the o-tolyl moiety in H**L1**$_{o\text{-tolyl}}$, we were intrigued by the possibility of blocking the o-CH-position of the aryl group and to examine whether the C-H activation would still occur by activating sp^2-CH bonds on the pyridine ring or sp^3 CH bonds of the blocking group. Hence, the reactions of H**L1**$_{2,6\text{-Me2Ph}}$ and H**L1**$_{2,4,6\text{-Me3Ph}}$ with $Pd(OAc)_2$ were studied. At room temperature in toluene (**Figure 3.19**) free ligand was found to be completely consumed after 48 h to give (H**L1**$_{2,6\text{-Me2Ph}}$)$Pd(OAc)_2$ as the main product. This is supported in solution by ^{1}H NMR spectroscopy, with two 3H singlets at 1.18 and 1.22 ppm due to the two acetate groups. Crystals suitable for single crystal X-Ray diffraction were grown by layering a dichloromethane solution of the complex with petroleum ether (**Figure 3.20** and **Table 3.7**). The crystal structure confirmed that the product was the bis-acetate Pd(II) complex with an *N*,*N*-bidentate ligand; i.e. C-H activation had not occurred.

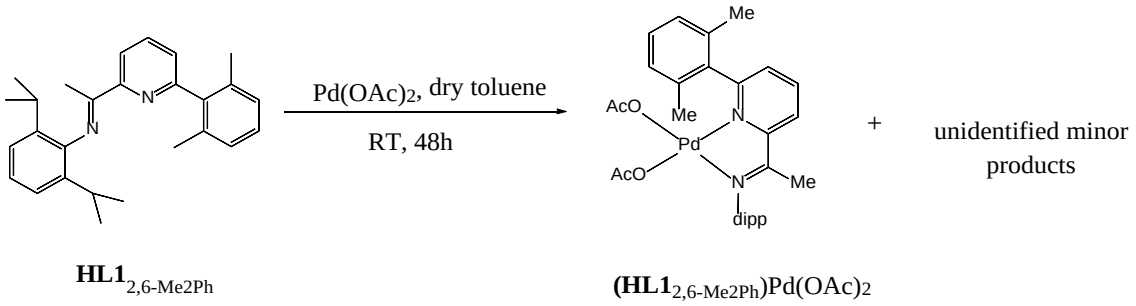

HL1$_{2,6\text{-Me2Ph}}$ **(HL1**$_{2,6\text{-Me2Ph}}$)$Pd(OAc)_2$

Figure 3.19 | Synthesis of (H**L1**$_{2,6\text{-Me2Ph}}$)$Pd(OAc)_2$

Table 3.7: Selected bond lengths (Å) and angles (°) for (H**L1**$_{2,6\text{-Me2Ph}}$)$Pd(OAc)_2$

	Bond length (Å)		Bond angles (°)
Pd(1)-N(1)	1.997(2)	C(9)-N(2)-Pd(1)	112.13(19)
Pd(1)-N(2)	2.043(2)	N(2)-Pd(1)-N(1)	80.15(10)
Pd(1)-O(1)	2.029(2)	C(7)-N(1)-Pd(1)	116.2(2)
Pd(1)-O(3)	1.998(2)	N(1)-Pd(1)-O(3)	91.73(9)

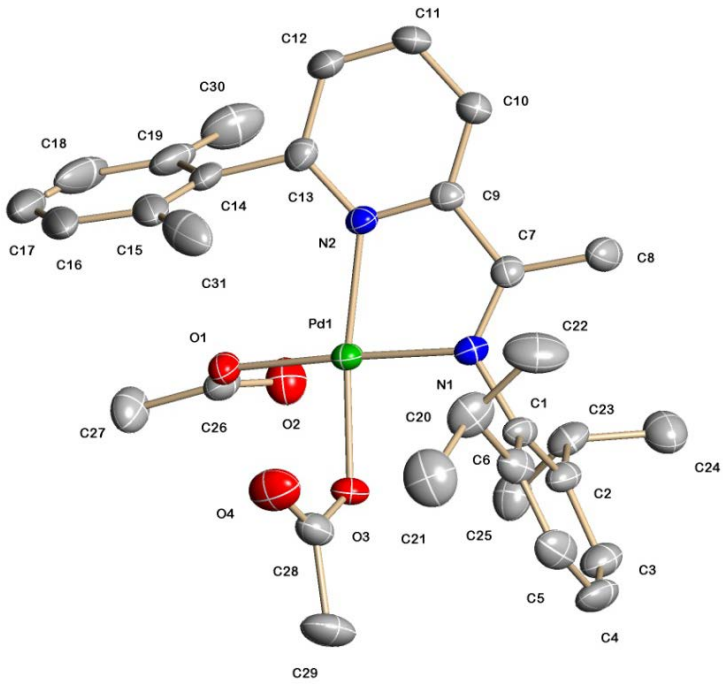

Figure 3.20 | Molecular Structure of (H**L1**$_{2,6\text{-Me2Ph}}$)Pd(OAc)$_2$

Following the failure to achieve C-H activation in the reaction of H**L1**$_{2,6\text{-Me2Ph}}$ with Pd(OAc)$_2$ at room temperature, the reaction was tried at 60 ^{o}C (**Figure 3.21**). The majority of the crude product was still the same non-activated bi-dentate complex (H**L1**$_{2,6\text{-Me2Ph}}$)Pd(OAc)$_2$ and unreacted free ligand along with minor amounts of a pyridine-activated bi-metallic species. This pyridine C-H activated species crystallized out upon slow evaporation of a dichloromethane and petroleum ether solution (**Figure 3.22** and **Table 3.8**).

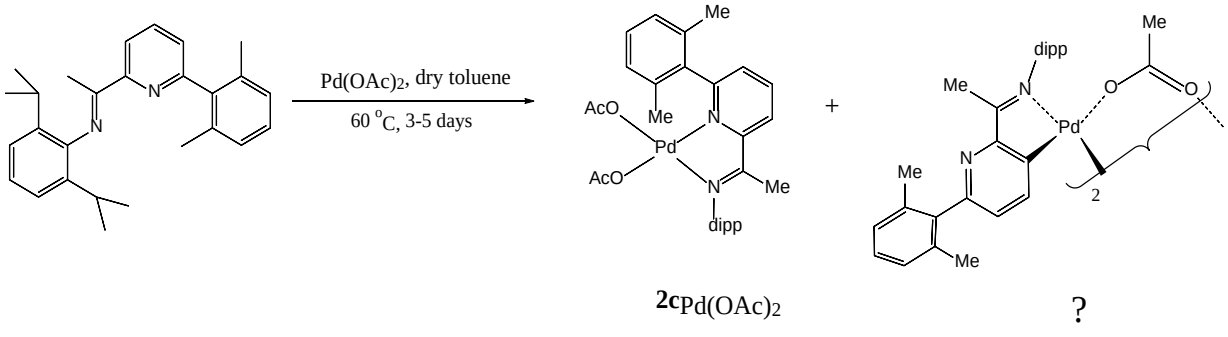

Figure 3.21 | Reaction of H**L1**$_{2,6\text{-Me2Ph}}$ with palladium acetate at 60^{o}C

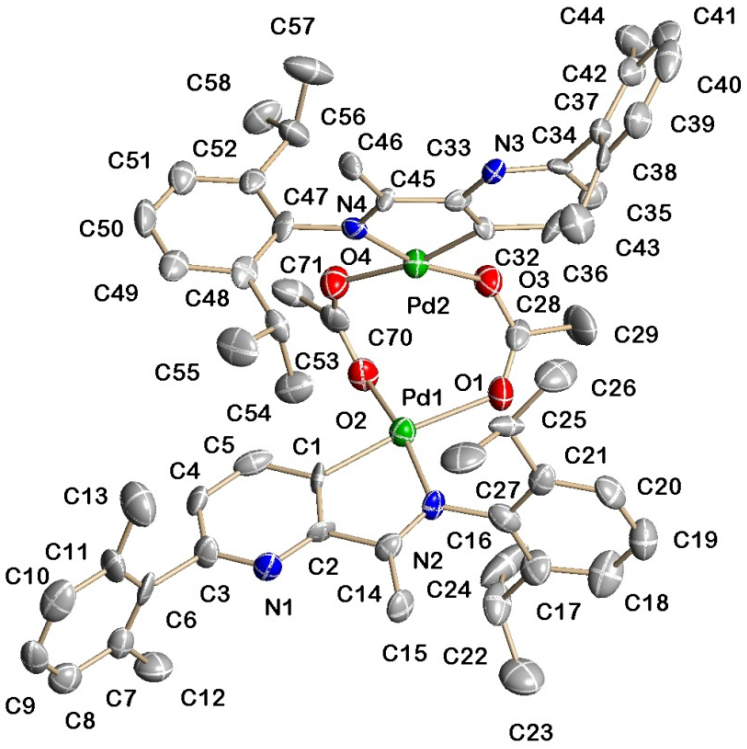

Figure 3.22 | Pyridine activated palladium complex of H**L1**$_{2,6\text{-Me2Ph}}$

Table 3.8: Selected bond lengths (Å) and angles (°)

	Bond length (Å)		Bond angles (°)
Pd(1)-C(1)	1.944(8)	C(2)-C(1)-Pd(1)	115.0(6)
Pd(1)-N(2)	2.024(7)	N(2)-Pd(1)-C(1)	79.4(3)
Pd(1)-O(1)	2.116(6)	C(14)-N(2)-Pd(1)	117.8(6)
Pd(2)-C(32)	1.962(8)	N(2)-Pd(1)-O(1)	95.3(3)

When the reaction of H**L1**$_{2,4,6\text{-Me3Ph}}$ with $Pd(OAc)_2$ was carried out at 60 °C, the major product was still the bi-dentate complex, with a very small amount of an un-identified species. Upon recrystallization, the sp^3 C-H activated product was crystallized out as single crystals suitable for an X-Ray diffraction study (**Figure 3.23** and **Table 3.9**). This was nevertheless only a minor product and there may be other low yielding species in the reaction pot. Keeping the reaction for more than five days did not increase the yield of the minor products, instead it led to decomposition. The several failed attempts at C-H activation of H**L1**$_{2,6\text{-Me2Ph}}$ and H**L1**$_{2,4,6\text{-Me3Ph}}$ pre-ligands indicate the difficulty in C-H activation when the most accessible activation site has been blocked.

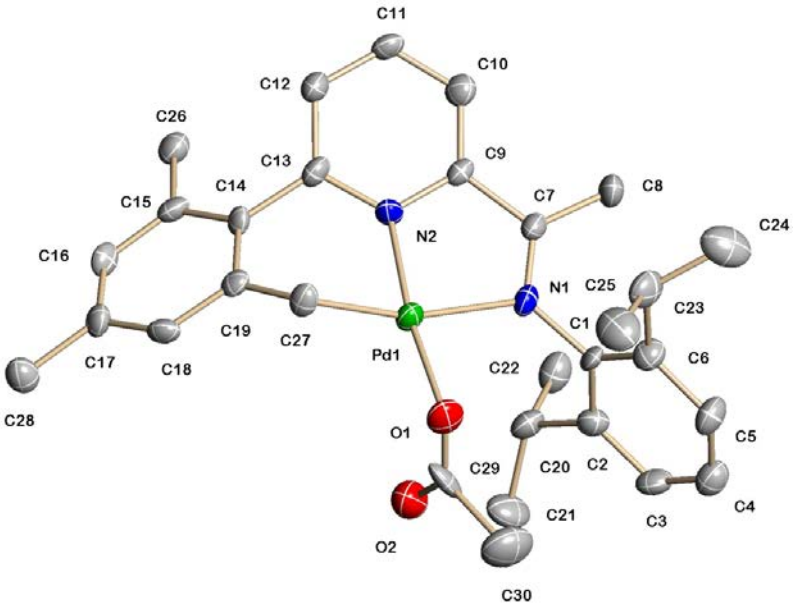

Figure 3.23 | Molecular structure of (**L1**$_{2,4,6\text{-Me3Ph}}$)PdOAc

Table 3.9: Selected bond lengths (Å) and angles (°) for (**L1**$_{2,4,6\text{-Me3Ph}}$)PdOAc

	Bond length (Å)		Bond angles (°)
Pd(1)-N(1)	2.149(5)	C(7)-N(1)-Pd(1)	111.0(4)
Pd(1)-N(2)	1.993(5)	N(2)-Pd(1)-N(1)	79.1(2)
Pd(1)-O(1)	2.042(4)	C(27)-Pd(1)-N(2)	89.5(2)
Pd(1)-C(27)	2.009(6)	C(19)-C(27)-Pd(1)	111.5(4)

3.4 Reactions of naphthyl substituted ligands: H**L1**$_{ket\text{-}nap}$, H**L1**$_{py\text{-}nap}$, H**L1**$_{ald\text{-}nap}$, H**L2**$_{nap}$ and H**L3**$_{nap}$

3.4.1 Reactions of ligands with $Pd(OAc)_2$

Following the investigations on the C-H activations of tolyl-armed and related ligands, the attention of the project was moved to the naphthyl-armed pyridyl-imines, H**L1**$_{ket\text{-}nap}$, H**L1**$_{py\text{-}nap}$, H**L1**$_{ald\text{-}nap}$, H**L2**$_{nap}$ and H**L3**$_{nap}$ – in each case the ligand has two possible activation sites on the naphthyl moiety.

The reaction of H**L1**$_{ket\text{-}nap}$ with palladium acetate was achieved via C-H activation with palladium acetate in toluene at 60 ^{o}C, as the reaction at room temperature resulted in less than 10% of conversion. There are two possible positions on the naphthalene ring that could be activated upon complexation with a metal, position a and b (**Figure 3.28**). However, after the characterization of the pure product, it was evident that position b had been activated, i.e. the peri activated product had been obtained.

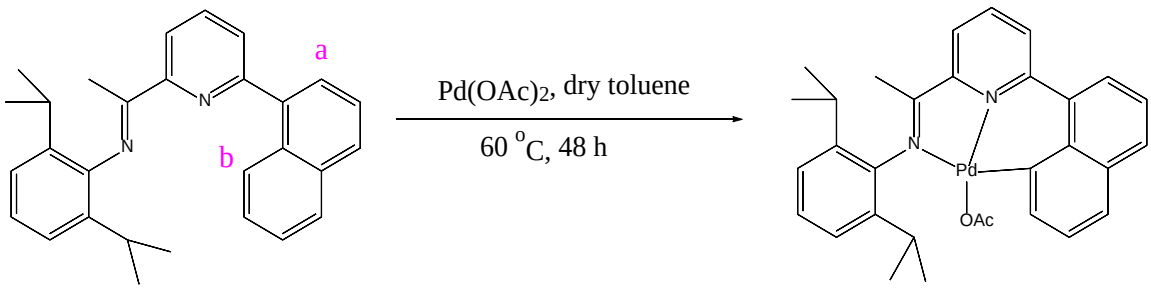

Figure 3.28 | Synthesis of peri-[(**L1**$_{ket\text{-}nap}$)PdOAc]

According to the 2D COSY spectrum of this compound, there are four groups of protons in the aromatic region and each group contains three protons correlated to each other, confirming that the C-H activated product shown in **Figure 3.28** had been obtained. The COSY spectrum of the product with position a activated—the ortho activated product (**Figure 3.29**)—would also show four groups of protons in the aromatic region, however in contrast to above, this is now two groups of three protons, one group of four protons and one group of two protons.

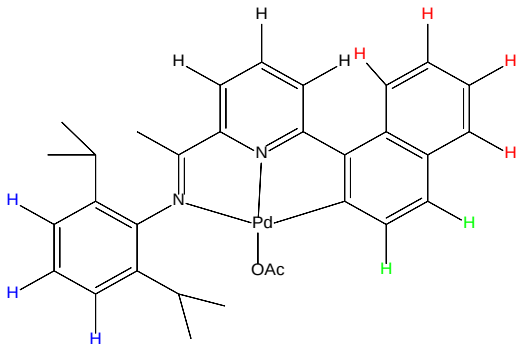

Figure 3.29 | Hypothetical *ortho*-[(**L1**$_{ket\text{-}nap}$)PdOAc]

The ESMS rendered a peak at m/z 511 assigned to the $[M\text{-}OAc]^{+}$ fragment of the complex as the acetate group could easily be detached from the palladium centre during the ESMS analysis, leaving the $[M\text{-}OAc]^{+}$ fragment. The peri activated structure was confirmed by

a single crystal X-Ray structure determination of the product (**Figure 3.30** and **Table 3.10**).

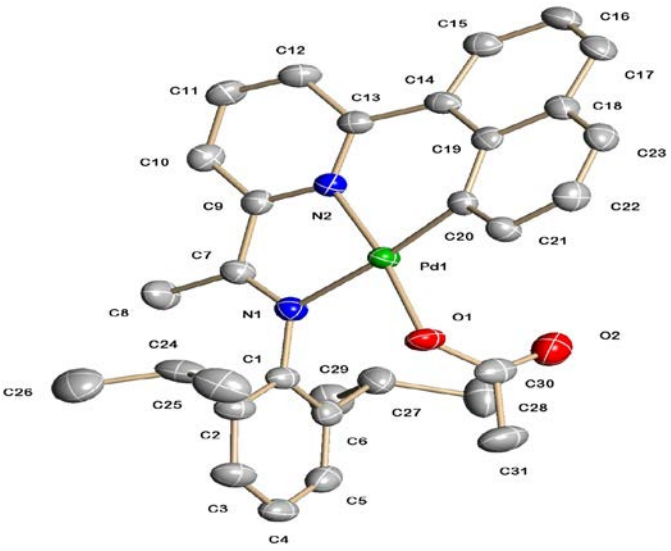

Figure 3.30 | X-Ray crystal structure of *peri*-[(**L1**$_{ket\text{-}nap}$)OAc]

Table 3.10: Selected bond lengths (Å) and angles (^{o}) for *peri*-[(**L1**$_{ket\text{-}naph}$)OAc]

	Bond length (Å)		Bond angles (^{o})
Pd(1)-N(1)	2.111(2)	N(2)-Pd(1)-C(20)	94.53(11)
Pd(1)-N(2)	1.996(2)	N(2)-Pd(1)-N(1)	80.63(9)
Pd(1)-C(20)	1.978(3)	C(20)-Pd(1)-O(1)	92.95(10)
Pd(1)-O(1)	2.029(2)	N(1)-Pd(1)-O(1)	91.83(9)

Heating *peri*-[(**L1**$_{ket\text{-}nap}$)PdOAc] in toluene at 60 ^{o}C or 100 ^{o}C gave no evidence for a peri-ortho interconversion. Only the unreacted starting material was observed after heating at 60 ^{o}C for 48h, while at 100 ^{o}C there were signs of decomposition (palladium black) after 24h and the NMR spectrum of the solution showed minor amounts of the free ligand.

The C-H activation of H**L1**$_{py\text{-}nap}$ can be achieved simply at room temperature by stirring a bench chloroform solution of H**L1**$_{py\text{-}nap}$ with palladium acetate. The bidentate intermediate (H**L1**$_{py\text{-}nap}$)Pd(OAc)$_2$, containing the N,N-bidentate ligand, can be isolated if the reaction is stopped after 2 h at room temperature (**Figure 3.24**).

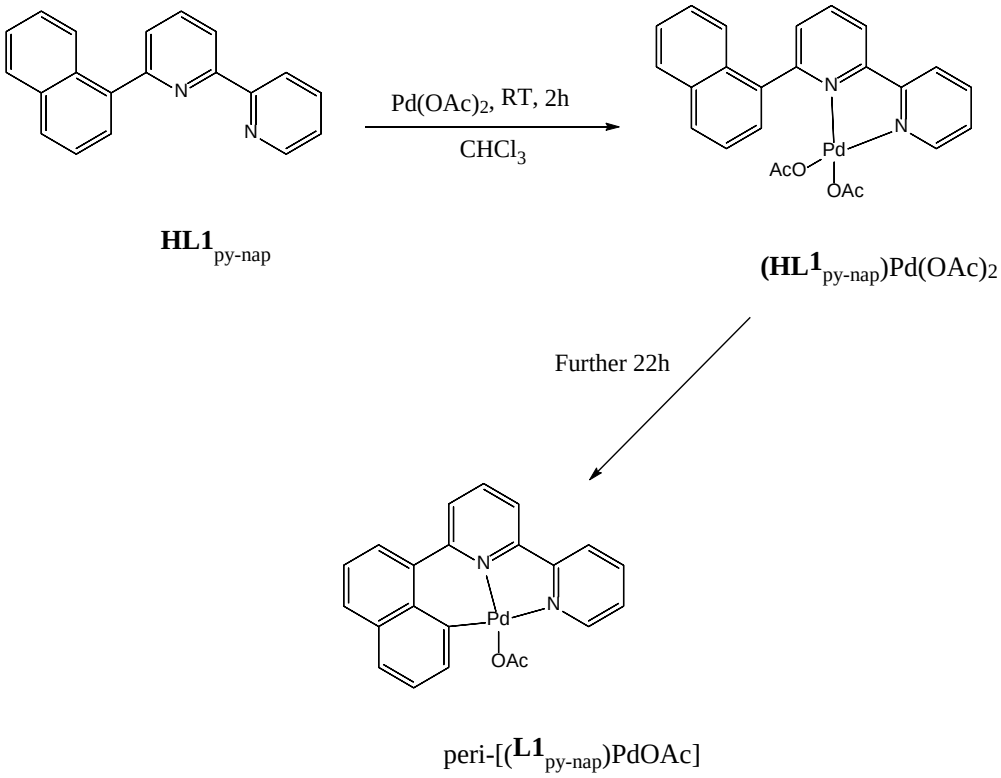

Figure 3.24 | The complexation of H**L1**$_{py\text{-}nap}$ with palladium acetate

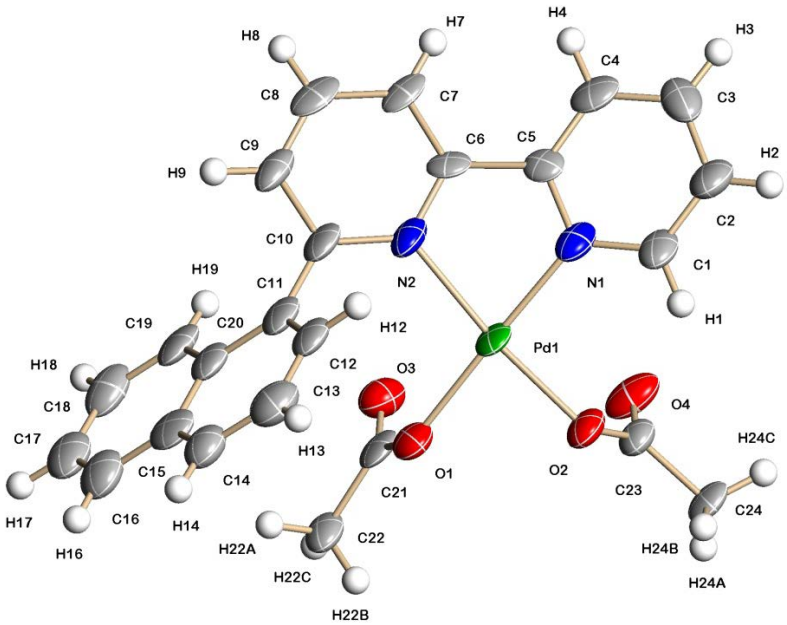

Figure 3.25 | Molecular Structure of (H**L1**$_{py\text{-}nap}$)Pd(OAc)$_2$

Table 3.11: Selected bond lengths (Å) and angles (°) for (H**L1**$_{py\text{-}nap}$)Pd(OAc)$_2$

	Bond length (Å)		Bond angles (°)

Pd(1)-N(1)	1.992(9)	C(6)-N(2)-Pd(1)	111.2(7)
Pd(1)-N(2)	2.063(8)	N(2)-Pd(1)-N(1)	80.2(3)
Pd(1)-O(1)	2.036(7)	C(5)-N(1)-Pd(1)	114.0(7)
Pd(1)-O(2)	2.001(7)	N(1)-Pd(1)-O(2)	93.1(3)

Layering the resultant chloroform with petroleum ether yielded crystals suitable for single crystal X-Ray diffraction. The molecular structure of the intermediate complex is presented in **Figure 3.25** with the selected bond length and angles in **Table 3.11**.

Keeping the reaction for a further 22 h at room temperature (**Figure 3.24**) yielded the C-H activated product peri-**[(L1**$_{py\text{-}nap}$)PdOAc] in a good yield. Only 13 proton signals were found in the proton NMR spectrum of the complex, indicating that C-H activation of the naphthyl ring had occured. Slow evaporation of a chloroform/petroleum ether solution of the product yielded crystals suitable for a single crystal X-Ray diffraction study. The molecular structure of the complex confirmed that the C-H activation had taken place on the *peri* position on the naphthyl moiety (**Figure 3.26** and **Table 3.12**).

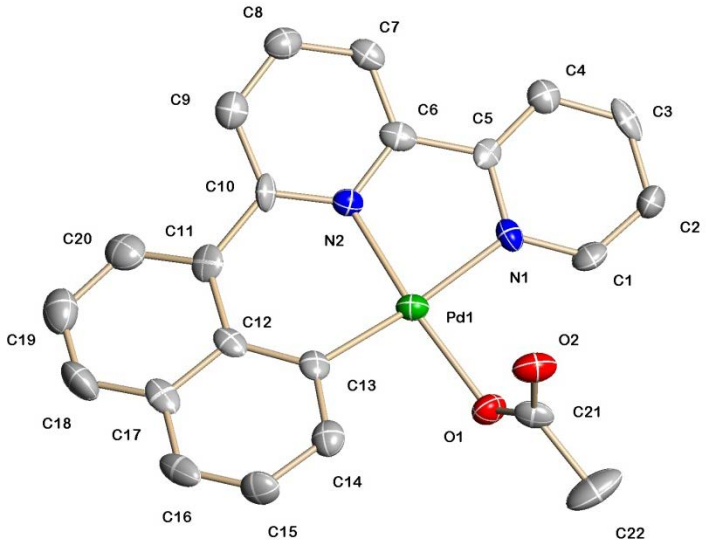

Figure 3.26 | Molecular Structure of *peri*-**[(L1**$_{py\text{-}nap}$)PdOAc]

Table 3.12: Selected bond lengths (Å) and angles (°) for *peri*-**[(L1**$_{py\text{-}nap}$)PdOAc]

	Bond length (Å)		Bond angles (°)

Pd(1)-N(1)	2.071(6)	N(2)-Pd(1)-C(13)	93.9(3)
Pd(1)-N(2)	2.005(5)	N(2)-Pd(1)-N(1)	81.0(3)
Pd(1)-C(13)	1.967(8)	C(13)-Pd(1)-O(1)	93.4(3)
Pd(1)-O(1)	2.040(5)	N(1)-Pd(1)-O(1)	91.9(2)

As seen for the bipyridyl ligand H**L1**$_{py\text{-}nap}$, the C-H activation of the aldimine-armed ligand H**L1**$_{ald\text{-}nap}$ can be achieved by reaction with $Pd(OAc)_2$ and full conversion to the C-H activated product was achieved after 16 h at room temperature (**Figure 3.27**). The proton NMR spectrum of the product showed 12 proton signals in the aromatic region, indicating the activation of the naphthyl ring. The 2D COSY spectrum of this compound revealed that there are four groups of protons in the aromatic region and each group contains three protons correlated to each other, confirming that the peri-activated product *peri*-[(**L1**$_{ald\text{-}nap}$)PdOAc] in **Figure 3.27** had been obtained.

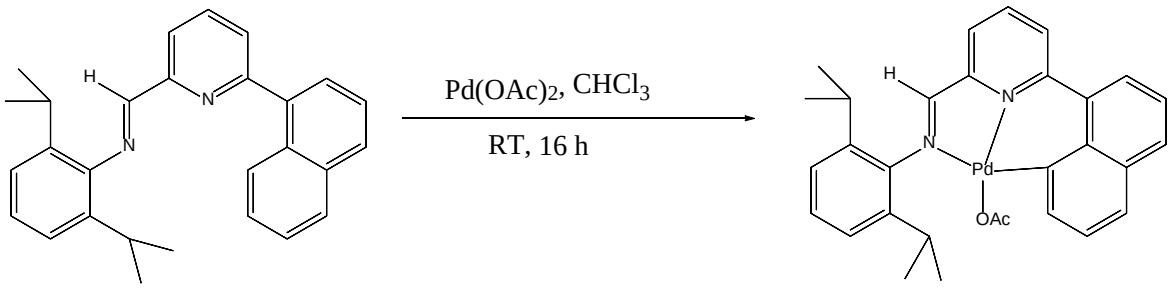

Figure 3.27 | Synthesis of *peri*-[(**L1**$_{ald\text{-}nap}$)PdOAc]

The C-H activation of H**L2**$_{nap}$ is similar to the reactions with H**L1**$_{ket\text{-}nap}$. The *peri*-C-H activated palladium complex *peri*-[(**L2**$_{nap}$)PdOAc] is obtained in excellent purity (**Figure 3.31**). Complex (**L2**$_{nap}$)PdOAc has a few interesting phenomenon in its proton NMR spectrum. Firstly, the methyl signal of ^{i}Pr in the free ligand appeared as one doublet. After coordination to palladium, it became four doublet peaks. Furthermore, the two CH on the diisopropyl group and the two methyl signals on $(CH_3)_2CNH$ moiety all appeared as different peaks indicating the inequivalency of these protons. This is induced by the lack of symmetry in the molecule. Another strong indicator of this lack of symmetry in structure is the presence of two septets assigned to the two CH protons on the diisopropyl

moieties. As discussed earlier for the palladium-acetate complex (**L2**$_{o\text{-tolyl}}$)PdOAc, the amine proton H1 signal (**Figure 3.32**) is seen at a very downfield chemical shift of 8.0 ppm, suggesting hydrogen bonding between the amine proton and the –OAc group in solution. A single crystal X-Ray diffraction study of the complex confirmed peri-activation of the pre-ligand and the presence of a hydrogen bond between the amine proton and the acetate oxygen (2.286 Å) (**Figure 3.32** and **Table 3.13**) in the solid state.

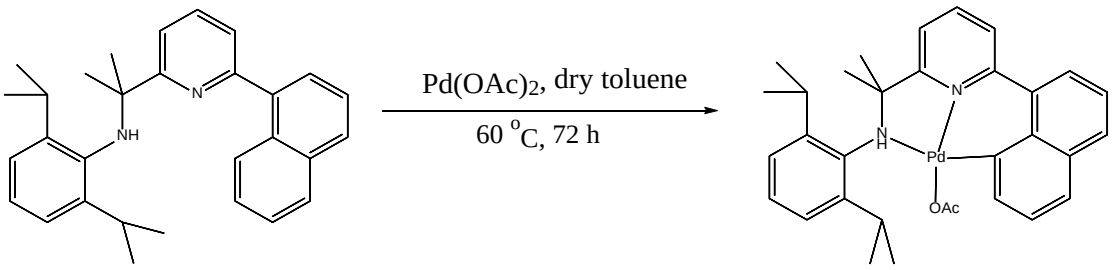

HL2$_{nap}$ peri-[(**L2**$_{nap}$)PdOAc]

Figure 3.31 | Synthesis of *peri*-[(**L2**$_{nap}$)PdOAc]

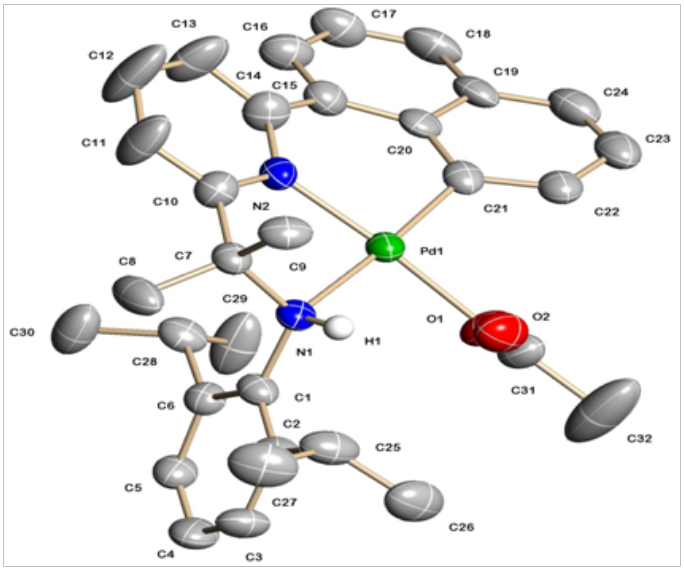

Figure 3.32 | Molecular Structure of *peri*-[(**L2**$_{nap}$)PdOAc]

Table 3.13: Selected bond lengths (Å) and angles (°) for *peri*-[(**L2**$_{nap}$)PdOAc]

	Bond length (Å)		Bond angles (°)
Pd(1)-N(1)	2.171(4)	N(2)-Pd(1)-C(21)	93.20(19)
Pd(1)-N(2)	1.990(4)	N(2)-Pd(1)-N(1)	83.08(15)
Pd(1)-C(21)	1.981(5)	C(21)-Pd(1)-O(1)	90.24(18)
Pd(1)-O(1)	2.035(4)	N(1)-Pd(1)-O(1)	93.60(15)

The C-H activation of the alcohol-armed ligand H**L3**$_{naph}$ was tried next with the same reaction conditions as that used in the previous ligands (**Figure 3.33**). As seen for the o-tolyl substituted analogue, the C-H activation of this alcohol armed ligand is more difficult than those for the imine and amine counterparts.

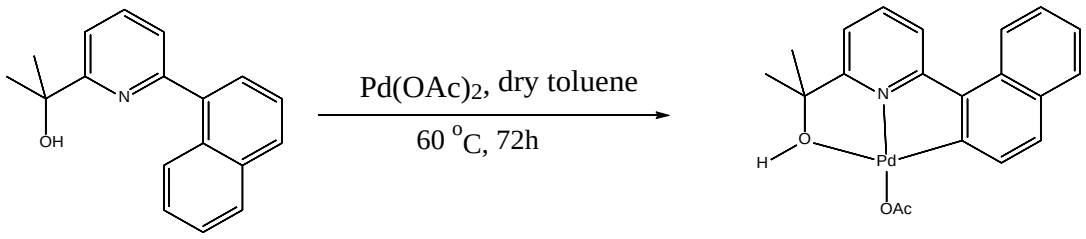

HL3$_{naph}$ ortho-**[(L3**$_{naph}$**)**PdOAc]

Figure 3.33 | C-H activation of H**L3**$_{naph}$

The C-H activated product was obtained in a 49% yield after 72 h at 60 °C. Interestingly, the X-Ray molecular structure of **L3**$_{naph}$PdOAc exhibited an unexpected ortho-activated structure (**Figure 3.34** and **Table 3.14**). As shown in **Table 3.14**, Pd(1)-O(1) bond length is 2.2 Å, which is slightly longer than the other palladium-oxygen bond Pd(1)-O(2) (2.0 Å), indicating that the palladium-tertiary alcohol (Pd-O) bond is weaker than a palladium-acetate bond. This can be explained by the difference of the two Pd-O bonds in nature. The hydroxy oxygen is neutral and it binds to the palladium by sharing a loan pair of electrons. The acetate oxygen, on the other hand, is negatively charged and it forms an electrostatic bond with palladium. Thus the latter Pd-O bond is stronger than the former. The bond angles are significantly different to those for the imine/amine analogues as well due to the fomation of a five-membered ring with a more strained bite angle of 82.5° (N(1)-Pd(1)-C(16)) than a six-membered ring.

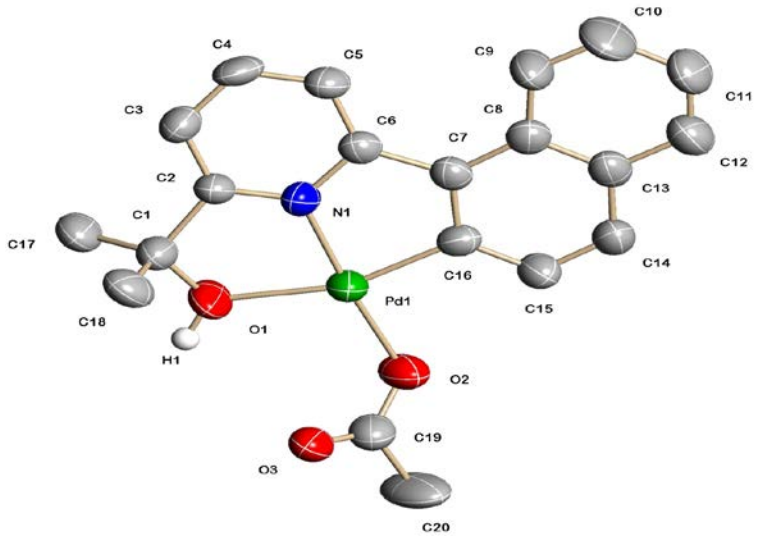

Figure 3.34 | Molecular Structure of *ortho*-[(**L3**$_{nap}$)PdOAc]

Table 3.14: Selected bond lengths (Å) and angles (°) for *ortho*-[(**L3**$_{nap}$)PdOAc]

	Bond length (Å)		Bond angles (°)
Pd(1)-N(1)	1.952(6)	N(1)-Pd(1)-C(16)	82.5(3)
Pd(1)-O(1)	2.139(5)	N(1)-Pd(1)-O(1)	78.4(2)
Pd(1)-O(2)	2.040(5)	C(16)-Pd(1)-O(2)	93.6(3)
Pd(1)-C(16)	1.957(7)	O(1)-Pd(1)-O(2)	105.1(2)

3.4.2 The mechanism of C-H activation reactions of H**L1**$_{ket\text{-}nap}$ and H**L3**$_{nap}$

Resulting in the different C-H activated products, the initial mechanisms of the C-H activation process must go through different routes with these ligands. C–H activation of H**L1**$_{ket\text{-}naph}$ seems to proceed in four steps, the first being the coordination of the palladium to the two nitrogen donors and the dissociation of one acetate to give [(N,N-pyridylarylimine)Pd(k^2-OAc)]$^+_{peri}$ precursor, **A** (**Figure 3.35**). k^2–k^1-displacement of the -OAc ligand by the incoming peri-C–H bond gives the transition state **B**. C–H activation then occurs via an AMLA-6 pathway[57] to give the cyclo-metallated **C**. Deprotonation

would then give the peri- C-H activated product peri-[(**L1**$_{ket\text{-}naph}$)PdOAc]. The rareness of the palladium pincer complexes of the 1-(pyridine-2-yl)-alkylalcohol ligands is partly due to the labile nature of the OH donor.[56] It has been reported that with monodentate naphthyl ligands the ortho-activated product is the major product with no or a minor amount of the peri-activated product (**Figure 3.36**).[47-49] Thus, in the case of the alcohol-armed ligand H**L3**$_{naph}$, the C-H activation seems to occur using only the monodentate pyridine as the directing group, leading to the ortho-activated product being predominant. The –OH donor seems to coordinate as the last step of the process (**Figure 3.37**).

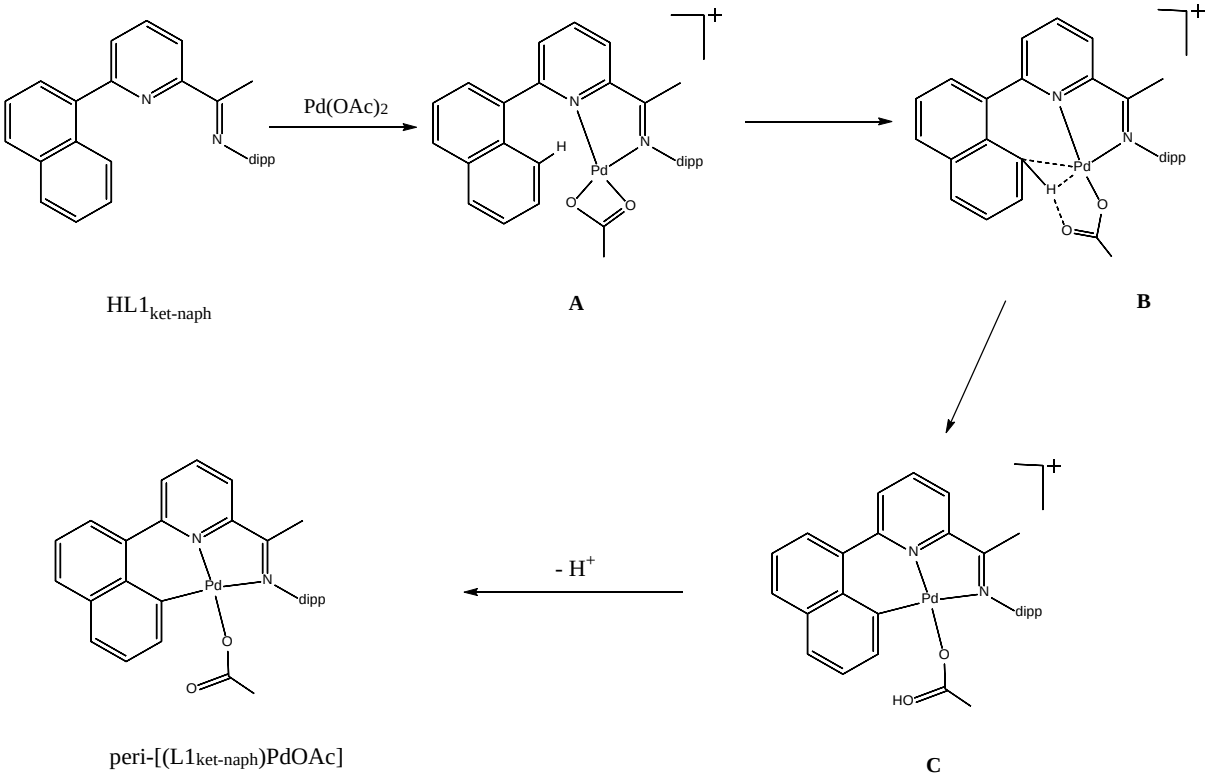

Figure 3.35 | C-H activation of H**L1**$_{ket\text{-}naph}$

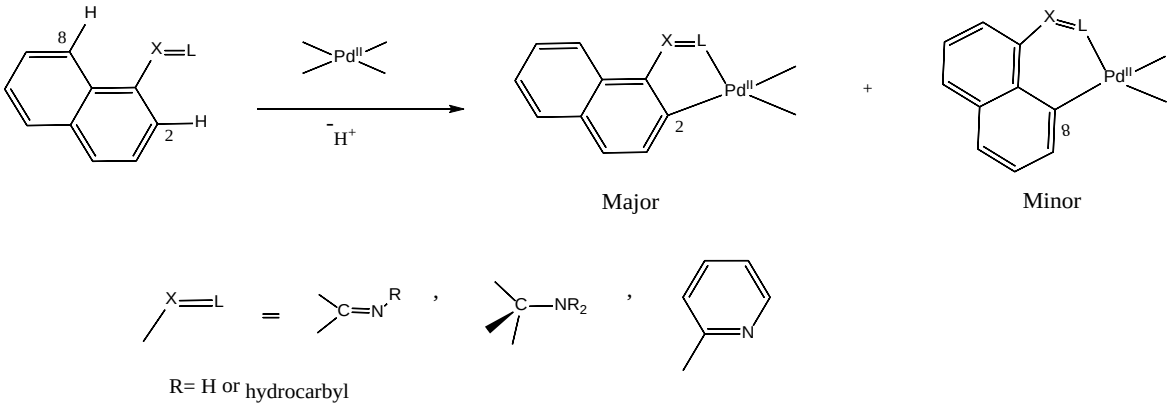

Figure 3.36 | Ortho vs. peri- activation of naphthyl rings using imine, amine and pyridine as directing groups

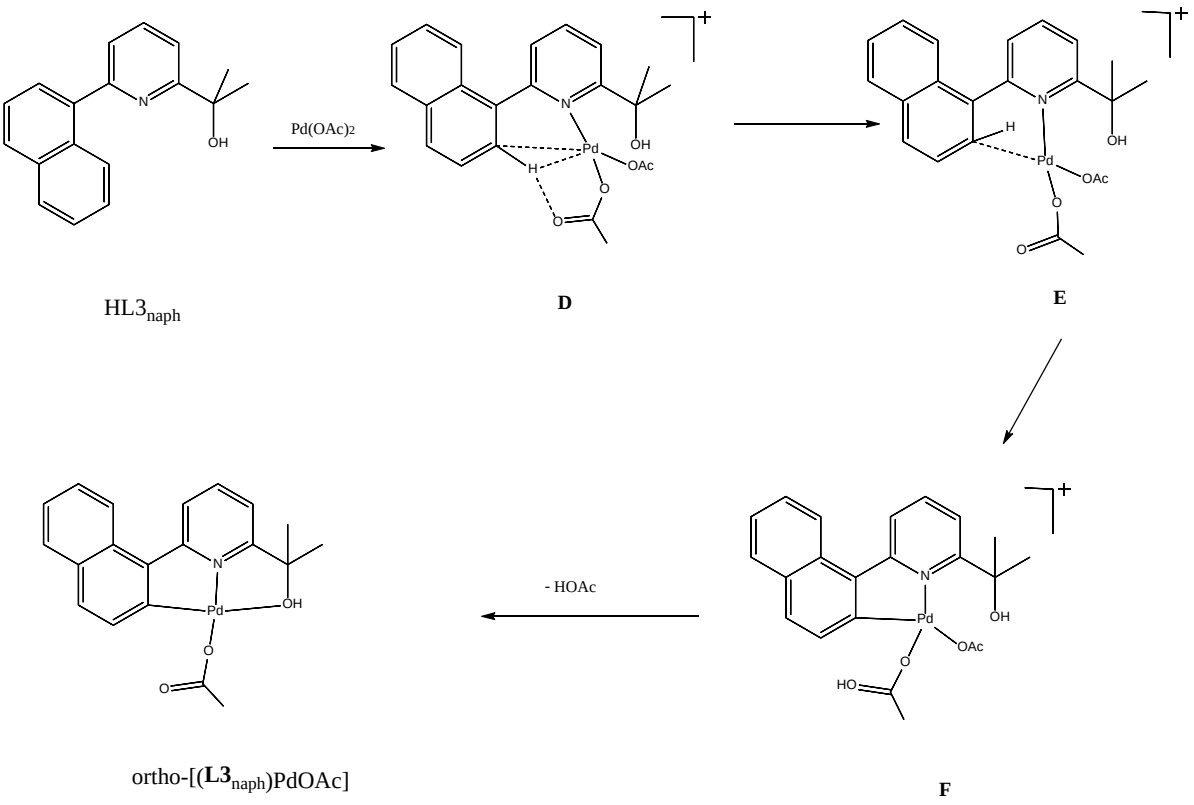

Figure 3.37 | C-H activation of H**L3**$_{naph}$

3.4.3 Reactions of **L**PdOAc with NaCl (L=H**L1**$_{ket-nap}$, H**L2/3**$_{nap}$)

In view of the relative reactivity and synthesis of the ligands used in section 3.4.1, the work hereafter is focused on the ketimine, amine and alcohol armed ligands H**L1**$_{ket}$, H**L2**$_{naph}$ and H**L3**$_{naph}$. The exchange of the –OAc with –Cl is achieved by reaction of the palladium acetate complexes of these three ligands with saturated sodium chloride solutions (**Figure 3.38**). The palladium chloride complex of ligand H**L1**$_{ket-nap}$ was characterized by ^{1}H and ^{13}C{^{1}H} NMR spectroscopy. The absence of the 3H singlet at 1.38 ppm corresponding to the methyl group on acetate moiety revealed that the acetate group had been successfully replaced by the chloride ligand.

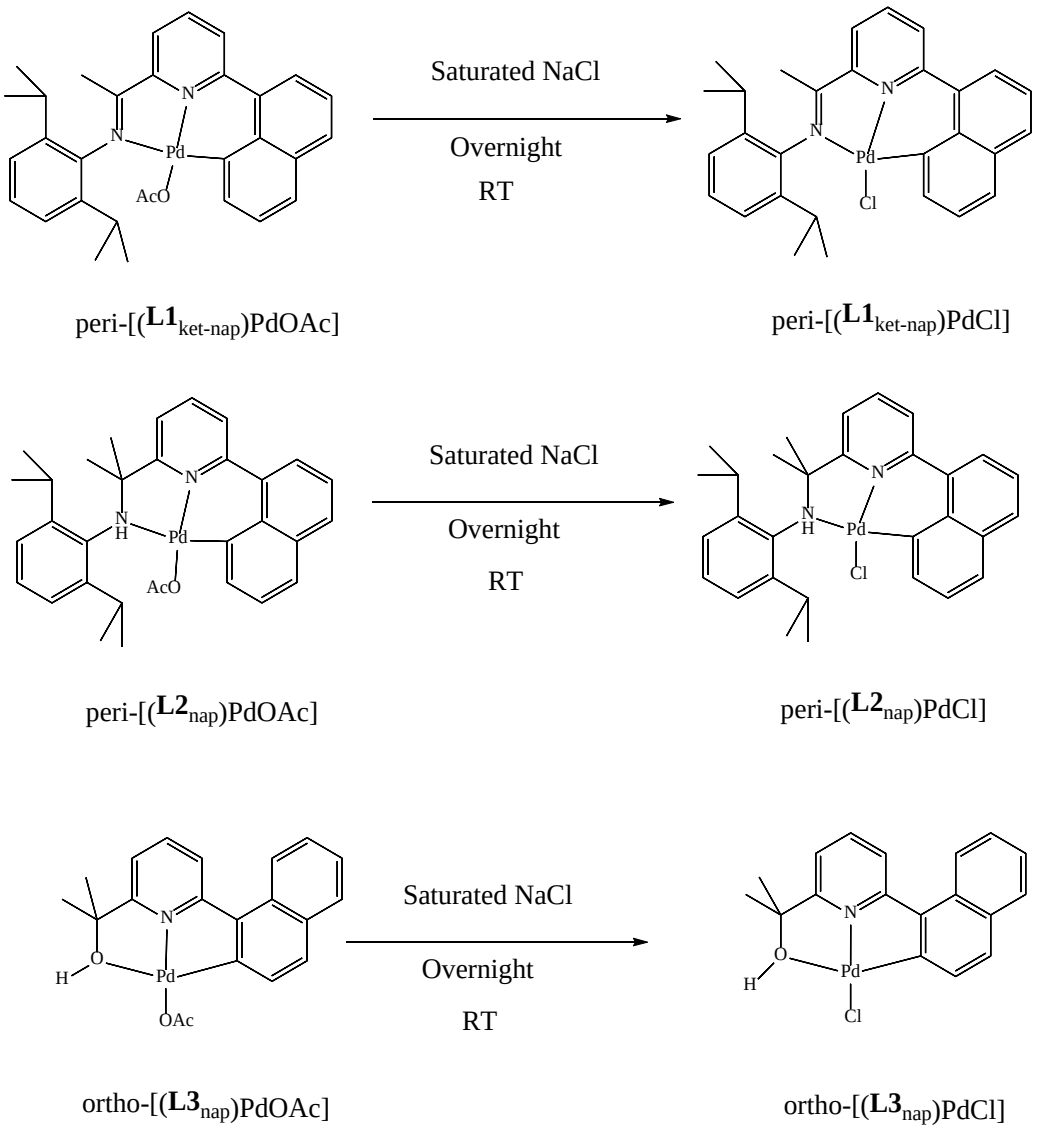

Figure 3.38 | Acetate exchange for chloride

Furthermore, the signals associated with acetate carbon atoms were not detected in the ^{13}C NMR spectrum of this complex confirming that *peri*-[(**L1**$_{ket\text{-}nap}$)PdCl] had been obtained in excellent purity. ESI spectra of the compound revealed a peak at 511.1377 corresponding to the [M-Cl^{35}] fragment. The X-Ray crystal structure of the complex unambiguously confirmed that the product is the –Cl analogue of the peri-[(**L1**$_{ket\text{-}nap}$)PdOAc] (**Figure 3.39** and **Table 3.15**).

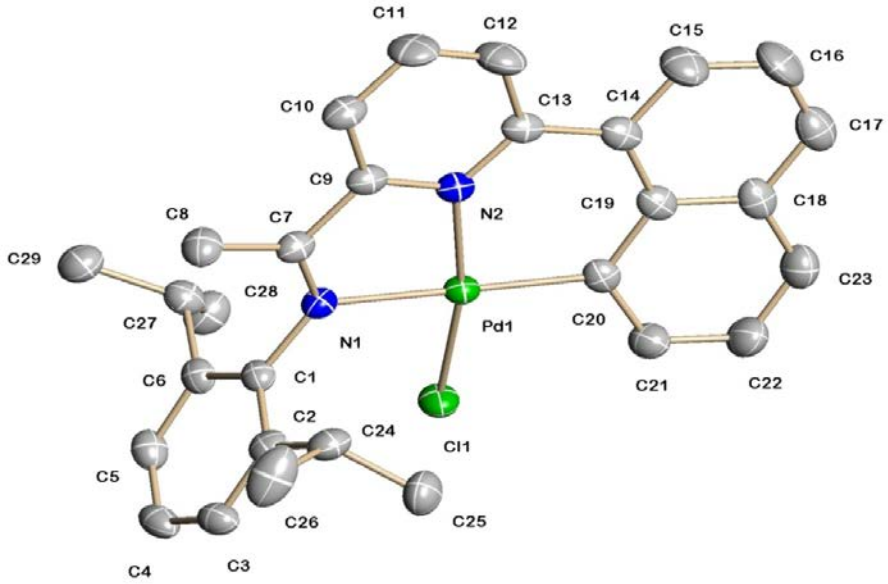

Figure 3.39 | X-ray crystal structure of *peri*-[(**L1**$_{ket\text{-}nap}$)PdCl]

Table 3.15: Selected bond lengths (Å) and angles (°) for *peri*-[(**L1**$_{ket\text{-}nap}$)PdCl]

	Bond length (Å)		Bond angles (°)
Pd(1)-N(1)	2.104(2)	N(2)-Pd(1)-C(20)	94.14(11)
Pd(1)-N(2)	2.018(2)	N(2)-Pd(1)-N(1)	80.68(9)
Pd(1)-C(20)	1.987(3)	C(20)-Pd(1)-Cl(1)	95.02(9)
Pd(1)-Cl(1)	2.326(8)	N(1)-Pd(1)-Cl(1)	90.87(6)

The palladium chloride complex *peri*-[(**L2**$_{nap}$)PdCl] was obtained via the reaction of *peri*-[(**L2**$_{nap}$)PdOAc] with a saturated sodium chloride solution. The amine proton of this complex appeared as a clear singlet at 5.67 ppm in its proton NMR spectrum, indicating the absence of the hydrogen bonding with the acetate moiety, providing confirmation of

the exchange of the acetate group with chloride. Crystals suitable for single crystal X-Ray diffraction were grown by layering a dichloromethane solution of the complex with hexane. The X-Ray crystallography results revealed the structure of the complex to be the chlorinated analogue of *peri*-[(**L2**$_{nap}$)PdOAc] (**Figure 3.40** and **Table 3.16**).

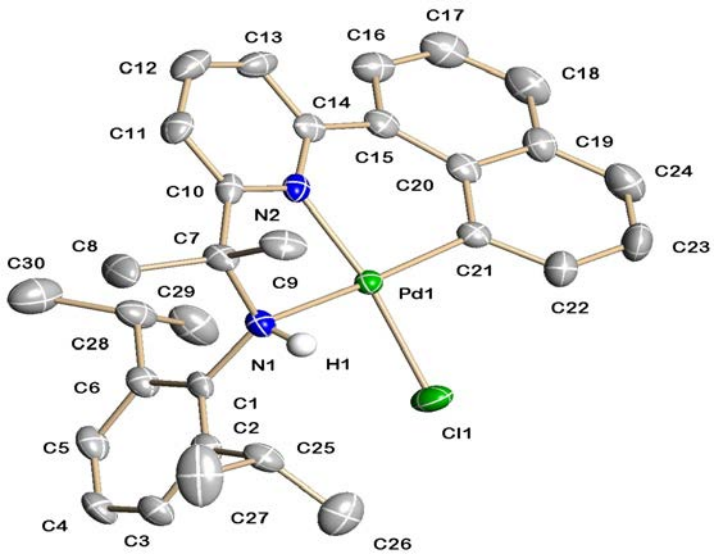

Figure 3.40 | Molecular Structure of *peri*-[(**L2**$_{nap}$)PdCl]

Table 3.16: Selected bond lengths (Å) and angles (°) for *peri*-[(**L2**$_{nap}$)PdCl]

	Bond length (Å)		Bond Angle (°)
Pd(1)-N(1)	2.158(3)	N(2)-Pd(1)-C(21)	93.31(14)
Pd(1)-N(2)	2.013(3)	C(21)-Pd(1)-Cl(1)	94.94(11)
Pd(1)-C(21)	1.983(4)	N(1)-Pd(1)-Cl(1)	89.07(9)
Pd(1)-Cl(1)	2.313(11)	N(2)-Pd(1)-N(1)	83.02(12)

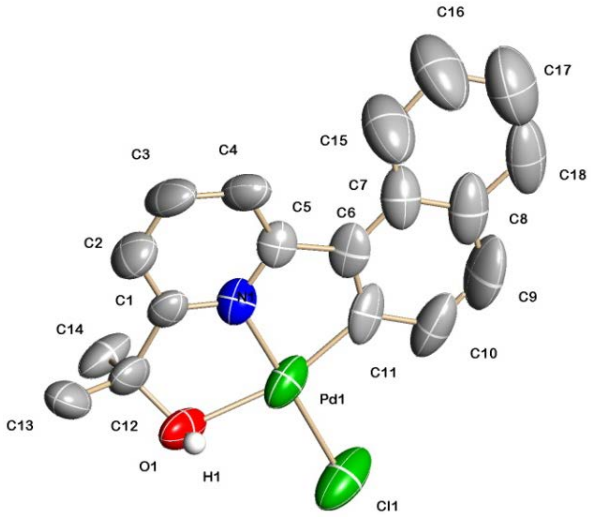

Figure 3.41 | Molecular Structure of *ortho*-[(**L3**$_{naph}$)PdCl]

Table 3.17: Selected bond lengths (Å) and angles (°) for *ortho*-[(**L3**$_{naph}$)PdCl]

	Bond length (Å)		Bond angles (°)
Pd(1)-N(1)	1.962(13)	N(1)-Pd(1)-C(11)	82.7(4)
Pd(1)-O(1)	2.186(11)	N(1)-Pd(1)-O(1)	78.9(5)
Pd(1)-Cl(1)	2.303(5)	C(11)-Pd(1)-Cl(1)	98.6(2)
Pd(1)-C(11)	1.978(4)	O(1)-Pd(1)-Cl(1)	99.7(3)

Similarly in the H**L3**$_{nap}$ – palladium reaction, the absence of the acetate methyl signals in the proton and carbon NMR spectra of the new complex suggested that the exchange of the acetate with chloride has been successful. The X-Ray molecular structure of the compound confirmed the complex obtained to be the desired chlorinated analogue (**Figure 3.41** and **Table 3.17**).

3.4.4 C-H activation of H**L1**$_{ald\text{-}nap}$ and H**L1**$_{ket\text{-}nap}$ with Na_2PdCl_4

Given the regioselectivity for peri-activation observed on reaction of H**L1**$_{ald\text{-}nap}$ and H**L1**$_{ket\text{-}nap}$ with $Pd(OAc)_2$ we decided to explore their reactivity towards other common palladium(II) reagents such as $Na_2[PdCl_4]$.

Considering the insolubility of Na_2PdCl_4 in organic solvents, the reactions were carried out in acetic acid at 100 ^oC. A yellow precipitate was formed after 60 h in the reaction of H**L1**$_{ket\text{-}nap}$ with Na_2PdCl_4 (**Figure 3.42**). After filtration, the pure product was obtained as a bright yellow powder with extremely low solubility in organic solvents.

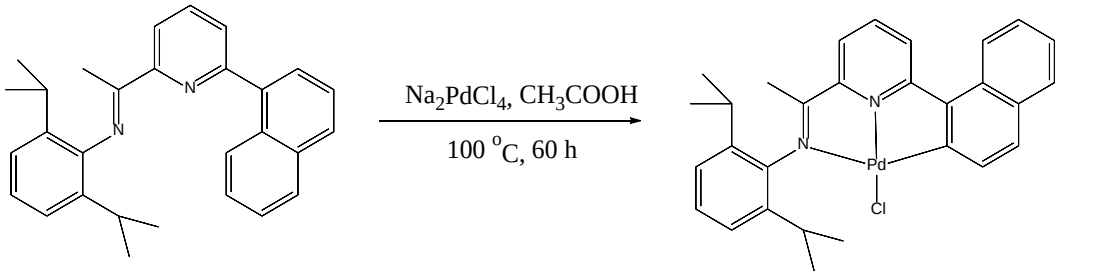

HL1$_{ket\text{-}nap}$ ortho-[(**L1**$_{ket\text{-}nap}$)PdCl]

Figure 3.42 | Synthesis of ortho-[(**L1**$_{ket\text{-}nap}$)PdCl]

The proton NMR spectrum of the product confirmed that C-H activation on the naphthyl moiety had been accomplished by the presence of signals for only 12 protons in the aromatic region. The 2D COSY spectrum of the complex showed four groups of protons in the aromatic region, two groups of three protons, one group of four protons and one group of two protons. This is quite different from that observed in the COSY spectrum of the peri-product. Furthermore, the chemical shifts and splitting patterns of the peaks in the proton NMR spectrum are distinctly different from those of the peri-activated product, indicating the formation of a different C-H activated product. A single crystal X-ray diffraction studies confirmed that the complex was the ortho-activated product (**Figure 3.43** and **Table 3.18**).

Table 3.18: Selected bond lengths (Å) and angles (^{o}) for *ortho*-[(**L1**$_{ket\text{-}nap}$)PdCl]

	Bond length (Å)		Bond angles (^{o})
Pd(1)-N(1)	2.123(5)	N(2)-Pd(1)-C(15)	82.1(3)
Pd(1)-N(2)	1.954(5)	N(2)-Pd(1)-N(1)	79.7(2)
Pd(1)-C(15)	1.960(7)	C(15)-Pd(1)-Cl(1)	98.6(2)
Pd(1)-Cl(1)	2.2976(18)	N(1)-Pd(1)-Cl(1)	99.86(15)

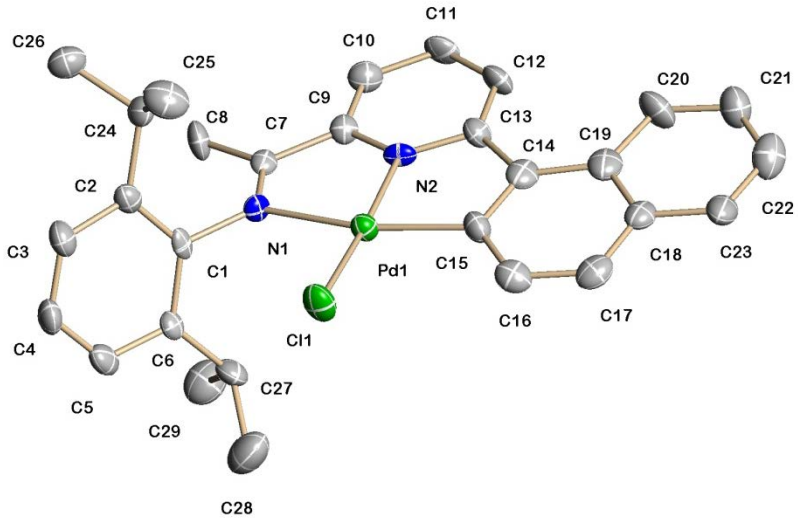

Figure 3.43 | Molecular Structure of *ortho*-[(**L1**$_{ket\text{-}nap}$)PdCl]

Interestingly, the reaction of H**L1**$_{ald\text{-}nap}$ with Na_2PdCl_4 did not result in the formation of the analogous ortho-activated product (**Figure 3.44**). After 24 h of reaction, a large amount of orange precipitate was formed.

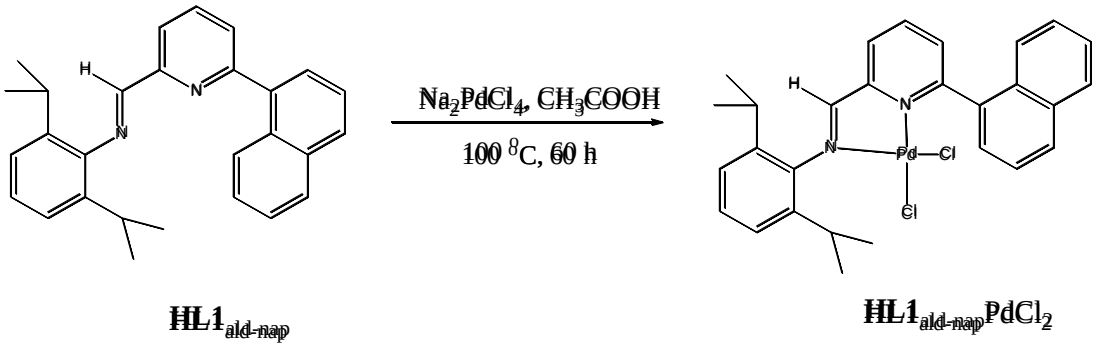

Figure 3.44 | Synthesis of (H**L1**$_{ald\text{-}nap}$)$PdCl_2$

After filtration, the orange powder, which was extremely insoluble in organic solvents, was dissolved in a large volume of dichloromethane and layered with hexane from which orange crystals suitable for single crystal X-Ray diffraction study were obtained. The X-Ray results confirmed that the product was the non C-H activated di-chloride complex of H**L1**$_{ald\text{-}nap}$ (**Figure 3.45** and **Table 3.19**). The extreme insolubility of the this complex (H**L1**$_{ald\text{-}nap}$)$PdCl_2$, that may be an "intermediate" in the reaction pathway, may explain why C-H activation did not occur for this pro-ligand H**L1**$_{ald\text{-}nap}$. Once (H**L1**$_{ald\text{-}nap}$)$PdCl_2$

had been formed and had precipitated out of the solution, further reaction to give a C-H activation species could not occur.

Table 3.19: Selected bond lengths (Å) and angles (°) for (H**L1**$_{ald\text{-}nap}$)$PdCl_2$

	Bond length (Å)		Bond angles (°)
Pd(1)-N(1)	2.088(6)	C(6)-N(1)-Pd(1)	110.5(6)
Pd(1)-N(2)	2.006(7)	N(2)-Pd(1)-N(1)	79.4(3)
Pd(1)-Cl(1)	2.292(2)	C(7)-N(2)-Pd(1)	115.0(6)
Pd(1)-Cl(2)	2.266(2)	N(1)-Pd(1)-Cl(1)	99.0(2)

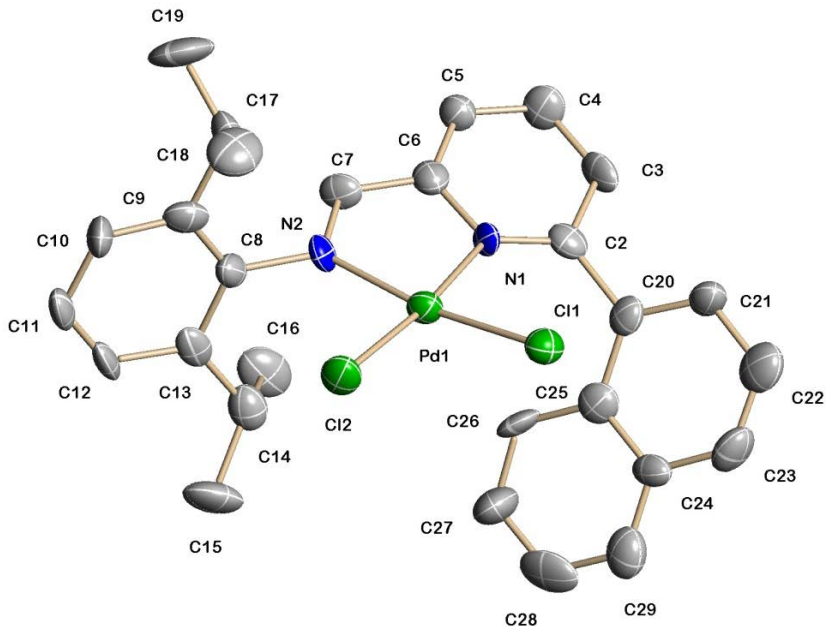

Figure 3.45 | Molecular Structure of (H**L1**$_{ald\text{-}nap}$)$PdCl_2$

3.4.5 C-H activation of H**L1**$_{ket\text{-}nap}$ with $PdCl_2(NCMe)_2$

Following the C-H activation reactions with Na_2PdCl_4, the C-H activation of H**L1**$_{ket\text{-}nap}$ with another palladium (II) chloride—$PdCl_2(NCMe)_2$ —was also investigated (**Figure 3.46**).

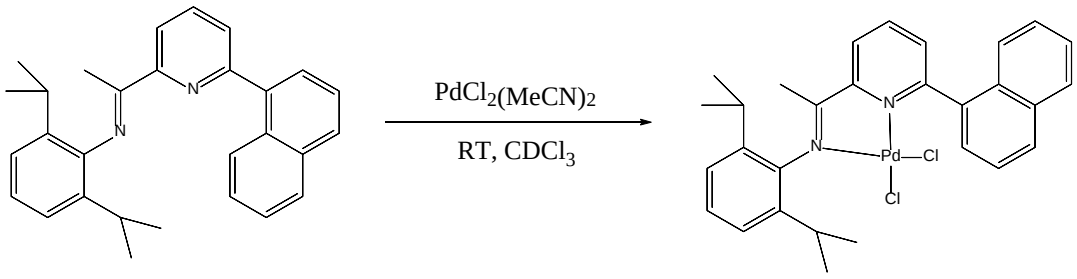

HL1$_{ket\text{-}nap}$ **HL1**$_{ket\text{-}nap}$$PdCl_2$

Figure 3.46 | Synthesis of (H**L1**$_{ket\text{-}nap}$)$PdCl_2$

After overnight reaction at room temperature in an NMR tube, crystals suitable for single crystal X-ray diffraction had precipitated from the solution. The X-ray structural investigation revealed that the structure of the resultant complex was the non C-H activated product [(H**L1**$_{ket\text{-}nap}$)$PdCl_2$] (**Figure 3.47** and **Table 3.20**).

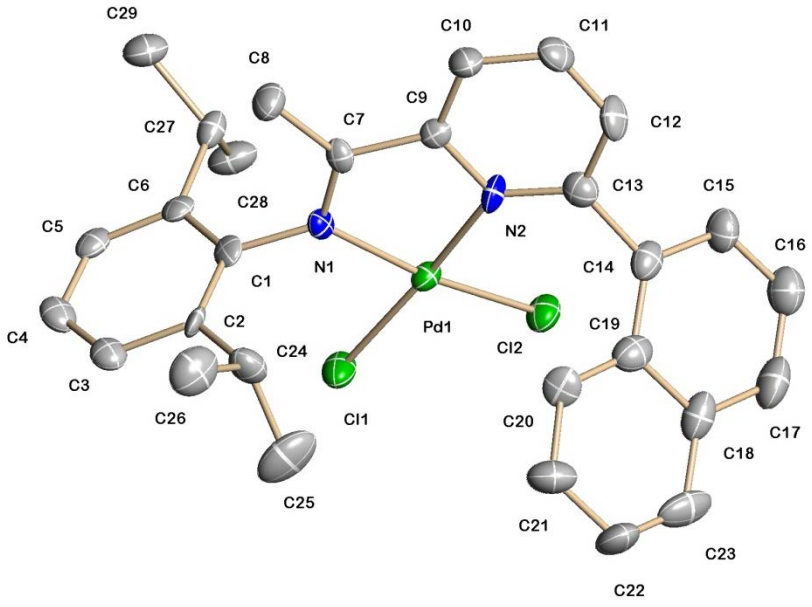

Figure 3.47 | Molecular Structure of (H**L1**$_{ket\text{-}nap}$)$PdCl_2$

Table 3.20: Selected bond lengths (Å) and angles (°) for (H**L1**$_{ket\text{-}nap}$)$PdCl_2$

	Bond length (Å)		Bond angles (°)
Pd(1)-N(1)	2.010(6)	C(7)-N(1)-Pd(1)	114.7(5)
Pd(1)-N(2)	2.059(6)	N(2)-Pd(1)-N(1)	80.4(3)

Pd(1)-Cl(1)	2.270(2)	C(9)-N(2)-Pd(1)	111.3(5)
Pd(1)-Cl(2)	2.298(2)	N(1)-Pd(1)-Cl(1)	93.56(19)

3.4.6 Exchange of –Cl for –OAc

To lay the ground work for the following study on the interconversion chemistry of the peri- and ortho- C-H activated products of H**L1**$_{ket\text{-}nap}$, the acetate-chloride exchange reaction, to generate the ortho-activated palladium acetate complex of H**L1**$_{ket\text{-}nap}$, was investigated. In the first attempt, a dichloromethane solution of ortho-[(**L1**$_{ket\text{-}nap}$)PdCl] was stirred overnight at room temperature with a saturated sodium acetate solution, from which only the unreacted starting materials were obtained (**Figure 3.48**).

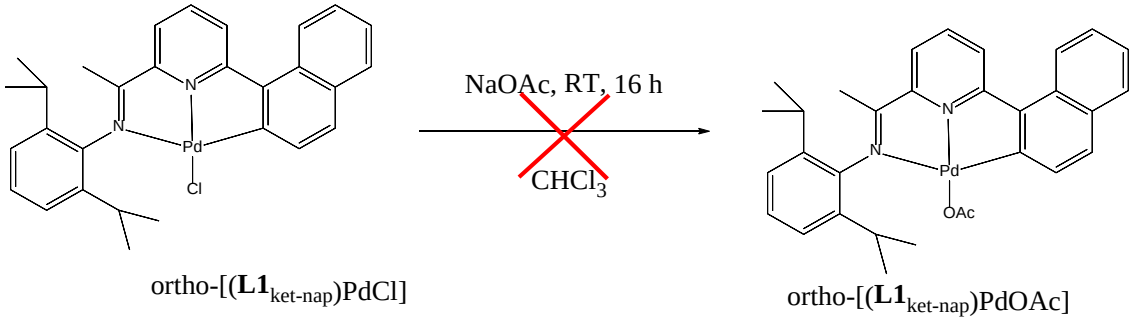

ortho-[(**L1**$_{ket\text{-}nap}$)PdCl] ortho-[(**L1**$_{ket\text{-}nap}$)PdOAc]

Figure 3.48 | Failed synthesis of ortho-[(**L1**$_{ket\text{-}nap}$)PdOAc]

Since the exchange of the chloride with acetate had not been successful with NaOAc, a silver salt—AgOAc—was used instead, since the precipitation of AgCl would be expected to drive the reaction in the desired direction. The reaction of ortho-[(**L1**$_{ket\text{-}nap}$)PdCl] with 1 equivalent of AgOAc in chloroform at room temperature yielded the expected acetate analogue of the complex in a quantitative yield (**Figure 3.49**). After the filtration of the AgCl precipitate and evaporation of the solvent, ortho-[(**L1**$_{ket\text{-}nap}$)PdOAc] was obtained as an orange solid with excellent purity. The X-Ray crystal structure of the complex confirmed the exchange of the chloride for acetate had been achieved (**Figure 3.50** and **Table 3.21**).

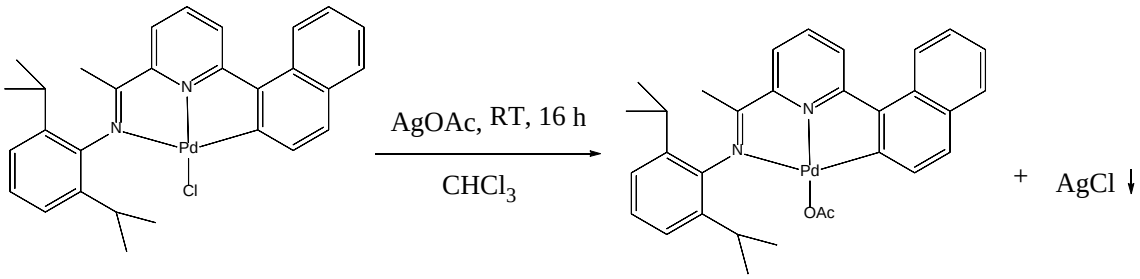

Figure 3.49 | Synthesis of *ortho*-[(**L1**$_{ket-nap}$)PdOAc]

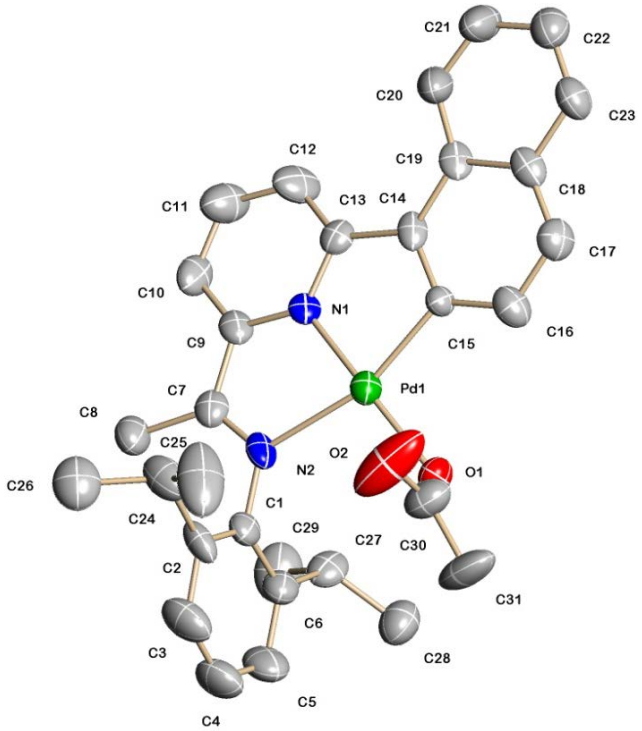

Figure 3.50 | Molecular Structure of *ortho*-[(**L1**$_{ket-nap}$)PdOAc]

Table 3.21: Selected bond lengths (Å) and angles (°) for *ortho*-[(**L1**$_{ket-nap}$)PdOAc]

	Bond length (Å)		Bond angles (°)
Pd(1)-N(1)	1.918(6)	N(1)-Pd(1)-C(15)	81.7(3)

Pd(1)-N(2)	2.147(6)	N(2)-Pd(1)-N(1)	79.0(3)
Pd(1)-C(15)	1.974(7)	C(15)-Pd(1)-O(1)	98.8(3)
Pd(1)-O(1)	2.033(5)	N(2)-Pd(1)-O(1)	100.6(2)

3.4.7 Interconversion chemistry

Given the interesting regiospecific C-H activations on the naphthyl ring, a series of experiments were tried to explore the interconversion of the peri- and ortho-activated materials. Thus, the non-activated dichloride complex (H**L1**$_{ket\text{-}nap}$)$PdCl_2$ was heated in toluene or in acetic acid. Heating in toluene for 12 h at 60 ^{o}C gave 70 % of the starting material and a 15%:15% mixture of the peri- and ortho- activated products. No changes in these ratios were observed on further heating.

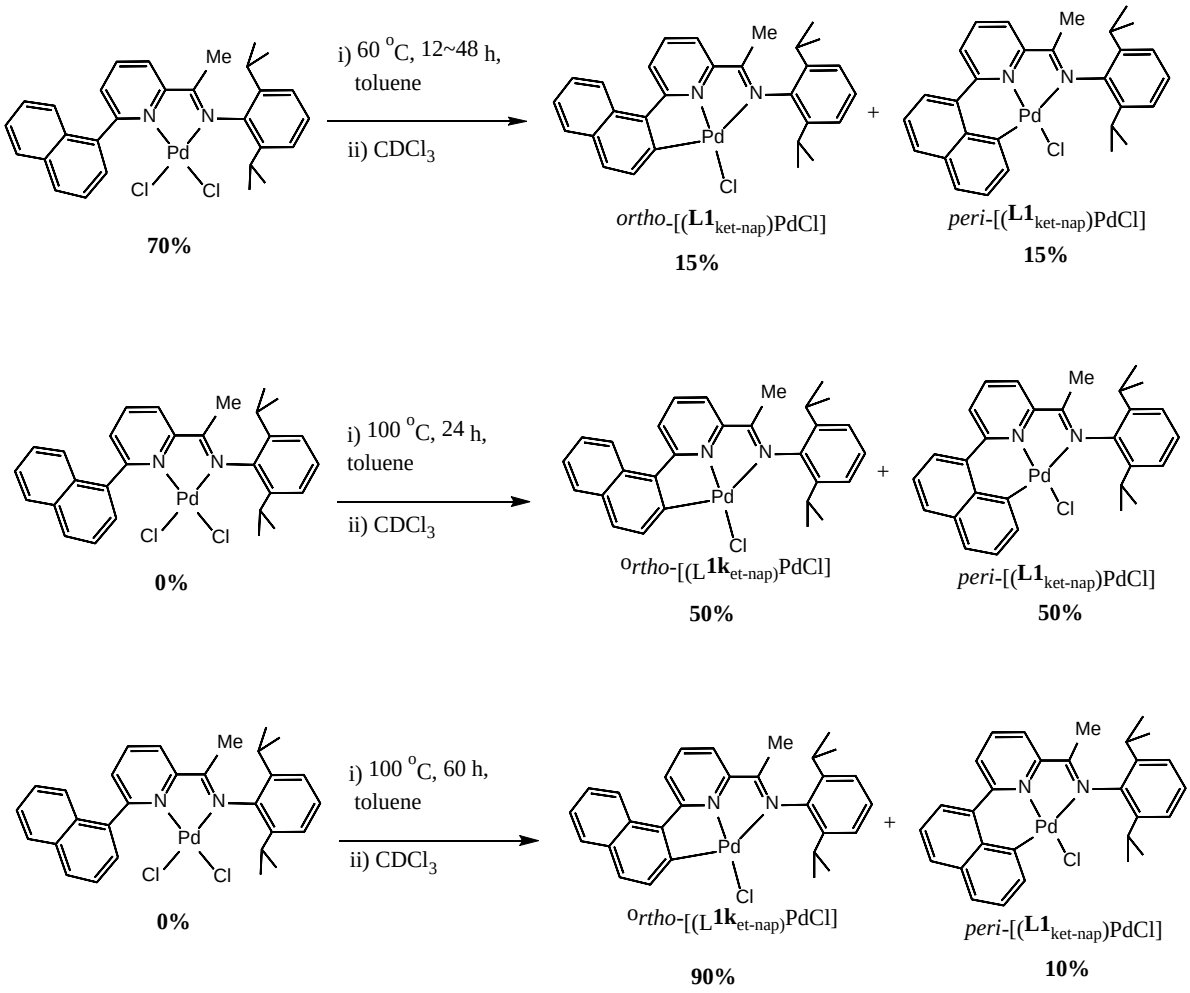

Figure 3.51 | Heating (H**L1**$_{ket\text{-}nap}$)$PdCl_2$ in toluene at 60/100 ^oC

On raising the temperature to 100 ^oC, a 50:50 mixture of the peri- and ortho-activated products were obtained after 24h, with no starting material. Further heating at 100 ^oC for 60 h resulted in the conversion of the peri-activated product into ortho-activated species to leave the products in a final ratio of 10:90 (**Figure 3.51**). Undertaking the same experiments with a different solvent, i.e. acetic acid, gave almost exclusively the ortho-activated product after 12h, with a minor amount of the peri-species (**Figure 3.52**). After heating for 60 h, the amount of the peri-activated product had dropped to less than 5%. Alternatively, heating the 50:50 mixture, which had been obtained from the experiment in toluene, in acetic acid led to the same results (*peri*- to *ortho*- 1:9). To back up this result, heating of a pure sample of *peri*-[(**L1**$_{ket\text{-}naph}$)PdCl] at 100 ^oC in acetic acid was monitored for 60 h and, again, the same results (*peri*- to *ortho*- 1:9) were obtained as above. This suggests that, in acetic acid, the C-H activation prefers the ortho- position of the naphthyl ring.

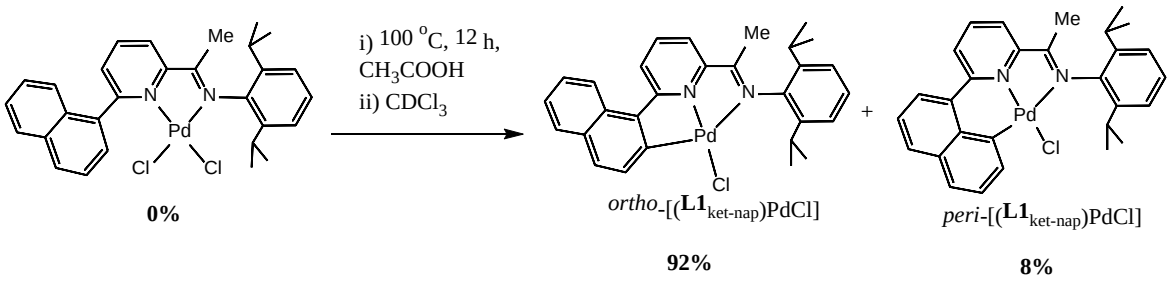

0%

ortho-[(**L1**$_{ket\text{-}nap}$)PdCl]

92%

peri-[(**L1**$_{ket\text{-}nap}$)PdCl]

8%

Figure 3.52 | Heating (H**L1**$_{ket\text{-}nap}$)$PdCl_2$ in acetic acid at 100 ^oC

To further confirm the interconversion between the peri- and ortho-activated products, the C-H activation of the pro-ligand H**L1**$_{ket\text{-}naph}$ was carried out in deuterated acetic acid. The proton NMR spectrum of the product revealed that the product formed is an ortho-activated species, in which the peri-proton of the naphthyl ring has been deuterated (**Figure 3.53**). These results confirm that there is interconversion between *peri*-[(**L1**$_{ket\text{-}naph}$)PdCl] and *ortho*-[(**L1**$_{ket\text{-}naph}$)PdCl] in acetic acid. The C-H activation initially occurs at the peri-position and this species converts into the ortho-activated product at a higher temperature and over a longer time.

On the other hand, reaction of the non activated complex (H**L1**$_{ket\text{-}nap}$)$PdCl_2$ with 2 equivalents of AgOAc gave the peri- C-H activated AgCl adduct *peri*-[(**L1**$_{ket\text{-}naph}$)PdOAc]·AgCl rather than the non activated di-acetate analogue after overnight of reaction at RT (**Figure 3.54**), which is evidenced by the presence of signals for only 12 aromatic protons in the proton NMR spectrum of this AgCl adduct. The subsequent exchange of (-OAc.AgCl) for -Cl by reaction with saturated sodium chloride solution gives peri-[(**L1**$_{ket\text{-}naph}$)PdCl], which can be evidenced by proton NMR spectroscopy (**Figure 3.54**). This suggests that the rapid *peri*- C-H activation of the putative [(H**L1**$_{ket\text{-}nap}$)$Pd(OAc)_2$] intermediate occurs rather than the isolation of the non-activated product seen for palladium-dichloride complex (H**L1**$_{ket\text{-}nap}$)$PdCl_2$.

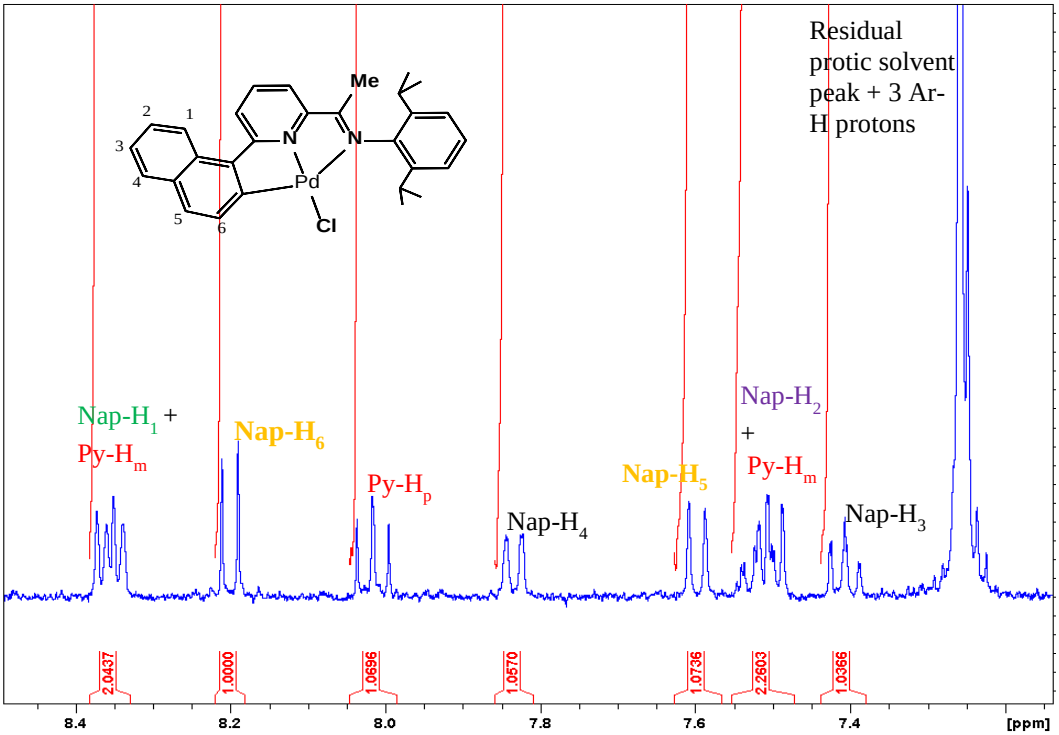

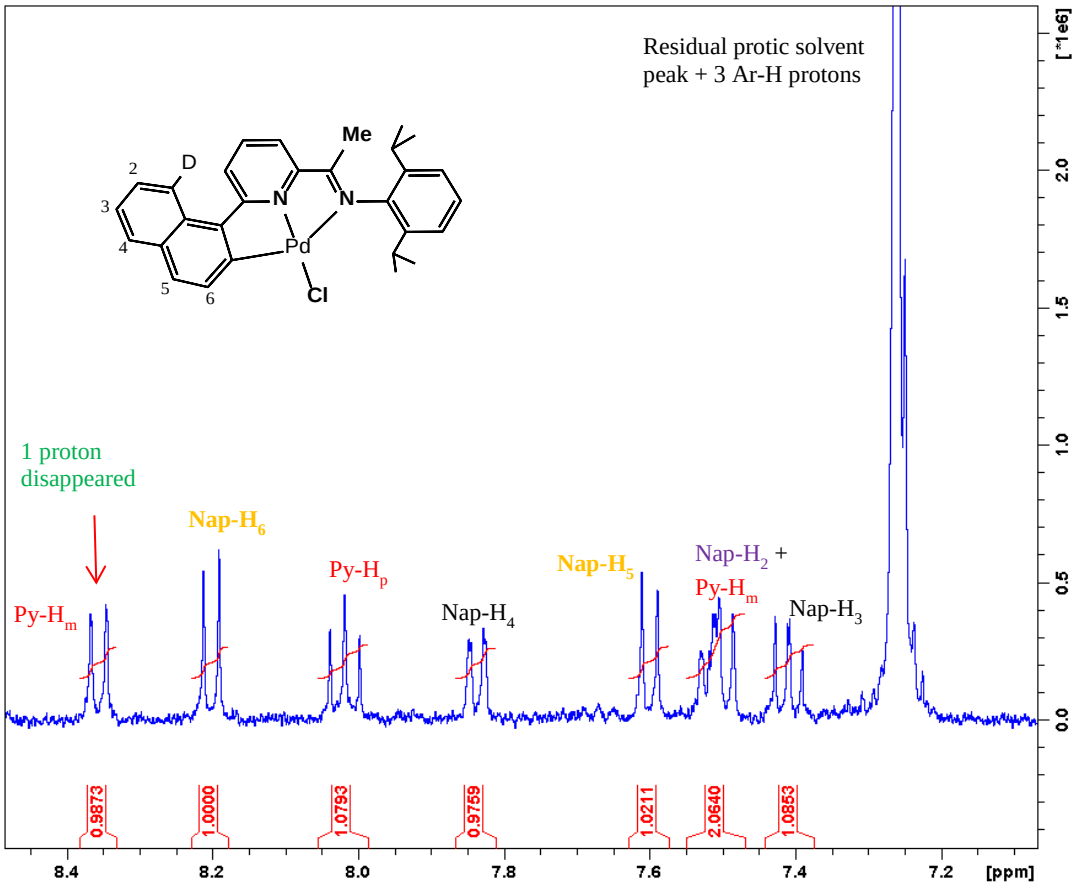

Figure 3.53 | *ortho*-Palladated [(**L1**$_{dipp}$ketimine)PdCl]: protio- versus deuterio-labelled *peri*-position

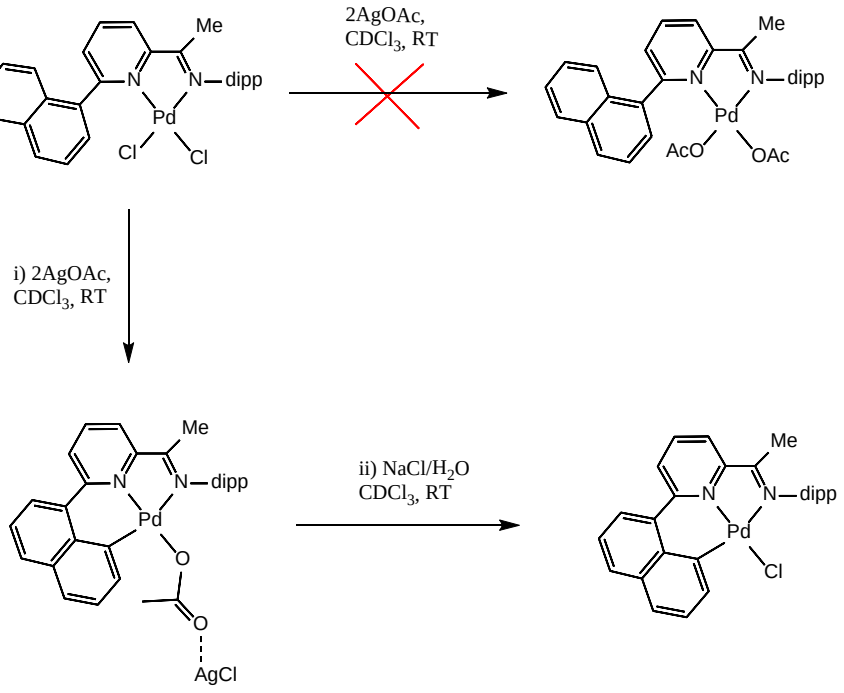

Figure 3.54 | Reaction of (H**L1**$_{ket\text{-}nap}$)$PdCl_2$ with 2 eq. of AgOAc

3.5 **Structural discussion on the palladium pincer complexes:** single crystal X-ray diffraction studies

The tridentate palladium complexes synthesized and characterized in this chapter generally adopt a square planar geometry which is typical for palladium pincer complexes. However, there are slight differences in the bond lengths between the different types of palladium species. In the cases of 5- or 6-membered chelate rings, the bond angles at palladium also vary. Thus, the bond lengths and angles of the palladium pincer complexes of ligands H**L1**$_{o\text{-}tol}$, H**L1**$_{ket\text{-}nap}$ and H**L2/3**$_{nap}$ are summarized and compared in **Tables 3.22** and **3.23**.

The N_{Py}-Pd-C and N_{Py}-Pd-$N_{imine/amine}$/$O_{alcohol}$ angles in the 5-membered chelate rings, i.e. ortho-[(**L1**$_{ket\text{-}nap}$)PdCl] and **L3**$_{nap}$PdCl, are obviously smaller (closer to 90^o) than those in the 6-membered chelating systems—*peri*-[(**L1**$_{ket\text{-}nap}$)PdCl] and **L2**$_{nap}$PdCl, indicating that the 5-membered chelate systems suit the square planaer geometry of the palladium complexes better than the 6-membered chelate rings. This explains why the ortho-[(**L1**$_{ket\text{-}nap}$)PdCl] being the thermodynamically stable product while its peri-analogue is the kinetically favoured one.

Table 3.22: Bond length (Å) for the palladium pincer complexes

Complex	Pd-C	Pd-N_{Py}	Pd-N_{imine}	Pd-N_{amine}	Pd-$O_{alcohol}$	Pd-Cl	Pd-OAc
L1$_{o\text{-}tol}$PdOAc	1.960(7)	1.958(5)	2.171(5)	-	-	-	2.034(4)
L1$_{o\text{-}tol}$PdCl	1.977(5)	1.952(4)	2.161(4)	-	-	2.3167(14)	-
L2$_{o\text{-}tol}$PdOAc	1.960(3)	1.956(2)	-	2.221(2)	-	-	2.056(2)
L2$_{o\text{-}tol}$PdCl	1.970(4)	1.964(3)	-	2.205(3)	-	2.313(10)	-
L3$_{o\text{-}tol}$PdOAc	1.938(6)	1.948(4)	-	-	2.174(4)	-	2.042(4)
L3$_{o\text{-}tol}$PdCl	1.948(4)	1.966(3)	-	-	2.211(3)	2.3335(11)	-

Peri-[(**L1**$_{ket\text{-}nap}$)PdOAc]	1.978(3)	1.996(2)	2.111(2)	-	-	-	2.029(2)
Peri-[(**L1**$_{ket\text{-}nap}$)PdCl]	1.987(3)	2.018(2)	2.104(2)	-	-	2.326(8)	-
L2$_{nap}$PdOAc	1.981(5)	1.990(4)	-	2.171(4)	-	-	2.035(4)
L2$_{nap}$PdCl	1.983(4)	2.013(3)	-	2.158(3)	-	2.313(11)	-
L3$_{nap}$PdOAc	1.957(7)	1.952(6)	-	-	2.139(5)	-	2.040(5)
L3$_{nap}$PdCl	1.978(4)	1.962(13)	-	-	2.186(11)	2.303(5)	-

Table 3.23: Bond angles (°)- 5-membered vs. 6-membered

Complexes	Ring type	N_{Py}-Pd-C	N_{Py}-Pd-$N_{imine/amine}$	N_{Py}-Pd-$O_{alcohol}$
Peri-[(**L1**$_{ket\text{-}nap}$)PdCl]	6-membered	94.14(11)	80.68(9)	-
Ortho-[(**L1**$_{ket\text{-}nap}$)PdCl]	5-membered	82.1(3)	79.7(2)	-
L2$_{nap}$PdCl	6-membered	93.31(14)	83.02(12)	-
L3$_{nap}$PdCl	5-membered	82.5(3)	-	78.4(2)

The two types of complexes, i.e. the palladium acetate species and their chlorinated analogues, exhibit very similar yet slightly different structures. **L2**$_{o\text{-}tolyl}$PdOAc and **L2**$_{o\text{-}tolyl}$PdCl, for example, exhibit a distorted square-planar coordination geometry. In both structures, the palladium atom is coordinated by nitrogen atoms from the pyridine and amine groups and by one carbon atom, C(16), from the 6-phenyl ring. The square-planar geometry is completed by an oxygen atom, O(1) from an acetate group in **L2**$_{o\text{-}tolyl}$PdOAc, and by a chloride atom in **L2**$_{o\text{-}tolyl}$PdCl. The slightly longer Pd-N_{amine} bond in **L2**$_{o\text{-}tolyl}$PdOAc as compared to **L2**$_{o\text{-}tolyl}$PdCl is probably due to an intramolecular hydrogen bonding between the acetate unit and the hydrogen on the amine group. The Pd(1)-C(16) bond lengths of either structure match well the values reported for other pincer Pd^{II} systems.[55] The two bite angles [N(2)-Pd(1)-C(16): 81.78(11)° in **L2**$_{o\text{-}tolyl}$PdOAc; 81.60(15)° in **L2**$_{o\text{-}tolyl}$PdCl; N(1)-Pd(1)-N(2): 81.84(10)° in **L2**$_{o\text{-}tolyl}$PdOAc ; 81.88(12)° in **L2**$_{o\text{-}tolyl}$PdCl] are comparable in either structure, while the coordination angle N(2)-Pd(1)-

O(1) of 174.68(9)° in **L2**$_{o\text{-}tolyl}$PdOAc and the coordination angle N(2)-Pd(1)-Cl(1) of 179.05(9)° in **L2**$_{o\text{-}tolyl}$PdCl are significantly different. In both solid-state structures, the 2,6-diisopropylphenyl moiety is, as expected, tilted away from the coordination plane, probably due to the interactions between the acetate and CMe_2.

3.6 Reactions of H**L1**$_{ket\text{-}nap}$ and H**L2**$_{nap}$ with K_2PtCl_4

After seeing different site activations on the napthyl moiety with different palladium salts, we were intrigued to look at the C-H activation of these naphthyl-armed ligands with a different metal. Hence, the reactions of two naphthyl-armed pro-ligands H**L1**$_{ket\text{-}nap}$ and H**L2**$_{nap}$ **with** K_2PtCl_4 were investigated. The pro-ligand H**L1**$_{ket\text{-}nap}$ and K_2PtCl_4 were heated at reflux in acetic acid for 60 h to give a dark red precipitate (**Figure 3.55**).

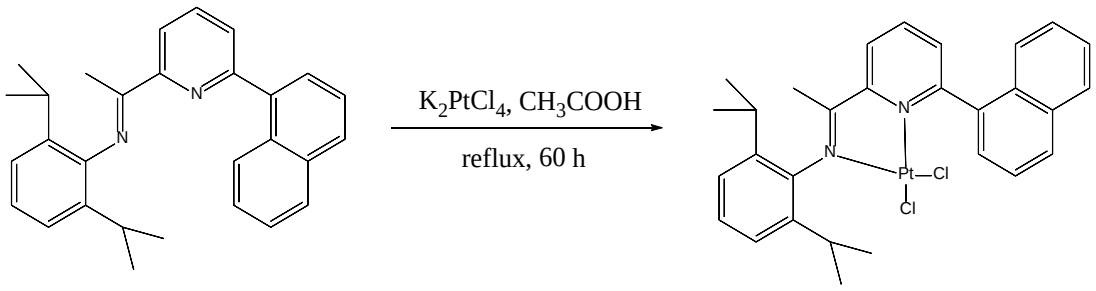

Figure 3.55 | C-H activation of H**L1**$_{ket\text{-}nap}$ with K_2PtCl_4

After filtration and recrystallization, the product was obtained as a red powder. The aromatic proton signals were mixed with the residual proton signal of the $CDCl_3$ thus were difficult to give an accurate integration. Hence, the proton NMR spectroscopy was taken in deuterated dichloromethane. The integration of the aromatic proton signals revealed thirteen Aryl/Pyridine-protons in the molecule, which indicated the generation of the non C-H activated product H**L1**$_{ket\text{-}nap}$ $PtCl_2$. The FAB analysis of the complex showed a peak at 642.2257 m/z, which is assigned to the $[(M\text{-}2Cl)+MeCN]^{2+}$ peak (M = $C_{29}H_{30}N_2Cl_2Pt$), confirming the product to be the non activated bidentate species. The reason why the C-H activation is not observed in this reaction might due to the insolubility of the bidentate complex H**L1**$_{ket\text{-}nap}$ $PtCl_2$ in acetic acid.

The same reaction conditions were used in the synthesis of *ortho*-[(**L2**$_{nap}$)PtCl] (**Figure 3.56**). ^{1}H NMR spectroscopy of the product showed 12 protons in the aromatic region, confirming the C-H activation of naphthyl ring had been successful. As seen before with

the previous ligands when using Na_2PdCl_4, at high temperature and in acetic acid, this reaction gave the ortho-activated product. During the recrystallization, red crystals suitable for single crystal X-Ray diffraction were grown. The X-Ray results confirmed the structure of the product to be the ortho-activated platinum complex in solid state (**Figure 3.57** and **Table 3.24**). The reason why this amine ligand undergoes C-H activation with K_2PtCl_4, while its ketimine analogue does not, might be that the bidentate complex of the ligand has a better solubility in acetic acid, thus enables the reaction to proceed to the C-H activation step in solution.

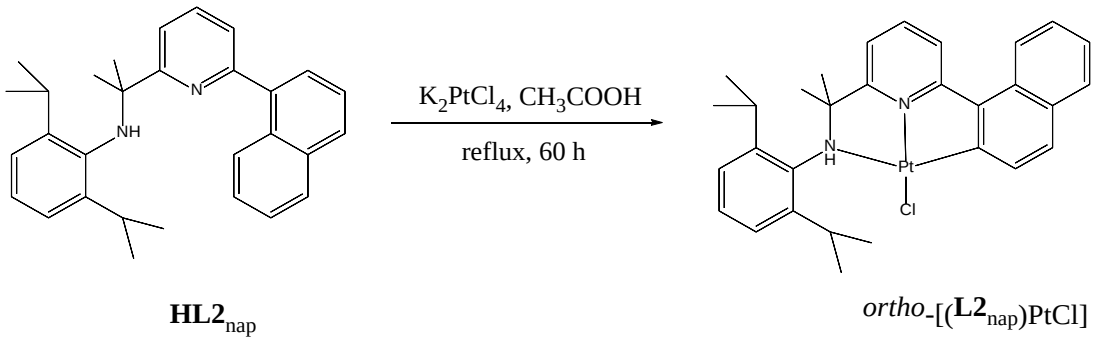

HL2$_{nap}$ *ortho*-[(**L2**$_{nap}$)PtCl]

Figure 3.56 | Synthesis of *ortho*-[(**L2**$_{nap}$)PtCl]

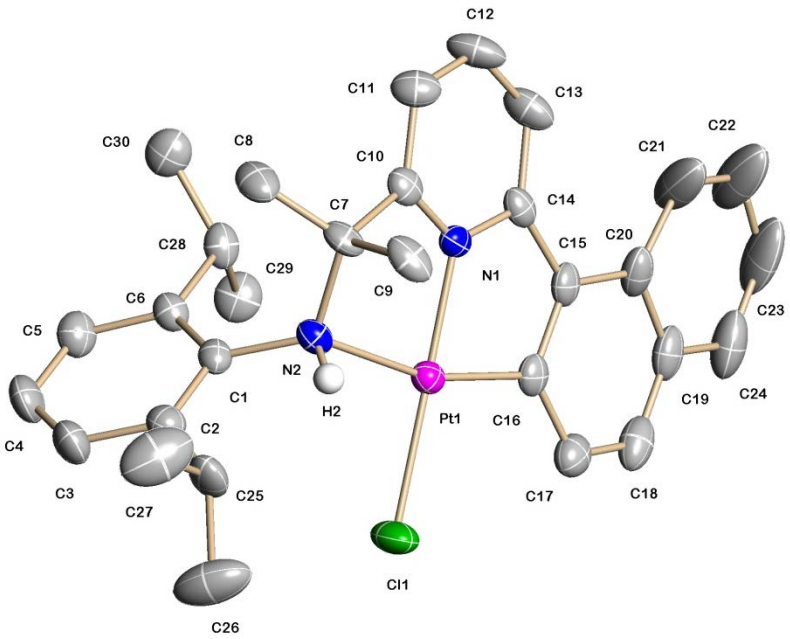

Figure 3.57 | Molecular Structure of *ortho*-[(**L2**$_{nap}$)PtCl]

Table 3.24: Selected bond lengths (Å) and angles (°) for *ortho*-[(**L2**$_{nap}$)PtCl]

	Bond length (Å)		Bond angles (°)
Pt(1)-N(1)	1.948(3)	N(1)-Pt(1)-C(16)	81.25(15)
Pt(1)-N(2)	2.170(3)	N(2)-Pt(1)-N(1)	82.87(12)
Pt(1)-C(16)	1.973(4)	C(16)-Pt(1)-Cl(1)	100.62(12)
Pt(1)-Cl(1)	2.2941(11)	N(2)-Pt(1)-Cl(1)	95.34(8)

3.7 Summary and conclusions

The reactions of the aryl-containing pincer ligands H**L1-3** with various transition metal salts are discussed in this chapter. The pincer complexes obtained are fully characterized by proton/carbon NMR, IR and ESMS spectroscopies and, in most cases, by X-Ray diffraction. The 'tolyl-armed' ligands H**L1**$_{o\text{-tolyl}}$, H**L2**$_{o\text{-tolyl}}$ and H**L3**$_{o\text{-tolyl}}$ were successfully C-H activated at the ortho-site while the activation of 'site-blocked' ligands H**L1**$_{2,6\text{-Me2Ph}}$ and H**L1**$_{2,4,6\text{-Me3Ph}}$ gave poor yielding reactions with products arising from pyridine or Ar-CH_3 C-H activation reactions.

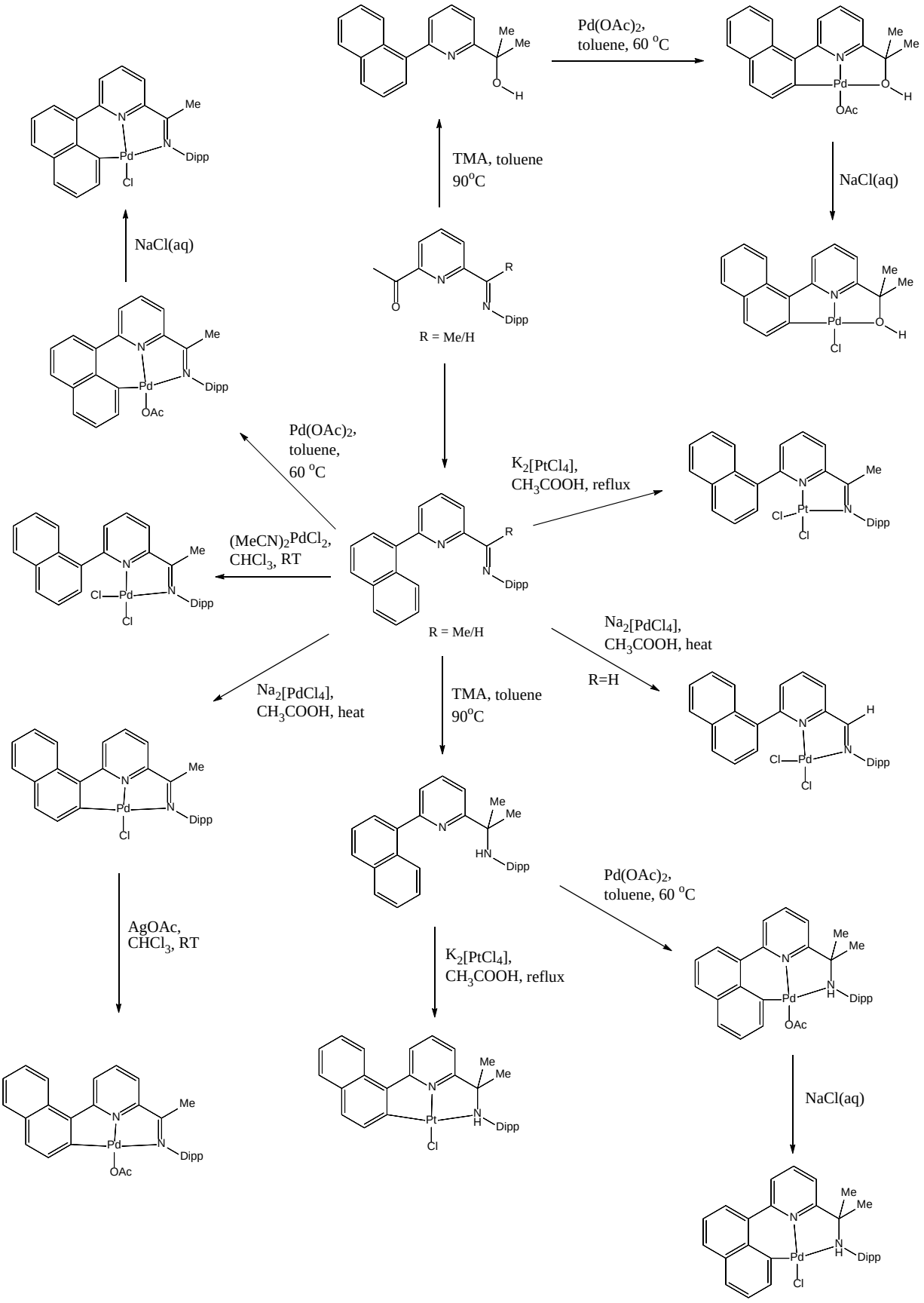

Scheme 3.1: C-H activations with ‘naphthyl-armed’ ligands

The isolation and characterisation of the intermediate complex during the C-H activation process has been achieved in the case of the bipyridyl ligand H**L1**$_{py\text{-}nap}$. The ketimine, bipyridine, aldimine and amine naphthyl-armed ligands H**L1**$_{ket\text{-}nap}$, H**L1**$_{py\text{-}nap}$, H**L1**$_{ald\text{-}nap}$ and H**L2**$_{nap}$ all gave the peri-activated products upon reaction with $Pd(OAc)_2$, whilst their alcohol-armed analogue, H**L3**$_{nap}$, exhibited ortho-C-H activation on the naphthyl moiety. This is most likely to be due to the oxygen on the hydroxyl group being a weaker donor than nitrogen.

The peri- and ortho-activations on the naphthyl ring in the previous ligands H**L1**$_{ket\text{-}nap}$ and H**L3**$_{nap}$ revealed the influence of the different donor atoms upon C-H activation, thus the influence of using a different palladium source was studied subsequently. Since the research was aimed at the activation of different sites on the naphthyl ring, the naphthyl-armed imine ligands H**L1**$_{ket\text{-}nap}$ and H**L1**$_{ald\text{-}nap}$ were chosen to be examined in reaction with two other palladium salts—Na_2PdCl_4 and $PdCl_2(MeCN)_2$. The reaction of H**L1**$_{ket\text{-}nap}$ with $PdCl_2(MeCN)_2$ gave the non C-H activated product H**L1**$_{ket\text{-}nap}PdCl_2$, while with Na_2PdCl_4 the ortho-activated palladium (II) product was obtained exclusively.

Without much surprise, the platinum counterpart of Na_2PdCl_4, K_2PtCl_4, also gave the ortho-activated product for ligand H**L2**$_{nap}$. However, upon reaction with H**L1**$_{ket\text{-}nap}$, it gave the non-C-H activated platinum complex (H**L1**$_{ket\text{-}nap}$)$PtCl_2$. In a similar way to the observations for the Pd(II) species, this is considered to due to the insolubility of the intermediate bidentate complex, preventing the C-H activation from proceeding. An overall summary of the reactions of all the 'naphthyl-armed' ligands with various metal salts is illustrated in **Scheme 3.1**.

References

1 M. van der Boom and D. Milstein, *Chem. Rev*., 2003, **103**, 1759.

2 J. Singleton, *Tetrahedron,* 2003, **59**, 1837.

3 D. Bentio-Garagorri and K. Kirchner, *Acc. Chem. Res*., 2008, **41**, 201.

4 N. Selander and K. Szabo, *Dalton Trans*., 2009, 6267.

5 N. Selander and K. Szabo, *Chem. Rev.,* 2011, **111**, 2048.

6 K. Takenaka, M. Minakawa and Y. Uozumi, *J. Am. Chem. Soc*., 2005, **127,** 12273.

7 M. Hung and L. Liang, *Organometallics,* 2004, **23**, 2813.

8 M. Albrecht and G. van Koten, *Angew. Chem., Int. Ed.,* 2001, **40**, 3750.

9 G. Hamasaka, F. Sakuraiab and Y. Uozumi, *Chem. Commun.,* 2015, **51**, 3886.

10 M. Asay and D. Morales-Morales, *Dalton Trans*., 2015, 44, 17432.

11 B. Arndtsen, R. Bergman, T. Mobely and T. Peterson, *Acc. Chem. Res*. 1995, **28**, 154.

12 A. Shilov and G. Shul'pin, *Chem. Rev*., 1997, **97**, 2879.

13 G. Dyker, *Angew. Chem., Int. Ed*., 1999, **38**, 1698.

14 Y. Guari, S. Sabo-Etienne and B. Chaudret, *Eur. J. Inorg. Chem*., 1999, **7**, 1047.

15 V. Ritleng, C. Sirlin and M. Pfeffer, *Chem. Rev.,* 2002, **102**, 1731.

16 A. Ryabov, *Chem. Rev*., 1990, **90**, 403.

17 C. Jun, C. Moon and D. Lee, *Chem. Eur. J.*, 2002, **8**, 2423.

18 F. Kakiuchi, S. Sekine, Y. Tanaka, A. Kamatani, M. Sonoda, N. Chatani and S. Murai, *Bull. Chem. Soc. Jpn.*, 1995, **68**, 62.

19 F. Kakiuchi, T. Sato, M. Yamauchi, N. Chatani and S. Murai, *Chem. Lett*., 1999, 19.

20 C. Lenges and M. Brookhart, *J. Am. Chem. Soc.*, 1999, **121**, 6616.

21 L. Johansson, M. Tilset, J. Labinger and J. Bercaw, *J. Am. Chem. Soc*., 2000, **122**, 10846.

22 H. Zhong, J. Labinger and J. Bercaw, *J. Am. Chem. Soc*., 2002, **124**, 1378.

23 R. Periana, Y. Liu and G. Bhalla, *Chem. Commun*., 2002, 3000.

24 A. Dick, K. Hull and M. Sanford, *J. Am. Chem. Soc.,* 2004, **126**, 2300.

25 M. Boele, G. van Strijdonck, A. de Vries, P. Kamer, J. de Vries and P. van Leeuwen, *J. Am. Chem. Soc*., 2002, **124**, 1586.

26 L. Desai, K. Hull and M. Sanford, *J. Am. Chem. Soc*., 2004, **126**, 9542.

27 K. Orito, A. Horibata, T. Nakamura, H. Ushito, H. Nagasaki, M. Yuguchi, S. Yamashita and M. Tokuda, *J. Am. Chem. Soc*., 2004, **126**, 14342.

28 J. Oxgaard, R. Muller, W. Goddard and R. Periana, *J. Am. Chem. Soc*., 2004, **126**, 352.

29 J. Dupont, C. Consorti and J. Spencer, *Chem. Rev*., 2005, **105**, 2527.

30 D. Leow, G. Li, T.-S. Mei and J.-Q. Yu, *Nature*, 2012, **486**, 518.

31 A. Ryabov, I. Sakodinskaya and A. Yatsimirsky, *J. Chem. Soc., Dalton Trans*., 1985, 2629

32 P. Burger and R. Bergman, *J. Am. Chem. Soc*., 1993, **115**, 10462

33 A. Canty and G. van Koten, *Acc. Chem. Res*., 1995, **28**, 406

34 M. Gomez, J. Granell and M. Martinez, *Organometallics*, 1997, **16**, 2539.

35 M. Gomez, J. Granell and M. Martinez, *J. Chem. Soc., Dalton Trans*., 1998, 37

36 A. Vigalok, O. Uzan, L. Shimon, Y. Ben-David, J. Martin and D. Milstein, *J. Am. Chem. Soc*., 1998, **120**, 12539.

37 C. Webster, Y. Fan, M. Hall, D. Kunz and J. Hartwig, *J. Am. Chem. Soc*., 2003, **125**, 858.

38 M. Lafrance and K. Fagnou, *J. Am. Chem. Soc*., 2006, **128**, 16496.

39 D. Garcia-Cuadrado, P. de Mendoza, A. Braga, F. Maseras and A. Echavarren, *J. Am. Chem. Soc*., 2007, **129**, 6880.

40 D. Davies, S. Donald and S. Macgregor, *J. Am. Chem. Soc*., 2005, **127**, 13754.

41 Y. Boutadla, D. L. Davies, S. A. Macgregor and A. I. Poblador-Bahamonde, *Dalton Trans*., 2009, 5887-5893.

42 M. Pfeffer, N. Sutter-Beydoun, A. De Cian and J. Fischer, *J. Organomet. Chem*., 1993, **453**, 139.

43 D. Narayan, P. Das, A. Biswas and P. Bandypadhyay, *Polyhedron*, 2006, **25**, 2149.

44 D. Narayan, A. Biswas, P. Das, R. Bhawmick and P. Bandypadhyay, *Inorg. Chim. Acta*, 2007, **360**, 2181.

45 I. Phillips and P. Steel, *J. Organomet. Chem*., 1991, **410**, 247.

46 L. Kind, A. Kaus, P. Rys and V. Gramlich, *Helv. Chim. Acta*, 1988, **81**, 307.

47 J. Albert, R. Bosque, J. M. Cadena, S. Delgado and J. Granell, *J. Organomet. Chem.*, 2001, **634**, 83.

48 D. Kalyani, A. Dick, W. Anani and M. Sanford, *Tetrahedron*, 2006, **62**, 11483.

49 D. Hockless, P. Gugger, P. Leung, R. Mayadunne, M. Pabel and S. Wild, *Tetrahedron*, 1997, **53**, 4083.

50 B. O'Keefe and P. Steel, *Organometallics*, 2003, **22**, 1281.

51 K. Gehrig, M. Hugentobler, A. Klaus and P. Rys, *Inorg. Chem*., 1982, **21**, 2493.

52 J. Albert, J. Granell, A. Luque, M. Font-Bardia and X. Solans, *J. Organomet. Chem*., 1997, **545**, 131.

53 K. Nakamoto, *IR and Raman Spectra of Inorganic and Coordination Compounds*, 5th ed., Wiley, New York, 1997, Part B, p.271.

54 C. Bianchini, G. Lenoble, W. Oberhauser, S. Parisel and F. Zanobini, *Eur. J. Inorg. Chem*., 2005, 4794.

55 G. Minghetti, M. Cinellu, G. Chelucci, S. Gladiali, F. Demartin and M. Manassero, *J. Organomet. Chem.*, 1986, **307**, 107.

56 S. Jie, P. Ai, Q. Zhou and B.-G. Li, *J. Organomet. Chem*., 2011, **696**, 1465.

57 Y. Boutadla, D. L. Davies, S. Macgregor and A. Poblador-Bahamonde, *Dalton Trans.*, 2009, 5820.

Chapter Four

Sp^3 C-H activation of alkyl-containing pyridine-based ligands

4.1 Introduction

4.1.1 Transition metal bidentate complexes of pyridine-based ligands—catalytic chelating systems

Transition metal bidentate complexes are of great interest due to their broad applications in light-emiting devices,[1] image display apparatus,[1] electrochemical sensors[2] and, widely recognized, alkene polymerizations.[3] There are myriad chelating ligand systems which can be associated with various transition metals to generate active catalysts to be used in efficient chemical synthesis. For instance, the monoanionic bidentate systems **xi** (**Figure 4.1**) have been studied as homogeneous catalysts not only in Ziegler–Natta-type polymerisations [4–8] but also in asymmetric organic reactions.[9,10] Another important example of this type of chelating ligand systems are the neutral pyridine N-oxide aldimines or ketimines **xii**, which are the neutral analogues of monoanionic systems **xi** (see **Figure 4.1**). Metal complexes of these ligand systems have been reported[11-15] but, in comparison with their phenolic analogues, there is still not sufficient knowledge about their interesting chemistry. Their N,N-chelating counterparts, ligand system **xiii** in **Figure 4.1**, have recently been explored by the preparation of their transition metal complexes and analyzing the structural differences and coordination behaviour of these ligand systems,[16] although the catalytic activities of the bidentate complexes obtained have not been described.

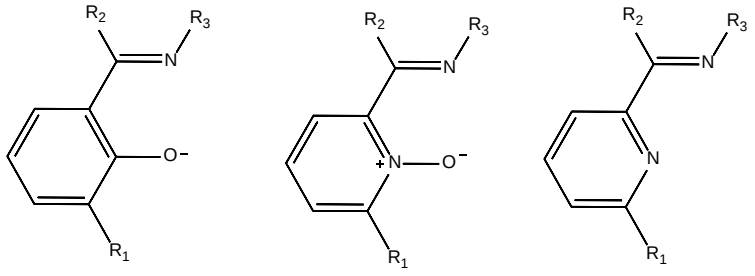

Figure 4.1 | Bidentate chelating ligand systems

Elsewhere, the *N,N*-chelating ligand systems are reported to be highly active in catalytic olefin polymerization reactions upon complexation with various transition metals.[17] Among them, palladium and nickel bidentate complexes of unsymmetrical pyridinylimine ligands are reported to be particularly useful for the polymerization of

norbornene[18] (**Figure 4.2**) because of the unique structure of the pyridinylimine ligands to combine specific features from the bipyridine-type alkene oligomerization catalysts[19] and the sterically hindered α-diimine-based polymerization system.[20]

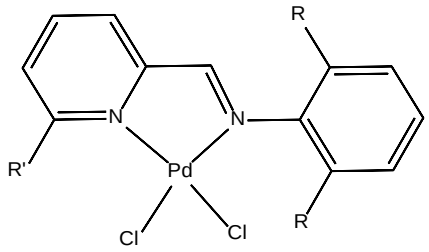

xiv: R= ^{i}Pr; R'= H
xv: R= Me; R'= H
xvi: R= ^{i}Pr; R'= Me

Catalyst	$m_{cat.}$ (mg)	$n_{norbornene}$:$n_{cat.}$	Yield (g)	Conversion (%)
xiv/MAO	25	400	2.16	100
xiv/MAO	25	800	4.22	100
xv/MAO	25	400	2.29	94
xv/MAO	25	800	4.74	98
xvi/MAO	25	400	2.10	100
xvi/MAO	25	800	4.11	100

Figure 4.2 | Palladium bidentate complexes as active catalysts for the polymerization of norbornene[18]

4.1.2 C(sp^3)-H activation reactions with transition metals

The use of transition metal catalyzed C-H activations to achieve highly efficient synthetic routes in organic synthesis has been a great focus in organometallic chemistry over the past decade.[21] As discussed in Chapter 3, the process of C-H activation is widely accepted to go through a pathway recognized as concerted metalation-deprotonation (CMD) or ambiphilic metal-ligand activation (AMLA).[22,23] However, comparing to the extensively studied C(sp^2)-H activation reactions, relatively few examples of C(sp^3)-H activation are known[24] because of the difficulties in cleaving the C(sp^3)-H bonds due to their less acidic nature and their lack of nearby empty low-energy orbitals that can readily interact with the orbitals of the metal.

Examples of sp^3 C-H activations in the presence of C(sp^2)-H bonds using directing groups have been reported. As illustrated in **Figure 4.3**, Sames and co-workers have described a

sp^3 C-H activation directed by an imine group with stoichiometric palladium chloride(II).[25]

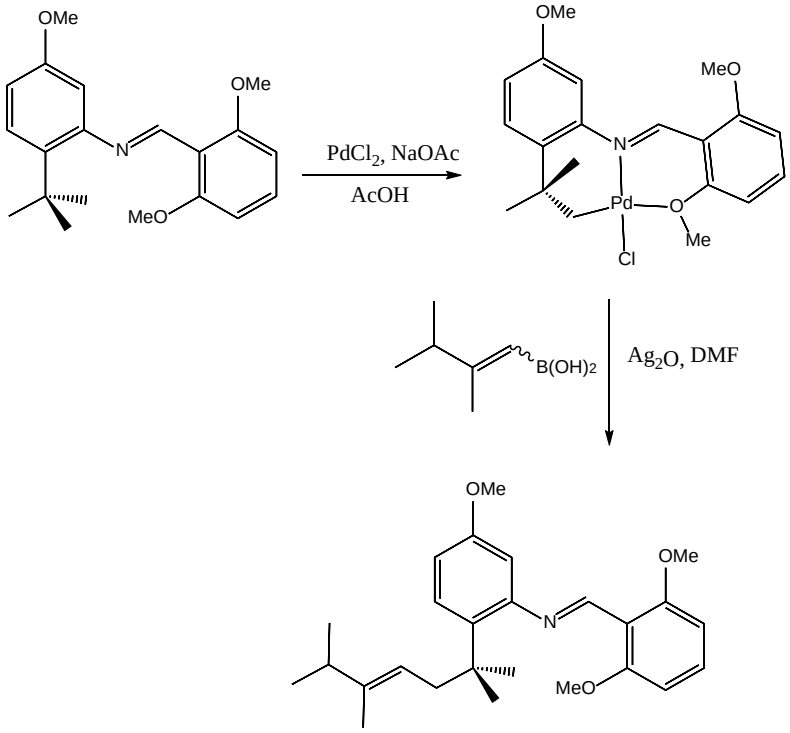

Figure 4.3 | Imine-directed C(sp^3)-H activation [25]

Yu *et al.* have, later, reported the first example of palladium(II)-catalyzed β-arylation of a C(sp^3)-H bond in carboxylic acids with arylboronic reagents (**Figure 4.4**).[26]

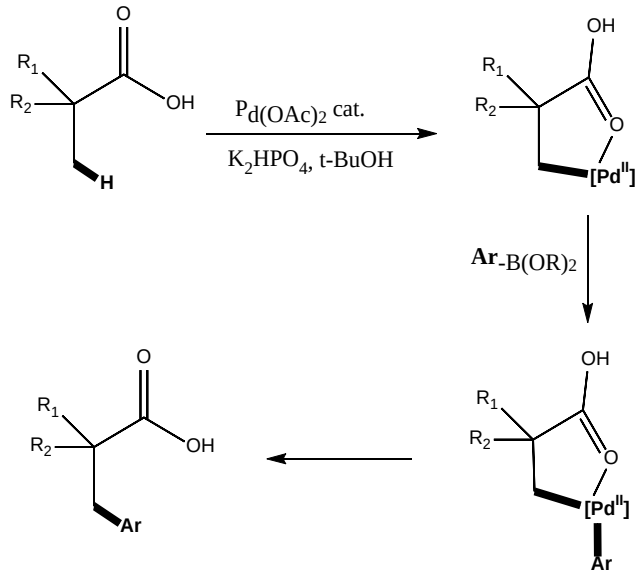

Figure 4.4 | Palladium(II)-catalyzed β-arylation of carboxylic acids [26]

Cross and co-workers reported the first well-established example of undirected C(sp^3)-H activation, in which the C-H activation is considered to proceed via a CMD or AMLA pathway, with the co-operation of the metal and a weakly basic ligand (**Figure 4.5**).[27] Their DFT calculation studies support their assumption that the C-H activation of the α-C(sp^3)-H bond with $[Cp^*IrCl_2]_2$ and NaOAc occurs under kinetic control.

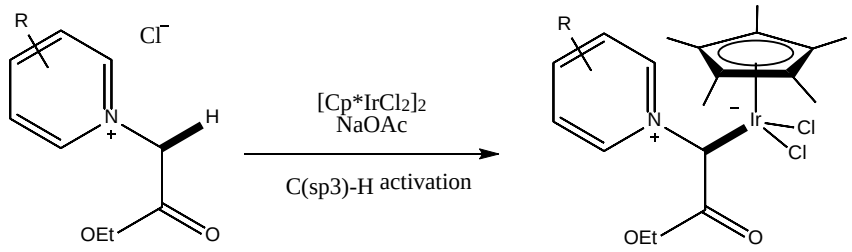

Figure 4.5 | C(sp^3)-H activation to give N-ylide complexes[27]

4.1.3 Aims and objectives

As described above, the activation of a C(sp^3)-H bond has not been studied overwhelmingly but several examples of transition metals activating small molecules through a monodentate coordination have been reported. However, there are scarce examples of transition metal pincer complexes adopting a $C_{(sp3),}N,N$-chelate structure. The alkyl-containing pyridyl ligands H**L4**$_{iPr}$ and H**L4**$_{tBu}$ have been reported to undergo complexation with transition metals such as Fe, Co, Ni.[16] Nevertheless, the complexes obtained adopted the bidentate structure by coordination of the pyridine- and imine-nitrogen atoms (**Figure 4.6**), rather than activating the alkyl arms to give the *C,N,N*-pincer complexes. To the best of our knowledge, no examples of a C(sp^3)-H activation with these types ($N_{imine}N_{py}C_{alkyl}$) of ligands have been described so far.

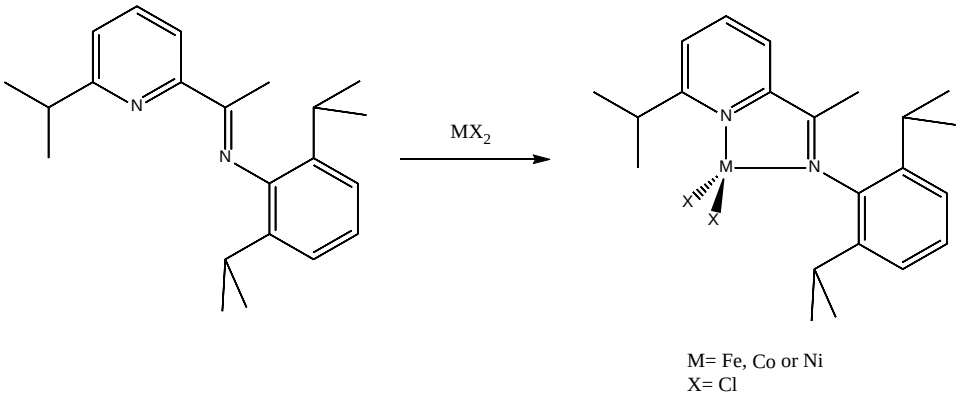

Figure 4.6 | The complexation of transition metals with H**L4**$_{i\text{Pr}}$

Since the palladium chemistry of the aryl-containing *C*,*N*,*N*- and *C*,*N*,*O*- tridentate ligands, i.e. the C(sp^2)-H activation, has been described in detail in the last chapter, the work in this chapter seeks to explore the complexation chemistry of these three alkyl-containing ligands (H**L4**) to examine the potential of C(sp^3)-H activation in these systems.

4.2 C(sp^3)-H activation of alkyl-containing pyridine-based ligands

4.2.1 Reactions with the ethyl-armed ligand H**L4**$_{\text{Et}}$

The attempted C(sp^3)-H activation of H**L4**$_{\text{Et}}$ was initially tried with Pd(OAc)$_2$ at room temperature to 60 ^{o}C in MeOH (**Figure 4.7**). As illustrated in **Figure 4.7**, the reaction of H**L4**$_{\text{Et}}$ with Pd(OAc)$_2$ gives the non C-H activated diacetate product (H**L4**$_{\text{Et}}$)Pd(OAc)$_2$ in a 98% yield at room temperature and at 60 ^{o}C. Raising the reaction temperature or prolonging the reaction time yielded no different results and gave a small amount of palladium black after 48h.

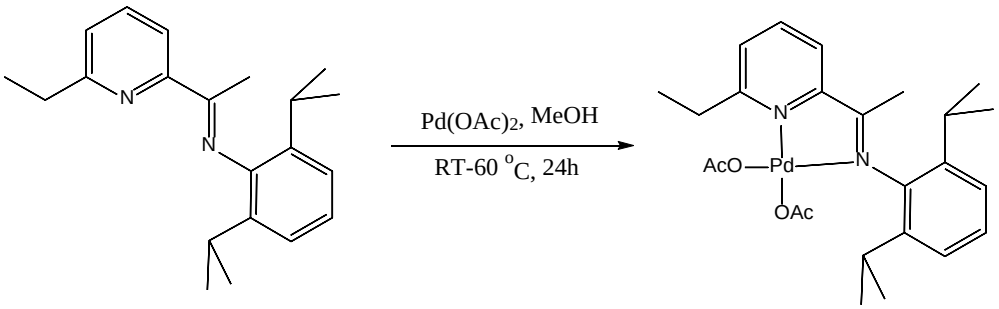

Figure 4.7 | Complexation of H**L4**$_{\text{Et}}$ with Pd(OAc)$_2$

The proton NMR spectrum of the complex revealed two 6H doublets at 1.09 and 1.51 ppm assigned to the four diisopropyl methyl groups. In agreement with this, the ^{13}C NMR spectrum shows two methyl signals for these methyl moieties. Thus, in line with the palladium complexes in Chapter 3, the two ^{i}Pr groups on the diisopropylphenyl moiety are symmetrical along the N-dipp axes while the two methyls on the same ^{i}Pr group are not, hence, resulting in two different proton/carbon environments for these four methyl groups. The two –OAc signals appear at 1.29 and 1.97 ppm respectively, which is consistent with that observed for the other diacetate palladium complexes in the previous chapter. The 3H quartet and 2H triplet, which are indicative of the ethyl moiety, are obviously shifted compared to those resonances for the free ligand, but are still evident in the proton NMR spectrum of the complex, indicating the formation of a non C-H activated product. The FAB analysis revealed a peak at 414.1314; calculated for $C_{21}H_{28}N_2Pd$ $[M\text{-}2OAc]^{2+}$ 414.1319. Single crystals suitable for an X-ray diffraction study were obtained by layering a dichloromethane solution of the complex with hexane. The X-ray crystal structure of the complex strongly supported the other data and confirmed the product to be the diacetate palladium complex of H**L4**$_{Et}$ (**Figure 4.8** and **Table 4.1**).

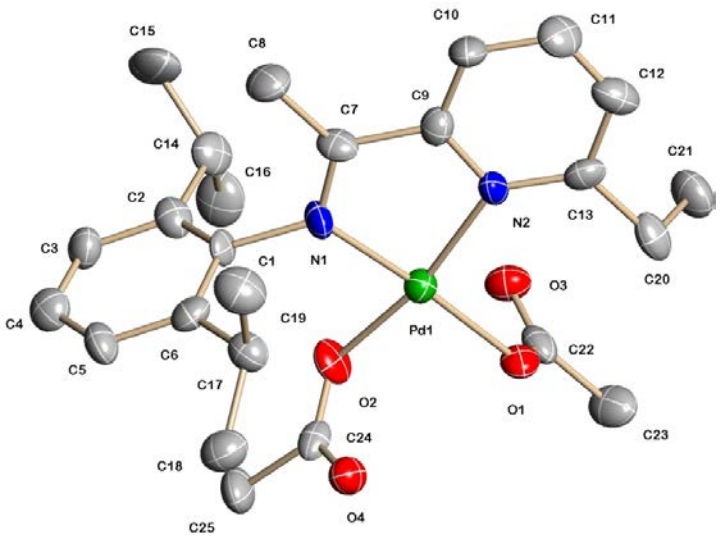

Figure 4.8 | Molecular structure of (H**L4**$_{Et}$)Pd(OAc)$_2$

Table 4.1: Selected bond lengths (Å) and angles (°) for (H**L4**$_{Et}$)Pd(OAc)$_2$

	Bond length (Å)		Bond angles (°)
Pd(1)-N(1)	1.982(6)	C(9)-N(2)-Pd(1)	111.4(6)
Pd(1)-N(2)	2.063(7)	N(2)-Pd(1)-N(1)	80.6(3)
Pd(1)-O(1)	2.014(5)	C(7)-N(1)-Pd(1)	117.7(6)
Pd(1)-O(2)	1.995(6)	N(1)-Pd(1)-O(2)	90.5(3)

The chlorinated analogue of (H**L4**$_{Et}$)Pd(OAc)$_2$ was easily obtained by stirring a dichloromethane solution of the complex with saturated sodium chloride solution (**Figure 4.9**). (H**L4**$_{Et}$)PdCl$_2$ was formed after 1 h at room temperature in quantitative yield. The proton NMR spectrum of the complex indicated the exchange of the –OAc for –Cl had been successful by the absence of the two 3H acetate singlets.

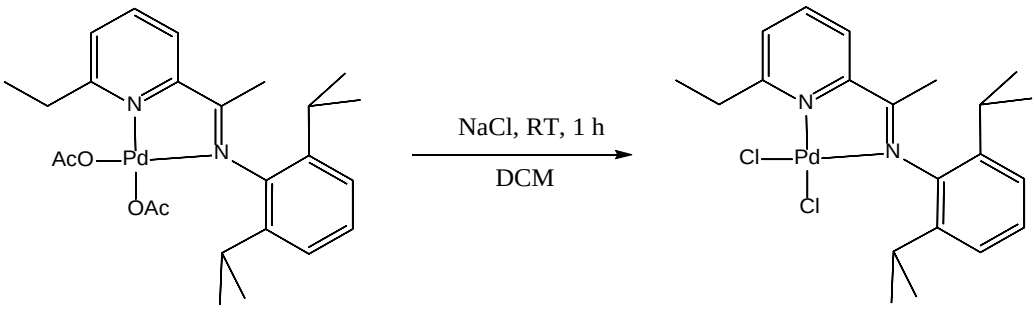

Figure 4.9 | Synthesis of (H**L4**$_{Et}$)PdCl$_2$ by ligand exchange

The same dichloride palladium complex was formed using a second palladium source, Na_2PdCl_4 (**Figure 4.10**). The reaction was undertaken in acetic acid at 100 °C for 24-48 h, and only the bidentate species and trace amounts of the free ligand were detected in the ^{1}H NMR spectrum. Hence, the C(sp^3)-H activation of the ethyl-armed ligand H**L4**$_{Et}$ has not been achieved using either Pd(OAc)$_2$ or Na_2PdCl_4, and only the bidentate palladium complexes were formed.

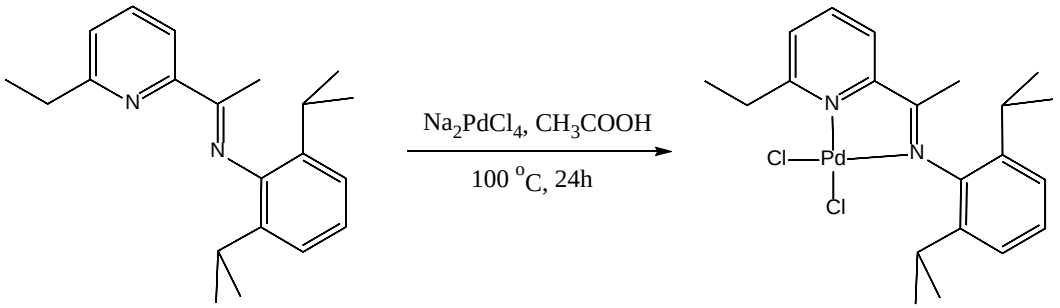

Figure 4.10 | Synthesis of (H**L4**$_{Et}$)$PdCl_2$ with Na_2PdCl_4

4.2.2 Reactions with the isopropyl-armed ligand H**L4**$_{iPr}$

Since the C(sp^3)-H activation of the ethyl-armed ligand H**L4**$_{Et}$ had not been successful, the reaction of the isopropyl-armed ligand H**L4**$_{iPr}$ with $Pd(OAc)_2$ was tried next. The reaction at room overnight temperature yielded the non activated diacetate species (H**L4**$_{iPr}$)$Pd(OAc)_2$ (**Figure 4.11**) with a yield of 89%.

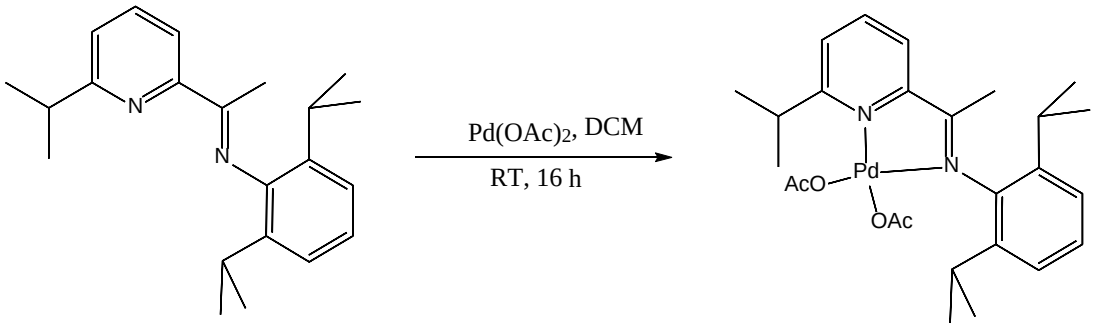

Figure 4.11 | Synthesis of (**HL4**$_{iPr}$)$Pd(OAc)_2$

The two 6H doublets at 1.01 and 1.43 ppm are assigned to be the signals of the two isopropyl groups on the diisopropyl phenyl moiety, which in the free ligand appeared as a single 12H doublet. This suggests coordination of the metal to the ligand. The two 3H singlets at 1.19 and 1.21 ppm are assigned to the two –OAc methyls, which is in line with the results that were previously observed for the ethyl-armed analogue of the complex. The 1H septet at 3.98 ppm and the 6H doublet at 1.22 ppm, which are the indicative of the free diisopropyl moiety, are shifted in comparison to those for the free ligand, but are still apparent in the proton NMR spectrum of the complex, indicating the formation of a

non C-H activated product. The FAB analysis of the product revealed a peak at 428.1417; calculated for $C_{22}H_{30}N_2Pd$ $[M\text{-}2OAc]^+$ 428.1413.

Attempts to grow single crystals suitable for an X-ray diffraction study have failed for (H**L4**$_{i\text{Pr}}$)Pd(OAc)$_2$. Thus the exchange of –OAc for –Cl/Br was tried, since crystals of the palladium chloride species have generally been easier to grow for most of the palladium complexes described in this thesis. The chlorination/bromination reactions were achieved by stirring a dichloromethane solution of (H**L4**$_{i\text{Pr}}$)Pd(OAc)$_2$ in saturated NaCl/NaBr solutions (**Figure 4.12**). The absence of the two acetate signals in the proton NMR spectra of (H**L4**$_{i\text{Pr}}$)PdCl$_2$ and (H**L4**$_{i\text{Pr}}$)PdBr$_2$ indicated that ligand exchange had been successful and the single crystal X-ray diffraction studies confirmed the two products to be the chlorinated and brominated analogues of the diacetate species (H**L4**$_{i\text{Pr}}$)Pd(OAc)$_2$ (**Figure 4.13 and Table 4.2).**

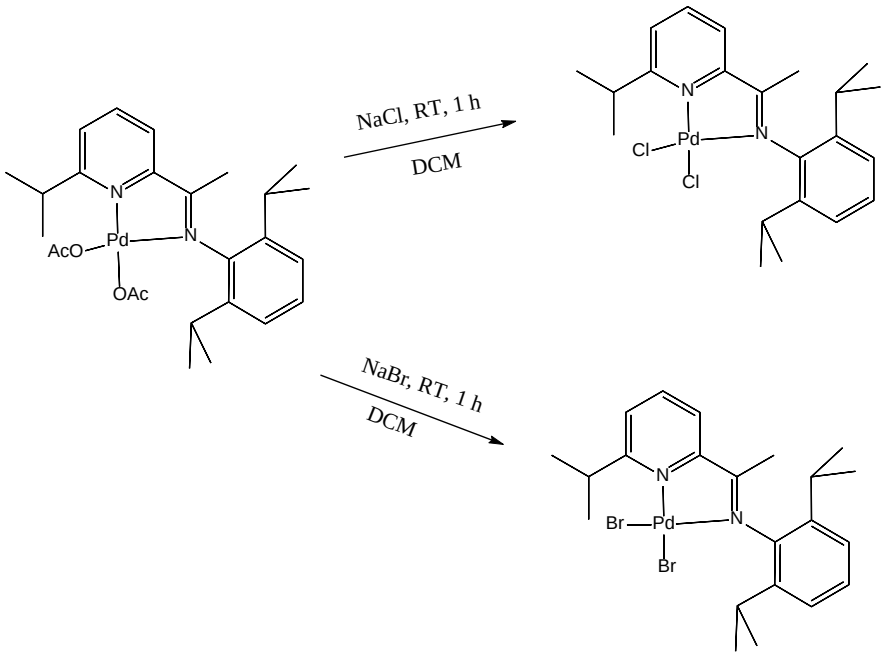

Figure 4.12 | Ligand exchange reactions of (H**L4**$_{i\text{Pr}}$)Pd(OAc)$_2$

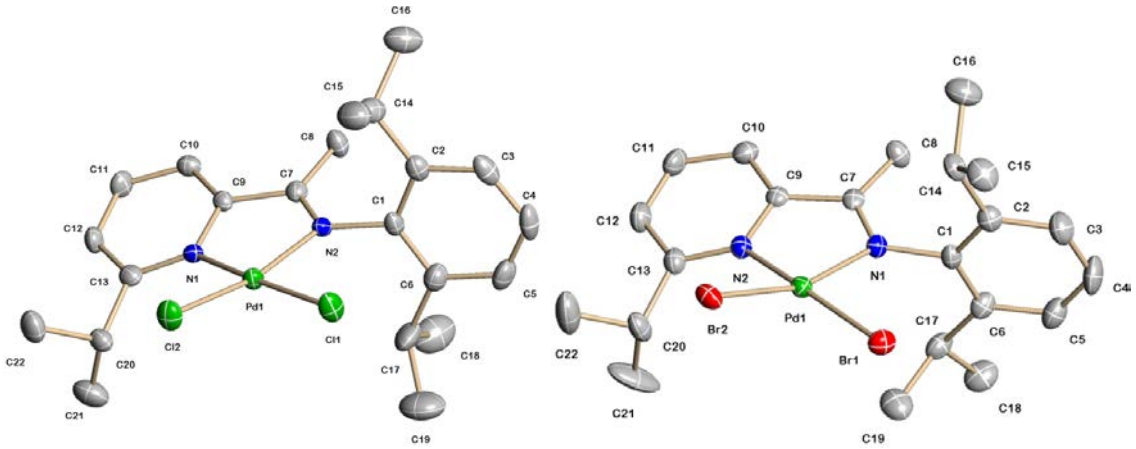

Figure 4.13 | Molecular structures of (H**L4**$_{i\text{Pr}}$)$PdCl_2$ and (H**L4**$_{i\text{Pr}}$)$PdBr_2$

Table 4.2: Selected bond lengths (Å) and angles (°) for (H**L4**$_{i\text{Pr}}$)$PdCl_2$ and (H**L4**$_{i\text{Pr}}$)$PdBr_2$

Bond length (Å)/ angles (°)	(H**L4**$_{i\text{Pr}}$)$PdCl_2$	(H**L4**$_{i\text{Pr}}$)$PdBr_2$
Pd-$N_{pyridine}$	2.062(3) Å	2.058(3) Å
Pd-N_{imine}	2.008(3) Å	2.034(3) Å
Pd-X(1)	2.2744(11) Å	2.4215(6) Å
Pd-X(2)	2.2918(11) Å	2.4223(6) Å
$N_{pyridine}$-Pd-N_{imine}	79.80(12) °	79.49(11) °
$N_{pyridine}$-Pd-X(2)	99.75(9) °	97.00(8) °
N_{imine}-Pd-X(1)	93.82(9) °	95.39(8) °

The reaction of H**L4**$_{i\text{Pr}}$ with $Pd(OAc)_2$ was then carried out at 60 °C in chloroform to examine the C(sp^3)-H activation of the isopropyl arm (**Figure 4.14**). As illustrated in **Figure 4.15**, in the proton NMR spectrum of the crude product, the doublet of doublets at 2.46 ppm and the 'quartet' at 3.45 ppm, each integrated to one proton, were assigned to protons H_b and H_a. The complexity of the signals might due to the long range coupling of these two protons to H_c. The 4H signal at 2.92 ppm is due to the overlapping of the resonances for H_c with the diisopropyl septet. The signal of the methyl moiety (Me_1) was found at 1.36 ppm as a 3H doublet; while the imine methyl (Me_2) appeared as a 3H singlet at 2.11 ppm. These findings suggest that the major product in the reaction mixture is the C(sp^3)-H activated product (**L4**$_{i\text{Pr}}$)Pd(OAc). The signals in the 5.5-7.0 ppm region

indicated that, at least two minor species, which contain vinyl protons in their molecules, are present in the crude product. Attempts to purify the product mixture to give a better quality spectrum for (**L4**$_{iPr}$)Pd(OAc) yielded no useful results, as well as the attempts to grow crystals of the complex suitable for single crystal X-ray diffraction studies.

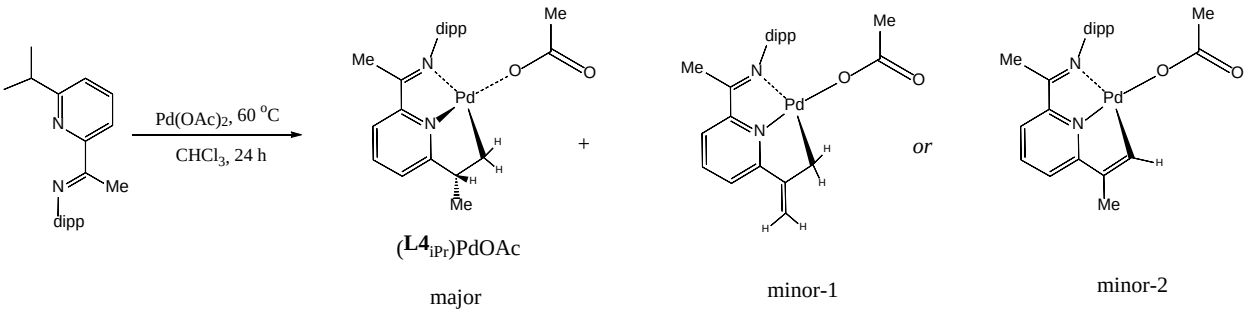

Figure 4.14 | C-H activation of H**L4**$_{iPr}$ with $Pd(OAc)_2$

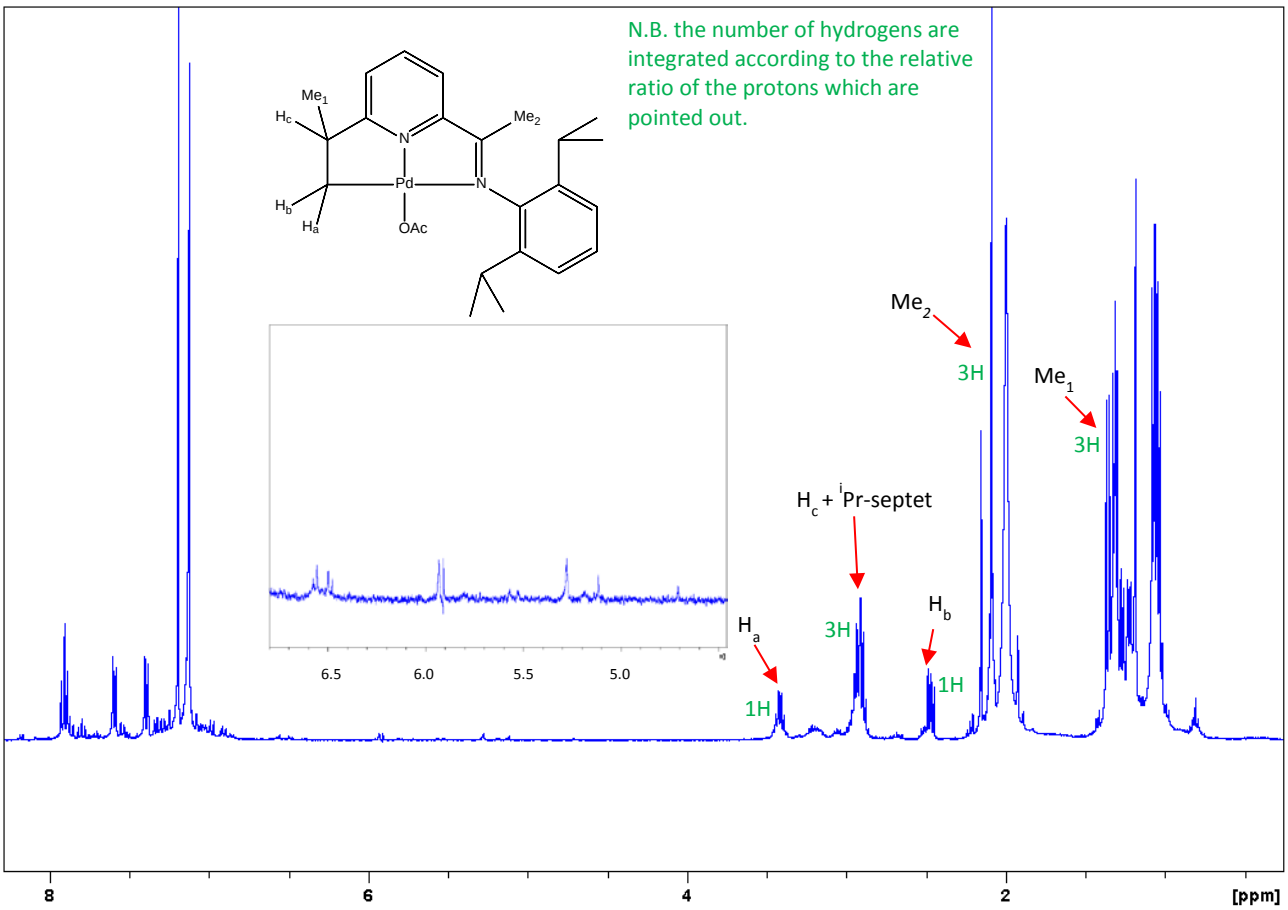

Figure 4.15 | ^{1}H NMR for the C-H activation of H**L4**$_{iPr}$ with $Pd(OAc)_2$

In line with the work on the previous Pd-OAc complexes in this thesis, the chlorination and bromination of the crude reaction mixture was undertaken in attempts to get crystals for the C-H activated complex. After being stirred with saturated NaCl at room temperature for overnight and the subsequent aqueous work up, the crude ^{1}H NMR spectrum of the product showed the absence of the two –OAc signals. Recrystallization with dichloromethane/petroleum ether gave orange crystals suitable for single crystal X-ray diffraction. The crystallographic studies revealed that these crystals belong to the palladium species illustrated in **Figure 4.16**, which is the chlorinated analogue for the 'minor-1' palladium species in **Figure 4.14**.

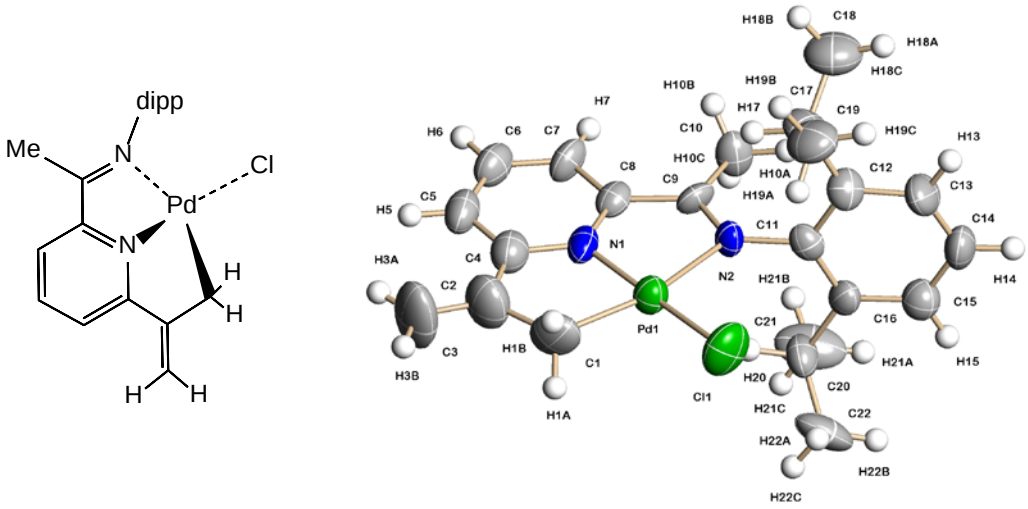

Figure 4.16 | Molecular structure of the chlorinated analogue for the 'minor-1' species

The acetate exchange for bromide (and the recrystallization from dichoromethane/petroleum ether) was carried out at room temperature, resulted in the isolation of the red crystals presented in **Figure 4.17**, which is the brominated analogue of the minor palladium species—'minor-2'—in **Figure 4.14**. The C1-C2 bond length (1.547(16) Å) in the chlorinated complex is significantly longer than the C2-C3 distance (1.339(15) Å) here. This is consistent with the assignment of C2-C3 as a double bond (**Table 4.3**). On the contrary, the C=C double bond comes at C1-C2 in the brominated complex with a bond length of 1.423(7) Å, and the longer "extra palladacycle" C2-C3 bond is consistent with the identification of C3 as a methyl group. In both complexes, the Pd-$N_{pyridine}$ bond length is shorter than their non-C-H activated analogues (H**L4**$_{iPr}$)$PdCl_2$

and (H**L4**$_{iPr}$)PdBr$_2$ (**Table 4.2**), indicating the more strained nature of the 5-membered palladacycles in the C-H activated complexes.

Table 4.3: Selected bond lengths (Å) and angles (°) for chlorinated analogue of 'minor-1' and the brominated analogue of 'minor-2'

Bond length (Å)/ angles (°)	'minor-1'-Cl	'minor-2'-Br
Pd-N$_{pyridine}$	1.973(8) Å	1.961(3) Å
Pd-C	2.013(11) Å	2.001(5) Å
C1-C2	1.547(16) Å	1.423(7) Å
C2-C3	1.339(15) Å	1.484(7) Å
N$_{pyridine}$-Pd-C	82.9(4) °	82.82(19) °

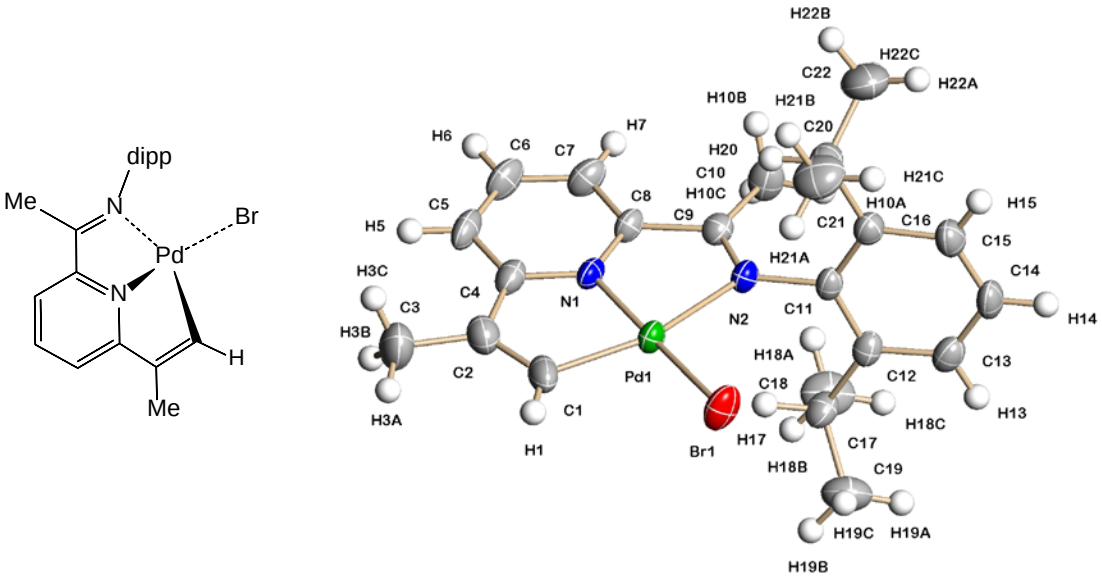

Figure 4.17 | Molecular structure of the brominated analogue for the 'minor-2' species

The two minor species are isomeric and appear to be generated from (**L4**$_{iPr}$)Pd(OAc) by loss of dihydrogen. It is tempting to speculate that the liberated acetate is reduced at the same time, but no evidence for ethanal or ethanol could be found in the NMR spectra. (However, a small amount of palladium black was observed for the reaction of H**L4**$_{iPr}$ with Pd(OAc)$_2$, so it can be assumed that the reduction of Pd(II) to Pd(0) must be happening.) A related oxidation was observed in the minor product of reaction of 2-(3-

biphenyl-2-ol)-6-(methylamine)pyridine with $Pd(OAc)_2$ in toluene at 60 °C (**Figure 4.18**).[28] Here, it was suggested that adventitious amounts of oxygen may have been involved in the oxidation, although the authors also speculated that a metal-ligand cooperation reaction via dearomatisation-aromatisation involving the pyridine ring[29] may have been involved.

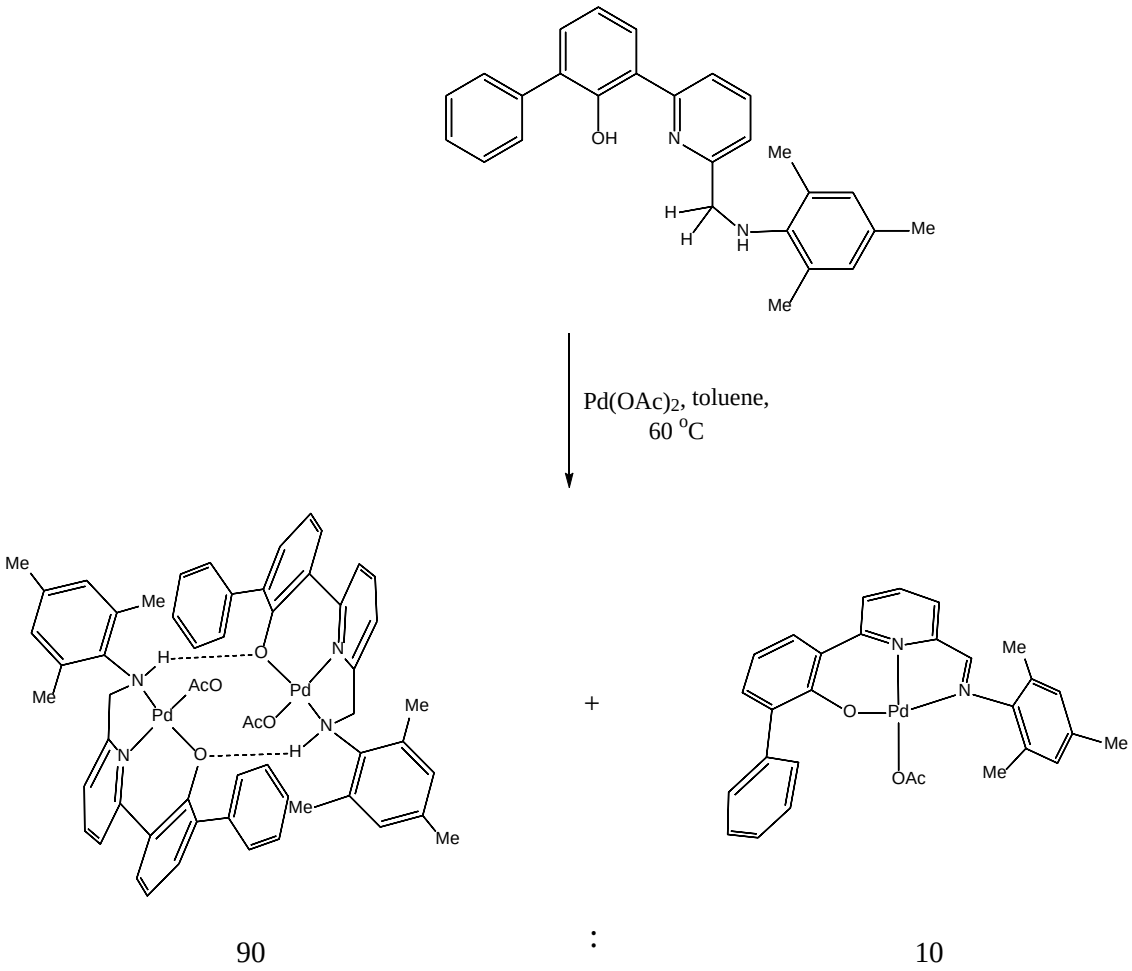

Figure 4.18 | The reaction of 2-(3-biphenyl-2-ol)-6-(methylamine)pyridine with $Pd(OAc)_2$

The reaction of H**L4**$_{i\text{Pr}}$ with Na_2PdCl_4 was then carried out at 100 °C in acetic acid (**Figure 4.19**). After 60 h of heating, the reaction gave a mixture of the sp^3 C-H activated palladium complex (**L4**$_{i\text{Pr}}$)PdCl and the previously described non C-H activated dichloride species (H**L4**$_{i\text{Pr}}$)$PdCl_2$ in a ratio of 1.5:1 (**Figure 4.20**). Other than (**L4**$_{i\text{Pr}}$)PdCl and (H**L4**$_{i\text{Pr}}$)$PdCl_2$, no other species were detected in the proton NMR spectrum from this reaction. However, upon recrystallization, only single crystals of the dichloride species

(H**L4**$_{i\text{Pr}}$)$PdCl_2$ could be isolated. Unfortunately, recrystallization to give a pure material of the C-H activated palladium complex (**L4**$_{i\text{Pr}}$)PdCl failed.

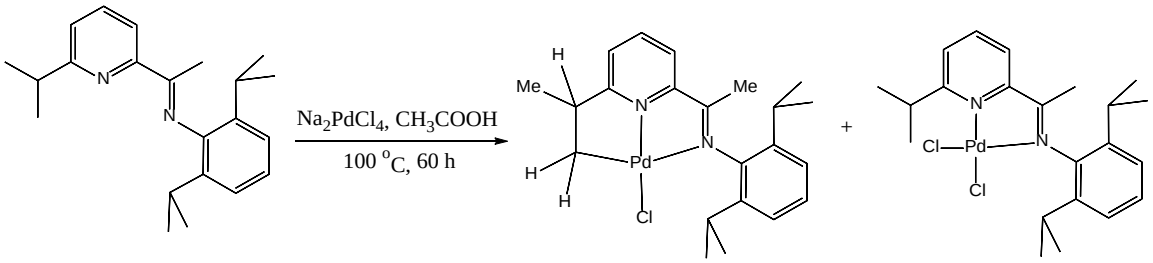

1.5 : 1

Figure 4.19 | C-H activation of H**L4**$_{i\text{Pr}}$ with Na_2PdCl_4

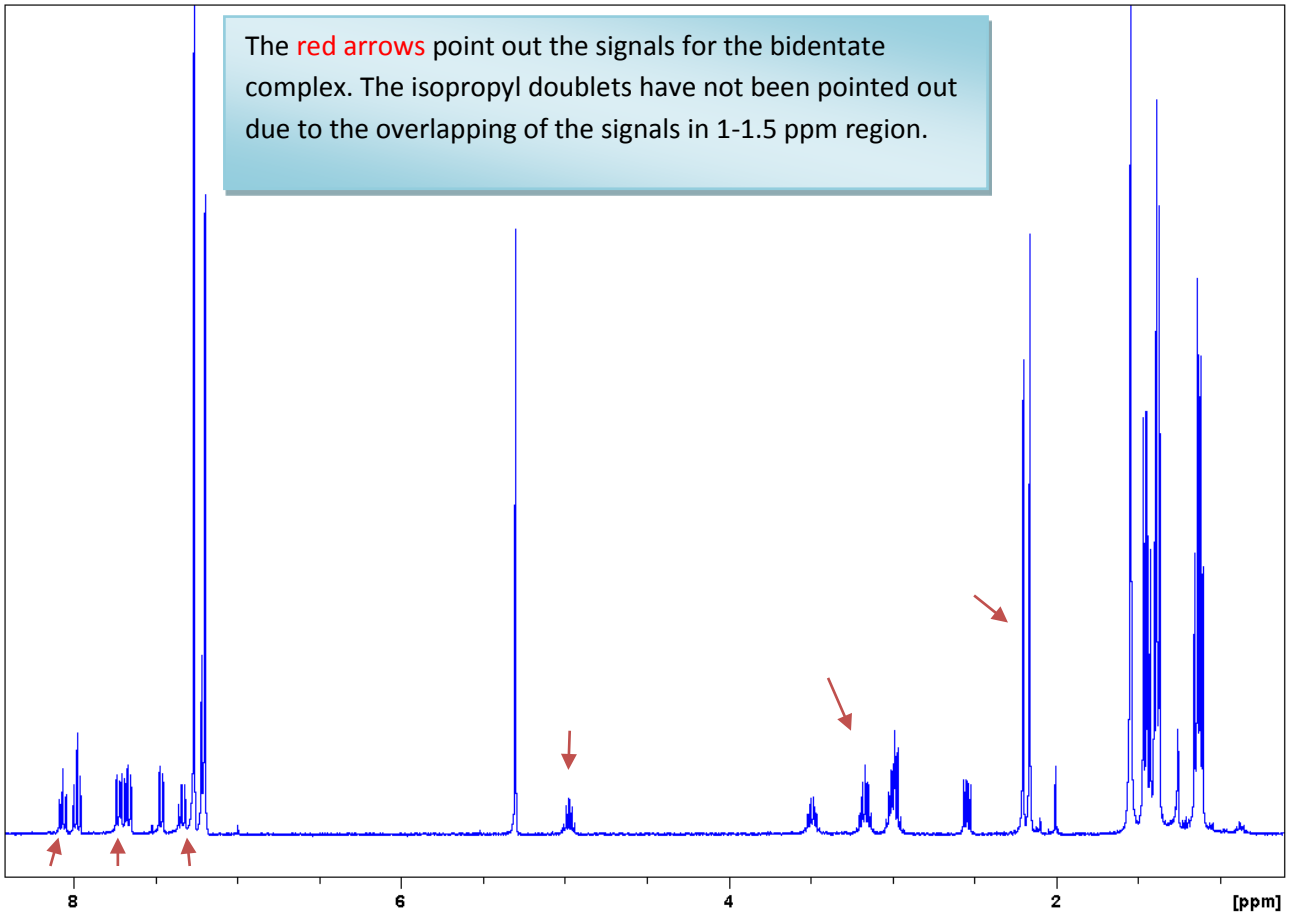

Figure 4.20 | ^{1}H NMR for the C-H activation of H**L4**$_{i\text{Pr}}$ with Na_2PdCl_4

4.2.3 Reactions with the tertbutyl-armed ligand H**L4**$_{tBu}$

Due to the shortage of the free ligand, the reaction of H**L4**$_{tBu}$ with $Pd(OAc)_2$ was not tried at room temperature, since the experience with the previous two ligands suggested that the non C-H activated di-acetate palladium complex would have been most likely to be obtained. Thus, the reaction was carried out initially at 60 ^oC in methanol (**Figure 4.21**) to see whether C(sp^3)-H activation of the tertbutyl arm could be achieved. After 48 h, the C(sp^3)-H activated palladium complex (**L4**$_{tBu}$)Pd(OAc) was obtained in a 66% yield. The proton NMR spectrum of the product revealed two 6H doublets at 1.06 and 1.30 ppm, assigned to the four diisopropyl methyls, indicating coordination of the ligand to palladium. The 9H strong singlet, as seen in the proton NMR spectrum of the free ligand, was not present in the spectrum of the complex. The two unactivated methyl groups on the 'former' ^{t}Bu-moiety appeared as a 6H singlet at 1.36 ppm while the C-H activated arm loses a proton and appeared as a 2H singlet at 2.72 ppm. These observations suggested that sp^3 C-H activation of the tertbutyl arm had been successful. Further confirmation comes from the FAB analysis of the product by revealing a peak at 441.1528; calculated for $C_{23}H_{31}N_2Pd$ $[M\text{-}OAc]^+$ 441.1531.

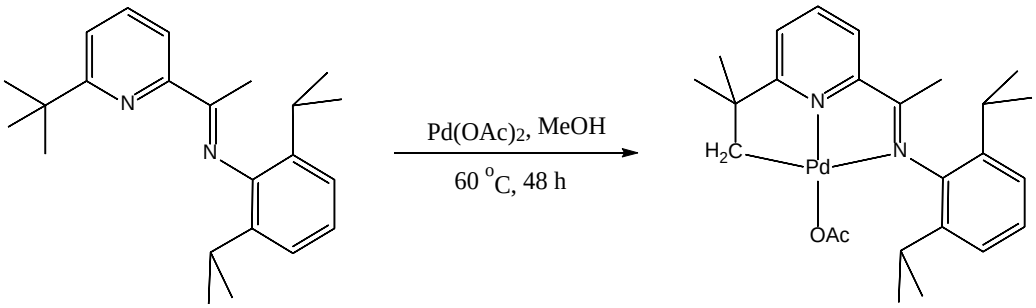

Figure 4.21 | C(sp^3)-H activation of H**L4**$_{tBu}$

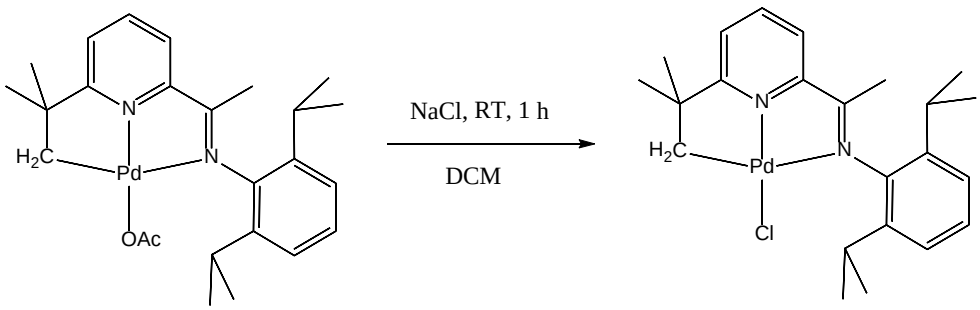

Figure 4.22 | Ligand exchange of (**L4**$_{tBu}$)Pd(OAc) to give (**L4**$_{tBu}$)PdCl

Several attempts to grow crystals suitable for a single crystal X-ray diffraction study were unsuccessful. Hence, the ligand exchange reaction with saturated sodium chloride solution was undertaken to replace the –OAc with –Cl (**Figure 4.22**). The reaction proceeded at room temperature and gave the chlorinated counterpart of (**L4**$_{tBu}$)Pd(OAc) in a quantitative yield. The proton NMR spectrum of the product suggested that the ligand exchange had been achieved by revealing the absence of the acetate signal.

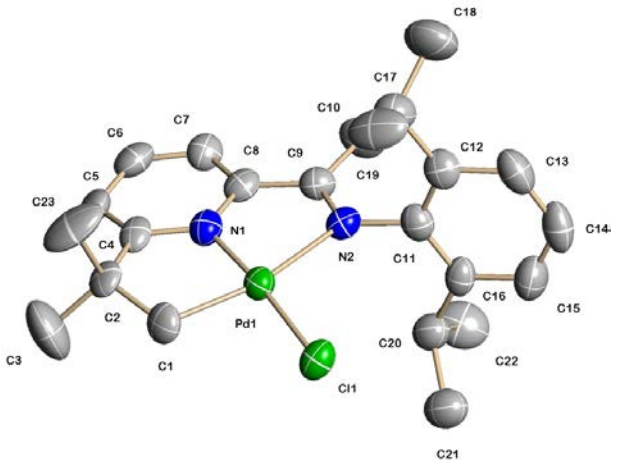

Figure 4.23 | Molecular structure of (**L4**$_{tBu}$)PdCl

Table 4.4: Selected bond lengths (Å) and angles (°) for (**L4**$_{tBu}$)PdCl

	Bond length (Å)		Bond angles (°)
Pd(1)-N(1)	1.929(9)	N(1)-Pd(1)-C(1)	82.9(4)
Pd(1)-N(2)	2.188(8)	N(2)-Pd(1)-N(1)	78.8(4)
Pd(1)-C(1)	2.001(11)	C(4)-C(2)-C(1)	110.6(9)
Pd(1)-Cl(1)	2.309(3)	C(1)-Pd(1)-Cl(1)	93.6(4)

Crystals of (**L4**$_{tBu}$)PdCl were grown from dichloromethane/hexane. The single crystal X-ray diffraction study of the crystals confirmed the formation of the analogous palladium chloride complex and also strongly supported that the C(sp^3)-H activation of the tertbutyl moiety had been achieved (**Figure 4.23** and **Table 4.4**).

Following the C-H activation with $Pd(OAc)_2$, the C-H activation of H**L4**$_{tBu}$ with Na_2PdCl_4 was also tried. The reaction also gave the sp^3 C-H activated species (**L4**$_{tBu}$)PdCl, only in a much better yield (95%) (**Figure 4.24**). The proton and carbon NMR spectroscopy and

FAB analysis results are in agreement with the product obtained from the ligand exchange reaction of (**L4**$_{tBu}$)Pd(OAc).

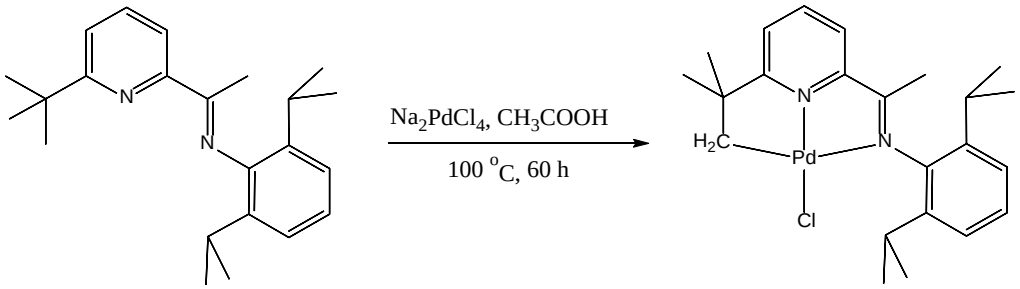

Figure 4.24 | Synthesis of (**L4**$_{tBu}$)PdCl using Na_2PdCl_4

4.3 Summary and conclusions

The rare C(sp^3)-H activations of pyridine-based alkyl-armed ligands H**L4** have been explored in this chapter. The reactions of the ethyl-armed ligand H**L4**$_{Et}$ with two palladium reagents ($Pd(OAc)_2$ and Na_2PdCl_4) yielded the non C-H activated bidentate species (H**L4**$_{Et}$)$Pd(OAc)_2$ and (H**L4**$_{Et}$)$PdCl_2$ in excellent yields. These bidentate species could potentially be useful for catalytic olefin polymerization reactions.

The reaction of $Pd(OAc)_2$ with H**L4**$_{iPr}$ at room temperature gave the palladium diacetate complex H**L4**$_{iPr}$$Pd(OAc)_2$, while the subsequent ligand exchange reactions with NaCl and NaBr gave the chlorinated and brominated analogues of the complex. When the reaction was carried out at 60 °C in chloroform, the C(sp^3)-H activated product (**L4**$_{iPr}$)Pd(OAc) was obtained as the major product, with minor amounts of two vinyl containing C-H activated species. The solid state structures of these minor species were confirmed by the subsequent ligand exchange reactions with NaCl/ NaBr of the reaction mixture and recrystallization of the resulting products from chloroform/petroleum ether. The reaction of this isopropyl-armed ligand with Na_2PdCl_4 resulted in a mixture of products, containing the C-H activated palladium complex (**L4**$_{iPr}$)PdCl and the non C-H activated dichloride species (H**L4**$_{iPr}$)$PdCl_2$ in a ratio of 1.5:1. Although the isolation of pure material for these C(sp^3)-H activated palladium complexes (**L4**$_{iPr}$)Pd(OAc) and (**L4**$_{iPr}$)PdCl has not been successful, their formation has been confirmed by proton NMR spectroscopy and solid state X-ray analyses.

The C-H activation of the ^{t}Bu-armed ligand was then examined in the reaction with $Pd(OAc)_2$ at 60 ^{o}C, which gave the C-H activated palladium complex (**L4**$_{tBu}$)Pd(OAc) in 66% yield. The exchange of the acetate group for chloride has yielded the chlorinated analogue—(**L4**$_{tBu}$)PdCl. Other than the NMR and FAB analysis, the solid state X-ray structure of the latter complex confirmed the formation of the material as a rare sp^3 C-H activated palladium complex. The reaction of this ligand with the Na_2PdCl_4 also resulted in the successful C-H activation of the ^{t}Bu-arm to give (**L4**$_{tBu}$)PdCl with a yield of 95%. These results confirm the ease of sp^3 C-H activation of the ^{t}Bu-armed ligand H**L4**$_{tBu}$, in comparison to its isopropyl- or ethyl-armed counterparts H**L4**$_{iPr}$ and H**L4**$_{Et}$.

References

1 J. Kamatani, R. Ooishi, S. Okada and T. Takiguchi, "*Organic compound for light-emitting device based on a transition metal complex having mono-valent bidentate ligands, light-emitting device, and image display apparatus"*, 2007, *U.S. Patent No.* ***20070231600***. New York : U.S.

2 F. Mao and A. Heller, "*Transition metal complexes with (pyridyl)imidazole ligands*", 2003, *U.S. Patent No.* ***20030096997.*** San Francisco: U.S.

3 T. Fujita, M. Mitani, Y. Yoshida, T. Matsugi, Y. Suzuki, S. Ishii, Y. Tohi, H. Makio, Y. Inoue and J. Saito, *PMSE Preprints*, 2002, **86**, 299.

4 M. Mitani, J. Saito, S.-I. Ishii, Y. Nakayama, H. Makio, N. Matsukawa, S. Matsui, J. Mohri, R. Furuyama, H. Terao, H. Bando, H. H. Tanaka and T. Fujita, *Chem. Rec*., 2004, **4**, 137.

5 M. Mitani, J. Mohri, Y. Yoshida, J. Saito, S. Ishii, K. Tsuru, S. Matsui, R. Furuyama, T. Nakano, H. Tanaka, S. Kojoh, T. Matsugi, N. Kashiwa and T. Fujita, *J. Am. Chem. Soc*., 2002, **124**, 3327.

6 D. J. Jones, V. C. Gibson, S. M. Green and P. J. Maddox, *Chem. Commun*., 2002, **10**, 1038.

7 R. O'Reilly, V. Gibson, A. White and D. Williams, *J. Am. Chem. Soc.*, 2003, **125**, 8450.

8 T. Younkin, E. Conner, J. Henderson, S. Friedrich, R. Grubbs and D. Bansleben, *Science*, 2000, 287, 460.

9 N. Josephsohn, M. Snapper and A. Hoveyda, *J. Am. Chem. Soc*., 2004, **126**, 3734.

10 K. Murphy and A. Hoveyda, *J. Am. Chem. Soc*., 2003, 125, 4690.

11 G. Chelucci, G. Murineddu and G. A. Pinna, *Tetrahedron: Asymmetry*, 2004, **15**, 1373.

12 R. Boca, M. Nemecková, M. Vrbová, P. Baran, I. Svoboda and H. Fuess, *Polyhedron*, 2000, **19**, 835.

13 E. Bermejo, R. Carballo, A. Castineiras, R. Dominguez, C. Maichle-Mossmer, J. Strahle and D. West, *Polyhedron*, 1999, **18**, 3695.

14 M. Boca, D. Valigura and W. Linert, *Tetrahedron*, 2000, **56**, 441.

15 B. Tao, M. Lo and G. Fu, *J. Am. Chem. Soc*. 2001, **123**, 353.

16 K. Nienkemper, V. Kotov, G. Kehr, G. Erker and R. Fröhlich, *Eur. J. Inorg. Chem*., 2006, 366.

17 V. Gibson and S. Spitzmesser, *Chem. Rev*. 2003, **103**, 283.

18 T. Laine, U. Piironen, K. Lappalainen, M. Klinga, E. Aitola and M. Leskela, *J. Organomet. Chem.*, 2000, **606**, 112.

19 C.M. Killian, L.K. Johnson and M. Brookhart, *Organometallics*, 1997, **16**, 2005.

20 L.K. Johnson, C.M. Killian and M. Brookhart, *J. Am. Chem. Soc*. 1995, **117**, 6414.

21 L. Ackermann, *Chem. Rev*., 2011, **111**, 1315.

22 S. Gorelsky, D. Lapointe and K. Fagnou, *J. Am. Chem. Soc*., 2008, **130**, 10848.

23 Y. Boutadla, D. L. Davies, A. Macgregor and A. Poblador-Bahammonde, *Dalton Trans*., 2009, 5820.

24 O. Baudoin, *Chem. Soc. Rev*., 2011, **40**, 4902.

25 B. D. Dangel, K. Godula, S. W. Youn, B. Sezen and D. Sames, *J. Am. Chem. Soc.*, 2002, **124**, 11856.

26 R. Giri, N. Maugel, J.-J. Li, D.-H. Wang, S. P. Breazzano, L. B. Saunders and J.-Q. Yu, *J. Am. Chem. Soc*., 2007, **129**, 3510.

27 W. Cross, S. Razak, K. Singh and A. Warner, *Chem. Eur. J*., 2014, **20**, 13203.

28 O. Adeyi, W. B. Cross. G. Forrest, L. Godfrey, E. G. Hope, A. Mcleod, A. Singh, K. Singh, G. A. Solan, Y. Wang and L. A. Wright, *Dalton Trans*., 2013, **42**, 7710.

29 M. Feller, Y. Diskin-Posner, L. J. W. Shimon, E. Ben-Ari and D. Milstein, *Organometallics*, 2012, **31**, 4083.

Chapter Five

Reactivity of N,N,C- and O,N,C-palladium pincer complexes

5.1 Introduction

5.1.1 Halide abstraction reactions of palladium complexes

Cationic palladium species with highly labile coordinating ligands can create a pathway for conveniently synthesizing new palladium complexes due to the easily substituted nature of the labile coordinating ligand. For example, Lloyd-Jones and co-workers have demonstrated the synthesis of an array of phosphine-containing palladium complexes, which have been used in the synthetic and mechanistic studies of asymmetric allylic alkylation reactions, by simply using $[(allyl)Pd(NCCH_3)]^{2+}$ as the synthetic precursor.[1,2] This type of cationic palladium species has also been reported to be useful as catalysts for the polymerization and oligomerization of 1,3-dienes and strained olefins.[3,4] Facile applications of cationic palladium complexes in catalytic alkene hydrogenation have been demonstrated by Albrecht et. al.[5] The synthesis of these cationic palladium complexes are quite straightforward and are often achieved by halide abstraction reactions of the neutral palladium complexes with silver salts, such as $AgBF_4$ (**Figure 5.1**).[6]

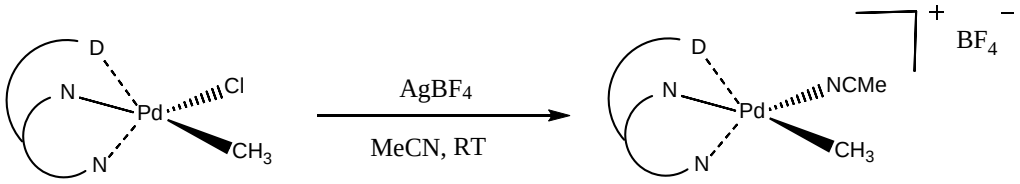

D = Donor atom, O or P

Ligands used:

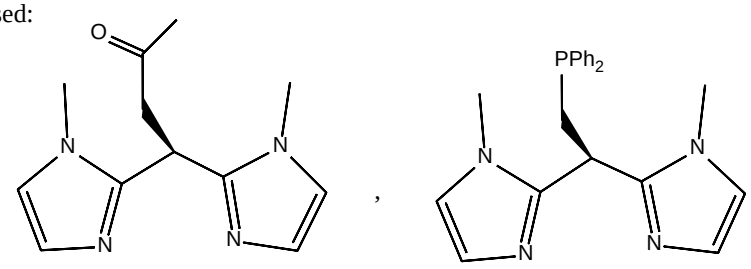

Figure 5.1 | Halide abstraction with $AgBF_4$ to give cationic complexes of palladium

Due to the highly labile nature of the acetonitrile ligand, these type of reactions are usually carried out in acetonitile as the solvent and substrate. The labile –NCMe ligand can then be substituted by other two electron donors such as pyridines, phosphines, isocyanides etc, generating many types of cationic transition metal complexes.[7, 8]

5.1.2 Catalytic allylic arylation reactions

Allylic substitution (Tsuji–Trost) reactions, which were first developed in 1960s, have been exploited in natural product synthesis and in the synthesis of pharmaceuticals.[9] A number of transition metal complexes have been generated and applied as effective catalysts in allylic arylation with arylboron reagents.[10,11]

However, harsh reaction conditions, such as relatively high temperatures and large catalyst loadings (1-10 mol%), are often required (**Figure 5.2**). Thus, studies on the establishment of a highly active catalyst for allylic arylation reactions under mild reaction conditions and with low catalyst loading has attracted considerable interest. Although a poly(imidazole-palladium) composite, as an efficient catalyst for allylic arylation reactions, has recently been reported (**Figure 5.3**),[12] the development of a catalytically active yet simple palladium complex is still desirable.

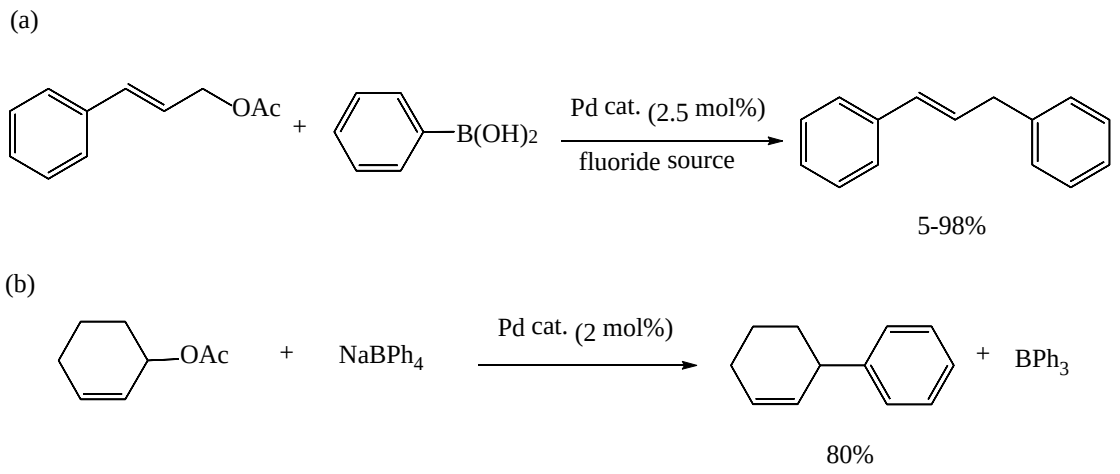

Figure 5.2 | Palladium catalyzed allylic arylation of: (a) cinnamyl acetate with phenyl boronic acid; (b) cyclohexenyl acetate with sodium tetraphenylborate.

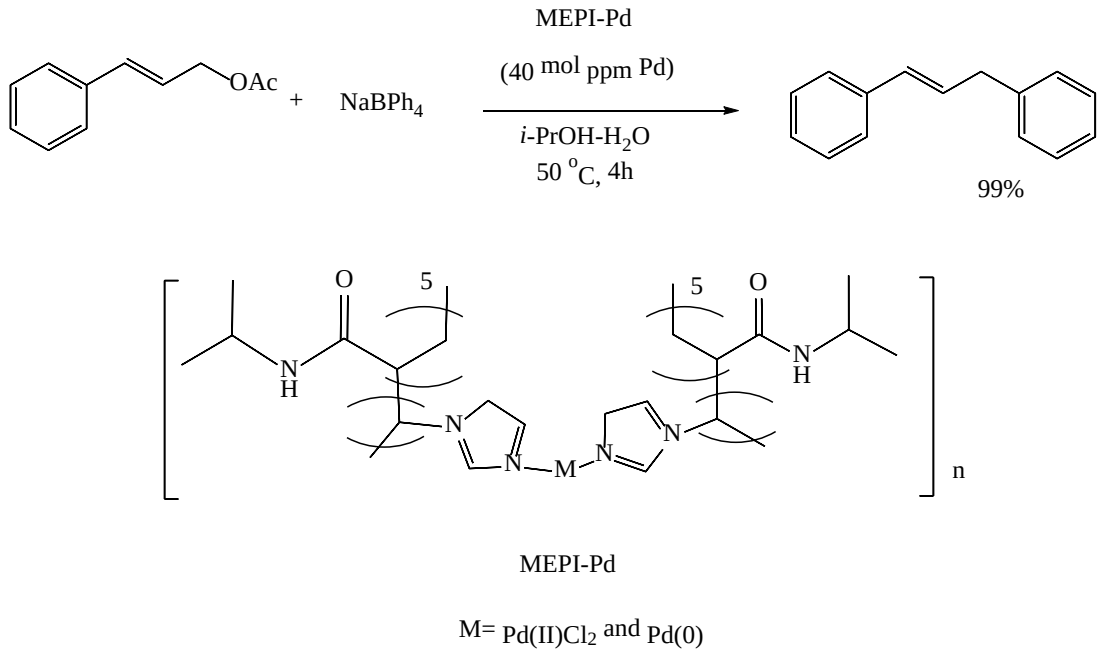

Figure 5.3 | Self-Assembled Poly(imidazole-palladium) as an active catalyst for allylic arylation

5.1.3 Aims and objectives

The reactivity of some of the palladium pincer complexes outlined in Chapters 3 & 4 is explored in this chapter. The stoichiometric reactions of the palladium-chloride type complexes, (**L1**$_{\text{o-tolyl}}$)PdCl, *peri*-[(**L1**$_{\text{ket-nap}}$)PdCl], (**L2**$_{\text{o-tolyl}}$)PdCl and *ortho*-[(**L3**$_{\text{nap}}$)PdCl] (**Figure 5.4**), with $AgBF_4$ and the subsequent exchange of the coordinating ligand (L = MeCN) are discussed in section 5.2.

Ten tridentate palladium complexes, supported by N_{imine},N_{py},C_{aryl}-, N_{amine},N_{py},C_{aryl}- and $O_{alcohol}$,N_{py},C_{aryl}-pincer ligands and two bidentate palladium complexes, were selected from all the synthesized and well defined complexes in Chapters 3 & 4, and tested as catalysts in allylic arylation reactions of sodium tetraphenyl borate with various cinnamyl acetates, which is described in section 5.3.

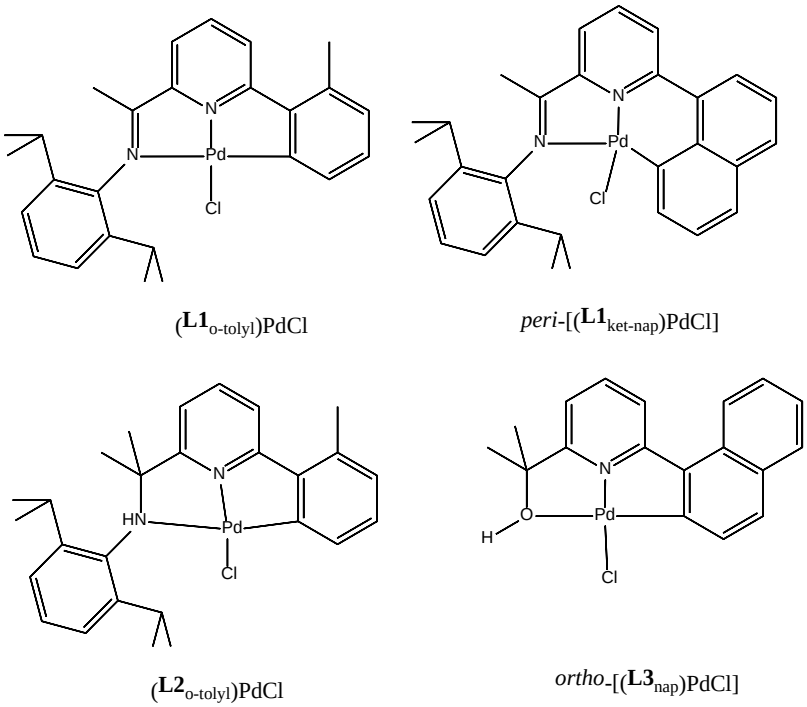

Figure 5.4 | The Pd-Cl complexes used in halide abstraction reactions

5.2 Stoichiometric reactions with silver salts

5.2.1 Halide abstraction in MeCN

5.2.1.1 Halide abstraction reactions of the Pd-Cl complexes with $AgBF_4$/$AgPF_6$

In order for the palladium complexes discussed in Chapters 3 and 4 to be active in catalytic reactions, one or more ligands have to dissociate from the metal centre. So, it was crucial that these palladium complexes showed reactivity in ligand exchange reactions. Although the interchange between the acetate and chloride ligands has been demonstrated in Chapter 3, attempts to exchange the acetate ligands for pyridines yielded no reaction. Thus, the halide abstractions with $AgBF_4$/$AgPF_6$ in MeCN were used, to remove/replace the Cl ligands in the palladium-chloride complexes. The acetonitrile ligand is considered to be relatively labile, so the expectation was to replace the chloride with acetonitile first, then exchanging the more labile ligand with pyridines. For all of the complexes, i.e. (**L1**$_{o\text{-tolyl}}$)PdCl, *peri*-[(**L1**$_{ket\text{-}nap}$)PdCl], (**L2**$_{o\text{-tolyl}}$)PdCl and *ortho*-

[(**L3**$_{nap}$)PdCl], the reaction with 1.1 to 1.5 eq. $AgBF_4$ successfully removed the chloride and afforded the cationic Pd-MeCN species [(**L1**$_{o\text{-}tolyl}$)Pd(NCMe)]$^+$[BF_4]$^-$, {*peri*-[(**L1**$_{ket\text{-}nap}$)Pd(NCMe)]}$^+$[BF_4]$^-$, [(**L2**$_{o\text{-}tolyl}$)Pd(NCMe)]$^+$[BF_4]$^-$ and {*ortho*-[(**L3**$_{nap}$)Pd(NCMe)]}$^+$[BF_4]$^-$ (**Figure 5.5**).

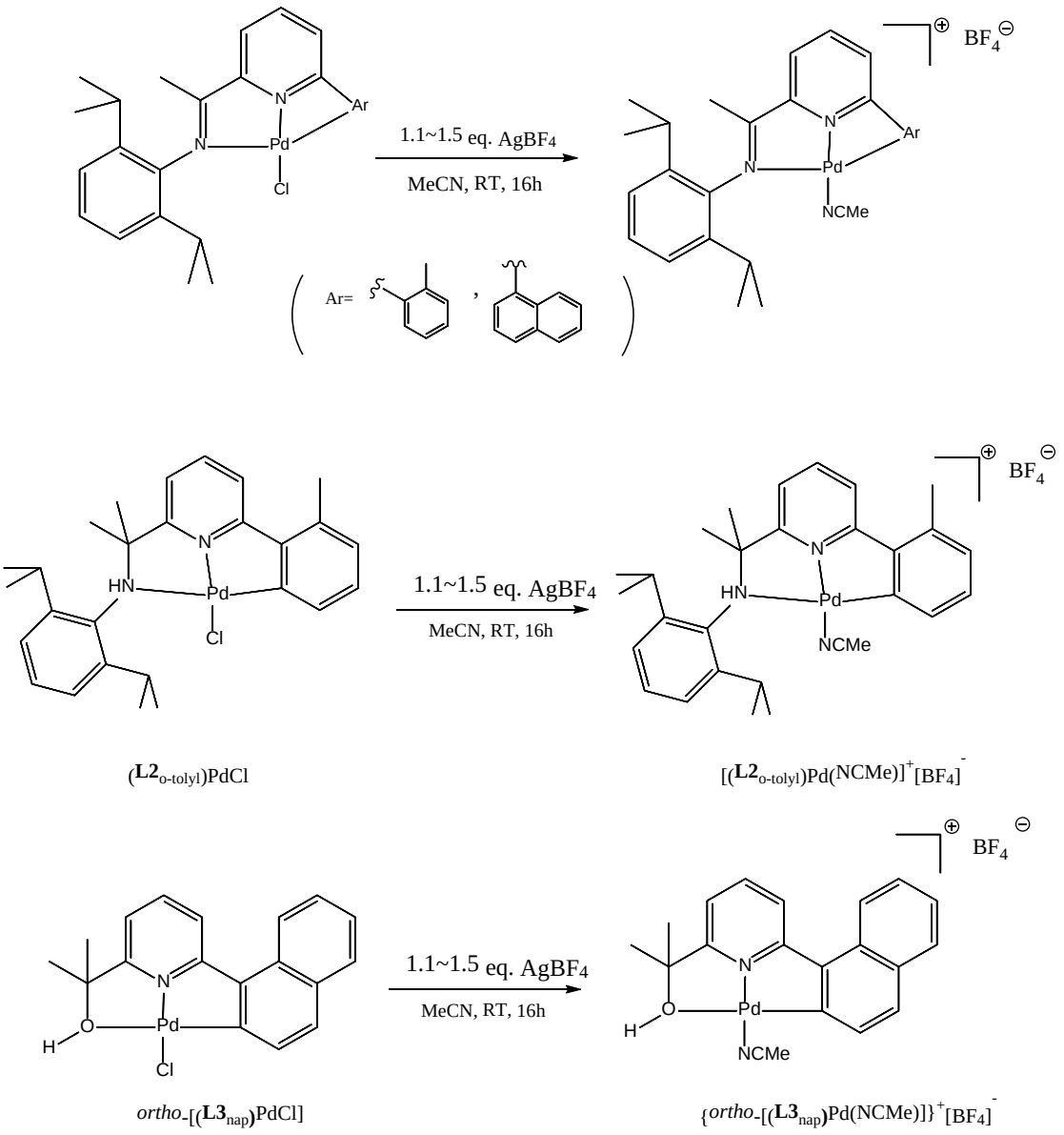

Figure 5.5 | Halide abstraction of (**L1**$_{o\text{-}tolyl}$)PdCl, *peri*-[(**L1**$_{ket\text{-}nap}$)PdCl], (**L2**$_{o\text{-}tolyl}$)PdCl and *ortho*-[(**L3**$_{nap}$)PdCl]

The appearance of a new 3H singlet at 1.99 ppm in the proton NMR spectrum of [(**L1**$_{o\text{-}tolyl}$)Pd(NCMe)]$^{+}$[BF_4]$^{-}$ (assigned to be the methyl protons on the acetonitrile moiety), the different splitting patterns of the aromatic protons and the more downfield chemical shift of the dipp-septet indicated the formation of the Pd-NCMe complex. The ^{19}F NMR spectrum revealed a strong peak at -152 ppm, indicating the presence of a BF_4 anion in the molecule. Similar features were observed for {peri-[(**L1**$_{ket\text{-}nap}$)Pd(NCMe)]}$^{+}$[BF_4]$^{-}$, [(**L2**$_{o\text{-}tolyl}$)Pd(NCMe)]$^{+}$[BF_4]$^{-}$ and {ortho-[(**L3**$_{nap}$)Pd(NCMe)]}$^{+}$[BF_4]$^{-}$ in their NMR spectra. ESMS spectroscopy of these four solvento complexes all revealed an [M-MeCN]$^{+}$ molecular ion peak respectively, while also showing a [BF_4]$^{-}$ peak at m/z 87.

5.2.1.2 Single crystal X-ray studies

Crystals suitable for single crystal X-ray diffraction studies were grown by layering the acetonitrile solution of these complexes with diethyl ether. The crystal structure analysis of the complexes {peri-[(**L1**$_{ket\text{-}nap}$)Pd(NCMe)]}$^{+}$[BF_4]$^{-}$ and {ortho-[(**L3**$_{nap}$)Pd(NCMe)]}$^{+}$[BF_4]$^{-}$ confirmed the exchange of the chloride group for acetonitile had been successful (**Figure 5.6**).

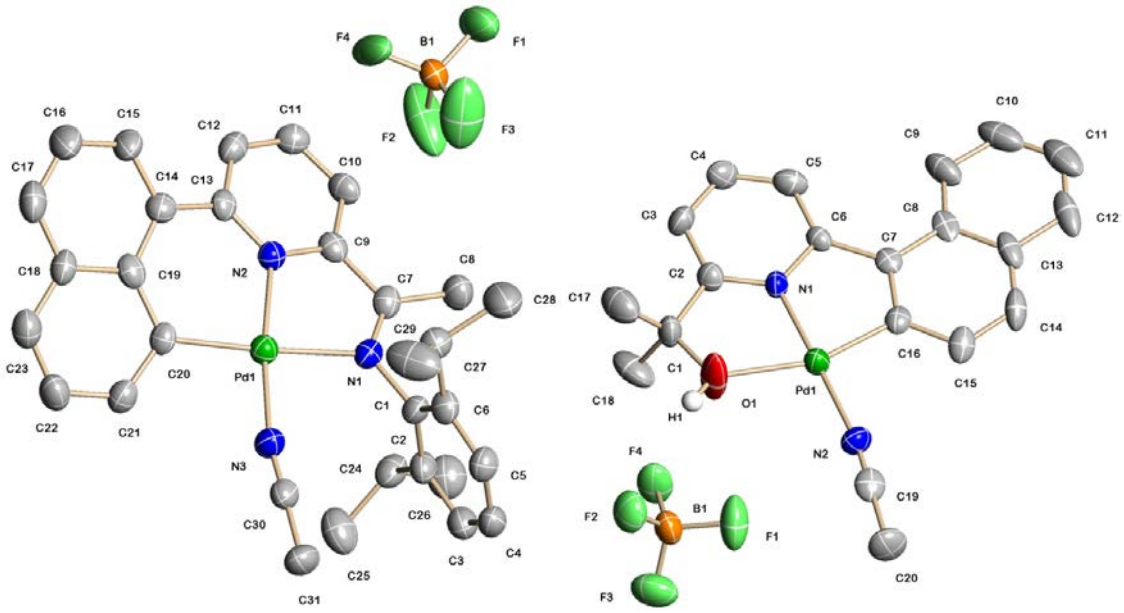

Figure 5.6 | Molecular structures of {*peri*-[(**L1**$_{ket\text{-}nap}$)Pd(NCMe)]}$^{+}$[BF_4]$^{-}$ and {*ortho*-[(**L3**$_{nap}$)Pd(NCMe)]}$^{+}$[BF_4]$^{-}$

The complex {peri-[(**L1**$_{ket-nap}$)Pd(NCMe)]}$^{+}$[BF_4]$^{-}$ adopts the square planar structure of the common palladium pincer complexes by showing angles very close to 90^{o} around the metal centre (80.62 Å for N(2)-Pd(1)-N(1) and 92.82 Å for N(1)-Pd(1)-N(3)). Similarly, the cationic complex {ortho-[(**L3**$_{nap}$)Pd(NCMe)]}$^{+}$[BF_4]$^{-}$ also presents a square planar geometry around the palladium atom and the hydrogen (H1) on the hydroxyl moiety shows intramolecular hydrogen bonding to one of the fluorine atoms of the BF_4^{-} anion with a distance of 1.854 Å.

Since the recrystalization of [(**L1**$_{o-tolyl}$)Pd(NCMe)]$^{+}$[BF_4]$^{-}$ to give crystals suitable for a single crystal X-Ray diffraction was not successful, the PF_6^{-} analogue of this complex was prepared, with the expectations that a different counter ion might result in a different solubility in organic solvents thus making it easier to grow better quality crystals (**Figure 5.7**).

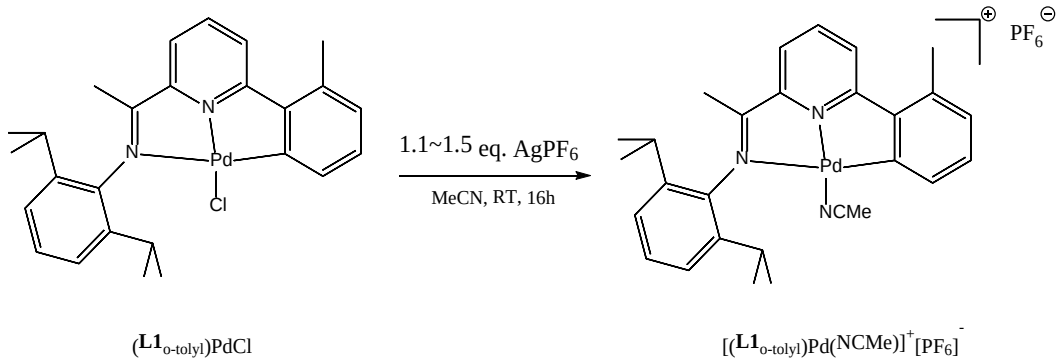

Figure 5.7 | Synthesis of [(**L1**$_{o-tolyl}$)Pd(NCMe)]$^{+}$[PF_6]$^{-}$

As hoped, layering the acetonitrile solution of this complex with diethyl ether and subsequent prolonged standing at room temperature yielded single crystals (**Figure 5.8**). The crystal structure analysis confirmed the cation and anion species wherein the PF_6^{-} anion is disordered over two sites. In comparison with {*peri*-[(**L1**$_{ket-nap}$)Pd(NCMe)]}$^{+}$[BF_4]$^{-}$, this complex presents a slightly distorted square planar geometry. But the same trend has been observed for the complexes supported by the tolyl-armed ligands (see Chapter 3).

The selected bond length (Å) and angles (^{o}) for complexes {*peri*-[(**L1**$_{ket-nap}$)Pd(NCMe)]}$^{+}$[BF_4]$^{-}$, {*ortho*-[(**L3**$_{nap}$)Pd(NCMe)]}$^{+}$[BF_4]$^{-}$ and [(**L1**$_{o-tolyl}$)Pd(NCMe)]$^{+}$[PF_6]$^{-}$ are compared with their starting materials (the corresponding Pd-

Cl complexes) in **Table 5.1**. In the solvento complexes, the Pd-$N_{pyridine}$ distances are generally slightly shorter than those in their starting materials; indicating a strengthening of the Pd-$N_{pyridine}$ bonds in these cationic solvento complexes.

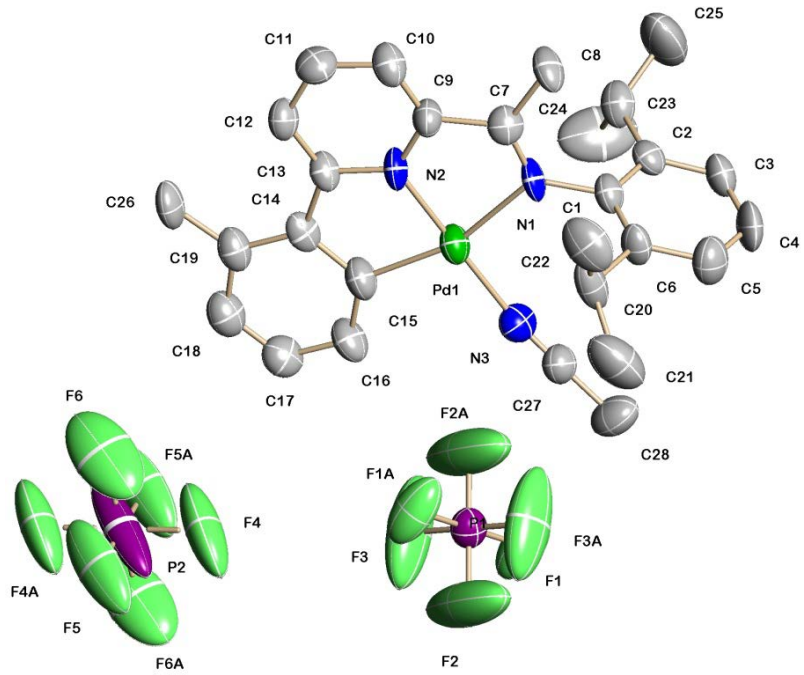

Figure 5.8 | Molecular structure of [(**L1**$_{o\text{-tolyl}}$)Pd(NCMe)]$^{+}$[PF_6]$^{-}$

Table 5.1: Selected bond lengths (Å) and angles (°) for the solvento complexes and their precursors

L	L-L-L	Pd-N_{py}	Pd-N_{imine}/$O_{alcohol}$	Pd-C	Pd-L	N_{py}-Pd-C
MeCN	Imine-py-nap	1.993(4) Å	2.105(5) Å	1.991(5) Å	2.011(5) Å	93.5(2) °
Cl		2.018(2) Å	2.104(2) Å	1.987(3) Å	2.326(8) Å	94.14(11) °
MeCN	Imine-py-tolyl	1.935(7) Å	2.141(6) Å	1.992(8) Å	2.014(8) Å	81.9(3) °
Cl		1.952(4) Å	2.161(4) Å	1.977(5) Å	2.3167(14) Å	81.24(19) °
MeCN	Alcohol-py-nap	1.958(5) Å	2.145(5) Å	1.951(7) Å	2.004(6) Å	81.7(2) °
Cl		1.962(13) Å	2.186(11) Å	1.978(4) Å	2.303(5) Å	82.5(3) °

5.2.2 The unexpectedly close Ag….Pd interaction in the Pd-NCMe solvento complexes

Interestingly, when the amount of $AgBF_4$ was increased to 3 eq. in the halide abstraction of **L1**$_{o\text{-tolyl}}$PdCl, a silver adduct [(**L1**$_{o\text{-tolyl}}$)(NCMe)Pd$^{\cdots}$Ag-(NCMe)$_3$][BF_4]$_2$ was isolated (**Figure 5.9**).

An X-ray diffraction analysis of single crystals revealed the unambiguous formation of an Ag adduct with an unusually short Pd-Ag contact of 2.8630 (11) Å (**Figure 5.10** and **Table 5.2**). Two MeCN solvent molecules complete the linear coordination geometry around the silver centre, while the palladium retains its planar configuration with the Ag moiety binding to it from outside the 'Pd-ligand' plane. Only two examples of this type of Pd-Ag species were found in the Cambridge structural database, both of which show a longer Pd-Ag distance (2.8701(6) Å[13] and 3.1120 (10) Å[14]) (**Figure 5.11**), suggesting a stronger intermetallic interaction in the complex in this work.

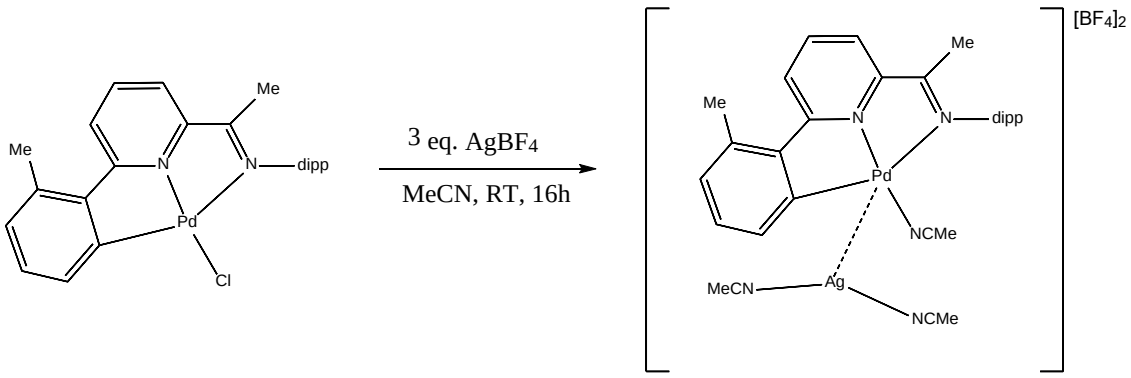

(**L1**$_{o\text{-tolyl}}$)PdCl

[(**L1**$_{o\text{-tolyl}}$)(NCMe)Pd$^{\cdots}$Ag-(NCMe)$_2$][BF_4]$_2$

Figure 5.9 | Formation of the bimetallic complex [(**L1**$_{o\text{-tolyl}}$)(NCMe)Pd$^{\cdots}$Ag-(NCMe)$_2$][BF_4]$_2$

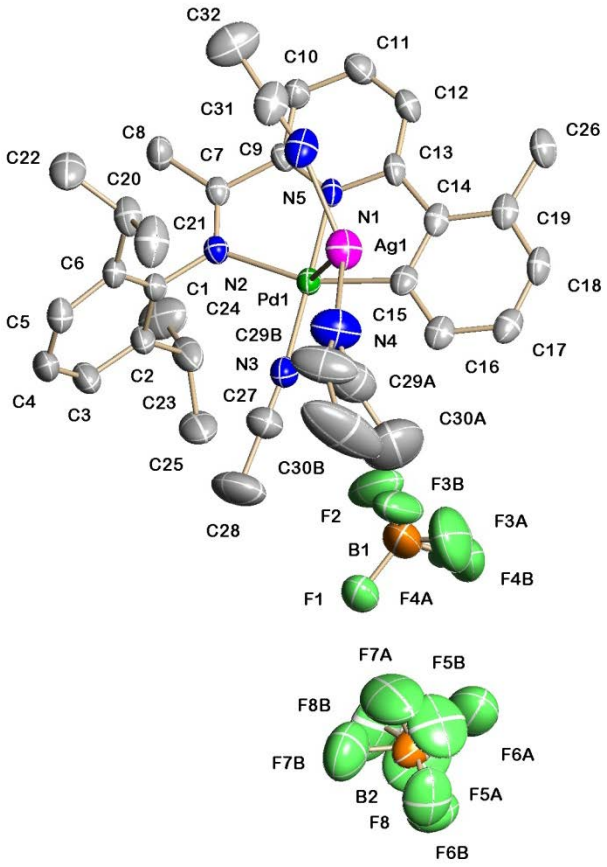

Figure 5.10 | Molecular structure of the dimetallic complex [(**L1**$_{o\text{-tolyl}}$)(NCMe)Pd···Ag-(NCMe)$_2$][BF$_4$]$_2$

Table 5.2: Selected bond lengths (Å) and angles (°) for [(**L1**$_{o\text{-tolyl}}$)(NCMe)Pd···Ag-(NCMe)$_2$][BF$_4$]$_2$

	Bond length (Å)		Bond angles (°)
Pd(1)-Ag(1)	2.8603(11)	N(1)-Pd(1)-C(15)	99.1(3)
Pd(1)-N(1)	1.931(5)	N(3)-Pd(1)-Ag(1)	88.06(17)
Pd(1)-C(15)	1.989(7)	C(15)-Pd(1)-Ag(1)	60.00(19)
Pd(1)-N(3)	1.987(6)	C(15)-Pd(1)-N(3)	99.1(3)

The fact that the proton NMR spectrum of this bi-metallic complex does not show characteristic differences from the solvento palladium complex, [(**L1**$_{o\text{-tolyl}}$)Pd(NCMe)]$^+$[BF$_4$]$^-$, suggests that dissociation of the Ag from the palladium complex is occurring in solution. The other Pd-Ag bimetallic species found in the literature (**Figure 5.11**) exhibited similar behaviour by showing dissociation of the Ag adduct in solution

and no characteristic peaks in the proton/carbon NMR spectra for the two MeCN solvent molecules on the silver (**Figure 5.12**).[13,14]

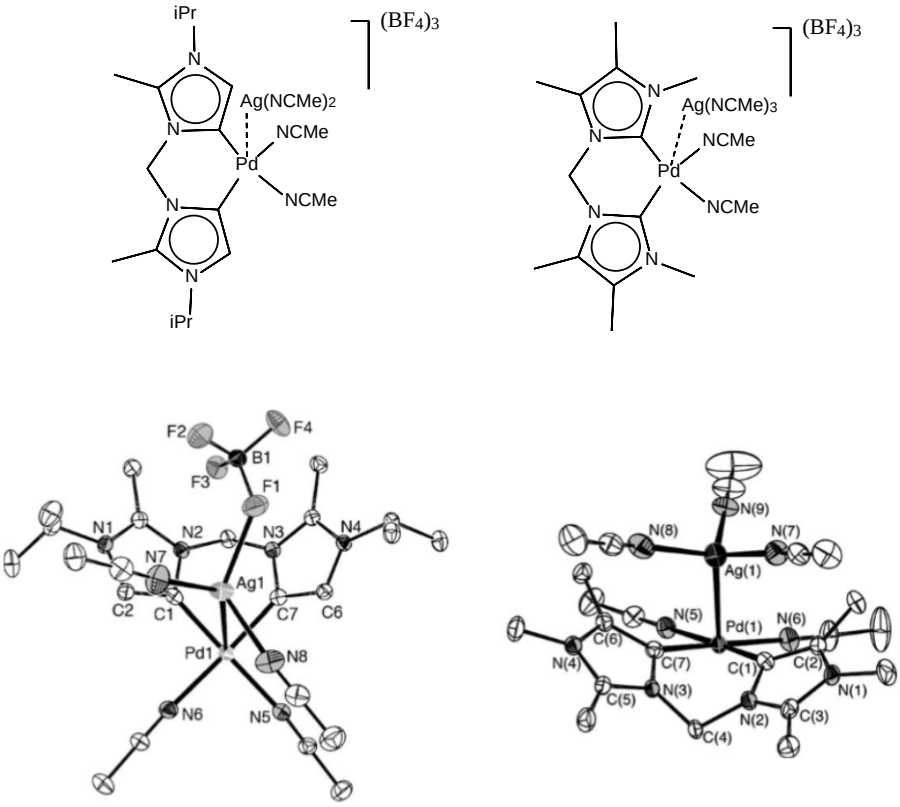

Figure 5.11 | The literature examples of the Ag-Pd dimetallic species[13,14]

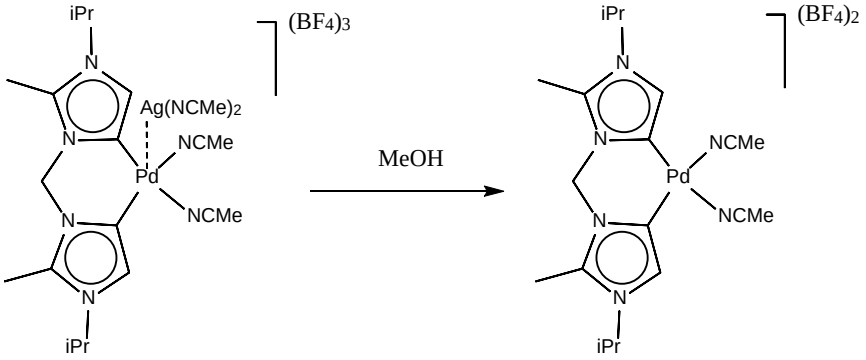

Figure 5.12 | Dissociation of the Ag adduct in solution[13]

This type of Pd-Ag interaction was found not to be unique to (**L1**$_{o\text{-tolyl}}$)PdCl. Increasing the amount of $AgBF_4$ (3 eq.) also led to the isolation of a Pd-Ag species, as crystals, upon reaction with (**L2**$_{o\text{-tolyl}}$)PdCl, which is supported by an amine side armed ligand (**Figure 5.13** and **Table 5.3**).

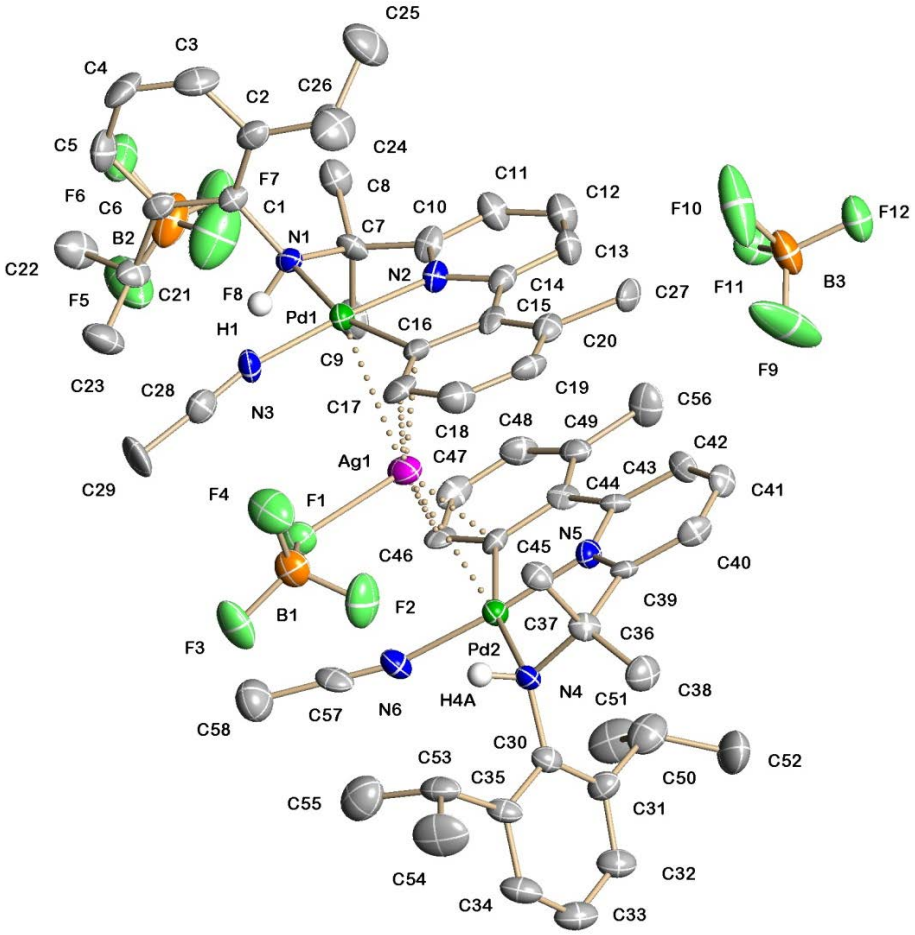

Figure 5.13 | Molecular structure of the trimetallic Pd-Ag adduct [(**L2**$_{o\text{-tolyl}}$)(NCMe)Pd$\cdots$AgBF$_4\cdots$Pd(**L2**$_{o\text{-tolyl}}$)(NCMe)][BF$_4$]$_2$

Table 5.3: Selected bond lengths (Å) and angles (^{o}) for trimetallic Pd-Ag adduct [(**L2**$_{o\text{-tolyl}}$)(NCMe)Pd$\cdots$AgBF$_4\cdots$Pd(**L2**$_{o\text{-tolyl}}$)(NCMe)][BF$_4$]$_2$

	Bond length (Å)		Bond angles (^{o})
Pd(1)-Ag(1)	2.9125(11)	Pd(1)-Ag(1)-Pd(2)	169.73(3)
Pd(2)-Ag(1)	2.9613(11)	N(3)-Pd(1)-Ag(1)	81.88(19)
Ag(1)-C(16)	2.357(8)	N(6)-Pd(2)-Ag(1)	83.9(2)
Ag(1)-C(17)	2.649(8)	C(16)-Pd(1)-N(2)	81.6(3)
Ag(1)-F(1)	2.510(4)	N(1)-Pd(1)-N(3)	99.2(2)
Ag(1)-C(45)	2.354(7)	C(45)-Pd(2)-N(5)	81.2(3)
Ag(1)-C(46)	2.609(7)	N(4)-Pd(2)-N(6)	99.7(3)

However, this Pd-Ag complex adopts a quite different configuration, with a silver atom in the middle coordinating to one palladium centre on each side. The three metal atoms Pd(1), Ag(1) and Pd(2) are almost in a line, by showing a value of 169.73(3)^{o} for the Pd(1)-Ag(1)-Pd(2) angle. Both of the palladium complex units retain their square planar geometry by presenting angles very close to 90^{o} around the Pd atom. The silver also shows coordination to two of the carbon atoms on the tolyl moiety on each of the palladium units and a fluoride ion from the BF_4^- counter ion. The Pd-Ag 'bond' length is slightly longer (2.9125(11) Å) than the previous Pd-Ag complex [(**L1**$_{o\text{-tolyl}}$)(NCMe)Pd$\cdots$Ag-(NCMe)$_2$][BF_4]$_2$ (2.8630 (11) Å). The amine proton H (4A) shows an intramolecular hydrogen bond to one of the fluorines (F2) of the BF_4^- ion with a value of 2.495 Å.

Complex *peri*-[(**L2**$_{\text{ket-nap}}$)PdCl] also rapidly transforms in the presence of 3 eq. $AgBF_4$ (MeCN solution) into the bimetallic complex {[*peri*-(**L2**$_{\text{ket-nap}}$)(NCMe)Pd]$\cdots$Ag(OH_2)$\cdots$[*peri*-(**L2**$_{\text{ket-nap}}$)Pd(NCMe)]}[BF_4]$_3$. Single crystals were isolated upon recrystallisation and the X-ray analysis revealed a silver adduct with a Pd-Ag-Pd structure (**Figure 5.14** and **Table 5.4**).

Table 5.4: Selected bond lengths (Å) and angles (^{o}) for {[*peri*-(**L2**$_{\text{ket-nap}}$)(NCMe)Pd]$\cdots$Ag(OH_2)$\cdots$[*peri*-(**L2**$_{\text{ket-nap}}$)Pd(NCMe)]}[BF_4]$_3$

	Bond length (Å)		Bond angles (^{o})
Pd(1)-Ag(1)	3.0981(11)	Pd(1)-Ag(1)-Pd(2)	167.32(3)
Pd(2)-Ag(1)	3.0449(11)	N(3)-Pd(1)-Ag(1)	97.4(2)
Ag(1)-C(20)	2.330(8)	N(6)-Pd(2)-Ag(1)	95.6(2)
Ag(1)-C(21)	2.604(9)	C(20)-Pd(1)-N(2)	93.2(3)
Ag(1)-O(1)	2.301(6)	N(1)-Pd(1)-N(3)	93.4(3)
Ag(1)-C(51)	2.386(8)	C(51)-Pd(2)-N(5)	92.3(4)
Ag(1)-C(52)	2.585(9)	N(4)-Pd(2)-N(6)	90.9(3)

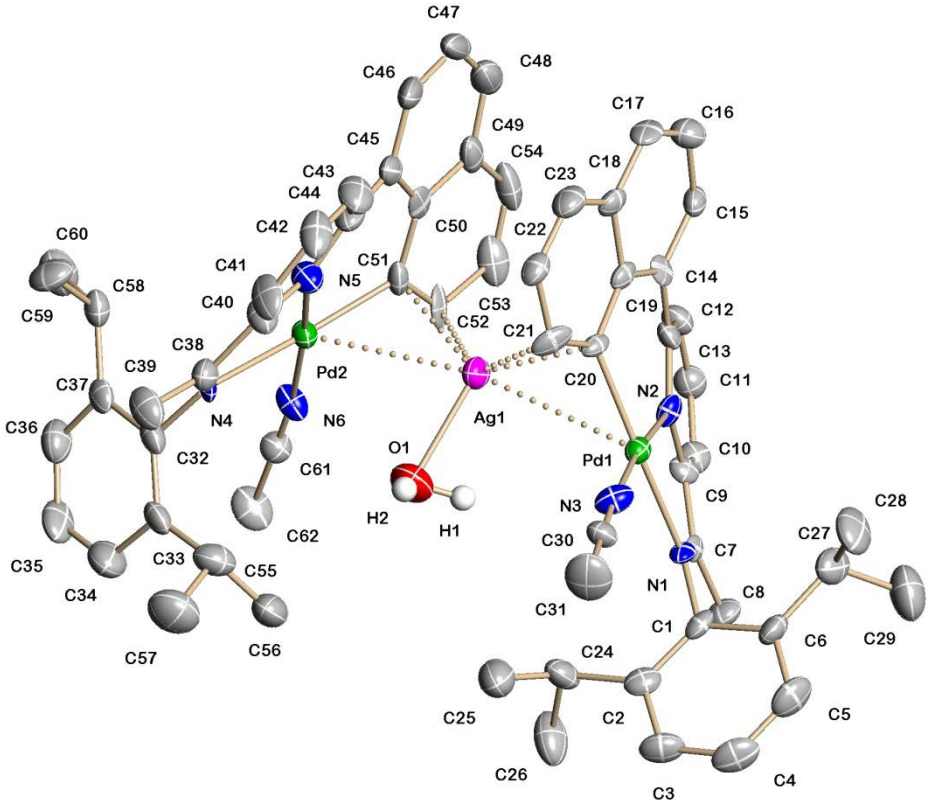

Figure 5.14 | Molecular structure of complex {[*peri*-(**L2**$_{ket\text{-}nap}$)(NCMe)Pd]····Ag(OH_2)····[*peri*-(**L2**$_{ket\text{-}nap}$)Pd(NCMe)]}$[BF_4]_3$. The BF_4^- anions have been omitted from the diagram.

In comparison to the previous Pd-Ag-Pd complex [(**L2**$_{o\text{-}tolyl}$)(NCMe)-Pd····$AgBF_4$····Pd(**L2**$_{o\text{-}tolyl}$)(NCMe)]$[BF_4]_3$ (Pd-Ag 2.9125(11) Å, Ag-C 2.649(8) Å), the Pd-Ag 'bond' lengths of this Pd-Ag complex are longer (3.0449(11) Å) and the Ag-C bond lengths are shorter (2.330(8) Å), resulting in a shift of the silver ion towards the aryl arms of the ligands.

Table 5.5: The Pd-Ag bond lengths of the Ag-Pd species

Ag-Pd complexes	Pd-Ag bond length
[(**L1**$_{o\text{-}tolyl}$)(NCMe)Pd····Ag-$(NCMe)_2$]$[BF_4]_2$	2.8603(11)
[(**L2**$_{o\text{-}tolyl}$) (NCMe)Pd····$AgBF_4$····Pd(**L2**$_{o\text{-}tolyl}$)(NCMe)]$[BF_4]_2$	2.9125(11) and 2.9613(11)
{[*peri*- (**L2**$_{ket\text{-}nap}$) (NCMe)Pd] ····Ag(OH_2) ····[*peri*- (**L2**$_{ket\text{-}nap}$)Pd(NCMe)]}$[BF_4]_3$	3.0981(11) and 3.0449(11)

Since the three complexes adopt different structures in terms of the numbers and types of coordinating ligands, and the number of metal atoms in one complex, it is not possible to directly compare the Pd-Ag distances. From the data here (**Table 5.5**), the Pd-Ag interaction is stronger when the ratio of the Ag and Pd atoms in the molecule is 1:1; while when it is 1:2, a slightly longer metal-metal 'bond' was observed. This might be because this type of metal-metal interaction comes from the palldium donating its electrons to silver, and while there are two palladium atoms donating into the same orbital of the silver atom, the interaction between the Ag and Pd is weakened, thus resulting in a longer Ag-Pd 'bond'.

Formation of such bimetallic complexes indicates that Pd-Ag bond formation may be a general process in halide abstractions of palladium complexes with silver salts. This behaviour may become attractive for exploiting new types of direct metal-metal interactions.[15] More importantly, the formation of Pd-Ag-Pd tri-metallic species suggests the possibility of linking the homodinuclear units through (weak) metal-metal bonding and the manufacture of coordination polymers.[16,17,18]

5.2.3 Exchange of the MeCN ligand for pyridines

After the synthesis and full characterization of the solvento palladium complexes, the relatively labile MeCN ligand opened a door to the exchange of the coordinating ligand to other moieties, i.e. pyridines, thus opening the possibility of making complexes that might exhibit catalytic activities. The exchange of the MeCN group for 3,5-dichloropyridine rapidly occurred in dichloromethane at room temperature (**Figure 5.15**). The methyl signals of the MeCN moiety disappeared in the proton NMR spectra of the products and three more proton signals appeared in the aromatic region. Along with the shift of the septet and doublet signals of the di-isopropyl moieties, these features indicate the formation of the palladium-pyridine complexes (**Figure 5.15**). The X-ray structural analysis of the products unambiguously confirmed that the exchange of the MeCN group for the 3,5-dichloropyridine moiety had been successful. **Figure 5.16** shows the X-ray structure of complex $[(\mathbf{L1}_{\text{o-tolyl}})Pd(NC_5H_3Cl_2\text{-}3,5)]^+[BF_4]^-$ with selected bond length and angles in **Table 5.6**. The complex retains its Pd cation and BF_4 anion configuration as in the original Pd-NCMe complex, only with a different coordinating ligand, 3,5-dichloropyridine.

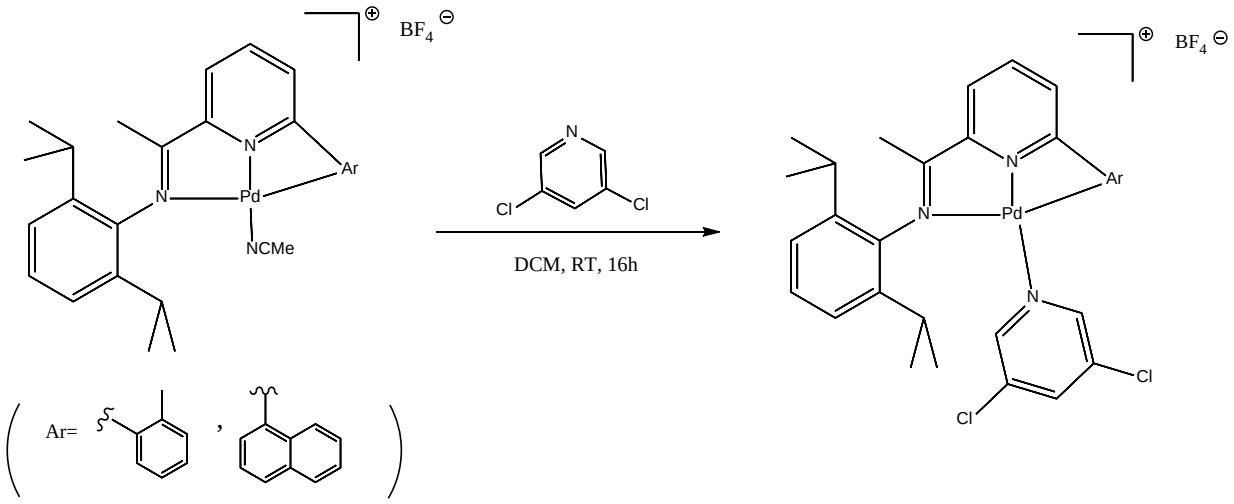

Figure 5.15 | Exchange of MeCN with 3,5-dichloropyridine

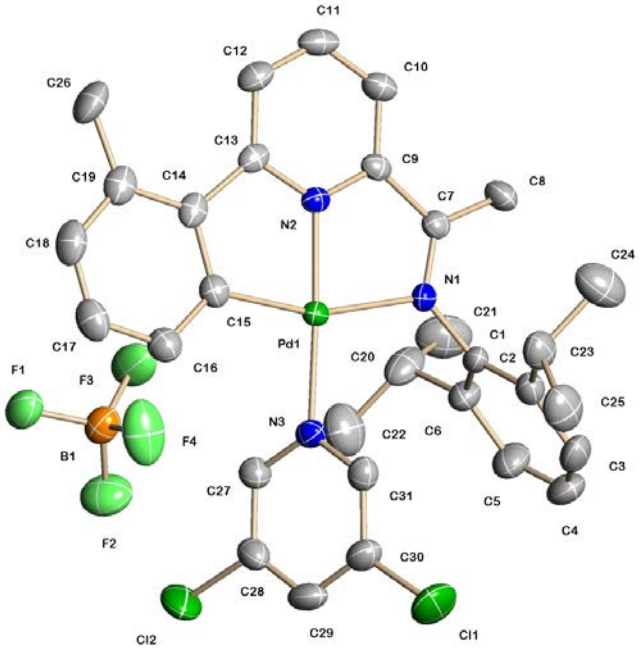

Figure 5.16 | Molecular structure of complex [(**L1**$_{o\text{-tolyl}}$)Pd($NC_5H_3Cl_2$-3,5)]$^+$[BF_4]$^-$

Table 5.6: Selected bond lengths (Å) and angles (°) for [(**L1**$_{o\text{-tolyl}}$)Pd($NC_5H_3Cl_2$-3,5)]$^+$[BF_4]$^-$

	Bond length (Å)		Bond angles (°)
Pd(1)-N(1)	2.142(3)	N(2)-Pd(1)-C(15)	81.83(13)
Pd(1)-N(2)	1.945(3)	N(2)-Pd(1)-N(1)	79.35(10)
Pd(1)-C(15)	1.979(3)	C(15)-Pd(1)-N(3)	97.75(12)
Pd(1)-N(3)	2.046(3)	N(1)-Pd(1)-N(3)	100.99(10)

The X-ray structural analysis of complex {*peri*-[(**L1**$_{ket\text{-}nap}$)Pd($NC_5H_3Cl_2$-3,5)]}$^+$[BF_4]$^-$ exhibits the usual square planar configuration around the palladium centre (**Figure 5.17** and **Table 5.7**). The bond lengths (Å) and angles (°) for both of the complexes {*peri*-[(**L1**$_{ket\text{-}nap}$)Pd($NC_5H_3Cl_2$-3,5)]}$^+$[BF_4]$^-$, [(**L1**$_{o\text{-}tolyl}$)Pd($NC_5H_3Cl_2$-3,5)]$^+$[BF_4]$^-$ are very similar to those of their Pd-NCMe precursors respectively (**Table 5.8**).

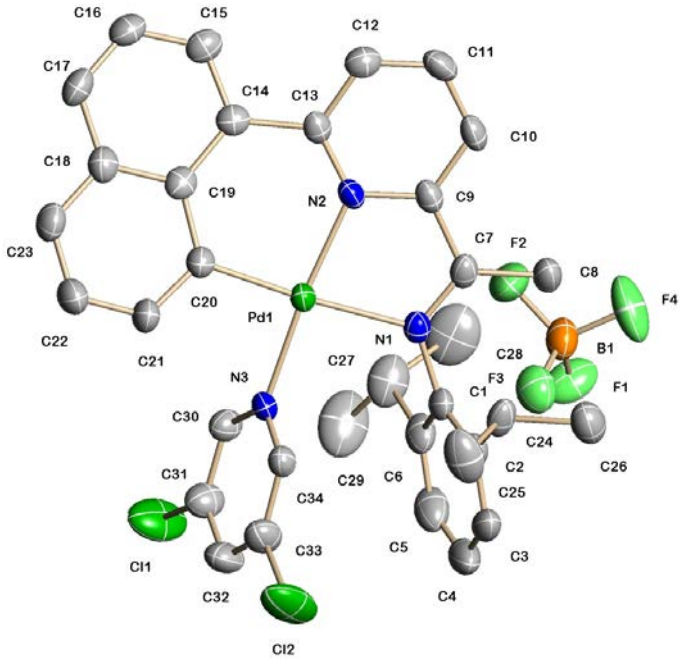

Figure 5.17 | Molecular structure of complex {*peri*-[(**L1**$_{ket\text{-}nap}$)Pd($NC_5H_3Cl_2$-3,5)]}$^+$[BF_4]$^-$

Table 5.7: Selected bond lengths (Å) and angles (°) for {*peri*-[(**L1**$_{ket\text{-}nap}$)Pd($NC_5H_3Cl_2$-3,5)]}$^+[BF_4]^-$

	Bond length (Å)		Bond angles (°)
Pd(1)-N(1)	2.127(5)	N(2)-Pd(1)-C(20)	94.3(2)
Pd(1)-N(2)	2.007(5)	N(2)-Pd(1)-N(1)	81.1(2)
Pd(1)-C(20)	2.000(6)	C(20)-Pd(1)-N(3)	92.0(2)
Pd(1)-N(3)	2.046(5)	N(1)-Pd(1)-N(3)	92.8(2)

Table 5.8: Selected bond lengths (Å) and angles (°) for the Pd-Cl_2Py complexes and their precursors

L	L-L-L	Pd-$N_{pyridine}$	Pd-N_{imine}	Pd-C	$N_{pyridine}$-Pd-C
MeCN	Imine-py-nap	1.993(4)	2.105(5)	1.991(5)	93.5(2)
Cl_2Py		2.007(5)	2.127(5)	2.000(6)	94.3(2)
MeCN	Imine-py-tol	1.935(7)	2.141(6)	1.992(8)	81.9(3)
Cl_2Py		1.945(3)	2.142(3)	1.979(3)	81.83(13)

Complex [(**L2**$_{o\text{-}tolyl}$)Pd(NCMe)]$^+[BF_4]^-$ behaves in exactly the same way when treated with 3,5-dichloropyridine in dichloromethane (**Figure 5.18**). The rapid substitution of the –NCMe ligand with a 3,5-dichloropyridine unit is evidenced by the disappearance of the methyl singlet of the acetonitrile group and the emergence of three new proton signals in the aromatic region in its proton NMR spectrum.

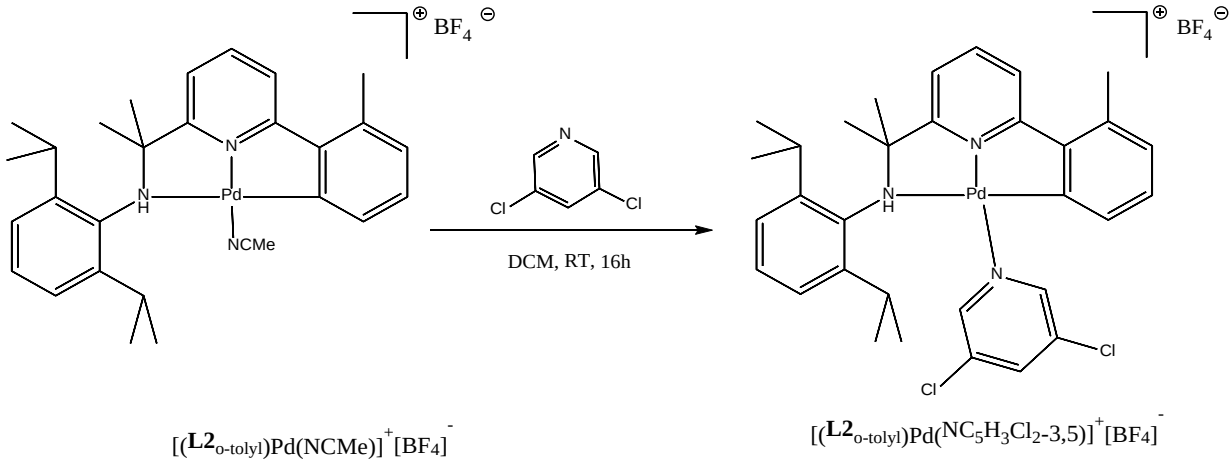

[(**L2**$_{o\text{-}tolyl}$)Pd(NCMe)]$^+[BF_4]^-$ [(**L2**$_{o\text{-}tolyl}$)Pd($NC_5H_3Cl_2$-3,5)]$^+[BF_4]^-$

Figure 5.18 | Synthesis of complex [(**L2**$_{o\text{-}tolyl}$)Pd($NC_5H_3Cl_2$-3,5)]$^+[BF_4]^-$

Further confirmation of the molecular structure of the complex was obtained by an X-ray diffraction analysis (**Figure 5.19** and **Table 5.9**). The structure is very similar to its imine-armed analogue—[(**L1**$_{o\text{-tolyl}}$)Pd($NC_5H_3Cl_2$-3,5)]$^+$[BF_4]$^-$—only with the amine proton showing intermolecular hydrogen bonding to one of the fluorine atoms on BF_4 ion with a value of 2.564 Å.

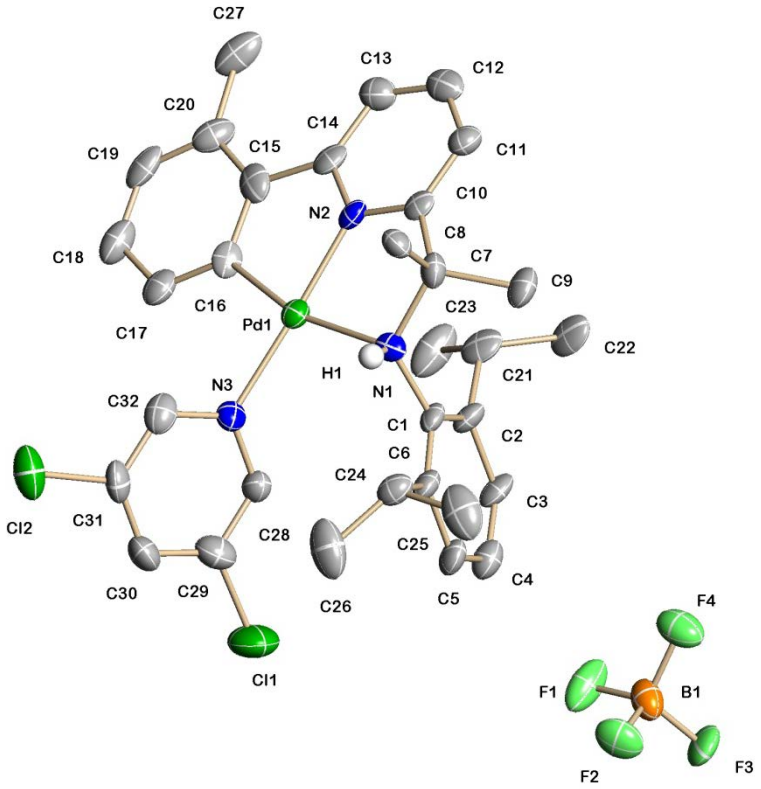

Figure 5.19 | Molecular structure of complex [(**L2**$_{o\text{-tolyl}}$)Pd($NC_5H_3Cl_2$-3,5)]$^+$[BF_4]$^-$

Table 5.9: Selected bond lengths (Å) and angles (°) for [(**L2**$_{o\text{-tolyl}}$)Pd($NC_5H_3Cl_2$-3,5)]$^+$[BF_4]$^-$

	Bond length (Å)		Bond angles (°)
Pd(1)-N(1)	2.166(6)	N(2)-Pd(1)-C(16)	82.1(3)
Pd(1)-N(2)	1.944(6)	N(2)-Pd(1)-N(1)	82.8(2)
Pd(1)-C(16)	1.989(8)	C(16)-Pd(1)-N(3)	96.8(3)
Pd(1)-N(3)	2.056(6)	N(1)-Pd(1)-N(3)	98.4(2)

Such Pd-3,5-dichloropyridine type complexes can also be obtained without going through the Pd-NCMe intermediate, by treating the Pd-Cl complexes with $AgBF_4$ and 3,5-dichloropyridine in dichloromethane (**Figure 5.20**).

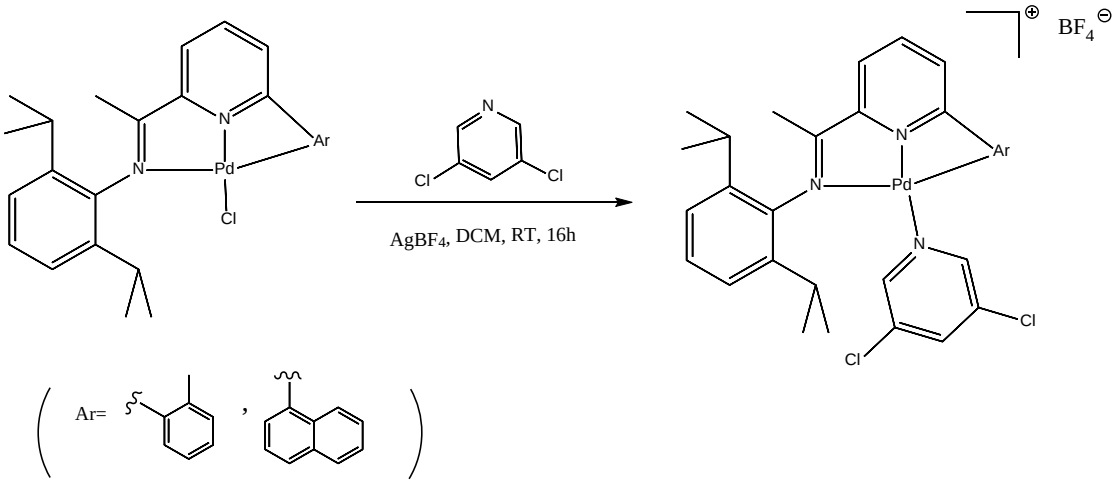

Figure 5.20 | Synthesis of Pd-Pyridine type complexes directly from Pd-Cl precursors

In light of these results, the exchange of the chloride ion with other pyridines was also tried, using *peri*- [(**L1**$_{ket\text{-}nap}$)PdCl] as an example (**Figure 5.21**). The single crystal X-ray diffraction analyses confirmed the validity of this route for replacing the chloride ion with various pyridines, by revealing the pyridine-substituted structure of the complexes. The molecular structures of these Pd-Pyridine type complexes are presented in **Figure 5.22**, with the bond lengths and angles compared in **Table 5.10**. Notably, the methyl groups on the 2,5-dimethyl pyridine moiety seem to result in the inequivalency of the two isopropyl groups on the diisopropyl phenyl unit. This is evidenced by the splitting of the 2H septet into two 1H septets and the two 6H doublets into four 3H doublets in the proton NMR spectrum of complex {*peri*-[(**L1**$_{ket\text{-}nap}$)Pd($NC_5H_3Me_2$-2,5)]}$^+$[BF_4]$^-$.

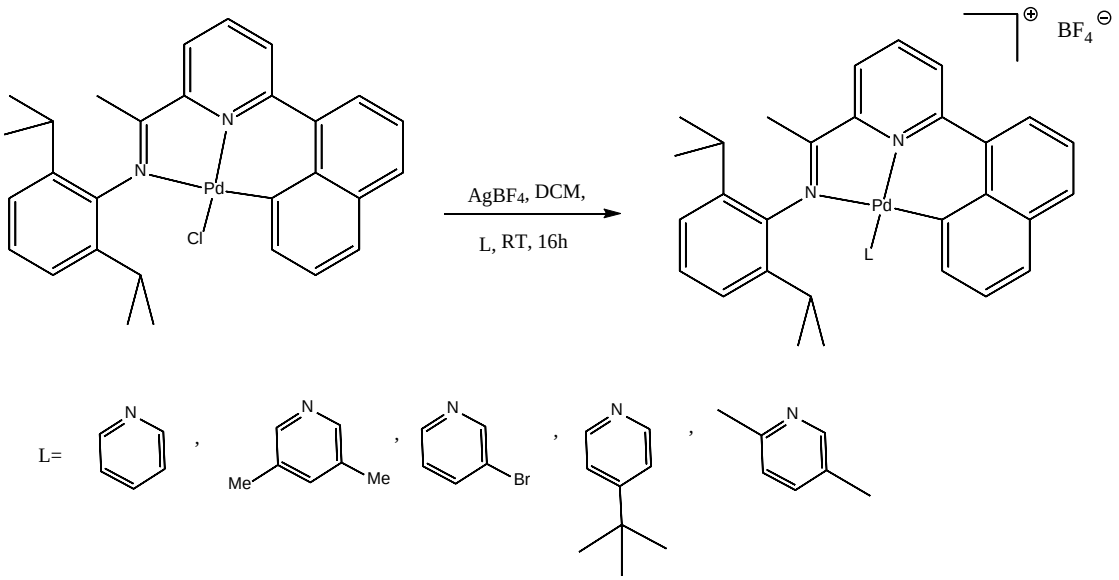

Figure 5.21 | Exchange of the chloride ion with various pyridines

Table 5.10: Selected bond lengths (Å) and angles (º) for the Pd-pyridine complexes

L / Bond/Angle	pyridine	3-bromo pyridine	4-tertbutyl pyridine	2,5-dimethyl pyridine	3,5-dichloro pyridine
Pd(1)-N(1)	2.120(4) Å	2.123(5) Å	2.123(3) Å	2.126(2) Å	2.127(5) Å
Pd(1)-N(2)	2.010(4) Å	2.002(5) Å	2.006(2) Å	2.006(2) Å	2.007(5) Å
Pd(1)-C(20)	2.008(5) Å	1.989(6) Å	2.010(3) Å	1.976(3) Å	2.000(6) Å
Pd(1)-N(3)	2.055(4) Å	2.059(5) Å	2.050(3) Å	2.053(2) Å	2.046(5) Å
C(20)-Pd(1)-N(2)	94.3(2) º	93.8(2) º	93.51(12) º	94.02(10) º	94.3(2) º
N(1)-Pd(1)-N(3)	91.96(16) º	92.75(18) º	92.23(10) º	94.53(9) º	92.8(2) º

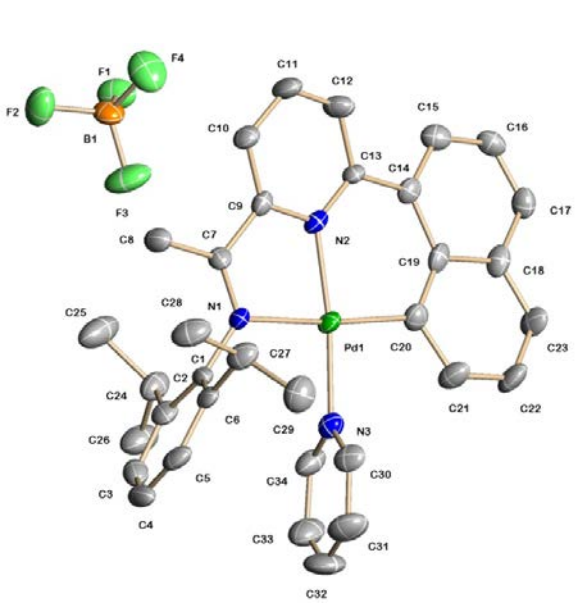

{*peri*-[(**L1**$_{ket\text{-}nap}$)Pd(NC_5H_5)]}$^+$[BF_4]$^-$

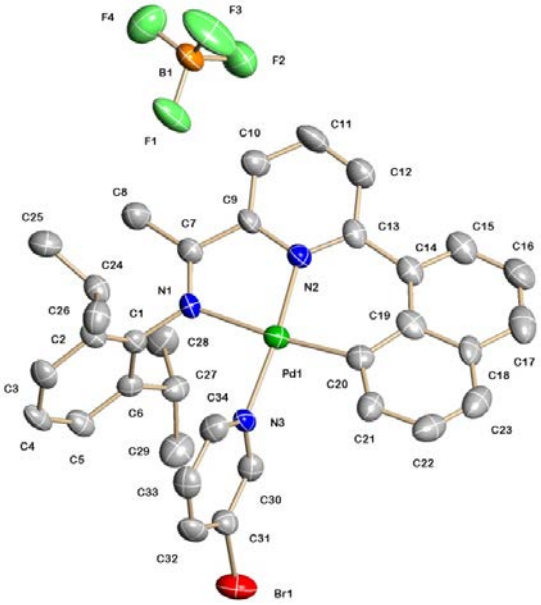

{*peri*-[(**L1**$_{ket\text{-}nap}$)Pd(NC_5H_4Br-3)]}$^+$[BF_4]$^-$

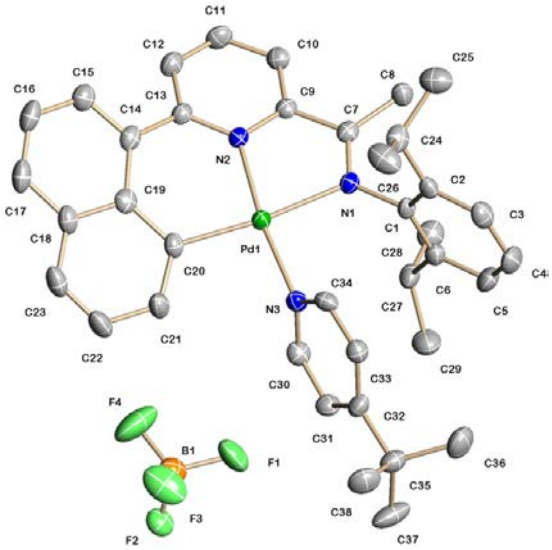

{*peri*-[(**L1**$_{ket\text{-}nap}$)Pd(NC_5H_4^{t}Bu-4)]}$^+$[BF_4]$^-$

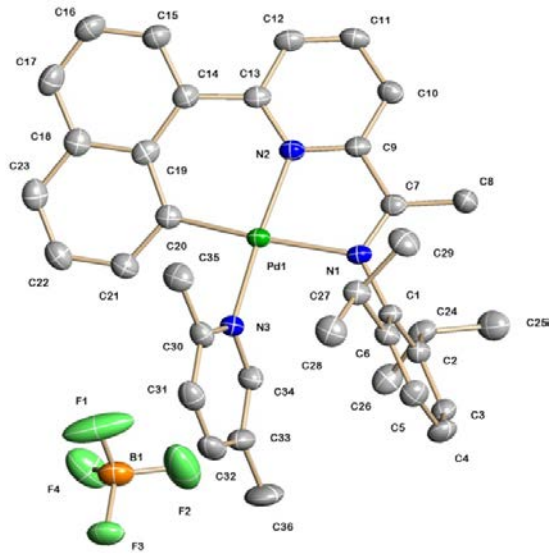

{*peri*-[(**L1**$_{ket\text{-}nap}$)Pd($NC_5H_3Me_2$-2,5)]}$^+$[BF_4]$^-$

Figure 5.22 | Molecular structures of Pd-Pyridine complexes

The Pd-N (pyridine and imine) distances do not vary significantly across the series of complexes, indicating that the substituents on the incoming pyridine ligands have little impact on the metal environment. The Pd-C distances show greater variation (1.976(3) – 2.010(3) Å) possibly as a result of the increased steric bulk of the 2,5-dimethyl pyridine ligand.

The rapid reactions of these ligands with the Pd-Cl complexes intrigued us to investigate the relative reactivity between these five different pyridines. Thus, 'competition reactions'—reacting two pyridines with 1 eq. of the Pd-Cl complex—were undertaken to 'rank' the reactivity of them (**Figure 5.23**).

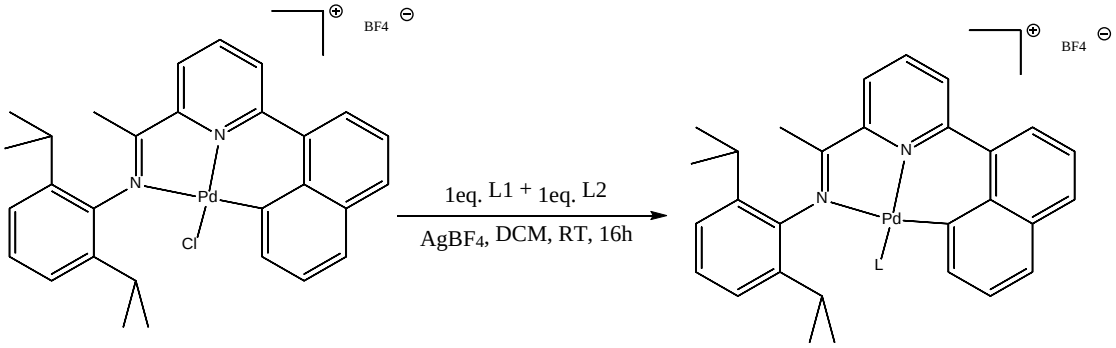

Figure 5.23 | The competition reactions with various pyridines

Table 5.11: Percentage of {*peri*-[(**L1**$_{ket\text{-}nap}$)Pd(L)]}$^{+}$[BF_4]$^{-}$ by ^{1}H NMR spectroscopy

L1	L2	% PdL1	% PdL2
3-bromo pyridine	pyridine	20	80
2,5-dimethyl pyridine	pyridine	29	71
4-tertbutyl pyridine	2,5-dimethyl pyridine	79	21
4-tertbutyl pyridine	3-bromo pyridine	98	2
3,5-dichloro pyridine	3-bromo pyridine	12	88
3,5-dichloro pyridine	4-tertbutyl pyridine	0	100
4-tertbutyl pyridine	pyridine	80	20
2,5-dimethyl pyridine	3,5-dichloro pyridine	78	22
pyridine	3,5-dichloro pyridine	79	21
2,5-dimethyl pyridine	3-bromo pyridine	65	35

The results were investigated by comparing the percentage of the two pyridine substituted complexes by ^{1}H NMR spectroscopy (**Table 5.11**).The outcome of the reactions presents the following order for the reactivity of the five pyridines (**Figure 5.24**):

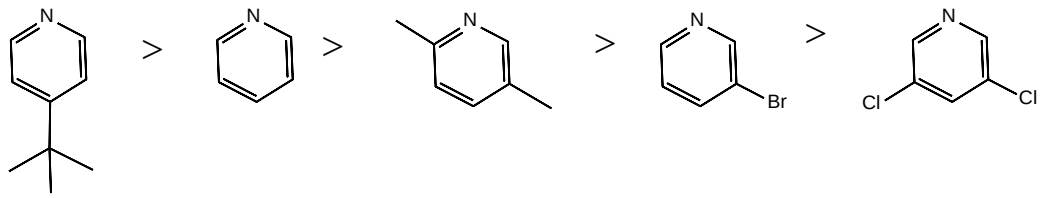

Figure 5.24 | The relative reactivity of the pyridines

The order of reactivity agrees with the predictions for the electronic and steric properties of these five pyridines. From the electronic point of view, the alkyl substituents, i.e. –^{t}Bu and –Me, are electron donating whilst the halide moieties, i.e. –Br and –Cl, are electron withdrawing. Thus, 4-^{t}Bu pyridine and 2,5-dimethyl pyridine are more reactive in this substitution reaction than the halide substituted pyridines. And sterically, the 2,5-dimethyl pyridine is more sterically strained than the pyridine while substituting the –MeCN or –Cl ligands on the palladium complexes. Hence, resulting in the pyridine being more reactive than 2,5-dimethyl pyridine in this case.

5.3 Catalytic reactions-allylic arylation

As an application of the palladium complexes, synthesized in this thesis, in catalysis, the allylic arylation of sodium tetraphenylborate and allylic acetates in the presence of ten palladium *NNC*- and *ONC*- pincer complexes and two *NN*-bidentate palladium complexes has been examined (**Figure 5.25**).

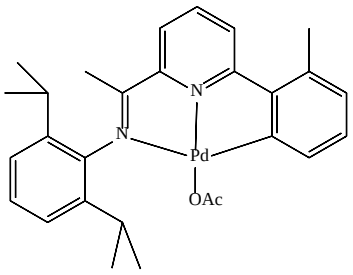

(**L1**$_{o\text{-tolyl}}$)PdOAc

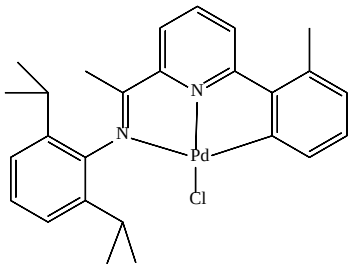

(**L1**$_{o\text{-tolyl}}$)PdCl

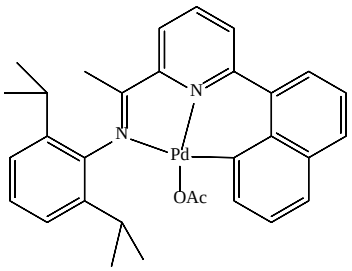

peri-[(**L1**$_{ket\text{-}nap}$)PdOAc]

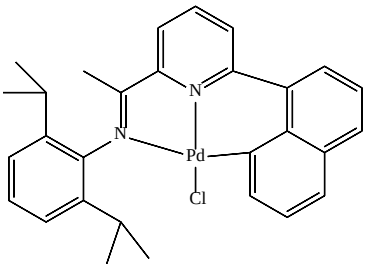

peri-[(**L1**$_{ket\text{-}nap}$)PdCl]

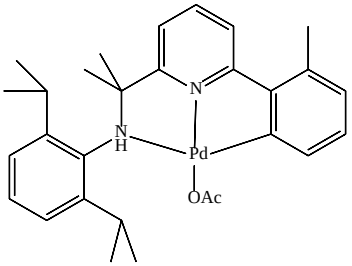

(**L2**$_{o\text{-tolyl}}$)PdOAc

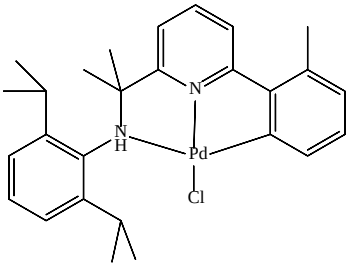

(**L2**$_{o\text{-tolyl}}$)PdCl

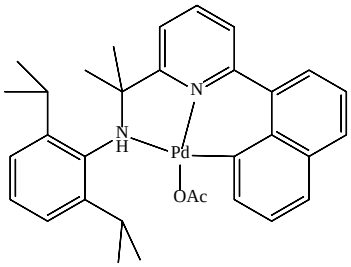

peri-[(**L2**$_{nap}$)PdOAc]

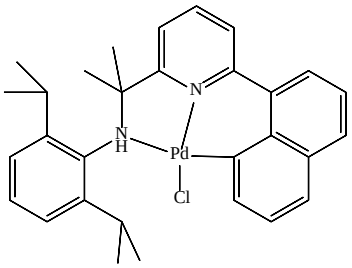

peri-[(**L2**$_{nap}$)PdCl]

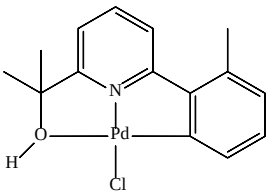

(**L3**$_{o\text{-tolyl}}$)PdCl

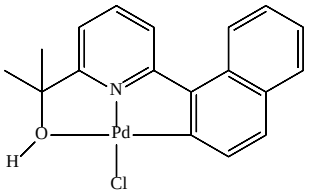

ortho-[(**L3**$_{nap}$)PdCl]

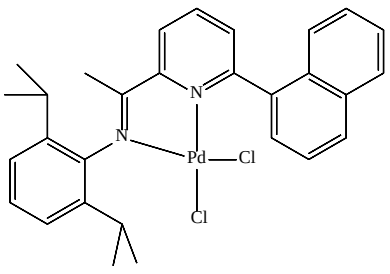

HL2$_{nap}$PdCl$_2$

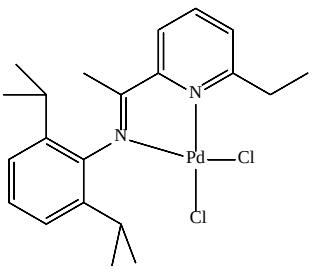

HL4$_{Et}$PdCl2

Figure 5.25 | The palladium pincer complexes tested as catalysts for allylic arylations

The allylic arylation of cinnamyl acetate with sodium tetraphenylborate was used as the catalyst screening reaction for the twelve metal complexes (**Figure 5.26**). The crude products were obtained in good to excellent conversions and purified by flash column chromatography to give the pure products with moderate to excellent isolated yields (**Table 5.12**).

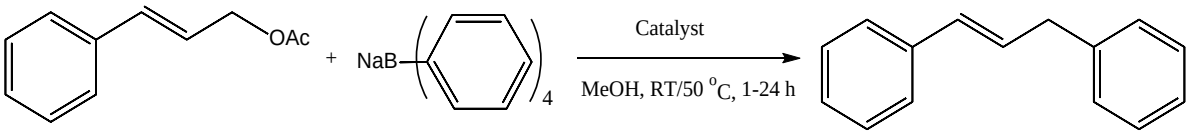

Figure 5.26 | The allylic arylation of cinnamyl acetate with sodium tetraphenylborate in the presence of palladium catalysts

It is notable that there is no reaction in the absence of the palladium catalyst at room temperature or 50 ^{o}C (**Table 5.12**, entry 1). There is also no reaction when dichloromethane was used as the solvent (**Table 5.12**, entry 6). While lowering the catalyst load to 0.01 mol%, the reaction yield drops to 21% at room temperature (24-48h) (**Table 5.12**, entry 4). Thus the reaction temperature was raised to 50 ^{o}C. The reaction reached completion after 1 h. Lowering the catalyst loading continuously to 1 mol ppm still results in 100% conversion after 1 h (**Table 5.12**, entry 7). Surprisingly, the reaction still reaches completion after 1 h (with an isolated yield of 91%) while 1 mol ppb of catalyst was used (**Table 5.12**, entry 8). Similar allyllic arylation reactions were reported in 2015, with a similar palladium NNC-pincer complex as catalyst, whilst only 27% yield was obtained with the same catalyst loading (1 mol ppb) in 24 h.[19] All the NNC- and NNO-tridentate palladium complexes (**Table 5.12** entries 8-17) gave the arylated products in 81-99% yield, while the bidentate palladium complexes **L1**$_{\text{ket-nap}}$PdCl$_2$ and **L4**$_{\text{Et}}$PdCl$_2$ showed slightly lower catalytic activities by giving yields of 68 and 70%, respectively. For both palladium catalysts with tridentate and bidentate ligands, the allylic arylation reactions proceeded smoothly with a catalyst load of 1 mol ppm. The o-tolyl-containing imine-armed palladium pincer complex (**L1**$_{\text{o-tolyl}}$)Pd(OAc) exhibited excellent catalytic performance even at an extremely low catalyst loading—1 mol ppb. Thus, a reaction condition of 50 ^{o}C in methanol in the presence of (**L1**$_{\text{o-tolyl}}$)Pd(OAc) at 1mol ppm level was defined as the optimum condition for this allylic arylation reaction. (Pd(OAc)$_2$

was also tested as a catalyst for this reaction. Although it gives a 98% isolated yield in 1h at RT with 0.01 mol% of catalyst load, and gives competitive results with our catalysts at ppb levels, it decomposes easily after prolonged standing in bench methanol while the catalysts in this work remained active even after a month.)

Table 5.12: The allylic arylation of cinnamyl acetate with sodium tetraphenylborate in the presence of *NNC*-, *ONC*- tridentate and *NN*-bidentate palladium complexes as catalysts

Entry	Catalyst	Catalyst load	Temperature (°C)	Time (h)	Yield (%)[a]
1	None	-	RT/50	24	nr[c]
2	(**L1**$_{o\text{-}tol}$)Pd(OAc)	0.1 mol%	RT	24	98
3	(**L1**$_{o\text{-}tol}$)Pd(OAc)	0.1 mol%	RT	1	97
4	(**L1**$_{o\text{-}tol}$)Pd(OAc)	0.01 mol%	RT	24-48	21
5	(**L1**$_{o\text{-}tol}$)Pd(OAc)	0.01 mol%	50	1	97
6[b]	(**L1**$_{o\text{-}tol}$)Pd(OAc)	0.1 mol%	RT/50	24	nr[c]
7	(**L1**$_{o\text{-}tol}$)Pd(OAc)	1 mol ppm	50	1	98
8	(**L1**$_{o\text{-}tol}$)Pd(OAc)	1 mol ppb	50	1	99
9	*peri*-[(**L1**$_{ket\text{-}nap}$)Pd(OAc)]	1 mol ppm	50	1	88
10	(**L1**$_{o\text{-}tol}$)PdCl	1 mol ppm	50	1	90
11	*peri*-[(**L1**$_{ket\text{-}nap}$)PdCl]	1 mol ppm	50	1	86
12	(**L2**$_{o\text{-}tolyl}$)Pd(OAc)	1 mol ppm	50	1	86
13	*peri*-[(**L2**$_{nap}$)Pd(OAc)]	1 mol ppm	50	1	82
14	(**L2**$_{o\text{-}tolyl}$)PdCl	1 mol ppm	50	1	87
15	*peri*-[(**L2**$_{nap}$)PdCl]	1 mol ppm	50	1	85
16	(**L3**$_{o\text{-}tolyl}$)PdCl	1 mol ppm	50	1	81
17	*ortho*-[(**L3**$_{nap}$)PdCl]	1 mol ppm	50	1	83
18	(**L1**$_{ket\text{-}nap}$)$PdCl_2$	1 mol ppm	50	1	68
19	(**L4**$_{Et}$)$PdCl_2$	1 mol ppm	50	1	70

[a] Isolated yield. [b] Dichloromethane was used as solvent. [c] nr = no reaction.

Following the catalyst screening and optimization of the reaction conditions, the substrate scope of the reaction was examined by investigating the allylic arylation of various allylic acetates with sodium tetraphenylborate in the presence of complex (**L1**$_{o\text{-}tolyl}$)Pd(OAc) (1 mol ppb) (**Figure 5.27**). The reactions of sodium tetraphenylborate with cinnamyl acetates containing electron-donating or electron-withdrawing substituents were tried. The reaction of (*E*)-3-(4-methylphenyl)-2-propen-1-ol acetate and (*E*)-3-(4-methoxyphenyl)-2-propen-1-ol acetate proceeded smoothly to give the (E)-1-(4-methylphenyl)-3-phenylpropene and (E)-1-(4-methoxyphenyl)-3-phenylpropene in 86 and 79% yield, respectively. The reaction of (*E*)-3-(4-nitrophenyl)-2-propen-1-ol acetate gave the arylated product (E)-1-(4-nitrophenyl)-3-phenylpropene in 98% yield. Reactions of the sterically hindered (*E*)-3-(2-methylphenyl)-2-propen-1-ol acetate, (*E*)-3-((2-methoxycarbonyl)phenyl)-2-propen-1-ol acetate and (*E*)-3-(2-nitrophenyl)-2-propen-1-ol acetate also gave the corresponding arylated products in 75-94% yields.

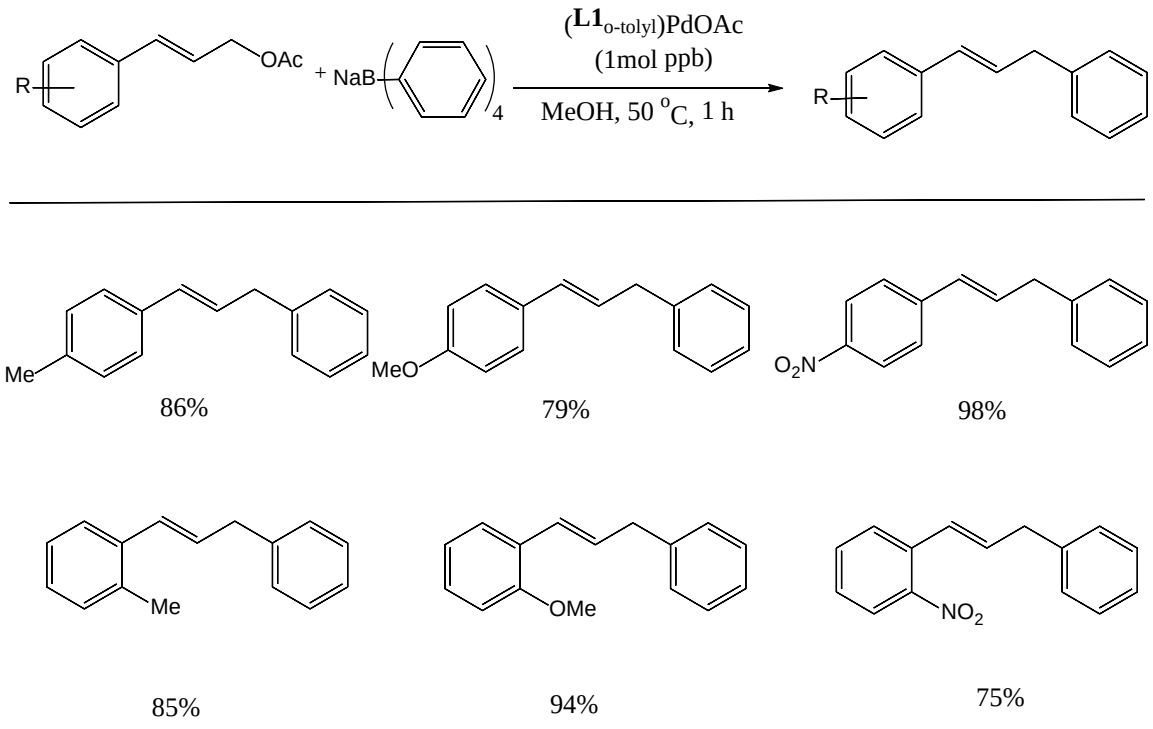

Figure 5.27| Allylic arylation of various allylic acetates with sodium tetraphenylborate in the presence of complex (**L1**$_{o\text{-}tolyl}$)Pd(OAc)

5.4 Summary and conclusions

Some reactivity of the palladium complexes synthesized in this thesis has been explored in this chapter. Halide abstraction reactions with silver salts were tried as an example of stoichiometric reactions of the complexes. Reactions in acetonitrile proceeded rapidly at room temperature and gave solvento cationic complexes in quantitative yields. Use of excess amounts of $AgBF_4$ resulted in the formation of bi- and tri-metallic palladium-silver species, which were identified in the solid state by X-ray crystallographic studies. Exchange of the labile –NCMe moiety with various pyridines readily produced a series of new palladium pincer cationic complexes with pyridines as the coordinating ligand. These results illustrate the stability of the NNC- and ONC-framework in these palladium pincer complexes under ligand exchange reaction conditions, thus indicating their potential to be applied in catalytic cycles.

Following the stoichiometric reactions, the catalytic activities of these palladium complexes were explored towards the allylic arylation of allylic acetates with sodium tetraphenylborate. Ten tridentate complexes and two bidentate palladium species were selected to be tested in a model reaction of cinnamyl acetate and sodium tetraphenylborate. The tridentate complexes exhibited considerably higher catalytic activities by giving the arylated products in good to excellent yields, especially with a 99% yield for (**L1**$_{o\text{-tolyl}}$)Pd(OAc), at 1 mol ppb levels. The allylic arylation of various allylic acetates with the phenylating reagent—sodium tetraphenylborate—was then examined in the presence of this complex with a catalyst loading of 1 mol ppb. The reactions of sodium tetraphenylborate with cinnamyl acetates containing electron-donating or electron-withdrawing substituents gave the corresponding phenylated products in good to excellent yields. Even the reactions of sterically hindered cinnamyl acetates smoothly gave the products in 75-94% yields. These results confirm that these NNC-/NNO-palladium complexes can be used as a class of novel transition metal catalysts for allylic arylation reactions, and could potentially be used for other palladium catalyzed cross-coupling reactions.

References

1 K. Bray, J. Charmant, I. Fairlamb and G. Lloyd-Jones, *Chem. Eur. J.*, 2001, **7**, 4205.

2 L. Gouriou, G. Lloyd-Jones, S. Vyskocil and P. Kocovsky, *J. Organomet. Chem*., 2003, **687**, 525.

3 A. O'Connor, P. White and M. Brookhart, *J. Am. Chem. Soc*., 2007, **129**, 4142.

4 A. O'Connor, S. Urbin, R. Moorhouse, P. White and M. Brookhart, *Organometallics*, 2009, **28**, 2372.

5 M. Heckenroth, E. Kluser, A. Neels and M. Albrecht, *Angew. Chem. Int. Ed*., 2007, **46**, 6293.

6 T. Ruther, M. Done, K. Cavell, E. Peacock, B. Skelton and A. White, *Organometallics*, 2001, **20**, 5522.

7 M. Fekete, O. Bayfield, S. Duckett, S. Hart, R. Mewis, N. Pridmore, P. Rayner and A. Whitwood, *Inorg. Chem*., 2013, **52**, 13453.

8 H. Brunner, T. Kurosawa, M. Muschiol, T. Tsuno and H. Ike, *Organometallics*, 2012, **31**, 3395.

9 B. Sundararaju, M. Achard and C. Bruneau, *Chem. Soc. Rev.*, 2012, **41**, 4467-4483.

10 F. Pigge, *Synthesis*, 2010, 1745.

11 D. Li, T. Tanaka, H. Ohmiya and M. Sawamura, *Org. Lett*., 2010, **12**, 3344.

12 Y. Yamada, S. Sarkar and Y. Uozumi, *J. Am. Chem. Soc*., 2012, **134**, 3190.

13 M. Heckenroth and M. Albrech, *Angew. Chem. Int. Ed*., 2007,**46**, 6293.

14 M. Heckenroth and M. Albrech, *Chem. Eur. J.*, 2009, **15**, 9375.

15 H. Schmidbaur, *Gold Bull*., 2000, **33**, 3.

16 J. K. Bera and K. R. Dunbar, *Angew.Chem. Int. Ed.*, 2002, **41**, 4453.

17 E. Fernandez, J. Lopez-de-Luzuriaga, M. Monge, M. Montiel, M. Olmos, J. Perez, A. Laguna, F. Mendizabal, A. Mohamed and J. Fackler, *Inorg. Chem*., 2004, **43**, 3573.

18 F. Pruchnik, P. Jakimowicz, Z. Ciunik, K. Stanislawek, L. Oro, C. Tejel and M. Ciriano, *Inorg. Chem. Commun*., 2001, **4**, 19.

19 G. Hamasaka, F. Sakurai and Y. Uozumi, *Chem. Commun*., 2015, **51**, 3886.

Chapter Six

Experimental

6.1 General

All reactions were carried out using Schlenk conditions under an atmosphere of dry, oxygen-free, nitrogen unless otherwise stated. Unless otherwise indicated, toluene, tetrahydrofuran (THF) and diethylether were dried by refluxing over sodium and benzophenone and then distilled prior to use; the same procedure was used for dichloromethane but with calcium hydride as the drying agent. All NMR spectroscopic data were collected on a Bruker ARX-400 spectrometer (400 MHz for ^{1}H, 100 MHz for ^{13}C, 375 MHz for ^{19}F) or a Bruker Avance III 500 spectrometer (500 MHz for ^{1}H, 125 MHz for ^{13}C), at ambient temperature unless otherwise stated; chemical shifts (ppm) are reported with relation to residual protio solvent peaks. Electrospray Mass Spectrometry (ESMS) data were collected by means of a micromass Quattra LC mass spectrometer with MeOH as a solvent. High resolution FAB (fast atom bombardment) mass spectra were recorded using a Kratos Concept spectrometer (xenon gas, 7kV) with NBA as a matrix. Elemental analyses were performed at the Science Technical Support Unit, London Metropolitan University. Infra Red (IR) data were obtained using a solid state Perkin Elmer Spectrum One instrument. All compounds, including n-BuLi (1.6M in hexane), trimethylsilyl cyanide, trimethylaluminium (2M solution in toluene), MeMgBr (3M solution in diethyl ether) and all the anilines, were purchased from Sigma Aldrich and rigorously maintained under a nitrogen atmosphere. $Pd(OAc)_2$, Na_2PdCl_4 and K_2PtCl_4 were purchased from Alfa-Aesar and used as obtained. $Pd(PPh_3)_4$,[1] $PdCl_2(NCMe)_2$,[2] 2-bromo-6-acetylpyridine,[3] 2-bromo-6-formylpyridine,[4] 1-naphthalene boronic acid,[5] 2-methylphenyl boronic acid,[6] 2,4,6-trimethylphenyl boronic acid,[7] 2,6-dimethylphenyl boronic acid[7] and 2-tributylstannylpyridine[8] were synthesized by literature routes. NMR solvents were kept over molecular sieves and were not distilled prior to use.

6.2 Experimental procedures for Chapter 2

6.2.1 Two step synthesis of H**L1**$_{o\text{-tolyl}}$

(a) Synthesis of 2-{2-MeC_6H_4}-6-CMeO-C_5H_3N

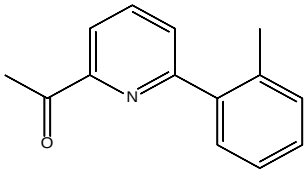

A 500 ml oven-dried three-necked round bottomed flask equipped with a magnetic stir bar was evacuated and backfilled with nitrogen. The flask was loaded with 2-bromo-6-acetyl pyridine (2.32 g, 11.68 mmol), $Pd(PPh_3)_4$ (0.27 g, 0.234 mmol, 0.02 eq.), dry toluene (40 ml) and an aqueous 2M solution of potassium carbonate (11.68 ml, 23.36 mmol, 2 eq). The solution was stirred for 15 min followed by the addition of the 2-methylphenylboronic acid (2.06 g, 15.18 mmol, 1.3 eq) in ethanol (22 ml). Following stirring and heating the solution at 90 ^oC for 48 h, the mixture was allowed to cool to room temperature and 30% hydrogen peroxide (0.8 ml) added. The solution was left to stir at room temperature for another 1 h. The product was extracted using diethylether (2 x 100 ml), washed with saturated sodium chloride solution and water (3 x 50 ml). The aqueous layer was then washed with chloroform (3 x 30 ml). The organic extracts were combined and dried over magnesium sulphate and the volatiles removed under reduced pressure to give a brown residue. The catalyst residues were removed using a short silica column employing dichloromethane:hexane (70:30; 2 x 200 ml) as the eluting solvent. After removing the solvent under reduced pressure, the product, 2-{2-MeC_6H_4}-6-CMeO-C_5H_3N, was obtained as a yellow oil (2.457 g, 99%). ^{1}H NMR ($CDCl_3$, 400 MHz): δ 2.37 (s, 3H, Ar-C*H*$_3$), 2.65 (s, 3H, C*H*$_3$-CO-pyridine), 7.16-7.26 (m, 3H, Ar-*H*), 7.34 (d, 1H, $^3J_{HH}$ = 7.2 Hz, Ar-*H*), 7.48 (d, 1H, $^3J_{HH}$ = 7.8 Hz, *m*-pyridine-*H*), 7.76 (t, 1H, $^3J_{HH}$ = 7.8 Hz, *p*-pyridine-*H*), 7.91 (d, 1H, $^3J_{HH}$ = 7.8 Hz, *m*-pyridine-*H*). ^{13}C{^{1}H} NMR ($CDCl_3$, 100 MHz): δ 20.7 (Py-C(O)-***C***H$_3$), 25.9 (o-Ar-***C***H$_3$), 119.4 (CH), 126.1 (CH), 127.4 (CH), 128.7 (CH), 129.8 (CH), 131.2 (CH), 136.3 (C), 137.2 (CH), 139.5 (C), 152.9 (C), 159.4 (C), 200.5 (Py-***C***(O)-CH$_3$). IR (solid state): 759 ν(C-H bend), 819 ν(C-H bend), 1581 ν(C=N)$_{pyridine}$, 1696 ν(C=O)$_{ketone}$, 2926 ν(C-H stretch) cm^{-1}. ESIMS (+ve, MeOH): *m/z* 212 $[M+H]^+$, 234 $[M+Na]^+$. HRMS (TOF): calculated for $C_{14}H_{14}NO$ $[M+H]^+$ 212.1036, found 212.1075.

(b) Synthesis of H**L1**$_{o\text{-tolyl}}$

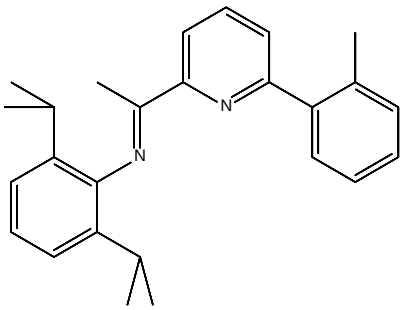

To a dry one-necked 50 mL round bottomed flask equipped with stir bar was added 2-{2-MeC_6H_4}-6-CMeO-C_5H_3N (4.00 g, 18.95 mmol), ethanol (25 mL) and 2,6-diisopropylaniline (6.72 g, 37.9 mmol, 2 eq.). After stirring the solution at reflux for 5 min, five drops of formic acid were added to the flask and a reflux condenser attached. Following stirring and heating at reflux for five days, the reaction mixture was cooled to room temperature and the resulting suspension filtered, washed with cold ethanol and dried to yield H**L1**$_{o\text{-tolyl}}$ as a pale yellow solid (5.095 g, 73%). ^{1}H NMR ($CDCl_3$, 400 MHz): δ 1.08 (d, 6H, $^3J_{HH}$ = 6.6 Hz, CH(C***H***$_3$)$_{2b}$), 1.10 (d, 6H, $^3J_{HH}$ = 6.6 Hz, CH(C***H***$_3$)$_{2a}$), 2.16 (s, 3H, Pyr-C(N)-C***H***$_3$), 2.43 (s, 3H, o-Ar-C***H***$_3$), 2.71 (sept, 2H, $^3J_{HH}$ = 6.6 Hz, C***H***-$(CH_3)_2$), 6.99-7.12 (m, 3H, Py/Ar-H), 7.21-7.31 (m, 3H, Py/Ar-H), 7.41-7.49 (m, 2H, Py/Ar-H), 7.80 (t, 1H, $^3J_{HH}$ = 7.8 Hz, Py/Ar-H), 8.24 (d, 1H, $^3J_{HH}$ = 8.0 Hz, Py/Ar-H). ^{13}C{^{1}H} NMR ($CDCl_3$, 100 MHz): δ 17.5 (Py-C(N)-***C***H_3), 20.8 (o-Ar-***C***H3), 23.0 (Ar-CH-***C***$H_{3(a)}$), 23.3 (Ar-CH-***C***$H_{3(b)}$), 28.4 (Ar-***C***H-$(CH_3)_2$), 119.1 (CH), 123.1 (CH), 123.6 (CH), 125.0 (CH), 126.1 (CH), 128.5 (CH), 130.0 (CH), 131.2 (CH), 135.9 (C), 136.3 (C), 136.8 (CH), 140.1 (C), 146.7 (C), 155.8 (C), 158.9 (C), 167.5 (Py-***C***(N)-CH_3). IR (solid state): 765 ν(C-H bend), 822 ν(C-H bend), 1587 ν(C=N)$_{pyridine}$, 1645 ν(C=N)$_{imime}$, 2926 ν(C-H stretch) cm^{-1}. ESIMS (+ve, MeOH): *m/z* 371 $[M+H]^+$, 393 $[M+Na]^+$. HRMS (TOF): calculated for $C_{26}H_{30}N_2$ $[M+H]^+$ is 371.2437, found 371.2487. m.p: 138-141 ºC.

6.2.2 Two step synthesis of H**L1**$_{ket\text{-}nap}$

(a) Synthesis of 2-{1-naphthalene}-6-CMeO-C_5H_3N

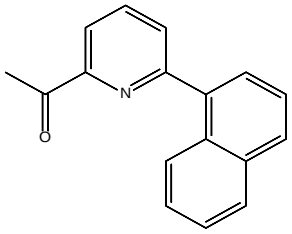

An oven-dried three-necked round bottomed flask equipped with a magnetic stir bar was evacuated and backfilled with nitrogen. The flask was loaded with 2-bromo-6-acetyl pyridine (2.685 g, 13.42 mmol), $Pd(PPh_3)_4$ (0.18 g, 0.15 mmol, 0.02 eq.), dry toluene (30 ml) and an aqueous 2M solution of potassium carbonate (13.42 ml, 26.84 mmol, 2 eq). The solution was stirred for 15 min followed by the addition of the 2-naphthalene boronic acid (3.00 g, 17.45 mmol, 1.3 eq) in ethanol (20 ml). After stirring and heating the solution at 90 ^oC for 72 h, the mixture was allowed to cool to room temperature and 30% hydrogen peroxide (0.8 ml) added. The mixture was left to stir at room temperature for further 1 h. The product was extracted using diethylether (3 x 30 ml), washed with saturated sodium chloride solution and water (3 x 30 ml). The aqueous layer was then washed repeatedly with chloroform until the extracts became colourless. The organic extracts were combined and dried over magnesium sulphate and the volatiles removed under reduced pressure to give a brown residue. The catalyst residues were removed using a short silica column employing dichloromethane:hexane (70:30; 2 x 200 ml) as the eluting solvent. After removing the solvent under reduced pressure, the product, 2-{1-naphthalene}-6-CMeO-C_5H_3N, was obtained as a pale yellow solid (3.248 g, 98%). ^1H NMR ($CDCl_3$, 400 MHz): δ 2.69 (s, 3H, O=C*Me*), 7.39-7.53 (m, 3H, ArH), 7.59 (d, $^3J_{HH}$ = 7.5 Hz, 1H, ArH), 7.70 (d, $^3J_{HH}$ = 8.0 Hz, 1H, ArH), 7.86-7.91 (m, 3H, ArH), 8.02 (dd, $^3J_{HH}$ = 8.0 Hz, $^4J_{HH}$ = 1.1 Hz, 1H, ArH), 8.10 (d, $^3J_{HH}$ = 8.0 Hz, 1H, ArH). $^{13}C\{^1H\}$ NMR ($CDCl_3$, 100 MHz): δ 25.9 (Py-C(O)-***C***H_3), 119.8 (CH), 125.4 (CH), 125.5 (CH), 126.06 (CH), 126.6 (CH), 127.9 (CH), 128.4 (CH), 128.5 (C), 129.4 (CH), 131.1 (CH), 134.1 (C), 137.3 (CH), 137.7 (C), 153.4 (C), 158.6 (C), 200.6 (Py-***C***(O)-CH_3). IR (solid state): 780 ν(C-H bend), 1585 $\nu(C{=}N)_{pyridine}$, 1695 $\nu(C{=}O)_{ketone}$ cm^{-1}. ESIMS (+ve, MeOH): *m/z* 248 $[M+H]^+$, 270 $[M+Na]^+$. HRMS (FAB): calculated for $C_{17}H_{13}NO$ $[M]^+$ 247.1033, found 247.1028. m.p: 119-122 ^oC. The NMR data are consistent with those reported in the literature.[9]

(b) Synthesis of H**L1**$_{ket\text{-}nap}$

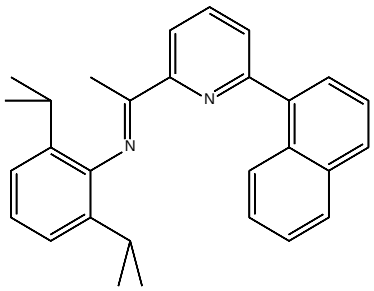

To a dry one-necked 50 mL round bottomed flask equipped with stir bar was added 2-{1-naphthalene}-6-CMeO-C_5H_3N (3.500 g, 14.15 mmol), ethanol (25 mL) and 2,6-diisopropylaniline (4.84 g, 37.9 mmol, 2 eq.); a reflux condenser was attached. After stirring the solution at reflux for 5 min, five drops of formic acid were added. The reaction mixture was then stirred and heated at reflux for four days. On cooling to room temperature a precipitate formed which was filtered, washed with cold ethanol and dried to yield H**L1**$_{ket\text{-}nap}$ as a pale yellow solid (4.366 g, 76%). ^{1}H NMR ($CDCl_3$, 400 MHz): δ 1.08 (d, 6H, $^3J_{HH}$ = 6.8 Hz, CH*(CH$_3$)$_2$*), 1.10 (d, 6H, $^3J_{HH}$ = 6.8 Hz, CH*(CH$_3$)$_2$*), 2.18 (s, 3H, *CH*=N), 2.73 (sept, 2H, $^3J_{HH}$ = 6.8 Hz, C*H*(CH_3)$_2$), 6.98 (t, 1H, $^3J_{HH}$ = 7.3 Hz, dipp-H), 7.06 (d, 2H, $^3J_{HH}$ = 7.3 Hz, dipp-H) 7.38-7.63 (m, 5H, Ar/PyH), 7.85 (m, 3H, Ar/PyH), 8.21 (d, 1H, $^3J_{HH}$ = 7.0 Hz, ArH), 8.32 (d, 1H, $^3J_{HH}$ = 7.8 Hz, PyH). ^{13}C{^{1}H} NMR ($CDCl_3$, 100 MHz): δ 17.5 (Py-C(N)-***C***H$_3$), 22.9 (Ar-CH-***C***H$_{3(a)}$), 23.3 (Ar-CH-***C***H$_{3(b)}$), 28.3 (Ar-***C***H-(CH_3)$_2$), 119.5 (CH), 123.0 (CH), 123.6 (CH), 125.4 (CH), 125.8 (CH), 125.9 (CH), 126.1 (CH), 126.4 (CH), 127.9 (CH), 128.5 (CH), 129.1 (C), 131.2 (CH), 134.1 (C), 135.9 (C), 136.9 (CH), 138.3 (C), 146.6 (C), 156.2 (C), 158.1 (C), 167.5 (Py-***C***(N)-CH_3). IR (solid state): 772 ν(C-H bend), 1562 ν(C=N)$_{pyridine}$, 1642 ν(C=N)$_{imime}$ cm^{-1}. ESIMS (+ve, MeOH): m/z 407 $[M+H]^+$, 429 $[M+Na]^+$. HRMS (FAB): calculated for $C_{29}H_{30}N_2$ $[M+H]^+$ 407.2055, found 407.2101. m.p: 183-186 ^{o}C. The NMR data are consistent with that reported in the literature.[10]

6.2.3 Two step synthesis of H**L1**$_{2,6\text{-Me2Ph}}$

(a) Synthesis of 2-(2,6-dimethylphenyl)-6-acetylpyridine

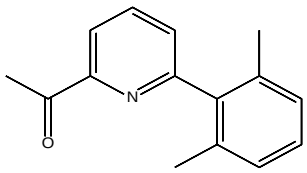

An oven-dried three-necked 100 ml round bottomed flask equipped with a magnetic stir bar was evacuated and backfilled with nitrogen. The flask was loaded with 2-bromo-6-acetylpyridine (0.906 g, 4.53 mmol), $Pd(PPh_3)_4$ (0.105 g, 0.09 mmol, 0.02 eq.), dry toluene (15 ml) and aqueous 2M solution of potassium carbonate (4.53 ml, 9.06 mmol, 2 eq). The solution was stirred for 15 min followed by the addition of the 2,6-dimethylphenylboronic acid (0.882 g, 5.88 mmol, 1.3 eq) in ethanol (10 ml). After stirring and heating the solution at 90 ºC for 72 h, the mixture was allowed to cool to room temperature and 30% hydrogen peroxide (0.8 ml) was introduced. The mixture was left to stir at room temperature for another 1 h. The product was extracted using diethylether (2 x 30 ml), washed with saturated sodium chloride solution and water (3 x 30 ml). The aqueous layer was then washed repeatedly with chloroform (3 x 40 ml). The organic extracts were combined and dried over magnesium sulphate and the volatiles removed under reduced pressure to give a brown residue. The catalyst residues were removed using a short silica column employing dichloromethane:hexane (70:30; 2 x 200 ml) as the eluting solvent. After removing the solvent under reduced pressure, 2-(2,6-dimethylphenyl)-6-acetylpyridine, was obtained as a yellow oil (0.889 g, 87%). ^{1}H NMR ($CDCl_3$, 400 MHz): δ 2.00 (s, 6H, Ar-C*H*$_3$), 2.61 (s, 3H, C*H*$_3$-CO-pyridine), 7.06 (d, 2H, $^3J_{HH}$ = 7.9 Hz, Ar-*H*), 7.15 (t, 1H, $^3J_{HH}$ = 7.5 Hz, Ar-*H*), 7.31 (dd, 1H, $^3J_{HH}$ = 7.7 Hz, $^4J_{HH}$ = 1.2 Hz, *m*-pyridine-*H*), 7.80 (t, 1H, $^3J_{HH}$ = 7.7 Hz, *p*-pyridine-*H*), 7.92 (dd, 1H, $^3J_{HH}$ = 7.9 Hz, $^4J_{HH}$ = 1.2 Hz, *m*-pyridine-*H*). ^{13}C{^{1}H} NMR ($CDCl_3$, 100 MHz): δ 20.4 (*o*-Ar-***C***H$_3$), 26.0 (Py-C(O)-***C***H$_3$), 119.5 (CH), 127.8 (CH), 128.1 (CH), 128.2 (CH), 135.9 (C), 137.0 (CH), 139.9 (C), 153.6 (C), 159.2 (C), 200.7 (Py-***C***(O)-CH$_3$). IR: 1694 ν(C=O)$_{ketone}$ cm^{-1}. ESIMS (+ve, MeOH): *m/z* 226 $[M+H]^+$, 248 $[M+Na]^+$. HRMS (FAB): calculated for $C_{15}H_{15}NO$ $[M+H]^+$ 226.2124, found 226.2119.

(b) Synthesis of H**L1**$_{2,6\text{-Me2Ph}}$

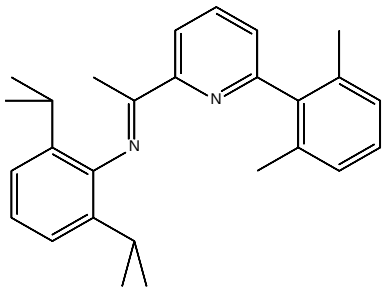

To a dry one-necked 50 mL round bottomed flask equipped with stir bar was added 2-(2,6-dimethylphenyl)-6-acetylpyridine (0.889 g, 3.95 mmol), ethanol (6 ml) and 2,6-diisopropylaniline (1.411 g, 37.9 mmol, 2 eq.). After stirring the solution at reflux for 5 min, five drops of formic acid were added and a reflux condenser attached. The reaction mixture was maintained at reflux for five days and then allowed to cool to room temperature. The resulting suspension was filtered, washed with cold ethanol and dried to yield H**L1**$_{2,6\text{-Me2Ph}}$ as a pale yellow solid (0.766 g, 51%). ^{1}H NMR ($CDCl_3$, 400 MHz): δ 1.08 (d, 6H, $^{3}J_{HH}$ = 6.8 Hz, CH-(C***H***$_3$)$_2$), 1.11 (d, 6H, $^{3}J_{HH}$ = 6.8 Hz, CH-(C***H***$_3$)$_2$), 2.08 (s, 6H, *o*-Ar-C***H***$_3$), 2.12 (s, 3H, Pyr-C(N)-C***H***$_3$), 2.73 (sept, 2H, $^{3}J_{HH}$ = 6.8 Hz, C***H***-(CH$_3$)$_2$), 7.01-7.09 (m, 3H, Ar-H), 7.11-7.17 (m, 3H, Ar-H), 7.27 (d, 1H, $^{3}J_{HH}$ = 7.6 Hz, Py-H), 7.81 (t, 1H, $^{3}J_{HH}$ = 7.9 Hz, Py-H), 8.25 (d, 1H, $^{3}J_{HH}$ = 8.2 Hz, Py-H). ^{13}C{^{1}H} NMR ($CDCl_3$, 100 MHz): δ 16.6 (Py-C(N)-***C***H$_3$), 19.5 (*o*-Ar-***C***H3), 21.9 (Ar-CH-***C***H$_{3(a)}$), 22.3 (Ar-***C***H-(CH$_3$)$_2$), 27.2 (Ar-CH-***C***H$_{3(b)}$), 118.1 (CH), 122.0 (CH), 122.5 (CH), 124.7 (CH), 126.8 (CH), 126.9 (C), 134.9 (C), 135.0 (CH), 135.5 (C), 139.3 (CH), 145.5 (C), 155.4 (C), 157.5 (C), 166.7 (Py-***C***(N)-CH$_3$). IR (solid state): 767 ν(C-H bend), 1566 ν(C=N)$_{pyridine}$, 1641 ν(C=N)$_{imime}$ cm^{-1}. ESIMS (+ve, MeOH): m/z 385 [M+H]$^{+}$, 407 [M+Na]$^{+}$. HRMS (FAB): calculated for $C_{27}H_{32}N_2$ [M+H]$^{+}$ 385.1088, found 385.1095. m.p: 160-163 ^{o}C.

6.2.4 Two step synthesis of H**L1**$_{2,4,6\text{-Me3Ph}}$

(a) Synthesis of 2-(2,4,6-trimethylphenyl)-6-acetylpyridine

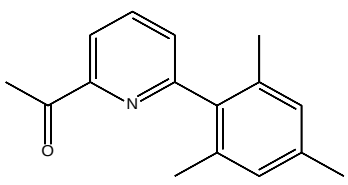

An oven-dried three-necked 100 ml round bottomed flask equipped with a magnetic stir bar was evacuated and backfilled with nitrogen. The flask was loaded with 2-bromo-6-acetylpyridine (0.906 g, 4.53 mmol), $Pd(PPh_3)_4$ (0.105 g, 0.09 mmol, 0.02 eq.), dry toluene (15 ml) and aqueous 2M solution of potassium carbonate (4.53 ml, 9.06 mmol, 2 eq). The solution was stirred for 15 min followed by the addition of the 2,4,6-trimethylphenylboronic acid (0.964 g, 5.88 mmol, 1.3 eq) in ethanol (10 ml). After stirring and heating the solution at 90 ^oC for 72 h, the mixture was allowed to cool to room temperature and 30% hydrogen peroxide (0.8 ml) was introduced. The mixture was left to stir at room temperature for another 1 h. The product was extracted using diethylether (2 x 30 ml), washed with saturated sodium chloride solution and water (3 x 30 ml). The aqueous layer was then washed repeatedly with chloroform (3 x 40 ml). The organic extracts were combined and dried over magnesium sulphate and the volatiles removed under reduced pressure to give a brown residue. The catalyst residues were removed using a short silica column employing dichloromethane:hexane (70:30; 2 x 200 ml) as the eluting solvent. After removing the solvent under reduced pressure, 2-(2,4,6-trimethylphenyl)-6-acetylpyridine, was obtained as a yellow oil (0.968 g, 73%). ^1H NMR ($CDCl_3$, 400 MHz): δ 2.10 (s, 6H, Me_o) 2.30 (s, 3H, Me_p), 2.70 (s, 3H, C*H*$_3$(C=O)), 7.00 (s, 2H, Ar-H), 7.40 (d, 1H, $^3J_{HH}$ = 7.5 Hz, Py-*H*), 7.85 (t, 1H, $^3J_{HH}$ = 7.7 Hz, Py-H), 8.00 (d, 1H, $^3J_{HH}$ = 7.7 Hz, Py-H). $^{13}C\{^1H\}$ NMR ($CDCl_3$, 100 MHz): δ 19.1 (Ar*Me*), 19.9 (Ar*M*e), 24.6 (*C*H_3(C=O), 118.2 (CH), 127.4 (CH), 127.7 (CH), 134.5 (C), 135.8 (C), 136.1 (CH), 136.5 (C), 152.4 (C), 158.11 (C), 198.9 (CH_3(*C*=O)). IR: 1699 ν(C=O)$_{ketone}$ cm^{-1}. ESIMS (+ve, MeOH): m/z 240 $[M+H]^+$, 262 $[M+Na]^+$.

(b) Synthesis of H**L1**$_{2,4,6\text{-}Me3Ph}$

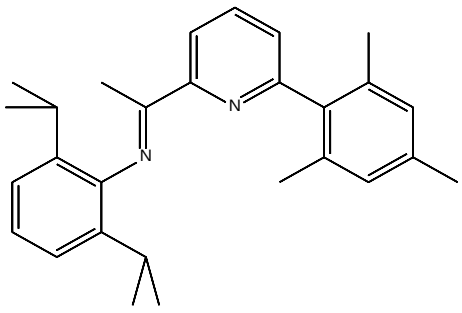

To a dry one-necked 50 mL round bottomed flask equipped with stir bar was added 2-(2,4,6-trimethylphenyl)-6-acetylpyridine (0.944 g, 3.95 mmol), ethanol (6 ml) and 2,6-

diisopropylaniline (1.411 g, 37.9 mmol, 2 eq.). After stirring the solution at reflux for 5 min, five drops of formic acid were added and a reflux condenser attached. The reaction mixture was maintained at reflux for five days and then allowed to cool to room temperature. The resulting suspension was filtered, washed with cold ethanol and dried to yield H**L1**$_{2,4,6\text{-}Me3Ph}$ as a pale yellow solid (0.539 g, 51%). ^{1}H NMR ($CDCl_3$, 400 MHz): δ 1.21 (d, 6H, $^{3}J_{HH}$ = 6.8 Hz, CH*Me*$_2$), 1.30 (d, 6H, $^{3}J_{HH}$ = 6.8 Hz, CH*Me*$_2$), 2.04 (s, 6H, Me$_o$), 2.09 (s, 3H, Me$_p$), 2.25 (s, 3H, C*H*$_3$C=N), 2.71 (sept, 2H, $^{3}J_{HH}$ = 6.6 Hz, C*H*Me$_2$), 6.89 (s, 2H, Ar-H$_m$), 7.06 (m, 3H, Ar-H), 7.22 (d, 1H, $^{3}J_{HH}$ = 7.7 Hz, py-H), 7.75 (t, 1H, $^{3}J_{HH}$ = 7.6 Hz, py-H), 8.17 (d, 1H, $^{3}J_{HH}$ = 7.7 Hz, py-H). ^{13}C{^{1}H} NMR ($CDCl_3$, 100 MHz): δ 16.4 (C*Me*=N), 19.7 (Ar-Me$_o$), 20.1 (Ar-Me$_p$), 21.9 (CH(*C*H$_3$)$_2$), 22.2 (CH(*C*H$_3$)$_2$), 27.2 (*C*H(CH$_3$)$_2$), 117.8 (CH), 121.9 (CH), 122.5 (CH), 123.8 (CH), 125.7 (CH), 128.9 (CH), 130.9 (CH), 134.8 (C), 135.0 (C), 135.6 (CH), 136.2 (C), 137.2 (C) 145.6 (C), 154.6 (C), 157.8 (C), 166.5 (CH$_3$*C*=N). IR (solid state): 1581 ν(C=N)$_{pyridine}$, 1640 ν(C=N)$_{imime}$ cm^{-1}. ESIMS (+ve, MeOH): m/z 399 [M+H]$^{+}$.

6.2.5 Two step synthesis of H**L1**$_{ald\text{-}nap}$

(a) Synthesis of 2-(1-naphthyl)-6-formylpyridine

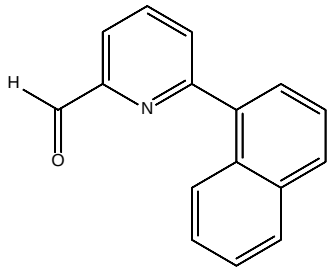

A Schlenk flask equipped with a stirrer bar was evacuated and backfilled with nitrogen, before it was charged with 2-bromo-6-formylpyridine (0.458 g, 2.46 mmol, 1 eq.), tetrakis(triphenylphosphine)palladium(0) (0.057 g, 0.0495 mmol), toluene (10 mL) and potassium carbonate (2.5 mL, 2M in water, 4.92 mmol). The yellow solution was stirred for 20 min before the addition of 1-naphthalene boronic acid (0.55 g, 3.20 mmol, 1.3 eq.) and ethanol (9 mL). The solution was stirred and heated to 90 ºC for 72 h. On cooling to room temperature the reaction mixture was treated with 30% hydrogen peroxide (0.2 mL). The crude product was washed with dichloromethane (3 x 50 mL) and water (20 mL) producing a golden yellow organic phase, which was washed with brine (30 mL) and then

dried over magnesium sulphate. Following filtration, the volatiles were removed under reduced pressure affording a brown oil. The crude product was purified by flash column chromatography using a 70:30 mixture of dichloromethane and petroleum ether (40/60) as eluent to give 2-(1-naphthyl)-6-formylpyridine as a yellow orange oil (0.389 g, 62%). ^{1}H NMR (300 MHz, $CDCl_3$): δ 7.47-7.55 (m, 2H, Ar/Py-*H*), 7.56-7.60 (m, 1H, Ar/Py-*H*), 7.64 (dd, 1H, $^{3}J_{HH}$ = 7.1 Hz, $^{4}J_{HH}$ = 1.2 Hz, Ar/Py-*H*), 7.83 (dd, 1H, $^{3}J_{HH}$ = 7.2 Hz, $^{4}J_{HH}$ = 3.3 Hz, Ar/Py-*H*), 7.90 – 8.03 (m, 5H, Ar/Py-*H*), 10.19 (s, 1H, -CO*H*). ESMS (+ve, MeOH): *m/z* 234 $[M+H]^+$. These data are consistent with those reported previously.[8]

(b) Synthesis of H**L1**$_{ald\text{-}nap}$

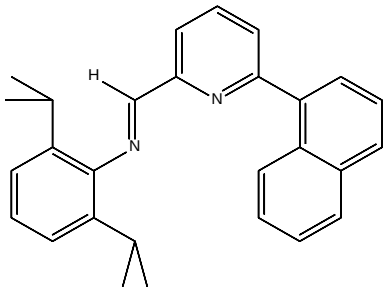

A 50 mL round bottomed flask, equipped with a stir bar and open to the air, was loaded with 2-(1-naphthyl)-6-formylpyridine (0.62 g, 2.58 mmol), 2,6-diisopropylaniline (0.689 g, 3.86 mmol) and ethanol (10 mL). The reaction mixture was warmed to 40 °C and stirred for 15 min. One drop formic acid was introduced to the flask before the mixture was left to stir overnight at 40 °C. Once cooled to room temperature, the precipitate was filtered and washed with ethanol and dried under reduced pressure yielding H**L1**$_{ald\text{-}nap}$ as a pale yellow solid (0.508 g, 48%). Crystals suitable for single crystal X-ray diffraction were grown by slow evaporation of a methanol solution containing the compound. ^{1}H NMR (300 MHz, $CDCl_3$): δ 1.20 (d, 12H, $^{3}J_{HH}$ = 6.8 Hz, CH(C*H*$_3$)$_2$), 3.02 (sept, 2H, $^{3}J_{HH}$ = 6.8 Hz, C*H*(CH$_3$)$_2$), 7.10-7.20 (m, 3H, Ar-H), 7.47-7.55 (m, 3H, Py-H), 7.71 (td, 2H, $^{3}J_{HH}$ = 7.1 Hz, $^{4}J_{HH}$ = 1.1 Hz, Nap-H), 7.91-7.96 (m, 2H, Nap-H), 7.99 (app-t, 1H, $^{3}J_{HH}$ = 7.9 Hz, Nap-H), 8.16-8.12 (m, 1H, Nap-H), 8.35 (dd, 1H, $^{3}J_{HH}$ = 7.8 Hz, $^{4}J_{HH}$ = 1.1 Hz, Nap-H), 8.42 (s, 1H, Imine-H). ^{13}C{^{1}H} NMR (75.42 MHz, $CDCl_3$): δ 23.5 (CH(*C*H$_3$)$_2$), 28.1 (*C*H(CH$_3$)$_2$), 119.5 (C), 123.1 (CH), 124.5 (CH), 125.4 (CH), 125.5 (CH), 126.1 (CH), 126.6 (CH), 126.8 (CH), 127.7 (CH), 128.5 (CH), 129.3 (CH), 131.2 (C), 134.1 (C), 137.1 (C), 137.2 (CH), 137.9 (C), 148.5 (C), 154.4 (C), 159.3 (C), 163.4 (H-C=N). IR (solid state): 2980 ν(H-C$_{aromatic}$), 1637 ν(C=N$_{imine}$) cm^{-1}. ESIMS (+ve MeOH): *m/z* 393. HRMS

(TOF): *m/z* calculated for $C_{28}H_{28}N_2$ $[M+H]^{+:}$ 393.2331. Found: 393.2334 $[M+H]^+$. mp 132-136 °C.

6.2.6 Synthesis of H**L2**$_{o\text{-tolyl}}$

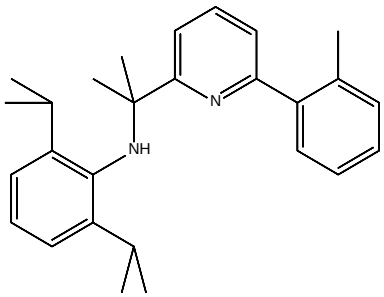

A clean and dry Schlenk flask equipped with a stir bar was evacuated and backfilled with nitrogen. To the flask was added H**L1**$_{o\text{-tolyl}}$ (0.555 g, 1.5 mmol, 1 eq.) which was dissolved in dry toluene (30 ml). $AlMe_3$ (2.3 ml, 4.5 mmol, 3 eq., 2M in toluene) was introduced dropwise and the reaction mixture stirred and heated to 95 ^oC overnight. The mixture was cooled to room temperature and de-ionized water (30 ml) added carefully. The mixture was stirred for 1 h and then the organic phase separated. The aqueous layer was washed with chloroform (2 × 30 ml). The organic extracts were combined, washed with saturated sodium chloride solution and dried over magnesium sulphate. The solvent was removed under reduced pressure to give H**L2**$_{o\text{-tolyl}}$ as a yellow oily solid (0.525 g, 91%). ^{1}H NMR ($CDCl_3$, 400 MHz): δ 0.97 (d, 12H, $^3J_{HH}$ = 6.9 Hz, CH-(C*H*$_3$)$_2$), 1.42 (s, 6H, HN-(C*H*$_3$)$_2$), 2.37 (s, 3H, o-Ar-C*H*$_3$), 3.17 (sept, 2H, $^3J_{HH}$ = 6.9 Hz, C*H*-(CH_3)$_2$), 4.17 (br s, 1H, *H*N-(CH_3)$_2$), 6.94-7.01 (m, 3H, Py/Ar-H), 7.04-7.25 (m, 5H, Py/Ar-H), 7.35-7.42 (m, 1H, Py/Ar-H), 7.63 (t, 1H, $^3J_{HH}$ = 7.73 Hz, Py/Ar-H). ^{13}C{^{1}H} NMR ($CDCl_3$, 100 MHz): δ 20.8 (o-Ar-*C*H_3), 24.1 (Ar-CH-(*C*H_3)$_2$), 28.3 (Ar-*C*H-(CH_3)$_2$), 29.3 (Py-C(NH)-(*C*H_3)$_2$), 59.5 (Py-*C*(NH)-(CH_3)$_2$), 117.1 (CH), 121.6 (CH), 123.0 (CH), 124.5 (CH), 125.9 (CH), 128.2 (CH), 129.9 (CH), 130.9 (CH), 136.1 (C), 136.5 (C), 140.6 (CH), 140.9 (C), 146.6 (C), 158.7 (C), 167.7 (C). IR (solid state): 794 ν(C-H bend), 815 ν(C-H bend), 1576 $\nu(C{=}N)_{pyridine}$, 2926 ν(C-H stretch), 3351 $\nu(N\text{-}H)_{amine}$ cm^{-1}. ESIMS (+ve, MeOH): m/z 387 [M+H]+. HRMS (FAB): calculated for $C_{27}H_{35}N_2$ $[M+H]^+$ 387.2747, found 387.2796. m.p: 81-84 ^oC.

6.2.7 Synthesis of H**L2**$_{nap}$

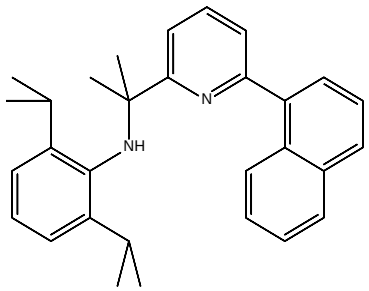

A small clean and dry Schlenk flask was charged with H**L1**$_{ket\text{-}nap}$ (2.045 g, 5.03 mmol, 1 eq) and the contents dissolved in toluene (40 mL). $AlMe_3$ (6.0 mL, 12 mmol, 2.4 eq, 2M in toluene) was added dropwise and the reaction mixture stirred and heated to 95 ^oC overnight. After cooling the reaction to room temperature, de-ionized water (10 mL) was carefully added (slowly at first to prevent the reaction from boiling over), and the mixture allowed to stir vigorously for 2 h. The organic layer was separated. The aqueous layer was washed with dichloromethane (3 x 30 mL) and the combined organic layers washed with brine (1 x 50 mL). The organic fractions were dried over magnesium sulphate and the solvent removed under reduced pressure to give H**L2**$_{nap}$ as a yellow oil (1.997 g, 88%). ^1H NMR ($CDCl_3$, 400 MHz): δ 0.95 (12H, d, $^3J_{HH}$ = 6.8 Hz, $CH(CH_3)_2$, 1.44 (s, 6H, $(CH_3)_2CNH$), 3.22 (sept, 2H, $^3J_{HH}$ = 7.1 Hz, $CH(CH_3)_2$), 4.27 (s, 1H, $(CH_3)_2CNH$), 6.97 (m, 3H, dipp-H), 7.34-7.40 (m, 3H, Ar/PyH) 7.46 (t, 2H, $^3J_{HH}$ = 8.3 Hz, Ar/PyH), 7.55(d, 1H, $^3J_{HH}$ = 6.8, Ar/PyH), 7.67 (t, 1H, $^3J_{HH}$ = 7.7, ArH), 7.80 (d, 2H, $^3J_{HH}$ = 8.0 Hz, Ar/PyH), 8.10 (d, 1H, $^3J_{HH}$ = 8.0 Hz, Ar/PyH). $^{13}C\{^1H\}$ NMR ($CDCl_3$, 100 MHz): δ 26.9 (Ar-CH-(CH_3)$_2$), 31.1 (Ar-*C*H-(CH_3)$_2$), 32.1 (Py-C(NH)-(CH_3)$_2$), 62.4 (Py-*C*(NH)-(CH_3)$_2$), 120.4 (CH), 125.5 (CH), 125.9 (CH), 127.2 (CH), 127.3 (CH), 128.2 (CH), 128.8 (CH), 129.1 (CH), 130.4 (CH), 131.3 (CH), 133.8 (C), 134.2 (CH), 136.9 (C), 139.5 (C), 141.9 (CH), 143.3 (C), 149.7 (C), 160.7 (C), 170.9 (C). IR: 3054 ν(N-H)$_{amine}$, 2960 ν(C-H stretch), 1570 ν(C=N)$_{pyridine}$, 1464, 1439, 1196, 798, 772 cm^{-1}. ESMS (+ve, MeCN): m/z 423 $[M]^+$. HRMS (FAB): calculated for $C_{30}H_{34}N_2$ $[M]^+$ 423.2788, found 423.2792. m.p: 89 – 92 ^oC.

6.2.8 Synthesis of H**L3**$_{o\text{-tolyl}}$

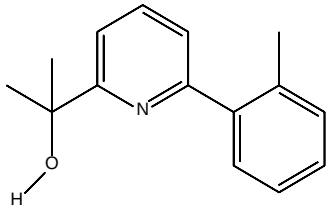

A small dry Schlenk flask was evacuated and backfilled with nitrogen. The flask was charged with 2-{2-MeC_6H_4}-6-CMeO-C_5H_3N (0.253 g, 1.2 mmol, 1 eq.) and the contents dissolved in toluene (10 ml). Trimethylaluminium (2.0 ml, 4 mmol, 3.3 eq., 2M in toluene) was added dropwise and the reaction stirred and heated to 95 ^oC overnight. The reaction mixture was cooled to room temperature and de-ionized water (10 ml) carefully added (a water-ice bath was placed under the flask to keep it cool). The mixture was stirred vigorously for 2 h after the addition of water. The organic layer was separated and the aqueous layer was washed with dichloromethane (3 × 15 ml). The organic layers were combined and washed with brine (1 × 30 ml) and dried over $MgSO_4$. Following filtration, the solvent was removed using a rotary evaporator and then under reduced pressure for 24 h to give H**L3**$_{o\text{-tolyl}}$ as a white solid (0.248 g, 91%). ^{1}H NMR ($CDCl_3$, 400 MHz): δ 1.49 (s, 6H, Pyr-C-(C***H***$_3$)$_2$), 2.29 (s, 3H, *o*-Ar-C***H***$_3$), 5.18 (s (broad), 1H, C-(CH_3)$_2$-O***H***), 7.16-7.22 (m, 5H, Py/Ar-H), 7.32 (d, 1H, $^3J_{HH}$ = 6.8 Hz, Py/Ar-H), 7.64 (t, 1H, $^3J_{HH}$ = 7.8 Hz, Py/Ar-H). $^{13}C\{^1H\}$ NMR ($CDCl_3$, 100 MHz): δ 20.7 (*o*-Ar-*C*H_3), 30.8 (Pyr-C-(*C*H_3)$_2$), 71.8 (Pyr-*C*-(CH_3)$_2$), 116.6 (CH), 122.1 (CH), 125.9 (CH), 128.5 (CH), 129.8 (CH), 131.0 (CH), 136.1 (C), 137.4 (CH), 139.9 (C), 157.8 (C), 165.3 (C). IR (solid state): 801 ν(C-H bend), 1563 ν(C=N)$_{pyridine}$, 3398 ν(O-H bond) cm^{-1}. ESIMS (+ve, MeOH): m/z 216 [M+H]$^+$, 238 [M+Na]$^+$. HRMS (FAB): calculated for $C_{14}H_{17}NO$ [M+H]$^+$ 216.2911, found 216.2914. m.p: 113-116 ^oC.

6.2.9 Synthesis of H**L3**$_{nap}$

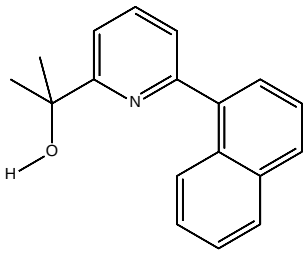

A clean and dry Schlenk flask was charged with 2-{1-naphthalene}-6-CMeO-C_5H_3N (0.30 g, 1.2 mmol, 1 eq) and the contents dissolved in toluene (10 mL). $AlMe_3$ (2.0 mL, 4.0 mmol, 3.3 eq., 2M in toluene) was added dropwise and the reaction mixture stirred and heated to 95 ^oC overnight. After cooling the reaction to room temperature, de-ionized water (10 mL) was carefully added (slow addition to prevent reaction boiling over), and the reaction allowed to stir vigorously for 2 h. The organic phase was separated, while the aqueous layer was washed with dichloromethane (3 x 15 mL). All the organic layers were combined and finally washed with brine (1 x 30 mL). The organic fractions were dried over magnesium sulphate and following filtration, the solvent was removed under reduced pressure affording H**L3**$_{nap}$ as a yellow oil (0.310 g, 98%). ^1H NMR ($CDCl_3$, 400 MHz): δ 1.47 (s, 6H, $(CH_3)_2COH$), 5.16 (s, 1H, $(CH_3)_2COH$), 6.97 (m, 3H, dipp-H), 7.20 (d, 1H, $^3J_{HH}$ = 7.9 Hz, Ar/PyH), 7.27 (d, 1H, $^3J_{HH}$ = 8.2 Hz, Ar/PyH), 7.30-7.33 (m, 2H, Ar/PyH) 7.37 (t, 1H, $^3J_{HH}$ = 8.2 Hz, Ar/PyH), 7.45 (d, 1H, $^3J_{HH}$ = 6.7 Hz, Ar/PyH), 7.59 (t, 1H, $^3J_{HH}$ = 7.9 Hz, ArH), 7.73 (d, 2H, $^3J_{HH}$ = 8.2 Hz, Ar/PyH), 7.98 (d, 1H, $^3J_{HH}$ = 8.0 Hz, Ar/PyH). $^{13}C\{^1H\}$ NMR ($CDCl_3$, 100 MHz): δ 29.7 (Py-C-$(CH_3)_2$), 70.9 (Py-*C*-$(CH_3)_2$), 115.8 (CH), 121.9 (CH), 124.2 (CH), 124.5 (CH), 124.8 (CH), 125.4 (CH), 126.6 (CH), 127.3 (C), 127.9 (CH), 129.9 (CH), 132.9 (C), 136.4 (CH), 137.0 (C), 155.5 (C), 164.8 (C). IR (solid state): 3409 ν(OH), 2972, 1571 $\nu(C{=}N)_{pyridine}$, 1444, 1391, 1366, 1176, 799 ν(C-H bend), 772 cm^{-1}. ESIMS (+ve, MeOH): *m/z* 264 $[M+H]^+$. HRMS (FAB): calculated for $C_{18}H_{18}NO$ $[M+H]^+$ 264.1372, found 264.1380. m.p: 110-112 ^oC.

6.2.10 Two step synthesis of H**L1**$_{py\text{-}nap}$

(a) Synthesis of 6-bromo-2,2'-bipyridine

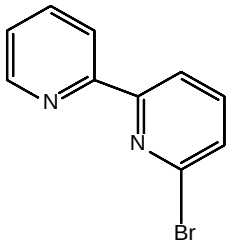

Based on a method described in the literature,[11] a Schlenk flask equipped with a stirrer bar was evacuated and backfilled with nitrogen. The flask was charged with 2,6-dibromopyridine (2.603 g, 10.99 mmol, 1.1 eq.), toluene (20 mL) and tetrakis(triphenylphosphine)palladium(0) (0.608 g, 0.526 mmol) producing a yellow

solution. The 2-tributylstannyl pyridine (3.802 g, 10.33 mmol, 1 eq.) was added to the solution and the reaction mixture stirred and heated to 90 ^{o}C for 45 h to give a dark brown solution. The solvent was removed under reduced pressure and the residue dissolved in dichloromethane (10 mL) and washed with dilute hydrochloric acid (3 x 10 mL). The solution was neutralised with 10% aqueous ammonia producing a cloudy pale brown solution. The organic phase was separated and the aqueous phase washed with dichloromethane (3 x 30 mL). The organic phases were combined and washed with water (2 x 30 mL). Following drying of the organic extracts over magnesium sulphate, all volatiles were removed under reduced pressure. The resulting solid was purified by flash column chromatography, using 50:50 petroleum ether to dichloromethane as the eluent, affording 6-bromo-2,2'-bipyridine as a pale orange solid (1.592 g, 66%). ^{1}H NMR (300 MHz, $CDCl_3$): δ 7.33 (app. t, 1H, $^{3}J_{HH}$ = 7.4 Hz), 7.49 (d, 1H, $^{3}J_{HH}$ = 7.4 Hz), 7.67 (app. t, 1H, $^{3}J_{HH}$ = 6.8 Hz), 7.82 (app. t, 1H, $^{3}J_{HH}$ = 8.0 Hz), 8.40 (app. t, 2H, $^{3}J_{HH}$ = 8.0 Hz), 8.67 (d, 1H, $^{3}J_{HH}$ = 5.1 Hz). ESIMS (+ve, MeOH): *m/z* 237 $[M+H]^{+}$. These data are consistent with those reported previously.[11]

(b) Synthesis of H**L1**$_{py\text{-}nap}$

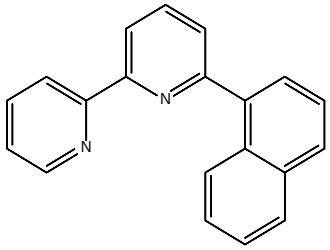

A Schlenk flask equipped with stirrer bar was evacuated and backfilled with nitrogen. The flask was charged with 6-bromo-2,2'-bipyridine (0.502 g, 2.14 mmol, 1 eq.), tetrakis(triphenylphosphine)palladium(0) (0.05 g, 0.043 mmol), aquesous potassium carbonate (2.13 mL, 4.25 mmol, 2 eq., 2M solution in water) and dry THF (10 mL) producing a pale orange solution. The solution was stirred for 20 min at room temperature followed by the addition of 1-naphthalene boronic acid (0.481 g, 2.80 mmol, 1.3 eq.) and ethanol (3 mL). The solution was stirred and heated to 90 ^{o}C for 72 h. On cooling to room temperature, 30% hydrogen peroxide (0.2 mL) was added and the mixture stirred for a further hour. The organic phase was separated and the aqueous phase extracted with dichloromethane (3 x 30 mL). The organic layers were combined and washed with brine (30 mL) before drying over $MgSO_4$. The solvent was removed under reduced pressure and the residue purified by flash chromatography using a 70:30 mixture of

dichloromethane to petroleum ether (40/60) as eluent, affording H**L1**$_{py\text{-}nap}$ as a pale orange solid (0.357 g, 61%). Crystals suitable for a single crystal X-ray diffraction study were grown by slow evaporation of a methanol solution of H**L1**$_{py\text{-}nap}$. ^{1}H NMR (300 MHz, $CDCl_3$): δ 7.30 (dd, 1H, $^{3}J_{HH}$ = 4.8 Hz, $^{4}J_{HH}$ = 2.0 Hz, Py-H_m), 7.48 (m, 1H, Nap-H_{C6}), 7.50 (m, 1H, Nap-H_{C3}), 7.53 (m, 1H, Nap-H_{C8}), 7.60 (dd, 1H, $^{3}J_{HH}$ = 7.7 Hz, $^{4}J_{HH}$ = 1.00 Hz, Nap-H_{C7}), 7.70 (d, 1H, $^{3}J_{HH}$ = 7.7 Hz, Py-H_m), 7.77 (app. t, 1H, $^{3}J_{HH}$ = 8.0 Hz, Py-H_p), 7.92 (m, 2H, Nap-$H_{C4,C5}$), 7.96 (d, 1H, $^{3}J_{HH}$ = 8.3 Hz, Py-H_m), 8.23 (d, 1H, $^{3}J_{HH}$ = 8.5 Hz, $^{4}J_{HH}$ = 2.2 Hz, Nap-H_{C2}), 8.50 (app. t, 2H, $^{3}J_{HH}$ = 8.4 Hz, Py-H_m), 8.70 (dq, 1H, $^{3}J_{HH}$ = 4.2 Hz, $^{4}J_{HH}$ = 0.9 Hz, Py-H_o). ^{13}C{^{1}H} NMR (75.42 MHz, $CDCl_3$): δ 119.2 (CH), 121.5 (CH), 123.8 (CH), 125.1 (CH), 125.4 (CH), 125.9 (CH), 126.4 (CH), 127.7 (CH), 128.4 (CH), 129.0 (CH), 131.3 (C), 132.1 (CH), 134.1 (C), 137.0 (CH), 137.4 (CH), 138.6 (C), 149.1 (CH), 155.8 (C), 156.3 (C), 158.6 (C). IR (solid state): 3045 ν(C-H)$_{alkenyl}$, 1578 ν(C=N)$_{pyridine}$, 1556, 1506, 1474, 1452, 1424, 1402 ν(C=C)$_{aromatic}$ cm^{-1}. ESIMS (-ve, MeOH): *m/z* 281 [M-H]$^{-}$. HRMS (TOF): *m/z* calc. for $C_{20}H_{14}N_2$ [M+H]$^{+}$: 283.1235, found: 283.1224. mp: 95 – 97 ºC.

6.2.11 Four step synthesis of H**L4**$_{Et}$

(a) Synthesis of 2-ethylpyridine N-oxide

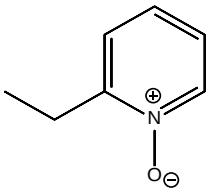

A 500 ml round bottomed flask equipped with a stir-bar was charged with 2-ethylpyridine (10.00 g, 93.458 mmol) and chloroform (100 ml) and the solution cooled to 0 °C. A solution of 3-chloroperoxybenzoic acid (mcpba) (23.993 g, 140.31 mmol, 1.5 eq.) previously dissolved in warm chloroform (100 ml) was added drop-wise over 1 h at this temperature *via* a pressure equalised dropping funnel. The resulting solution was allowed to warm to room temperature gradually and stirred for a further 12 h. After removal of solvent under reduced pressure the resulting oil was stirred overnight with sodium hydroxide (50 ml, 1.0 M). The aqueous layer was extracted rigorously with chloroform (5 x 50 ml) and the combined organic phase was dried over magnesium sulphate, filtered

and concentrated to give a dark yellow oil (10.35 g, 90%). Note: The oil is volatile and should be dried briefly (*ca.* 30 mins) under reduced pressure. ^{1}H NMR (300 MHz, $CDCl_3$): δ 1.32 (t, 3H, $^{3}J_{HH}$ = 7.4 Hz, C*H*$_3$), 2.96 (q, 2H, $^{3}J_{HH}$ = 7.4 Hz, C*H*$_2$), 7.23 (m, 3H, Py*H*). These data are consistent with those reported in the literature.[12]

(b) Synthesis of 2-ethyl-6-cyanopyridine

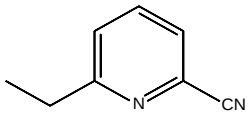

A 250 ml three neck flask equipped with a pressure equalised dropping funnel and a stirrer bar was evacuated and backfilled with nitrogen. The flask was charged with 2-ethylpyridine *N*-oxide (8.000 g, 65.57 mmol), trimethylsilylcyanide (7.807 g, 78.69 mmol, 1.2 eq.) and dry dichloromethane (100 ml). Dimethylcarbamylchloride (8.554 g, 78.69 mmol, 1.2 eq.) was added to the pressure equalised dropping funnel and added dropwise. The funnel was then rinsed with a portion of dry dichloromethane (20 ml). The resulting solution was stirred for 72 h at room temperature after which time a 20% potassium carbonate solution (50 ml) was added and the mixture stirred for a further 30 min. The organic phase was separated, dried over magnesium sulphate and, following filtration and solvent removal, the product was obtained as an orange oil (2.577 g, 30%). ^{1}H NMR (400 MHz, $CDCl_3$): δ 1.25 (t, 3H, $^{3}J_{HH}$ = 7.4 Hz, C*H*$_3$), 2.81 (q, 2H, $^{3}J_{HH}$ = 7.4 Hz, C*H*$_2$), 7.35 (d, 1H, $^{3}J_{HH}$ = 7.0 Hz, Py*H*), 7.47 (d, 1H, $^{3}J_{HH}$ = 7.0 Hz, Py*H*), 7.70 (t, 1H, $^{3}J_{HH}$ = 7.0 Hz, Py*H*). These data are consistent with those reported in the literature.[13]

(c) Synthesis of 2-ethyl-6-acetylpyridine

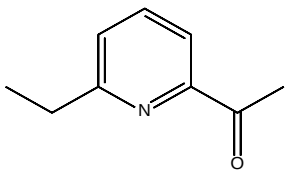

A dry three neck flask was evacuated and backfilled with nitrogen, before being charged with 2-ethyl-6-cyanopyridine (0.515 g, 3.90 mmol) and dry tetrahydrofuran (20 ml). The resulting solution was cooled to -15 °C (using an acetone/dry ice bath) and MeMgBr (2.0 ml, 0.702 g, 5.90 mmol, 1.5 eq., 3M solution in diethyl ether), added dropwise. The mixture was then stirred for 1 h at -15 °C and 2 h at room temperature. Saturated ammonium chloride solution (30 ml) was added and the mixture stirred for 10 min. The

organic layer was separated and the aqueous layer washed with diethyl ether (1 x 20 ml) and then dichloromethane (1 x 20 ml). The combined organic layers were then washed with brine (1 x 20 ml) and water (2 × 20 ml). The organic phase was then dried over magnesium sulphate, filtered and the solvent removed under reduced pressure to give the crude product as a deep yellow oil. The sample was purified by flash chromatography using a 40:60 mixture of ethyl acetate:petroleum ether affording 2-ethyl-6-acetylpyridine as a yellow oil (0.425 g, 73%). ^{1}H NMR (400 MHz, $CDCl_3$): δ 1.35 (t, 3H, $^{3}J_{HH}$ = 7.6 Hz, CH_2CH_3), 2.72 (s, 3H, C*H*$_3$C=O), 2.88 (q, 2H, $^{3}J_{HH}$ = 7.6 Hz, C*H*$_2$CH$_3$), 7.31 (d, 1H, $^{3}J_{HH}$ = 7.0 Hz, Py-H), 7.71 (t, 1H, $^{3}J_{HH}$ = 7.6 Hz, PyH), 7.84 (d, 1H, $^{3}J_{HH}$ = 7.2 Hz, PyH). ^{13}C{^{1}H} NMR ($CDCl_3$, 100 MHz): δ 13.5 (CH_2CH_3), 25.7 (*C*H$_3$C=O), 31.1 (*C*H$_2$CH$_3$), 118.6 (CH), 125.5(CH), 136.8 (CH), 153.2 (C), 163.1 (C), 200.8 (CH$_3$*C*=O). IR (solid state): 1695 ν(C=O)$_{ketone}$ cm^{-1}. ESIMS: *m/z* 150 [M + H]$^{+}$.

(d) Synthesis of H**L4**$_{Et}$

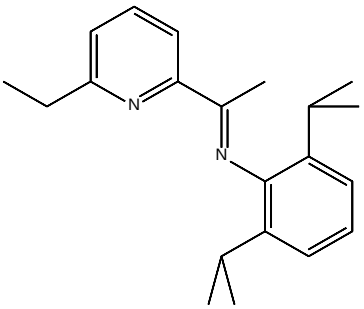

A round bottomed flask was charged with 2-ethyl-6-acetylpyridine (2.00 g, 13.422 mmol), 2,6-diisopropylaniline (2.850 g, 16.107 mmol, 1.2 eq.) and absolute ethanol (20 ml). A few drops of formic acid were added and the mixture stirred and heated to 100 °C for 48 h. On cooling to -30 °C, H**L4**$_{Et}$ was obtained as yellow powder which was filtered and washed with cold ethanol (2.400 g, 60%). ^{1}H NMR (400 MHz, $CDCl_3$): δ 1.15 (12H, d, $^{3}J_{HH}$ = 6.9 Hz, CH*Me*$_2$), 1.36 (t, 3H, $^{3}J_{HH}$ = 7.9 Hz, CH$_2$C*H*$_3$), 2.00 (s, 3H, C*H*$_3$C=N), 2.76 (sept, 2H, $^{3}J_{HH}$ = 6.9 Hz, C*H*Me$_2$), 2.87 (q, 2H, $^{3}J_{HH}$ = 7.9 Hz, C*H*$_2$CH$_3$), 7.00 (m, 1H, Ar-H), 7.09 (m, 2H, Ar/PyH), 7.13 (d, 1H, $^{3}J_{HH}$ = 7.3 Hz, PyH), 7.61 (d, 1H, $^{3}J_{HH}$ = 7.3 Hz, PyH), 8.11 (d, 1H, $^{3}J_{HH}$ = 7.4 Hz, PyH). ^{13}C{^{1}H} NMR ($CDCl_3$, 100 MHz): 13.7 (CH_2CH_3), 17.3 (*Me*C=N), 22.9 (CH*Me*$_2$) 23.3 (CH*Me*$_2$), 28.3 (*C*HMe$_2$), 31.3 (*C*H$_2$CH$_3$), 118.3 (CH), 123.0 (CH), 123.4(CH), 135.9 (C), 136.3 (CH), 136.6 (CH), 146.7 (C), 155.8 (C), 162.4 (C), 167.6 (Me*C*=N). IR (solid state): 1644 ν(C=N)$_{imine}$, 1585 ν(C=N)$_{pyridine}$, 1361, 1089, 821 cm^{-1}. ESIMS: m/z 310 [M + H]. HRMS (FAB): calculated for $C_{21}H_{29}N_2$ [M+H]$^{+}$ 310.2332, found 310.2324. mp: 194–196 °C.

6.2.12 Five step Synthesis of H**L4**$_{i\text{-}Pr}$

(a) Synthesis of 2-isopropyl pyridine

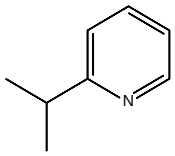

Using a method based on that described in the literature,[14] a 500 ml three neck flask equipped with a pressure equalised dropping funnel and stirrer bar was evacuated and backfilled with nitrogen. The vessel was charged with 2-ethylpyridine (10.0 ml, 87.57 mmol) and dry tetrahydrofuran (60 ml). The solution was cooled to -30 ^{o}C (using a dry ice/acetonitrile bath) and a solution of *n*-butyllithium (60.0 ml, 96.30 mmol, 1.1 eq., 1.6M in hexanes) added dropwise over 30 min; upon addition the solution turned deep red. The dropping funnel was rinsed with a portion of tetrahydrofuran (10 ml) and charged with methyl iodide (6.5 ml, 105 mmol, 1.2 eq.) which was added dropwise over 30 min to the stirred solution maintained at -30 °C. The reaction mixture was then stirred for an additional 30 min at this temperature. After warming to room temperature, water (50 ml) was added followed by conc. hydrochloric acid (13 ml) and the solution stirred for 10 min. The mixture was then extracted with diethyl ether (3 × 50 ml). The aqueous phase was treated with a saturated solution of potassium carbonate (*ca*. 20 ml) and re-extracted with diethyl ether (3 × 50 ml). The combined organic phases were dried over magnesium sulphate, filtered and evaporated to dryness to yield 2-isopropyl pyridine as a pale yellow oil (10.08 g, 89%). ^{1}H NMR (400 MHz, $CDCl_3$): δ 1.31 (d, 6H, $^{3}J_{HH}$ = 7.1 Hz, CH*Me*$_2$), 3.05 (sept, 1H, $^{3}J_{HH}$ = 7.1 Hz, C*H*Me$_2$), 7.80 (t, 1H, $^{3}J_{HH}$ = 5.2 Hz, Py*H*), 7.25 (d, 1H, $^{3}J_{HH}$ = 5.3 Hz, Py*H*), 7.60 (t, 1H, $^{3}J_{HH}$ = 5.2 Hz, Py*H*), 8.54 (d, 1H, $^{3}J_{HH}$ = 5.2 Hz, Py*H*). These data are consistent with those reported previously.[14]

(b) Synthesis of 2-isopropyl pyridine *N*-oxide

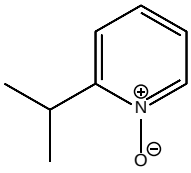

Using a method based on that described in the literature, a 500 ml round bottomed flask equipped with a pressure equalised dropping funnel and a stir-bar was charged with 2-

isopropylpyridine (10.00 g, 82.640 mmol) and chloroform (100 ml) and the solution cooled to 0 °C. A solution of 3-chloroperoxybenzoic acid (mcpba) (23.993 g, 140.31 mmol, 1.5 eq.) previously dissolved in warm chloroform (100 ml) was introduced to the pressure equalised dropping funnel and added dropwise over 1 h at this temperature. The resulting solution was allowed to warm gradually to room temperature and stirred for a further 12 h. The solvent was reduced to half volume and solid potassium carbonate (19.363 g, 140.31 mmol, 1.5 eq.) was added and the thick suspension stirred vigorously for 30 min. The aqueous layer was then extracted rigorously with chloroform (5 x 50 ml) and the combined organic phase dried over magnesium sulphate, filtered and concentrated to give a dark yellow oil (10.19 g, 89%). Note: The oil is volatile and should be dried briefly (*ca.* 30 min) under reduced pressure. ^{1}H NMR (300 MHz, $CDCl_3$): δ 1.30 (d, 6H, $^{3}J_{HH}$ = 6.9 Hz, CH*Me*$_2$), 3.80 (sept, 1H, $^{3}J_{HH}$ = 6.9 Hz, C*H*Me$_2$), 7.13 (m, 2H, Py*H*), 7.25 (d, 1H, $^{3}J_{HH}$ = 6.4 Hz, Py*H*), 8.25 (d, 1H, $^{3}J_{HH}$ = 6.4 Hz, Py*H*). These data are consistent with those reported previously.[14]

(c) Synthesis of 2-isopropyl-6-cyanopyridine

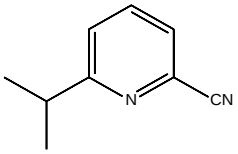

A 250 ml three neck flask equipped with a pressure equalised dropping funnel and a stirrer bar was evacuated and backfilled with nitrogen. The flask was then charged with 2-isopropylpyridine *N*-oxide (8.00 g, 65.04 mmol), trimethylsilylcyanide (7.743 g, 78.05 mmol, 1.2 eq.) and dry dichloromethane (100 ml). Dimethylcarbamylchloride (8.390 g, 78.05 mmol, 1.2 eq.) was added to the dropping funnel and added dropwise; the funnel was then rinsed with a portion of dry dichloromethane (20 ml). The resulting solution was stirred for 72 h at room temperature after which time 20% potassium carbonate solution (50 ml) was added and the mixture stirred for 30 min. The organic phase was separated, dried over magnesium sulphate, filtered and the solvent removed in vacuo to give 2-isopropyl-6-cyanopyridine as a red/brown oil (2.848 g, 30%). ^{1}H NMR (300 MHz, $CDCl_3$): δ 1.30 (d, 6H, $^{3}J_{HH}$ = 6.6 Hz, CH*Me*$_2$), 3.06 (sept, 1H, $^{3}J_{HH}$ = 6.4 Hz, C*H*Me$_2$), 7.40 (d, 1H, $^{3}J_{HH}$ = 8.0 Hz, Py*H*), 7.52 (d, 1H, $^{3}J_{HH}$ = 7.9 Hz, Py*H*), 7.80 (t, 1H, $^{3}J_{HH}$ = 8.0 Hz, Py*H*). These data are consistent with those reported previously.[14]

(d) Synthesis of 2-isopropyl-6-acetylpyridine

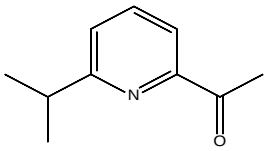

A dry three neck flask was evacuated and backfilled with nitrogen. To this was added 2-isopropyl-6-cyanopyridine (1.953 g, 13.38 mmol) and dry tetrahydrofuran (20 ml). This was then cooled to -15 °C (using a dry ice/acetone bath). MeMgBr (11.5 ml, 2.388 g, 20.07 mmol, 1.5 eq., 3M solution in diethyl ether), was added dropwise. The mixture was then stirred for 1 h at -15 °C and 2 h at room temperature. Saturated ammonium chloride solution (30 ml) was then added and the solution was stirred for 10 min. The organic phase was then separated and the aqueous layer washed with diethyl ether (1 x 20 ml) then dichloromethane (1 x 20 ml). The combined organic layers were then washed with brine (20 ml) and water (2 × 20 ml). The organic phase was then dried over magnesium sulphate, filtered and the solvent removed under reduced pressure to give the crude product as a deep red oil. Purification of the crude product by column chromatography, on silica gel, using 30:70 mixture of ethyl acetate:petroleum ether as eluent, gave 2-isopropyl-6-acetylpyridine as a yellow oil (1.638 g, 75%). ^{1}H NMR (400 MHz, $CDCl_3$): δ 1.29 (d, 6H, $^{3}J_{HH}$ = 7.0 Hz, $CH(CH_3)_2$), 2.68 (s, 3H, $COCH_3$), 3.07 (sept, 1H, $^{3}J_{HH}$ = 7.0 Hz, $CH(CH_3)_2$), 7.28 (dd, 1H, $^{3}J_{HH}$ = 7.7 Hz, $^{4}J_{HH}$ = 1.2 Hz, Py-*H*), 7.67 (t, 1 H, $^{3}J_{HH}$ = 7.7 Hz, Py-*H*), 7.79 (dd, 1H, $^{3}J_{HH}$ = 7.7 Hz, $^{4}J_{HH}$ = 1.2 Hz, Py-*H*). These data are consistent with those reported previously.[14]

(e) Synthesis of H**L4**$_{i\text{-}Pr}$

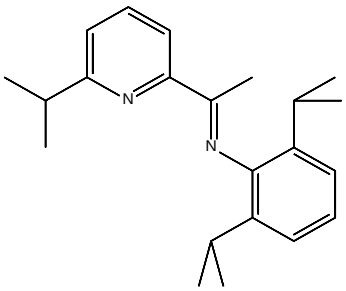

A round bottomed flask was charged with 2-isopropyl-6-acetylpyridine (1.500 g, 9.20 mmol), 2,6-diisopropylaniline (1.955 g, 11.04 mmol, 1.2 eq.) and absolute ethanol (20 ml). A few drops of formic acid were added and the mixture stirred and heated at reflux for 48 h. On cooling to -30 °C, H**L4**$_{i\text{-}Pr}$ was obtained as a yellow powder which was

filtered and washed with cold ethanol (1.926 g, 65%). ^{1}H NMR (400 MHz, $CDCl_3$): δ 1.08 (d, 12H, $^{3}J_{HH}$ = 6.9 Hz, CH(CH_3)$_{2ar}$), 1.29 (d, 6H, $^{3}J_{HH}$ = 6.9 Hz, CH(CH_3)$_{2Py}$), 2.14 (s, 3H, $CNCH_3$), 2.69 (sept, 2H, $^{3}J_{HH}$ = 6.9 Hz, C*H*(CH_3)$_{2ar}$), 3.05 (sept, 1H, $^{3}J_{HH}$ = 6.9 Hz, C*H*(CH_3)$_2$py), 7.01 (m, 1H, Ar-H), 7.09 (m, 2H, Ar-H), 7.18 (d, 1H, $^{3}J_{HH}$ = 7.7 Hz, Py-H), 7.63 (t, 1H, $^{3}J_{HH}$ = 7.7 Hz, Py-H), 8.08 (br. d, 1H, Py-H). ^{13}C{^{1}H} NMR (100 MHz, $CDCl_3$): δ 17.2 (*C*H_3C=N), 22.6 (CH(*C*H_3)$_{2py}$), 23.0 (CH(*C*H_3)$_{2ar}$), 23.3 (CH(*C*H_3)$_{2ar}$), 28.3 (*C*H(CH_3)$_{2ar}$), 36.3 (*C*H(CH_3)$_{2py}$), 118.2 (CH), 121.7 (CH), 122.9 (CH), 123.4 (CH), 135.8 (C), 136.7 (CH), 146.8 (C), 155.6 (C), 166.1 (C), 167.7 (CH_3*C*=N). IR (solid state): 1584 ν(C-$N_{pyridine}$), 1635 ν(C=N_{imine}) cm^{-1}. ESIMS: *m/z* 323 $[M + H]^+$. HRMS (FAB): calculated for $C_{22}H_{31}N_2$ $[M+H]^+$ 323.2426, found 323.2418. mp.: 89-91 °C.

6.2.13 Five step synthesis of H**L4**$_{t\text{-}Bu}$

(a) Synthesis of 2-*tert*-butyl pyridine

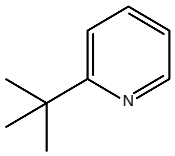

Using a modified route to that described in the literature,[14] a dry 250 ml three neck flask was evacuated and backfilled with nitrogen. The flask was loaded with ^{t}BuOK (3.400 g, 30.00 mmol, 1.5 eq.), dry THF (30 ml) and diisopropylamine (3.036 g, 4.2 ml, 30.00 mmol, 1.5 eq.). The mixture was cooled to -70 °C (using a dry ice/acetone bath) and *n*-BuLi (18.4 ml, 30.00 mmol, 1.5 eq., 1.6M in hexanes) added dropwise. The mixture was then warmed to -50 °C (by adding acetone to the dry ice/acetone bath) over 15 min before adding 2-isopropylpyridine (2.420 g, 20.00 mmol). After 30 min of metalation at -50 °C, the mixture was cooled to -75 °C and iodomethane (3.0 ml, 50 mmol, 2.5 eq.) added dropwise. The reaction mixture was stirred for a further 2 h at -75 °C. After warming to room temperature, water (35 ml) was added and the mixture was stirred for 1 h. The mixture was then extracted with dichloromethane (3 x 30 ml). Following drying over magnesium sulphate, the solvent was removed under reduced pressure. Purification of the crude product was carried out using column chromatography, on silica gel, using a 1:10 mixture of ethyl acetate/petroleum ether as eluent affording 2-*tert*-butyl pyridine as a

yellow oil (1.728 g, 64%). ^{1}H NMR (400 MHz, $CDCl_3$): δ 1.36 (s, 9H, C*Me*$_3$), 7.04 (t, 1H, $^{3}J_{HH}$ = 5.3 Hz, Py*H*), 7.31 (d, 1H, $^{3}J_{HH}$ = 5.3 Hz, Py*H*), 7.57 (t, 1H, $^{3}J_{HH}$ = 5.2 Hz, Py*H*), 8.56 (d, 1H, $^{3}J_{HH}$ = 5.2 Hz, Py*H*). These data are consistent with those reported previously.[14]

(b) Synthesis of 2-*tert*-butyl pyridine N-oxide

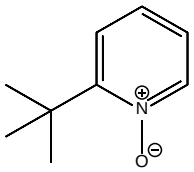

A 500 ml round bottomed flask equipped with a pressure equalised dropping funnel and a stir-bar was charged with with 2-*tert*-butylpyridine (1.500 g, 11.10 mmol) and chloroform (15 ml) and the solution cooled to 0 °C. A solution of 3-chloroperoxybenzoic acid (mcpba) (3.000 g, 16.65 mmol, 1.5 eq.) previously dissolved in warm chloroform (10 ml) was introduced to the pressure equalised dropping funnel and added dropwise over 1 h at this temperature. The resulting solution was allowed to warm gradually to room temperature and stirred for a further 12 h. The solvent was reduced to half volume and solid potassium carbonate (2.298 g, 16.65 mmol, 1.5 eq.) was added and the thick suspension stirred vigorously for 30 min. The aqueous layer was then extracted rigorously with chloroform (5 x 10 ml) and the combined organic phases dried over magnesium sulphate, filtered and concentrated to give 2-*tert*-butyl pyridine *N*-oxide as a dark yellow oil (1.424 g, 85%). Note: The oil is volatile and should be dried briefly (*ca.* 30 min) under reduced pressure. ^{1}H NMR (400 MHz, $CDCl_3$): δ 1.53 (s, 9H, C*Me*$_3$), 7.11 (m, 1H, Py*H*), 7.20 (m, 1H, Py*H*), 7.34 (d, 1H, $^{3}J_{HH}$ = 6.4 Hz, Py*H*), 8.19 (d, 1H, $^{3}J_{HH}$ = 6.4 Hz, Py*H*). These data are consistent with those reported previously.[14]

(c) Synthesis of 2-*tert*-butyl-6-cyanopyridine

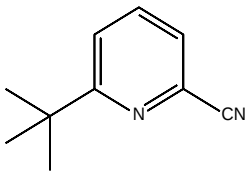

A 250 ml three neck flask equipped with a pressure equalised dropping funnel and a stirrer bar was evacuated and backfilled with nitrogen. The flask was charged with 2-*tert*-

butylpyridine *N*-oxide (2.316 g, 15.34 mmol), trimethylsilylcyanide (1.826 g, 18.41 mmol, 1.2 eq.) and dry dichloromethane (10 ml). Dimethylcarbamylchloride (1.988 g, 18.41 mmol, 1.2 eq.) was added to the pressure equalised dropping funnel and introduced dropwise; the dropping funnel was rinsed with a portion of dry dichloromethane (5 ml). The solution was stirred for 72 h after which time 20% aqueous potassium carbonate solution (15 ml) was added and stirred for 30 min. The organic phase was separated, dried over magnesium sulphate, filtered and concentrated to give 2-*tert*-butyl-6-cyanopyridine as a yellow oil (1.751 g, 71%). ^{1}H NMR (400 MHz, $CDCl_3$): δ 1.30 (s, 9H, C*Me*$_3$), 7.45 (dd, 1H, $^{3}J_{HH}$ = 7.9 Hz, $^{4}J_{HH}$ = 1.1 Hz, Py*H*), 7.53 (dd, 1H, $^{3}J_{HH}$ = 7.9 Hz, $^{4}J_{HH}$ = 1.1 Hz, Py*H*), 7.72 (t, 1H, $^{3}J_{HH}$ = 7.9 Hz, Py*H*). These data are consistent with those reported previously.[14]

(d) Synthesis of 2-*tert*-butyl-6-acetyl pyridine

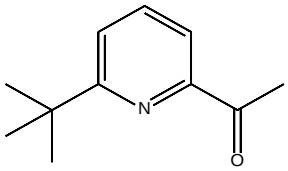

A large Schlenk flask was evacuated and backfilled with nitrogen before being charged with 2-*tert*-butyl-6-cyanopyridine (0.700 g, 4.37 mmol) and dry toluene (20 ml). Trimethylaluminium (7.0 ml, 13.11 mmol, 2 eq., 2 M in toluene) was added dropwise with caution. The solution was stirred and heated to 100 °C for 12 h. Upon cooling, the solvent was removed under reduced pressure until *ca.* 2-3 ml of red oil was left in the flask. The flask was cooled to 0 °C and bench chloroform (10 ml) added with stirring. Water was then added dropwise under **extreme caution** until the effervescence stops (NOTE: 1-2 drops per minute is sufficient in the first instance). The solution was diluted with a further portion of chloroform (10 ml) and the mixture stirred for 2 h. After filtration to remove any aluminium by-products, the organic phase was separated and the aqueous phase washed with chloroform (2 × 10 ml). The combined organic phases were washed with water (1 × 20 ml). The organic layer was then dried over magnesium sulphate, filtered and the solvent removed under reduced pressure to give 2-*tert*-butyl-6-acetyl pyridine as a brown oil (0.464 g, 60%). ^{1}H NMR (300 MHz, $CDCl_3$): δ 1.40 (s, 9H, $C(CH_3)_3$), 2.72 (s, 3H, $COCH_3$), 7.50 (dd, 1H, $^{3}J_{HH}$ = 7.7 Hz, $^{4}J_{HH}$ = 1.3 Hz, Py-H), 7.72 (t, 1H, $^{3}J_{HH}$ = 7.7 Hz, Py-H), 7.82 (dd, 1H, $^{3}J_{HH}$ = 7.7 Hz, $^{4}J_{HH}$ = 1.3 Hz, Py-H), These data are consistent with those reported previously.[14]

(e) Synthesis of H**L4**$_{t\text{-}Bu}$

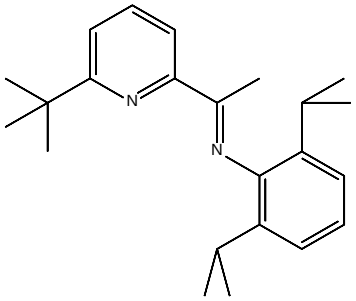

A round bottomed flask was charged with 2-*tert*-butyl-6-acetylpyridine (0.590 g, 3.33 mmol), 2,6-diisopropylaniline (0.649 g, 3.66 mmol, 1.2 eq.) and *n*-butanol (5 ml). A catalytic amount of *p*-toluenesulfonic acid (0.02 eq.) was added and the mixture stirred and heated at reflux for 72 h. On cooling to -30 °C, H**L4**$_{t\text{-}Bu}$ was obtained as yellow powder which was filtered and washed with cold ethanol (0.337 g, 25%). ^{1}H NMR (300 MHz, $CDCl_3$): δ 1.07 (d, 12H, $^{3}J_{HH}$ = 6.8 Hz, CH(CH_3)$_2$), 1.34 (s, 9H, C(CH_3)$_3$), 2.13 (s, 3H, $CNCH_3$), 2.69 (sept, 2H, $^{3}J_{HH}$ = 6.8 Hz, CH(CH_3)$_2$), 7.00 (m, 1H, Ar-H), 7.08 (m, 2H, Ar-H), 7.32 (d, 1H, $^{3}J_{HH}$ = 7.8 Hz, Py-H), 7.63 (t, 1H, $^{3}J_{HH}$ = 7.8 Hz, Py-H), 8.07 (br. d, 1H, Py-H). ^{13}C{^{1}H} NMR (100 MHz, $CDCl_3$): δ 16.1 (CH_3C=N), 21.9 (C(CH_3)$_3$), 22.2 (CH(CH_3)$_2$), 27.2 (CH(CH_3)$_2$), 29.2 (CH(CH$_3$)$_2$), 36.6 (C(CH$_3$)$_3$), 116.8 (CH), 118.9 (CH), 121.9 (CH), 122.3 (CH), 134.8 (C), 135.4 (CH), 145.7 (C), 153.9 (C), 166.7 (C), 167.0 (CH_3C=N). IR (solid state): 1644 ν(C=N)$_{imine}$, 1587 ν(C=N)$_{pyridine}$. ESIMS *m/z*: 359.3 [M + Na]$^{+}$, 337.3 [M + H]$^{+}$. mp.: 122-124 °C.

6.3 Experimental procedures for Chapter 3

6.3.1 Synthesis of (**L1**$_{o\text{-}tolyl}$)PdOAc

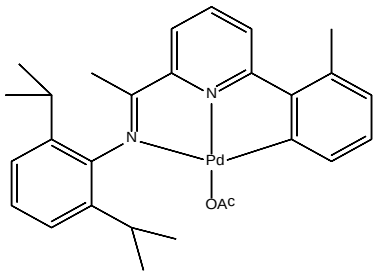

A clean dry Schlenk flask equipped with a magnetic stir bar was evacuated and backfilled with nitrogen. The flask was then charged with $Pd(OAc)_2$ (0.183 g, 0.81 mmol) and H**L1**$_{o\text{-}tolyl}$ (0.300 g, 0.81 mmol) and the contents dissolved in dry toluene (30 ml). The solution was stirred and heated to 60 ºC for 48 h. On cooling to room temperature, the reaction mixture was filtered through a thin layer of Celite. The Celite cake was washed thoroughly with dichloromethane and dried under reduced pressure to give (**L1**$_{o\text{-}tolyl}$)PdOAc as a deep yellow solid (0.416 g, 96%). ^{1}H NMR ($CDCl_3$, 400 MHz): δ 1.04 (d, 6H, $^3J_{HH}$ = 6.9 Hz, Ar-CH-C***H***$_{3(a)}$CH$_{3(b)}$), 1.31 (d, 6H, $^3J_{HH}$ = 6.7 Hz, Ar-CH-CH$_{3(a)}$C***H***$_{3(b)}$), 1.63 (s(broad), 3H, OCOC***H***$_3$), 2.13 (s, 3H, Pyr-C(N)-C***H***$_3$), 2.53 (s, 3H, *o*-Ar-C***H***$_3$), 3.08 (sep, 2H, $^3J_{HH}$ = 6.8 Hz, C***H***-(CH$_3$)$_2$), 6.77 (d, 1H, $^3J_{HH}$ = 7.4 Hz, Py/Ar-***H***), 6.91 (t, 1H, $^3J_{HH}$ = 7.6 Hz, Py/Ar-***H***), 7.04 (d, 1H, $^3J_{HH}$ = 7.8 Hz, Py/Ar-***H***), 7.11-7.21 (m, 3H, Py/Ar-***H***), 7.35-7.40 (m, 1H, Py/Ar-***H***), 7.83-7.88 (m, 1H, Py/Ar-***H***). ^{13}C{^{1}H} NMR ($CDCl_3$, 100 MHz): δ 17.6 (Py-C(N)-***C***H$_3$), 23.3 (*o*-Ar-***C***H$_3$), 23.5 (Ar-CH-***C***H$_{3(a)}$), 24.0 (Ar-CH-***C***H$_{3(b)}$), 28.7 (Ar-***C***H-(CH$_3$)$_2$), 29.7 (OCO***C***H$_3$), 120.8 (CH), 123.4 (CH), 123.5 (CH), 124.4 (CH), 127.1 (CH), 129.3 (C), 130.1 (CH), 131.3 (CH), 135.6 (C), 136.4 (C), 138.7 (CH), 141.1 (C), 145.5 (C), 154.0 (C), 155.4 (C), 166.1 (Py-***C***(N)-CH$_3$), 172.9 (O***C***OCH$_3$). IR: 766 ν(C-H bend), 801 ν(C-H bend), 1382 ν(COO)$_{symm.}$, 1558 ν(COO)$_{asym.}$, 1586 ν(C-N)$_{pyridine}$, 1604 ν(C=N)$_{imime}$, 2958 ν(C-H stretch) cm^{-1}. ESIMS (+ve, MeOH): *m/z* 475 [M-OAc]$^+$. HRMS (TOF): calculated for $C_{28}H_{32}N_2O_2Pd$ [M]$^+$ 534.1509, found 534.1510. m.p: > 270 ºC. Anal. calc. for ($C_{28}H_{32}N_2O_2Pd$·0.5CH_2Cl_2): C 59.28, H 5.76, N 4.85. Found C 59.31, H 5.07, N 4.87%.

6.3.2 Synthesis of (**L1**$_{o\text{-}tolyl}$)PdCl

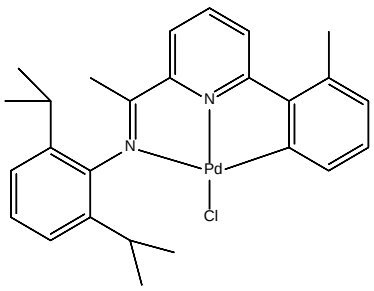

To a round bottomed flask, open to the air and equipped with a magnetic stir bar, was added (**L1**$_{o\text{-}tolyl}$)PdOAc (0.056 g, 0.10 mmol) and a saturated aqueous solution of sodium

chloride (10 ml). The mixture was then stirred vigorously overnight to obtain a yellow coloured reaction mixture. $CHCl_3$ (10 ml) was then introduced and the reaction mixture stirred for 5 min. The organic phase was then isolated and the aqueous layer washed with $CHCl_3$ (2 × 10 ml). The organic extracts were combined and dried over magnesium sulphate. The solvent was removed under reduced pressure to give the (**L1**$_{o\text{-tolyl}}$)PdCl as a light brown solid (0.054 g, 99%). Single crystals of (**L1**$_{o\text{-tolyl}}$)PdCl suitable for an X-ray structure determination were grown by slow evaporation from dichloromethane. ^{1}H NMR ($CDCl_3$, 400 MHz): δ 1.07 (d, 6H, $^3J_{HH}$ = 6.9 Hz, Ar-CH-C***H***$_{3(a)}$CH$_{3(b)}$), 1.31 (d, 6H, $^3J_{HH}$ = 6.7 Hz, Ar-CH-CH$_{3(a)}$C***H***$_{3(b)}$), 2.12 (s, 3H, Pyr-C(N)-C***H***$_3$), 2.56 (s, 3H, *o*-Ar-C***H***$_3$), 2.97 (sep, 2H, $^3J_{HH}$ = 6.8 Hz, C***H***-(CH$_3$)$_2$), 6.81 (d, 1H, $^3J_{HH}$ = 7.5 Hz, Py/Ar-***H***), 6.92 (t, 1H, $^3J_{HH}$ = 7.6 Hz, Py/Ar-***H***), 7.13-7.22 (m, 3H, Py/Ar-***H***), 7.44 (d, 1H, $^3J_{HH}$ = 7.3 Hz, Py/Ar-***H***), 7.74 (d, 1H, $^3J_{HH}$ = 7.7 Hz, Py/Ar-***H***), 7.86-7.96 (m, 2H, Py/Ar-***H***). ^{13}C{^{1}H} NMR ($CDCl_3$, 100 MHz): δ 17.8 (Py-C(N)-***C***H$_3$), 23.0 (*o*-Ar-***C***H$_3$), 23.8 (Ar-CH-(***C***H$_3$)$_2$), 28.7 (Ar-***C***H-(CH$_3$)$_2$), 120.6 (CH), 123.4 (CH), 123.5 (CH), 124.4 (CH), 126.9 (CH), 129.2 (C), 130.1 (CH), 130.9 (CH), 133.3 (C), 136.1 (C), 138.8 (CH), 141.0 (C), 145.1 (C), 154.0 (C), 154.8 (C), 172.3 (Py-***C***(N)-CH$_3$). IR: 764 ν(C-H bend), 798 ν(C-H bend), 1582 ν(C-N)$_{pyridine}$, 1614 ν(C=N)$_{imime}$, 2953 ν(C-H stretch) cm^{-1}. ESIMS (+ve, MeOH): m/z 511 [M]$^+$. HRMS (FAB): calculated for $C_{26}H_{29}N_2ClPd$ [M]$^+$ 510.1131, found 510.1151. m.p: > 270 ^{o}C.

6.3.3 Synthesis of *peri*-[(**L1**$_{ket\text{-}nap}$)PdOAc][15]

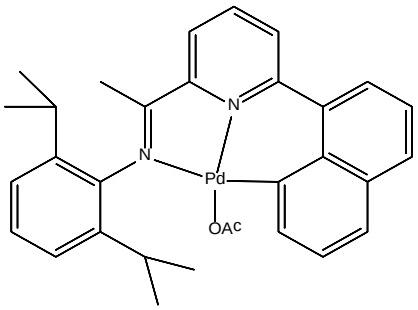

Based on the literature procedure,[15] a clean dry Schlenk flask equipped with a magnetic stir bar was evacuated and backfilled with nitrogen. The flask was then charged with Pd(OAc)$_2$ (0.113 g, 0.50 mmol), H**L1**$_{ket\text{-}nap}$ (0.211 g, 0.515 mmol) and the contents dissolved in dry toluene (20 ml). The solution was stirred and heated to 60 ^{o}C for 48 h. The reaction mixture was cooled to room temperature and filtered through a thin layer of Celite. The Celite cake was washed thoroughly with dichloromethane and the solvent

removed under reduced pressure to give *peri*-(**L1**$_{ket\text{-}nap}$)PdOAc as a deep yellow solid (0.292 g, 93%). ^{1}H NMR ($CDCl_3$, 400 MHz): δ 1.04 (d, 6H, $^{3}J_{HH}$ = 6.6, CH*(CH$_3$)$_2$*), 1.38 (s, 3H, Pd-OCOC*H$_3$*), 1.39 (d, 6H, $^{3}J_{HH}$ = 6.6 Hz, CH*(CH$_3$)$_2$*), 2.24 (s, 3H, *(CH$_3$)*C=N), 3.19 (sept, 2H, $^{3}J_{HH}$ = 6.6 Hz, C*H(CH$_3$)$_2$*), 7.18-7.27 (m, 4H, dipp/Ar/PyH), 7.39 (t, 1H, $^{3}J_{HH}$ = 7.6 Hz, Ar/Py-H) , 7.52 (d, 1H, $^{3}J_{HH}$ = 7.6 Hz, Ar/Py-H), 7.60 (d, 1H, $^{3}J_{HH}$ = 7.6 Hz, Ar/Py-H) , 7.79 (d, 2H, $^{3}J_{HH}$ = 7.6 Hz, Ar/Py-H) , 7.85 (t, 1H, $^{3}J_{HH}$ = 8.1 Hz, Ar/Py-H), 8.04 (d, 1H, $^{3}J_{HH}$ = 7.6 Hz, Ar/Py-H), 8.29 (d, 1H, $^{3}J_{HH}$ = 8.1 Hz, Ar/Py-H). ^{13}C{^{1}H} NMR ($CDCl_3$, 100 MHz): δ 18.9 (Py-C(N)-***C***H$_3$), 23.0 (Ar-CH-***C***H$_{3(a)}$), 23.6 (Ar-CH-***C***H$_{3(b)}$), 24.4 (Ar-***C***H-(CH$_3$)$_2$), 28.8 (OCO***C***H$_3$), 123.4 (CH), 123.6 (CH), 124.0 (CH), 125.4 (C), 126.4 (CH), 127.0 (CH), 128.0 (CH), 128.1 (CH), 129.7 (CH), 133.5 (CH), 134.1 (C), 134.6 (CH), 136.2 (C), 137.0 (C), 138.8 (CH), 139.5 (C), 141.1 (C), 155.6 (C), 156.1 (C), 170.7 (Py-***C***(N)-CH$_3$), 176.6 (O***C***OCH$_3$). IR: 763 ν(C-H bend), 797 ν(C-H bend), 1368 ν(COO)$_{symm.}$, 1567 ν(COO)$_{asym.}$, 1585 ν(C-N)$_{pyridine}$, 1615 ν(C=N)$_{imime}$, 2958 ν(C-H stretch) cm^{-1}. ESIMS (+ve, MeOH): m/z 511 [M-OAc]$^{+}$. HRMS (FAB): calculated for $C_{29}H_{29}N_2Pd$ [M-OAc]$^{+}$ 511.2053, found 511.2055. m.p: 248-251 ^{o}C. The data are consistent with those in the published report.[15]

6.3.4 Synthesis of *peri*-[(**L1**$_{ket\text{-}nap}$)PdCl]

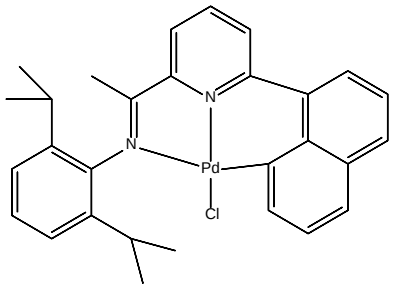

To a round bottomed flask, open to the air and equipped with a magnetic stir bar, was added *peri*-(**L1**$_{ket\text{-}nap}$)PdOAc (0.051 g, 0.09 mmol) in dichloromethane (10 ml) and a saturated solution of sodium chloride (10 ml). The mixture was then stirred vigorously overnight to obtain a yellow coloured reaction mixture. $CHCl_3$ (10 ml) was then introduced and the reaction mixture stirred for 5 min. The organic phase was then separated and the aqueous layer washed with $CHCl_3$ (2 × 10 ml). The organic extracts were combined and dried over magnesium sulphate. The solvent was removed under

reduced pressure to give *peri*-(**L1**$_{ket\text{-}nap}$)PdCl as a brown solid (0.053 g, 99%). ^{1}H NMR ($CDCl_3$, 400 MHz): δ 1.06 (d, 6H, $^{3}J_{HH}$ = 6.9 Hz, CH*(CH$_3$)$_2$*), 1.35 (d, 6H, $^{3}J_{HH}$ = 6.9 Hz, CH*(CH$_3$)$_2$*), 2.27 (s, 3H, NC*CH$_3$*), 3.05 (sept, 2H, $^{3}J_{HH}$ = 6.9 Hz, *CH*(CH_3)$_2$), 7.16-7.23 (m, 3H, dipp-H), 7.26 (d, 1H, $^{3}J_{HH}$ = 7.6 Hz, ArH) 7.47 (t, 1H, $^{3}J_{HH}$ = 7.8 Hz, ArH), 7.58 (d, 1H, $^{3}J_{HH}$ = 7.8 Hz, ArH), 7.85 (d, 1H, $^{3}J_{HH}$ = 7.6 Hz, ArH), 7.94 (d, 1H, $^{3}J_{HH}$ = 8.0, PyH), 8.10 (t, 1H, $^{3}J_{HH}$ = 8.0, PyH), 8.15 (d, 1H, $^{3}J_{HH}$ = 7.4, ArH), 8.40 (d, 1H, $^{3}J_{HH}$ = 8.0 Hz, PyH), 8.61 (d, 1H, $^{3}J_{HH}$ = 7.4 Hz, ArH). ^{13}C{^{1}H} NMR ($CDCl_3$, 100 MHz): δ 18.7 (Py-C(N)-***C***H$_3$), 23.8 (Ar-CH-(***C***H$_3$)$_{2a}$), 23.9 (Ar-CH-(***C***H$_3$)$_{2b}$), 28.81 (Ar-***C***H-(CH$_3$)$_2$), 120.2 (CH), 122.8 (CH), 123.3 (CH), 123.4 (C), 123.9 (CH), 125.5 (CH), 126.4 (CH), 127.2 (CH), 128.3 (CH), 129.3 (CH), 133.8 (C), 134.2 (CH), 134.8 (C), 137.3 (C), 139.0 (CH), 141.0 (C),142.1 (C), 155.6 (C), 156.3 (C), 171.2 (Py-***C***(N)-CH$_3$). IR: 754 ν(C-H bend), 795 ν(C-H bend), 1591 ν(C-N)$_{pyridine}$, 1627 ν(C=N)$_{imime}$, 2960 ν(C-H stretch) cm^{-1}. ESIMS (+ve, MeOH): m/z 547 [M]$^{+}$. HRMS(FAB): calculated for $C_{29}H_{29}N_2PdCl$ [M]$^{+}$ 547.2023 and $C_{29}H_{29}N_2Pd$ [M-Cl]$^{+}$ 511.1088, found 547.2017 and 511.1079. m.p: > 270 ^{o}C. Anal. calc. for ($C_{29}H_{29}N_2$ ClPd): C 63.63, H 5.34, N 5.12. Found C 63.57, H 5.46, N 5.39%.

6.3.5 Synthesis of *ortho*-[(**L1**$_{ket\text{-}nap}$)PdCl]

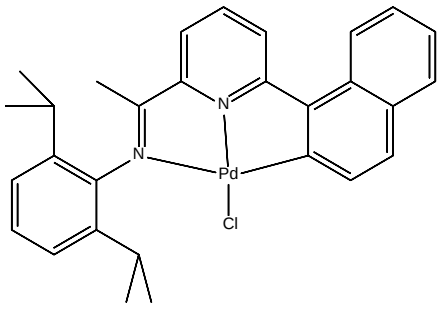

To a round bottom flask open to the air was added H**L1**$_{ket\text{-}nap}$ (0.100 g, 0.25 mmol), Na_2PdCl_4 (0.074 g, 0.25 mmol) and glacial acetic acid (5 ml). A condenser was attached and the mixture heated to 100 ^{o}C for 60 h. Upon cooling to room temperature, the resulting suspension was filtered to give *ortho*-(**L1**$_{ket\text{-}nap}$)PdCl as an orange powder (0.116 g, 85%). Recrystallization from dichloromethane/hexane yielded orange crystals suitable for a single crystal X-ray diffraction study. ^{1}H NMR ($CDCl_3$, 500 MHz): δ 1.16 (d, 6H, $^{3}J_{HH}$ = 6.9 Hz, CH*(CH$_3$)$_2$*), 1.39 (d, 6H, $^{3}J_{HH}$ = 6.9 Hz, CH*(CH$_3$)$_2$*), 2.22 (s, 3H, NC*CH$_3$*), 3.07 (sept, 2H, $^{3}J_{HH}$ = 6.9 Hz, *CH*(CH_3)$_2$), 7.25 (s, 3H, dipp-H), 7.41 (t, 1H, $^{3}J_{HH}$

= 7.6 Hz, ArH), 7.49-7.54 (m, 2H, Ar/Py-H), 7.60 (d, 1H, $^3J_{HH}$ = 7.8 Hz, Ar-H), 7.84 (d, 1H, $^3J_{HH}$ = 7.6 Hz, ArH), 8.02 (t, 1H, $^3J_{HH}$ = 8.0 Hz, Py-H), 8.20 (d, 1H, $^3J_{HH}$ = 8.0 Hz, Ar-H), 8.35 (d, 1H, $^3J_{HH}$ = 7.4 Hz, Ar-H), 8.37 (d, 1H, $^3J_{HH}$ = 8.0 Hz, Py-H). A $^{13}C\{^1H\}$ NMR spectrum could not be obtained due to the sample's poor solubility in $CDCl_3$ and other NMR solvents. IR: 755 ν(C-H bend), 796 ν(C-H bend), 1590 $\nu(C\text{-}N)_{pyridine}$, 1629 $\nu(C{=}N)_{imine}$, 2966 ν(C-H stretch) cm^{-1}. ESIMS (+ve, MeOH): m/z 547 $[M]^+$. HRMS(FAB): calculated for $C_{29}H_{29}N_2PdCl$ $[M]^+$ 547.2023 and $C_{29}H_{29}N_2Pd$ $[M\text{-}Cl]^+$ 511.1088, found 547.2017 and 511.1079. m.p: > 270 ºC. Anal. calc. for ($C_{29}H_{29}ClN_2Pd$): C 63.63, H 5.34, N 5.12. Found C 63.55, H 5.29, N 5.18%.

6.3.6 Synthesis of *ortho*-[(**L1**$_{ket\text{-}nap}$)PdOAc]

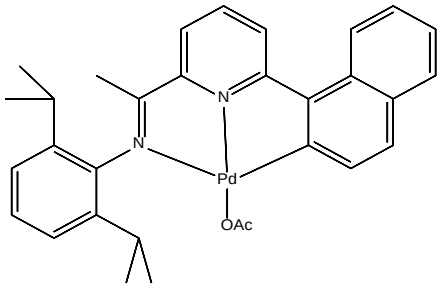

To a round bottom flask open to the air was added *ortho*-(**L1**$_{ket\text{-}nap}$)PdCl (0.100 g, 0.18 mmol), AgOAc (0.031 g, 0.18 mmol) and bench chloroform (5 ml). The solution was stirred at room temperature overnight. The resulting suspension was filtered and solvent removed under reduced pressure to give *ortho*-(**L1**$_{ket\text{-}nap}$)PdOAc as a yellow powder (0.102 g, 99%). Recrystallization from dichloromethane/hexane yielded yellow crystals suitable for a single crystal X-ray diffraction study. ^1H NMR ($CDCl_3$, 400 MHz): δ 1.04 (6H, d, $^3J_{HH}$ = 6.9 Hz, CH*(CH$_3$)$_2$*), 1.22 (6H, d, $^3J_{HH}$ = 6.9 Hz, CH*(CH$_3$)$_2$*), 1.49 (s, 3H, Pd-OCOC*H$_3$*), 2.16 (s, 3H, *(CH$_3$)*C=N), 3.00 (sept, 2H, $^3J_{HH}$ = 6.9 Hz, C*H(CH$_3$)$_2$*), 7.08-7.09 (m, 4H, dipp/Ar/PyH), 7.31 (t, 1H, $^3J_{HH}$ = 7.6 Hz, Ar/Py-H), 7.36 (d, 1H, $^3J_{HH}$ = 7.6 Hz, Ar/Py-H), 7.43 (t, 1H, $^3J_{HH}$ = 7.6 Hz, Ar/Py-H), 7.48 (d, 1H, $^3J_{HH}$ = 7.6 Hz, Ar/Py-H), 7.67 (br d, 1H, $^3J_{HH}$ = 8.0 Hz, Ar/Py-H), 7.97 (t, 1H, $^3J_{HH}$ = 7.6 Hz, Ar/Py-H), 8.08 (d, 1H, $^3J_{HH}$ = 8.0 Hz, Ar/Py-H), 8.17 (d, 1H, $^3J_{HH}$ = 8.0 Hz, Ar/Py-H). $^{13}C\{^1H\}$ NMR ($CDCl_3$, 100 MHz): δ 16.9 (Py-C(N)-***C***H$_3$), 21.6 (Ar-***C***H-(CH$_3$)$_2$), 22.7 (Ar-CH-***C***H$_{3(a)}$), 22.9 (Ar-CH-***C***H$_{3(b)}$), 27.7 (OCO***C***H$_3$), 120.1 (CH), 120.2 (CH), 122.5 (CH), 122.8 (C), 123.4 (CH), 123.8 (CH), 126.1 (CH), 126.4 (CH), 129.0 (CH), 129.4 (CH), 129.7 (C),

131.3 (CH), 132.1 (C), 137.8 (C), 139.0 (CH), 139.5 (C), 140.0 (C), 153.2 (C), 164.8 (C), 172.9 (Py-***C***(N)-CH_3), 176.2 (O***C***OCH_3). IR: 761 ν(C-H bend), 796 ν(C-H bend), 1372 $\nu(COO)_{symm.}$, 1564 $\nu(COO)_{asym.}$, 1591 $\nu(C\text{-}N)_{pyridine}$, 1610 $\nu(C{=}N)_{imime}$, 2951 ν(C-H stretch) cm^{-1}. ESIMS (+ve, MeOH): m/z 511 $[M\text{-}OAc]^+$. HRMS (FAB): calculated for $C_{29}H_{29}N_2Pd$ $[M\text{-}OAc]^+$ 511.2053, found 511.2055. m.p: 251-254 ^oC. Anal. calc. for ($C_{31}H_{32}N_2O_2Pd$): C 65.21, H 5.65, N 4.91. Found C 65.06, H 5.78, N 4.74%.

6.3.7 Synthesis of (H**L1**$_{ket\text{-}nap}$)$PdCl_2$

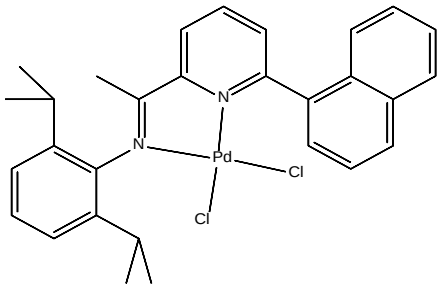

To a round bottom flask open to the air was added H**L1**$_{ket\text{-}nap}$ (0.100 g, 0.25 mmol), $(MeCN)_2PdCl_2$ (0.064 g, 0.25 mmol) and bench chloroform (5 ml). The mixture was then stirred at room temperature for 24 h. The solvent was removed under reduced pressure and the crude product recrystallized from dichloromethane/hexane to give (H**L1**$_{ket\text{-}nap}$)$PdCl_2$ as an orange powder (0.110 g, 75%). Slow evaporation of a chloroform solution of the product yielded orange crystals suitable for a single crystal X-ray diffraction study. ^{1}H NMR (CD_2Cl_2, 500 MHz): δ 1.19 (d, 3H, $^3J_{HH}$ = 6.9 Hz, CH*(*CH_3*)*$_2$), 1.23 (d, 3H, $^3J_{HH}$ = 6.8 Hz, CH*(*CH_3*)*$_2$), 1.42 (d, 3H, $^3J_{HH}$ = 6.9 Hz, CH*(*CH_3*)*$_2$), 1.46 (d, 3H, $^3J_{HH}$ = 6.8 Hz, CH*(*CH_3*)*$_2$), 2.31 (s, 3H, NCCH_3), 3.17 (sept, 1H, $^3J_{HH}$ = 6.9 Hz, *CH*$(CH_3)_2$), 3.27 (sept, 1H, $^3J_{HH}$ = 6.8 Hz, *CH*$(CH_3)_2$), 7.24 (d, 2H, $^3J_{HH}$ = 8.0 Hz, dipp-H), 7.36 (t, 1H, $^3J_{HH}$ = 8.0 Hz, dipp-H), 7.57-7.65 (m, 3H, Ar-H), 7.76 (dd, 1H, $^3J_{HH}$ = 7.6 Hz, $^4J_{HH}$ = 1.17 Hz, Ar-H), 7.91 (m, 1H, Py-H), 7.96-7.99 (m, 3H, Py-H), 8.03 (d, 1H, $^3J_{HH}$ = 8.2 Hz, Ar-H), 8.19 (t, 1H, $^3J_{HH}$ = 7.8 Hz, Ar-H). $^{13}C\{^1H\}$ NMR (CD_2Cl_2, 125 MHz,): δ 21.1 (*C*Me=N), 23.8 (Ar-CH*Me*$_2$), 23.8 (Ar-CH*Me*$_2$), 24.0 (Ar-CH*Me*$_2$), 26.6 (Ar-CH*Me*$_2$), 29.3 (Ar-*C*HMe$_2$), 29.4 (Ar-*C*HMe$_2$), 124.0 (*C*H), 124.1 (*C*H), 125.0 (*C*H), 125.4 (*C*H), 125.8 (*C*H), 126.6 (*C*H), 127.5 (*C*H), 128.8 (*C*H), 129.2 (*C*H), 130.1 (*C*H), 131.0 (*C*H), 131.9 (*C*), 133.9 (*C*), 134.0 (*C*H), 137.8 (*C*), 139.8 (*C*H), 140.4 (C), 140.5 (C), 141.4 (C), 157.0 (C), 164.8 (C), 178.3 (*C*Me=N). IR: 1595 $\nu(C{=}N)_{pyridine}$, 1614 $\nu(C{=}N)_{imime}$, 2956

ν(C-H stretch) cm^{-1}. ESIMS (+ve, MeOH): m/z 511 $[M\text{-}2Cl]^+$. HRMS (FAB): calculated for $C_{29}H_{30}N_2Pd$ $[M\text{-}2Cl]^+$ 511.1365, found 511.1382. m.p: 254-256 ºC. Anal. calc. for ($C_{29}H_{30}N_2Cl_2Pd{\cdot}0.5CHCl_3$): C 55.06, H 4.78, N 5.35. Found C 55.60, H 4.75, N 5.82 %.

6.3.8 Synthesis of (H**L1**$_{ket\text{-}nap}$)$PtCl_2$

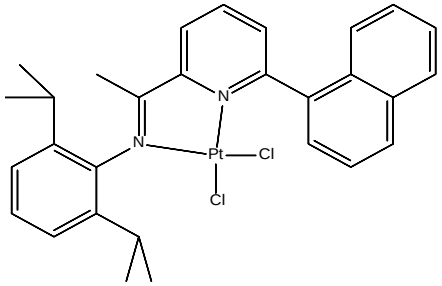

To a round bottom flask open to the air was added H**L1**$_{ket\text{-}nap}$ (0.100 g, 0.25 mmol), K_2PtCl_4 (0.104 g, 0.25 mmol) and acetic acid (10 ml). A reflux condenser was attached and the mixture stirred and heated to 100 ºC for 60 h. Upon cooling to room temperature, the resulting suspension was filtered to give (H**L1**$_{ket\text{-}nap}$)$PtCl_2$ as a brown powder (0.121 g, 76%). ^{1}H NMR (CD_2Cl_2, 500 MHz): δ 1.20 (d, 6H, $^3J_{HH}$ = 5.5 Hz, CH*(CH$_3$)$_2$*), 1.35 (d, 6H, $^3J_{HH}$ = 5.5 Hz, CH*(CH$_3$)$_2$*), 2.24 (s, 3H, NC*CH$_3$*), 3.13 (sept, 2H, $^3J_{HH}$ = 5.5 Hz, *CH*(CH_3)$_2$), 7.35 (m, 3H, dipp-H), 7.47 (t, 1H, $^3J_{HH}$ = 6.2 Hz, Ar-H), 7.54 (d, 1H, $^3J_{HH}$ = 6.2 Hz, Ar-H), 7.60 (t, 1H, $^3J_{HH}$ = 6.3 Hz, Ar-H), 7.76 (d, 1H, $^3J_{HH}$ = 6.8 Hz, Ar-H), 7.88 (d, 1H, $^3J_{HH}$ = 6.7 Hz, Py-H), 8.03 (t, 1H, $^3J_{HH}$ = 6.3 Hz, Ar-H), 8.11 (m, 2H, Py-H), 8.40 (d, 1H, $^3J_{HH}$ = 6.6 Hz, Ar-H), 8.46 (d, 1H, $^3J_{HH}$ = 6.9 Hz, Ar-H). A ^{13}C NMR spectrum has not been obtained due to the sample's poor solublity in NMR solvents. IR: 1591 $\nu(C{=}N)_{pyridine}$, 1619 $\nu(C{=}N)_{imine}$, 2937 ν(C-H stretch) cm^{-1}. ESIMS (+ve, MeOH): m/z 601 $[M\text{-}2Cl]^+$. HRMS (FAB): calculated for $C_{29}H_{30}N_2Pt$ $[M+H]^+$ 672.1502, found 672.1515. m.p > 270 ºC.

6.3.9 Synthesis of (H**L1**$_{2,6\text{-Me2Ph}}$)Pd(OAc)$_2$

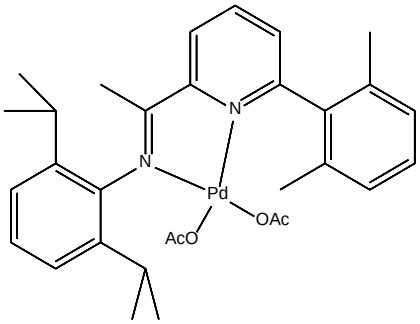

A dry Schlenk flask was evacuated and backfilled with nitrogen. To the flask was added H**L1**$_{2,6\text{-Me2Ph}}$ (0.100 g, 0.26 mmol), Pd(OAc)$_2$ (0.058 g, 0.26 mmol) and dry toluene (10 ml). The resulting solution was then stirred at room temperature for 24 h to give a light brown solid. Recyrstallization from dichloromethane/hexane yielded (H**L1**$_{2,6\text{-Me2Ph}}$)Pd(OAc)$_2$ as an orange powder (0.097 g, 61%). ^{1}H NMR (400 MHz, $CDCl_3$): δ 1.05 (d, 6H, $^3J_{HH}$ = 7.0 Hz, CH-(*CH$_3$)$_2$*)), 1.18 (s, 3H, Pd-O-C(O)*CH$_3$*), 1.22 (s, 3H, Pd-O-C(O)*CH$_3$*), 1.40 (d, 6H, $^3J_{HH}$ = 6.8 Hz, CH-(*CH$_3$)$_2$*)), 2.20 (s, 3H, N=C*CH$_3$*), 2.42 (s, 6H, *o*-Ar-*CH$_3$)*, 3.22 (sept, 2H, $^3J_{HH}$ = 6.8 Hz, C*H*-CH$_3$)$_2$), 7.02 – 7.12 (m, 5H, Ar-H), 7.19 – 7.23 (m, 1H, Ar-H), 7.42 (d, 1H, $^3J_{HH}$ = 7.6 Hz, Py-*H$_m$)*, 7.73 (d, 1H, $^3J_{HH}$ 7.7 = Hz, Py-*H$_m$)*, 8.09 (t, 1H, $^3J_{HH}$ = 7.7 Hz, Py-*H$_p$)*. ^{13}C{^{1}H} NMR (100 MHz, $CDCl_3$): δ 19.2 (*C*Me=N)**,** 21.0 (Ar-*Me*$_o$), 21.5 (Pd-OC(O)-*C*H$_3$), 22.4 (Pd-OC(O)-*C*H$_3$), 23.5 (Ar-CH*Me*$_2$), 24.4 (Ar-CH*Me*$_2$), 29.0 (Ar-*C*HMe$_2$), 123.8 (*C*H), 124.5 (*C*H), 126.8 (CH), 128.3 (*C*H), 129.6 (*C*H), 132.9 (*C*H), 134.8 (*C*), 136.0 (*C*), 136.4 (*C*), 139.2 (*C*H), 139.5 (*C*), 140.6 (C), 155.9 (C), 166.5 (*C*Me=N), 176.5 (Pd-O*C*(O)Me), 177.9 (Pd-O*C*(O)Me). IR (solid state): 1598 ν(C=N)$_{pyridine}$, 1655 ν(C=N)$_{imine}$**.** ESIMS (+ve, MeOH) *m/:* 549 [M-OAc]$^+$. HRMS(TOF) (MeCN): *m/z* 549 [M-OAc]$^+$, 530 [M-OAc+MeCN]$^+$. Anal. calc. for ($C_{31}H_{38}N_2O_4Pd$): C 61.13, H 6.29, N 4.60. Found C 61.35, H 6.19, N 4.45%. m.p.: >270 ^{o}C.

6.3.10 Synthesis of (H**L1**$_{ald\text{-}nap}$)$PdCl_2$

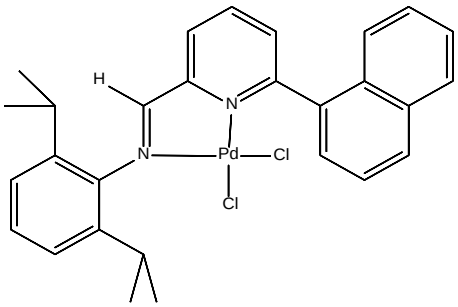

To a round bottom flask open to the air was added H**L1**$_{ald\text{-}nap}$ (0.050 g, 0.14 mmol), Na_2PdCl_4 (0.040 g, 0.14 mmol) and acetic acid (5 ml). A reflux condenser was attached and the mixture stirred and heated to 100 ºC for 24 h (until an orange precipitate was apparent). Upon cooling to room temperature, the resulted suspension was filtered to give (H**L1**$_{ald\text{-}nap}$)$PdCl_2$ as an orange powder (0.065 g, 81%). Recrystallization from dichloromethane/hexane gave orange crystals suitable for a single crystal X-ray diffraction. ^{1}H NMR (CD_2Cl_2, 500 MHz): δ 1.24 (d, 3H, $^3J_{HH}$ = 6.5 Hz, CH*(CH$_3$)$_2$*), 1.30 (d, 3H, $^3J_{HH}$ = 6.5 Hz, CH*(CH$_3$)$_2$*), 1.44 (d, 3H, $^3J_{HH}$ = 6.4 Hz, CH*(CH$_3$)$_2$*), 1.47 (d, 3H, $^3J_{HH}$ = 6.4 Hz, CH*(CH$_3$)$_2$*), 3.41 (sept, 1H, $^3J_{HH}$ = 6.4 Hz, *CH*(CH$_3$)$_2$), 3.49 (sept, 1H, $^3J_{HH}$ = 6.5 Hz, *CH*(CH$_3$)$_2$), 7.27 (d, 2H, $^3J_{HH}$ = 5.8 Hz, dipp-H), 7.41 (t, 1H, $^3J_{HH}$ = 5.8 Hz, dipp-H), 7.65-7.70 (m, 3H, Ar-H), 7.79 (dd, 1H, $^3J_{HH}$ = 8.0 Hz, $^4J_{HH}$ = 1.0 Hz, Ar-H), 7.94-8.05 (m, 3H, Py-H), 8.09 (d, 1H, $^3J_{HH}$ = 5.8 Hz, Ar-H), 8.28 (t, 2H, $^3J_{HH}$ = 5.8 Hz, Ar-H). ^{13}C{^{1}H} NMR (CD_2Cl_2, 125 MHz,): δ 23.2 (Ar-CH*Me*$_2$), 23.3 (Ar-CH*Me*$_2$), 24.6 (Ar-CH*Me*$_2$), 24.7 (Ar-CH*Me*$_2$), 29.2 (Ar-*C*HMe$_2$), 29.3 (Ar-*C*HMe$_2$), 123.8 (*C*H), 123.9 (*C*H), 124.8 (*C*H), 125.4 (*C*H), 126.7 (*C*H), 127.4 (*C*H), 127.5 (*C*H), 128.8 (*C*), 129.1 (*C*H), 129.2 (*C*H), 130.1 (*C*H), 131.2 (*C*H), 132.0 (*C*), 133.8 (*C*), 134.2 (*C*H), 135.1 (*C*), 137.1 (C), 139.9 (*C*H), 141.1 (C), 141.4 (C), 155.2 (C), 170.1 (H*C*Me=N). IR: 1585 ν(C=N)$_{pyridine}$, 1626 ν(C=N)$_{imine}$. ESIMS (+ve, MeOH) *m/:* 498 [M-2Cl]$^+$. HRMS (FAB): calculated for $C_{28}H_{27}N_2Pd$ [M-HCl_2]$^+$ 497.1209, found 497.1235. m.p: 250-252 ºC. Anal. calc. for ($C_{28}H_{28}N_2Cl_2Pd$·0.5CH_2Cl_2): C 55.90, H 4.77, N 4.57. Found C 55.12, H 4.81, N 5.30 %.

6.3.11 Synthesis of *peri*-[(**L1**$_{ald\text{-}nap}$)PdOAc]

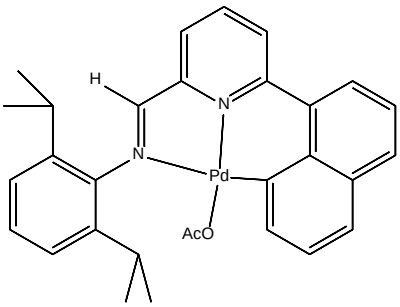

H**L1**$_{ald\text{-}nap}$ (0.049 g, 0.0125 mmol) and $Pd(OAc)_2$ (0.003 g, 0.0125 mmol) were dissolved in $CHCl_3$ in a round bottom flask open to the air. The mixture was stirred for 20 h at room temperature before the solvent was evaporated. The crude product was recrystallized from dichloromethane/petroleum ether (40:60) to give *peri*-(**L1**$_{ald\text{-}nap}$)PdOAc as a yellow powder (0.050 g, 60%). ^{1}H NMR (400 Hz, $CDCl_3$): δ 1.14 (d, 6H, $^3J_{HH}$ = 6.9 Hz, CH(CH_3)$_2$), 1.44 (d, 6H, $^3J_{HH}$ = 6.9 Hz, CH(CH_3)$_2$), 3.46 (sept, 2H, $^3J_{HH}$ = 6.9 Hz, CH), 7.25-7.31 (m, 3H, Ar-H), 7.38 (t, 1H, $^3J_{HH}$ = 8.0 Hz, Ar-H), 7.59 (t, 1H, $^3J_{HH}$ = 8.0 Hz, Ar-H), 7.68-7.74 (m, 2H, Py-H), 7.92 (d, 2H, $^3J_{HH}$ = 8.0, Nap-H), 8.01 (t, 1H, $^3J_{HH}$ = 8.0 Hz, Nap-H), 8.26 (s, 1H, Im-H), 8.27 (d, 1H, $^3J_{HH}$ = 8.0 Hz, Nap-H), 8.48 (d, 1H, $^3J_{HH}$ = 8.0 Hz, Nap-H). ^{13}C{^{1}H} NMR ($CDCl_3$, 100 MHz): δ 22.8 (Ar-CH-***C***H$_{3(a)}$), 24.6 (Ar-CH-***C***H$_{3(b)}$), 25.7 (Ar-***C***H-(CH$_3$)$_2$), 28.5 (OCO***C***H$_3$), 123.3 (CH), 123.6 (CH), 125.4 (CH), 126.2 (CH), 126.9 (CH), 127.1 (C), 127.5 (CH), 127.9 (CH), 130.0 (CH), 133.0 (C), 133.4 (C), 135.0 (CH), 136.7 (CH), 137.0 (CH), 137.5 (C), 139.8 (C), 140.4 (C), 143.5 (C), 154.3 (C), 155.0 (O***C***OCH$_3$), 163.9 (H*C*Me=N). IR (cm^{-1}): 2957 ν(H-C$_{aromatic}$), 1590 ν(C=N$_{imine}$). ESIMS (+ve, MeOH): *m/z* 557 [M+H]$^+$. m.p: 251-253 ^{o}C. Anal. calc. for ($C_{30}H_{30}N_2O_2Pd{\cdot}CH_2Cl_2$): C 58.00, H 5.02, N 4.36. Found C 57.80, H 5.12, N 5.25%.

6.3.12 Synthesis of (**L2**$_{o\text{-}tolyl}$)PdOAc

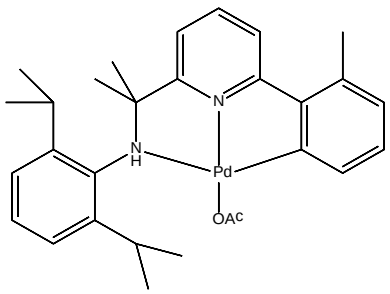

A clean dry Schlenk flask equipped with a magnetic stir bar was evacuated and backfilled with nitrogen. The flask was then charged with $Pd(OAc)_2$ (0.291 g, 1.3 mmol), H**L2**$_{o\text{-tolyl}}$ (0.500 g, 1.3 mmol) and the contents dissolved in dry toluene (30 ml). The solution was stirred and heated to 60 °C for 72 h. The reaction mixture was cooled to room temperature and filtered through a thin layer of Celite. The Celite cake was washed thoroughly with dichloromethane. Solvent romoved under reduced pressure to give (**L2**$_{o\text{-tolyl}}$)PdOAc as a light brown solid (0.736 g, 88%). ^{1}H NMR ($CDCl_3$, 400 MHz): δ 0.81 (d, 3H, $^3J_{HH}$ = 7.0 Hz, CH(C***H***$_3$)$_2$), 1.15-1.33 (m, 12H, Pd-OCOC*H*$_3$, CH(C***H***$_3$)$_2$), 1.91 (s, 3H, Py-C(NH)-(C***H***$_3$)$_2$), 1.97 (s, 3H, o-Ar-C***H***$_3$), 2.57 (s, 3H, Py-C(NH)-(C***H***$_3$)$_2$), 3.26 (sept, 1H, $^3J_{HH}$ = 7.0 Hz, C***H***-(CH$_3$)$_2$), 3.38 (sept, 1H, $^3J_{HH}$ = 7.1 Hz, C***H***-(CH$_3$)$_2$), 6.84 (d, 1H, $^3J_{HH}$ = 7.2 Hz, Py/Ar-***H***), 6.89 (s, 1H, N***H***), 6.92-7.10 (m, 5H, Py/Ar-***H***), 7.15-7.21 (m, 1H, Py/Ar-***H***), 7.69 (d, 1H, $^3J_{HH}$ = 8.2 Hz, Py/Ar-***H***), 7.75 (t, 1H, $^3J_{HH}$ = 8.0 Hz, Py/Ar-***H***). ^{13}C{^{1}H} NMR ($CDCl_3$, 100 MHz): δ 22.7 (Py-C(N)-***C***H$_3$), 23.2 (*o*-Ar-***C***H$_3$), 23.4 (Ar-CH-(***C***H$_3$)$_2$), 24.1 (Ar-CH-(***C***H$_3$)$_2$), 24.9 (Ar-CH-(***C***H$_3$)$_2$), 25.1 (Ar-CH-(***C***H$_3$)$_2$), 27.1 (Ar-*C*H-(CH$_3$)$_2$), 28.1 (Py-C(NH)-(***C***H$_3$)$_2$), 28.7 (Py-C(NH)-(***C***H$_3$)$_2$), 35.1 (Pd-OCOCH$_3$), 68.1 (Py-***C***(NH)-(CH$_3$)$_2$), 116.9 (CH), 120.4 (CH), 124.5 (CH), 124.7 (C), 126.2 (CH), 128.8 (CH), 128.8 (CH), 130.6 (C), 135.3 (CH), 137.1 (CH), 138.3 (C), 143.9 (C), 144.1 (CH), 144.9 (C), 153.9 (C), 164.2 (C), 169.5 (C), 178.9 (Pd-O***C***OCH$_3$). IR: 781 ν(C-H bend), 805 ν(C-H bend), 1373 ν(COO)$_{symm.}$, 1455 ν(C=N)$_{pyridine}$, 1566 ν(COO)$_{asym.}$, 1590 ν(N-H)$_{amine\ bend}$, 2926 ν(C-H stretch), 3230 ν(N-H)$_{amine\ stretch}$ cm^{-1}. ESIMS (+ve, MeCN): m/z 532 [(M-OAc)+MeCN]$^+$, 491 [M-OAc]$^+$, 550 [M]$^+$. HRMS (TOF): calculated for $C_{27}H_{33}N_2Pd$ [M-OAc]$^+$ 491.1667, found 491.1678. m.p: 255-258 °C.

6.3.13 Synthesis of (**L2**$_{o\text{-tolyl}}$)PdCl

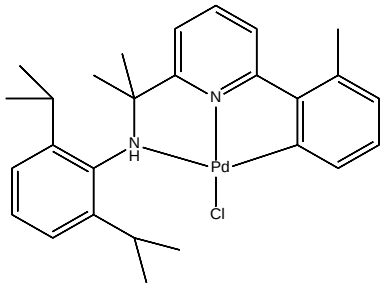

To a round bottomed flask, open to the air and equipped with a magnetic stir bar, was added (**L2**$_{o\text{-tolyl}}$)PdOAc (0.050 g, 0.090 mmol) in dichloromethane (5 ml) and a saturated aqueous solution of sodium chloride (10 ml). The mixture was then stirred vigorously overnight at room temperature to give a yellow coloured reaction mixture. The organic

phase was then isolated and the aqueous layer was washed with dichloromethane (2 × 10 ml). The organic extracts were combined and dried over magnesium sulphate. The solvent was removed under reduced pressure to give the (**L2**$_{o\text{-tolyl}}$)PdCl as a brown solid (0.047 g, 99%). ^{1}H NMR ($CDCl_3$, 400 MHz): δ 0.86 (d, 3H, $^{3}J_{HH}$ = 6.8 Hz, Ar-CH(C***H***$_3$)$_2$), 1.28 (s, 3H, Py-C(NH)-(C***H***$_3$)$_2$), 1.29 (d, 3H, $^{3}J_{HH}$ = 6.8 Hz, Ar-CH-(C***H***$_3$)$_2$), 1.31 (d, 3H, $^{3}J_{HH}$ = 6.8 Hz, Ar-CH-(C***H***$_3$)$_2$), 1.37 (d, 3H, $^{3}J_{HH}$ = 6.8 Hz, Ar-CH(C***H***$_3$)$_2$), 1.90 (s, 3H, Py-C(NH)-(C***H***$_3$)$_2$), 2.57 (s, 3H, o-Ar-C***H***$_3$), 3.01 (sept, 1H, $^{3}J_{HH}$ = 6.8 Hz, C***H***-(CH_3)$_2$), 3.32 (sept, 1H, $^{3}J_{HH}$ = 6.8 Hz, C***H***-(CH_3)$_2$), 5.18 (s, 1H, N***H***), 6.84 (d, 1H, $^{3}J_{HH}$ = 7.6 Hz, Py/Ar-***H***), 6.93 (t, 1H, $^{3}J_{HH}$ = 7.6 Hz, Py/Ar-***H***), 6.99 (d, 1H, $^{3}J_{HH}$ = 7.5 Hz, $^{4}J_{HH}$ = 1.4 Hz, Py/Ar-***H***), 7.02-7.12 (m, 3H, Py/Ar-***H***), 7.72 (dd, 1H, $^{3}J_{HH}$ = 7.8 Hz, $^{4}J_{HH}$ = 1.1 Hz, Py/Ar-***H***), 7.74-7.84 (m, 2H, Py/Ar-***H***). ^{13}C{^{1}H} NMR ($CDCl_3$, 100 MHz): δ 22.8 (Ar-CH-(***C***H$_3$)$_2$), 23.4 (Py-C(NH)-(***C***H$_3$)$_2$), 23.6 (Py-C(NH)-(***C***H$_3$)$_2$), 23.7 (Ar-CH-(***C***H$_3$)$_2$), 24.9 (Ar-CH-(***C***H$_3$)$_2$), 26.8 (Ar-CH-(***C***H$_3$)$_2$), 28.9 (Ar-***C***H-(CH_3)$_2$), 29.0 (Ar-***C***H-(CH_3)$_2$), 35.9 (o-Ar-***C***H$_3$), 68.9 (Py-***C***(NH)-(CH_3)$_2$), 116.9 (CH), 120.9 (CH), 123.6 (CH), 125.1 (C), 126.4 (CH), 128.8 (CH), 128.9 (CH), 134.2 (C), 135.5 (CH), 137.1 (CH), 138.7 (C), 141.9 (C), 143.2 (CH), 145.4 (C), 154.0 (C), 164.3 (C), 168.2 (C). IR: 789 ν(C-H bend), 802 ν(C-H bend), 1452 ν(C-N)$_{pyridine}$, 1590 ν(N-H)$_{amine\ bend}$, 2926 ν(C-H stretch), 3341 ν(N-H)$_{amine\ stretch}$ cm^{-1}. ESIMS (+ve, MeCN): m/z 526 [M]$^{+}$. HRMS (FAB): calculated for $C_{25}H_{31}N_2PdCl$: [M]$^{+}$ 526.1078, found 526.1082. m.p: > 270 ^{o}C. Anal. calc. for ($C_{27}H_{33}N_2ClPd$): C 61.48, H 6.31, N 5.31. Found C 61.42, H 6.38, N 5.29%.

6.3.14 Synthesis of *peri*-[(**L2**$_{nap}$)PdOAc][15]

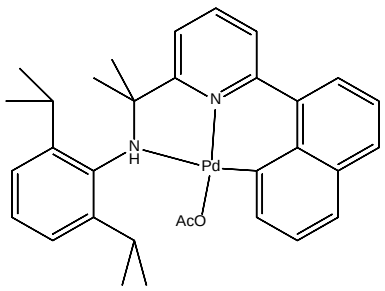

A small dry Schlenk flask equipped with stir bar was evacuated and backfilled with nitrogen. The flask was then loaded with $Pd(OAc)_2$ (0.051 g, 0.23 mmol, 1 eq.) and H**L2**$_{nap}$ (0.158 g, 0.27 mmol, 1.15 eq.) and the contents dissolved in toluene (10 mL). The resultant brown solution was stirred at 60 ^{o}C for 48 h. The reaction mixture was then filtered in the air through a thin layer of Celite and the Celite cake washed thoroughly with dichloromethane and sovent removed under reduced pressure to give *peri*-

(**L2**$_{nap}$)PdOAc as a yellow powder. Recrystallisation from dichloromethane/hexane (1:3 v/v) yielded yellow feathery crystals (0.126 g, 91%). ^{1}H NMR ($CDCl_3$, 400 MHz): δ 0.71 (d, 3H, $^{3}J_{HH}$ = 6.9 Hz, CH(C*H*$_3$)$_2$), 1.20 (d, 3H, $^{3}J_{HH}$ = 6.9 Hz, CH(C*H*$_3$)$_2$), 1.33 (d, 3H, $^{3}J_{HH}$ = 6.9 Hz, CH(C*H*$_3$)$_2$), 1.38 (d, 3H, $^{3}J_{HH}$ = 6.9 Hz, CH(C*H*$_3$)$_2$), 1.39 (s, 3H, Pd-OCO*CH*$_3$), 2.10 (s, 3H, HNC(C*H*$_3$)$_2$), 2.51 (s, 3H, HNC(C*H*$_3$)$_2$), 3.43 (sept, 1H, $^{3}J_{HH}$ = 6.9 Hz, C*H*(CH$_3$)$_2$), 3.57 (sept, 1H, $^{3}J_{HH}$ =6.9 Hz, C*H*(CH$_3$)$_2$), 7.04 (m, 1H, Ar-H), 7.16 (m, 2H, Ar-H), 7.24 (dd, 1H, $^{3}J_{HH}$ = 7.9 Hz, Py*H*), 7.36 (t, 1H, $^{3}J_{HH}$ = 7.7 Hz, Ar*H*), 7.53 (t, 1H, $^{3}J_{HH}$ = 7.7 Hz, Ar$_1$*H*), 7.66 (d, 1H, $^{3}J_{HH}$ = 7.8 Hz, Ar*H*), 7.72 (d, 1H, $^{3}J_{HH}$ = 7.3 Hz, Ar*H*), 7.91 (t, 1H, $^{3}J_{HH}$ = 7.9 Hz, Py*H*), 7.97 (d, 1H, $^{3}J_{HH}$ = 7.0 Hz, Ar*H*), 7.98 (s, 1H, (CH$_3$)$_2$CN*H*), 8.06 (d, 1H, $^{3}J_{HH}$ = 7.9 Hz, PyH), 8.14 (d, 1H, $^{3}J_{HH}$ = 7.0 Hz, Ar*H*). ^{13}C{^{1}H} NMR ($CDCl_3$, 400 MHz): δ 22.8 (CH(*C*H$_3$)$_2$), 24.5 (CH(*C*H$_3$)$_2$), 24.9 (CH(*C*H$_3$)$_2$), 25.8 (CH(*C*H$_3$)$_2$), 25.9 (*C*H(CH$_3$)$_2$), 26.0 (*C*H(CH$_3$)$_2$), 28.3 (Py-C(NH)-(***C***H$_3$)$_2$), 31.8 (Py-C(NH)-(***C***H$_3$)$_2$), 34.2 (Pd-OCOCH$_3$), 66.1 (Py-***C***(NH)-(CH$_3$)$_2$), 119.2 (CH), 121.8 (CH), 123.7 (CH), 124.3 (CH), 124.6 (C), 124.9 (CH), 125.2 (C), 125.5 (CH), 126.5 (CH), 128.0 (CH), 128.8 (CH), 133.4 (C), 135.2 (CH), 136.9 (C), 137.9 (C), 139.6 (CH), 141.0 (CH), 144.6 (C), 144.8 (C), 155.1 (C), 172.1 (C), 178.8 (Pd-O***C***OCH$_3$). IR: 3339 ν(N-H)$_{amine}$, 2919 ν(C-H stretch), 1379 ν(C=N)$_{pyridine}$, 803 ν(C-H bend), 767 ν(C-H bend) cm^{-1}. ESIMS (+ve, MeCN): m/z 586 [M]$^{+}$. HRMS (FAB): calculated for $C_{32}H_{36}N_2O_2Pd$ [M]$^{+}$ 586.1801, found 586.1806. m.p: 260-263 ºC. The data are consistent with those in the published report.[15]

6.3.15 Synthesis of *peri*-[(**L2**$_{nap}$)PdCl]

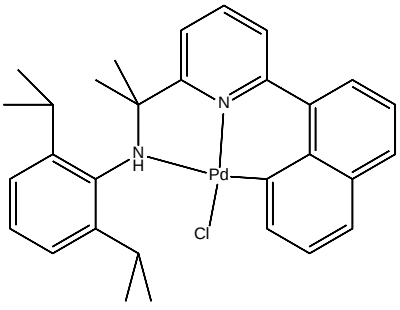

To a 50 mL round bottom flask, open to the air and equipped with stir bar, was added complex *peri*-(**L2**$_{nap}$)PdOAc (51.1 mg, 0.08 mmol) and dichloromethane (10 ml). A saturated solution of sodium chloride (10 ml) was added and the reaction mixture stirred at room temperature overnight. The organic layer was separated and the aqueous layer washed with dichloromethane (3 x 15 mL). All the organic layers were combined and

washed with brine (1 x 30 mL). The organic fractions were dried over magnesium sulphate and the solvent was removed under reduced pressure to give *peri*-(**L2**$_{nap}$)PdCl as yellow (45.9 mg, 99%). ^{1}H NMR ($CDCl_3$, 400 MHz): δ 0.67 (d, 3H, $^{3}J_{HH}$ = 7.0 Hz, CH(*CH*$_3$)), 1.10 (d, 3H, $^{3}J_{HH}$ = 7.0 Hz, CH(*CH*$_3$)), 1.31 (s, 3H, HNC(*CH*$_3$)), 1.34 (d, 3H, $^{3}J_{HH}$ = 7.0 Hz, CH(*CH*$_3$)), 1.44 (d, 3H, $^{3}J_{HH}$ = 7.0 Hz, CH(*CH*$_3$)), 2.37 (s, 3H, HNC(*CH*$_3$)) , 3.12 (sept, 1H, $^{3}J_{HH}$ = 7.0 Hz, C*H*(CH_3)$_2$), 3.20 (sept, 1H, $^{3}J_{HH}$ = 7.0 Hz, C*H*(CH_3)$_2$) , 5.67 (s, 1H, (CH_3)$_2$CN*H*), 6.94-7.04 (m, 3H, Aniline-H), 7.16 (d, 1H, $^{3}J_{HH}$ = 7.8 Hz, Ar*H*), 7.22 (t, 1H, $^{3}J_{HH}$ = 7.5 Hz, Ar*H*), 7.42 (t, 1H, $^{3}J_{HH}$ = 7.9 Hz, Py*H*), 7.53 (d, 1H, $^{3}J_{HH}$ = 7.9 Hz, Ar*H*), 7.83 (d, 1H, $^{3}J_{HH}$ = 8.2 Hz, Py*H*), 7.85 (d, 1H, $^{3}J_{HH}$ = 6.9 Hz, Ar*H*), 8.02 (d, 1H, $^{3}J_{HH}$ = 7.9 Hz, Ar*H*), 8.09 (d, 1H, $^{3}J_{HH}$ = 8.1 Hz, PyH), 8.32 (d, 1H, $^{3}J_{HH}$ = 7.2 Hz, Ar*H*). ^{13}C{^{1}H} NMR ($CDCl_3$, 100 MHz): δ 23.1 (CH(*C*H_3)$_2$), 24.7 (CH(*C*H_3)$_2$), 25.1 (CH(*C*H_3)$_2$), 25.7 (CH(*C*H_3)$_2$), 26.2 (*C*H(CH_3)$_2$), 26.9 (*C*H(CH_3)$_2$), 28.7 (Py-C(NH)-(***C***H_3)$_2$), 32.1 (Ar-CH-(***C***H_3)$_2$), 33.4 (Py-C(NH)-(***C***H_3)$_2$), 68.7 (Py-***C***(NH)-(CH_3)$_2$), 122.8 (CH), 124.5 (CH), 127.5 (CH), 127.9 (CH), 128.2 (C), 129.3 (CH), 129.9 (C), 130.7 (CH), 131.8 (CH), 132.1 (CH), 135.4 (CH), 136.3 (C), 137.8 (CH), 138.2 (C), 139.9 (C), 140.5 (CH), 143.9 (CH), 145.3 (C), 151.7 (C), 162.4 (C), 175.6 (C). IR: 3322 ν(N-H)$_{amine}$, 2958 ν(C-H stretch), 1464 ν(C=N)$_{pyridine}$, 800 ν(C-H bend), 765 ν(C-H bend) cm^{-1}. ESIMS (+ve, MeCN): *m/z* 562 [M]$^{+}$. HRMS (FAB): calculated for $C_{30}H_{34}ClPd$ [M]$^{+}$ 562.1352, found 562.1356. m.p: > 270 ^{o}C.

6.3.16 Synthesis of *ortho*-[(**L2**$_{nap}$)PtCl]

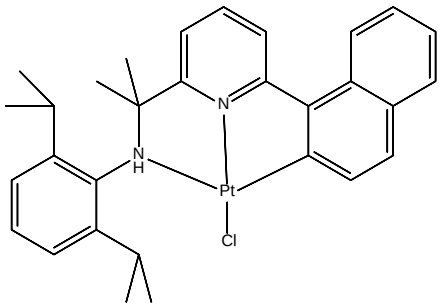

To a round bottom flask open to the air was added H**L2**$_{nap}$ (0.050 g, 0.12 mmol), K_2PtCl_4 (0.050 g, 0.12 mmol) and acetic acid (5 ml). A reflux condenser was attached and the mixture then stirred heated to 100 ^{o}C for 60 h. Upon cooling to room temperature, the resulting suspension was filtered to give *ortho*-(**L2**$_{nap}$)PtCl as a brown powder (0.065 g, 83%). ^{1}H NMR ($CDCl_3$, 400 MHz): δ 0.89 (d, 3H, $^{3}J_{HH}$ = 6.8 Hz, CH(*CH*$_3$)), 1.15 (d, 3H, $^{3}J_{HH}$ = 6.8 Hz, CH(*CH*$_3$)), 1.33 (d, 3H, $^{3}J_{HH}$ = 6.8 Hz, CH(*CH*$_3$)), 1.42 (d, 3H, $^{3}J_{HH}$ =

6.8 Hz, CH(*CH*$_3$)), 1.93 (s, 3H, HNC(*CH*$_3$)$_2$), 2.02 (s, 3H, HNC(*CH*$_3$)$_2$) , 3.07 (sept, 1H, $^3J_{HH}$ = 6.8 Hz, C*H*(CH$_3$)$_2$), 3.26 (sept, 1H, $^3J_{HH}$ = 6.8 Hz, C*H*(CH$_3$)$_2$) , 5.85 (s, 1H, (CH$_3$)$_2$CN*H*), 6.91 (d, 1H, $^3J_{HH}$ = 7.9 Hz, Py/Ar-H), 7.04-7.08 (m, 1H, Py/Ar-H), 7.11 (m, 2H, Py/Ar-H), 7.31 (td, 1H, $^3J_{HH}$ = 7.5 Hz, $^4J_{HH}$ = 1.0, Py/Ar-H), 7.43 (td, 1H, $^3J_{HH}$ =7.7 Hz, $^4J_{HH}$ = 1.5 Hz, Py/Ar-H), 7.57 (d, 1H, $^3J_{HH}$ = 8.3 Hz, Py/Ar-H), 7.75 (dd, 1H, $^3J_{HH}$ = 8.2 Hz, $^4J_{HH}$ = 1.4 Hz, Py/Ar-H), 7.88 (t, 1H, $^3J_{HH}$ = 8.0 Hz, Py/Ar-H), 8.09-8.11 (m, 2H, Py/Ar-H), 8.33 (d, 1H, $^3J_{HH}$ = 8.5 Hz, Py/Ar-H). ^{13}C{^{1}H} NMR (125 MHz, CDCl$_3$): δ 19.9 (*C*H$_3$C=N), 20.6 (CH*Me*$_2$), 21.9 (CH*Me*$_2$), 22.8 (CH*Me*$_2$), 23.8 (CH*Me*$_2$), 25.9 (*C*HMe$_2$), 27.6 (*C*HMe$_2$), 28.1 (Py-C(NH)-(***C***H$_3$)$_2$), 34.3 (Py-C(NH)-(***C***H$_3$)$_2$), 70.5 (Py-*C*(NH)-(CH$_3$)$_2$), 115.2 (CH), 119.8 (CH), 120.1 (CH), 122.3 (CH), 122.7 (CH), 124.5 (CH), 125.9 (CH), 126.0 (CH), 129.2 (CH), 129.6 (CH), 130.1 (C), 131.3 (C), 131.8 (CH), 136.5 (CH), 137.5 (C), 141.0 (C), 142.1 (C), 143.7 (C), 165.0 (C), 166.7 (C), 175.3 (C). IR: 3343 ν(N-H)$_{amine}$, 2945 ν(C-H stretch), 1483 ν(C=N)$_{pyridine}$, 809 ν(C-H bend), 779 ν(C-H bend) cm^{-1}. ESIMS (+ve, MeCN): m/z 651 [M]$^+$. HRMS (FAB): calculated for C$_{30}$H$_{34}$ClPd [M]$^+$ 651.1352, found 651.1359. m.p. > 270 ^{o}C.

6.3.17 Synthesis of (**L3**$_{o\text{-tolyl}}$)PdOAc

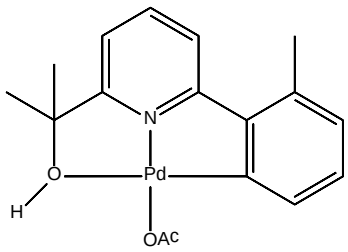

A clean dry Schlenk flask equipped with a magnetic stir bar was evacuated and backfilled with nitrogen. The flask was then charged with Pd(OAc)$_2$ (0.113 g, 0.50 mmol), H**L3**$_{o\text{-tolyl}}$ (0.116 g, 0.515 mmol) and the contents dissolved in dry toluene (20 ml). The solution was heated to 60 ^{o}C and stirred for 48 h. The reaction mixture was cooled to room temperature and filtered through a thin layer of Celite. The Celite cake was washed thoroughly with dichloromethane and dried under reduced pressure to give (**L3**$_{o\text{-tolyl}}$)PdOAc as a deep yellow solid (0.119 g, 59%). Single crystals of (**L3**$_{o\text{-tolyl}}$)PdOAc suitable for an X-ray structure determination were grown by recrystallization from dichloromethane: hexane (1:3). ^{1}H NMR (CDCl$_3$, 400 MHz): δ 1.79 (s, 6H, Pyr-C-(C*H*$_3$)$_2$), 2.15 (s,broad), 3H, OCOC***H***$_3$), 2.53 (s, 3H, *o*-Ar-C***H***$_3$), 6.79-6.95 (m, 3H, Py/Ar-H), 7.03 (m, 1H, Py/Ar-H), 7.59 (d, 1H, $^3J_{HH}$ = 8.1 Hz, Py/Ar-H), 7.81 (t, 1H, $^3J_{HH}$ = 8.1

Hz, Py/Ar-H). $^{13}C\{^{1}H\}$ NMR ($CDCl_3$, 100 MHz): δ 22.3 (*o*-Ar-*C*H_3), 27.8 (OCO***C***H_3), 33.1 (Pyr-C-(*C*H_3)$_2$), 79.3 (Pyr-*C*-(CH_3)$_2$), 116.8 (CH), 120.4 (CH), 128.4 (C), 128.7 (CH), 130.2 (CH), 135.1 (CH), 138.0 (C), 145.3 (CH), 153.6 (C), 163.3 (C), 166.8 (C), 170.9 (O***C***OCH_3). IR (solid state): 778 ν(C-H bend), 1559 $\nu(C\text{-}N)_{pyridine}$ cm^{-1}. ESIMS (+ve, MeOH): m/z 392 $[M+H]^+$, 414 $[M+Na]^+$. HRMS (FAB): calculated for $C_{17}H_{20}NO_3Pd$ $[M+H]^+$ 392.3270, found 392.3274. m.p: 234-237 ^oC.

6.3.18 Synthesis of (**L3**$_{o\text{-tolyl}}$)PdCl

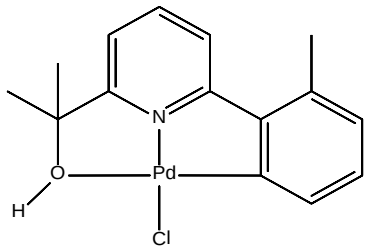

To a round bottomed flask, open to the air and equipped with a magnetic stir bar, was added (**L3**$_{o\text{-tolyl}}$)PdOAc (0.035 g, 0.09 mmol), dichloromethane (10 ml) and a saturated aqueous solution of sodium chloride (10 ml). The mixture was then stirred vigorously overnight to obtain a yellow coloured reaction mixture. Dichloromethane (10 ml) was then introduced and the reaction mixture stirred for 5 min. The organic phase was then isolated and the aqueous layer washed with dichloromethane (2 × 10 ml). The organic extracts were combined and dried over magnesium sulphate. The solvent was removed under reduced pressure to give the (**L3**$_{o\text{-tolyl}}$)PdCl as a brown solid (0.033 g, 99%). Single crystals of (**L3**$_{o\text{-tolyl}}$)PdCl suitable for an X-ray structural determination were grown by recrystallization from dichloromethane: hexane (1:3). ^1H NMR ($CDCl_3$, 400 MHz): δ 1.76 (s, 6H, Pyr-C-(C*H*$_3$)$_2$), 2.34 (s, 3H, *o*-Ar-C***H***$_3$), 6.42 (t, 1H, $^3J_{HH}$ = 7.7 Hz, Py/Ar-H), 6.61 (d, 1H, $^3J_{HH}$ = 7.6 Hz, Py/Ar-H), 6.86 (d, 1H, $^3J_{HH}$ = 8.0 Hz, Py/Ar-H), 6.91 (s (broad), 1H, C-(CH_3)$_2$-O*H*), 7.05 (d, 1H, $^3J_{HH}$ = 7.7 Hz, Py/Ar-H), 7.21 (d, 1H, $^3J_{HH}$ = 8.1 Hz, Py/Ar-H), 7.50 (t, 1H, $^3J_{HH}$ = 8.1 Hz, Py/Ar-H). $^{13}C\{^{1}H\}$ NMR ($CDCl_3$, 100 MHz): δ 21.9 (*o*-Ar-*C*H_3), 34.3 (Pyr-C-(*C*H_3)$_2$), 78.5 (Pyr-*C*-(CH_3)$_2$), 118.6 (CH), 123.7 (CH), 125.2 (C), 129.2 (CH), 129.9 (CH), 131.6 (CH), 137.4 (C), 138.3 (CH), 143.6 (C), 160.8 (C), 167.4 (C). IR (solid state): 749 ν(C-H bend), 1602 $\nu(C{=}N)_{pyridine}$ cm^{-1}. ESIMS (+ve, MeOH): m/z 368 $[M+H]^+$, 390 $[M+Na]^+$. HRMS (FAB): calculated for $C_{15}H_{17}NOPdCl$ $[M+H]^+$ 368.7471, found 368.7475. m.p: > 270 ^oC.

6.3.19 Synthesis of *ortho*-[(**L3**$_{nap}$)PdOAc][15]

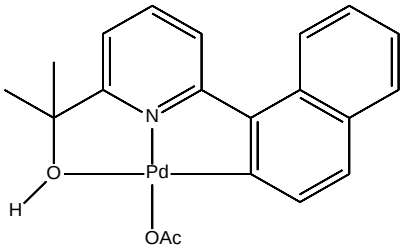

A small dry Schlenk flask equipped with stir bar was evacuated and backfilled with nitrogen. The flask was loaded with $Pd(OAc)_2$ (88 mg, 0.39 mmol, 1 eq), H**L3**$_{nap}$ (0.103 g, 0.4 mmol, 1.03 eq) and the contents dissolved in dry toluene (10 mL). The resultant solution was stirred at 60 ^oC for 48 h. The reaction mixture was then filtered in the air through a thin layer of CeliteCelite and the Celite cake washed thoroughly with dichloromethane and dried under reduced pressure to give *ortho*-(**L3**$_{nap}$)PdOAc as a yellow powder (0.142 g, 85% yield). ^1H NMR (400 MHz, $CDCl_3$): δ 1.73 (s, 3H, Pd-OCO*CH*$_3$), 1.96 (s, 6H, CH(*CH*$_3$)$_2$), 7.30 (t, 1H, $^3J_{HH}$ = 7.8 Hz, Py-H), 7.43 (t, 2H, $^3J_{HH}$ = 8.2 Hz, Ar_2H), 7.59 (d, 1H, $^3J_{HH}$ = 7.8 Hz, PyH), 7.77 (d, 1H, $^3J_{HH}$ = 7.9 Hz, Ar_1H), 7.81 (d, 1H, $^3J_{HH}$ = 7.9 Hz, Ar_1H), 7.87 (d, 1H, $^3J_{HH}$ = 8.5 Hz, Ar_2H), 7.95 (d, 1H, $^3J_{HH}$ = 8.1 Hz, Ar_2H), 8.04 (d, 1H, $^3J_{HH}$ = 7.8 Hz, PyH), 12.24-12.51 (brs, 1H, Pd-O*H*). A $^{13}C\{^1H\}$ NMR spectrum could not be obtained due to the poor solubility of the sample in common NMR solvents. IR (solid state): 771 ν(C-H bend), 1560 $\nu(C=N)_{pyridine}$ cm^{-1}. ESIMS (+ve, MeOH): m/z 428 $[M+H]^+$, 450 $[M+Na]^+$. HRMS (FAB): calculated for $C_{16}H_{20}NO_3Pd$ $[M+H]^+$ 428.0428, found 428.0441. m.p: 234-237 ^oC. The data are consistent with those in the published report.[15]

6.3.20 Synthesis of *ortho*-[(**L3**$_{nap}$)PdCl]

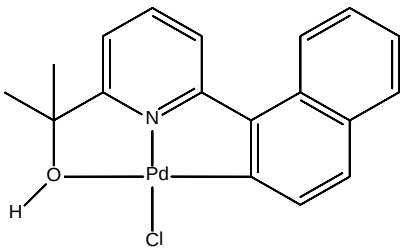

To a round bottomed flask, open to the air and equipped with a magnetic stir bar, was added *ortho*-(**L3**$_{nap}$)PdOAc (0.038 g, 0.09 mmol) in dichloromethane (10 ml) and a

saturated aqueous solution of sodium chloride (10 ml). The mixture was then stirred vigorously overnight to obtain a yellow coloured reaction mixture. $CHCl_3$ (10 ml) was then introduced and the reaction mixture stirred for 5 min. The organic phase was then isolated and the aqueous layer was washed with $CHCl_3$ (2 × 10 ml). The organic extracts were combined and dried over magnesium sulphate. The solvent was removed under reduced pressure to give the *ortho*-(**L3**$_{nap}$)PdCl as a brown solid (0.036 g, 99%). Single crystals of *ortho*-(**L3**$_{nap}$)PdCl suitable for an X-ray structural determination were grown by recrystallization from dichloromethane: hexane (1:3). ^{1}H NMR ($CDCl_3$, 400 MHz): δ 1.78 (s, 6H, Pyr-C-(C*H*$_3$)$_2$), 5.23 (br. s, 1H, C-(CH$_3$)$_2$-O*H*), 6.72 (t, 2H, $^3J_{HH}$ = 8.3 Hz, Py/Ar-H), 6.99 (d, 1H, $^3J_{HH}$ = 8.6 Hz, Py/Ar-H), 7.15-7.20 (m, 2H, Py/Ar-H), 7.31 (td, 1H, $^3J_{HH}$ = 7.4 Hz, $^4J_{HH}$ = 1.2 Hz, Py/Ar-H), 7.40 (d, 1H, $^3J_{HH}$ = 8.8 Hz, Py/Ar-H), 7.51 (d, 1H, $^3J_{HH}$ = 8.6 Hz, Py/Ar-H), 7.63 (d, 1H, $^3J_{HH}$ = 8.4 Hz, Py/Ar-H). ^{13}C{^{1}H} NMR ($CDCl_3$, 100 MHz): δ 29.7 (Pyr-C-(*C*H$_3$)$_2$), 73.5 (Pyr-*C*-(CH$_3$)$_2$), 115.9 (CH), 122.4 (CH), 125.8 (CH), 126.1 (CH), 126.6 (CH), 127.5 (CH), 128.3 (CH), 129.6 (C), 132.1 (C), 133.8 (CH), 139.0 (CH), 138.6 (C), 157.0 (C), 161.7 (C), 165.5 (C). IR (solid state): 755 ν(C-H bend), 1583 ν(C-N)$_{pyridine}$ cm^{-1}. ESIMS (+ve, MeOH): *m/z* 404 [M+H]$^+$, 426 [M+Na]$^+$. HRMS (FAB): calculated for $C_{18}H_{16}NOPdCl$ [M]$^+$ 403.7792, found 403.7796. m.p: > 270 ^{o}C. Anal. calc. for ($C_{18}H_{16}NOClPd$): C 53.49, H 3.99, N 3.47. Found C 53.48, H 3.82, N 3.53%.

6.3.21 Synthesis of (H**L1**$_{py\text{-}nap}$)Pd(OAc)$_2$

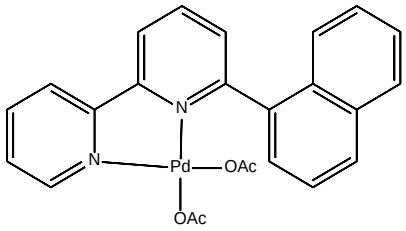

H**L1**$_{py\text{-}nap}$ (0.035 g, 0.124 mmol, 1 eq.) and palladium(II) acetate (0.030 g, 0.134 mmol, 1.1 eq were dissolved in $CHCl_3$ (8 ml) in a round bottom flask open to the air. The solution was stirred at room temperature for 2 h producing a dark yellow solution. The solvent was removed under reduced pressure affording (H**L1**$_{py\text{-}nap}$)Pd(OAc)$_2$ as a dark yellow microcrystalline solid (0.050 g, 78%). Yellow and needle-like crystals suitable for a single crystal X-ray diffraction study could be grown by layering a chloroform solution of the complex with petroleum ether (40:60). ^{1}H NMR (300 MHz, $CDCl_3$): δ 0.70 (s, 3H, Pd-OC(O)C*H*$_3$), 2.05 (s, 3H, Pd-OC(O)C*H*$_3$), 7.35 (m, 2H, $^3J_{HH}$ = 7.1 Hz, Py-*H*$_p$, Nap-

H_{C8}), 7.49 (d, 1H, $^3J_{HH}$ = 7.7 Hz, Py-H_m), 7.58 (dd, 1H, $^3J_{HH}$ = 7.0 Hz, Nap-H_{C6}), 7.62 (d, 1H, $^3J_{HH}$ = 7.0 Hz, Nap-H_{C3}), 7.71 (d, 1H, $^3J_{HH}$ = 7.7 Hz, Nap-H_{C7}), 7.95 (dd, 1H, $^3J_{HH}$ = 7.0, $^4J_{HH}$ = 4.5 Hz, Py-H_p), 8.00 (d, 2H, $^3J_{HH}$ = 9.1 Hz, Nap-$H_{C4,C5}$), 8.15 (d, 1H, $^3J_{HH}$ = 7.5 Hz, Nap-H_{C2}), 8.18 (d, 1H, $^3J_{HH}$ = 3.5 Hz, Py-H_m), 8.20 (d, 1H, $^3J_{HH}$ = 3.5 Hz, Py-H_o), 8.88 (d, 1H, $^3J_{HH}$ = 7.0 Hz, Py-H_m), 8.92 (d, 1H, $^3J_{HH}$ = 6.5 Hz, Py-H_m). A $^{13}C\{^1H\}$ NMR spectrum could not be obtained due to the poor solubility of the sample in NMR solvents. IR (solid state): 1629 $\nu(C=N)_{pyridine}$ cm^{-1}. ESIMS (-ve, MeOH): *m/z* 387 [(H**L1**$_{py\text{-}nap}$)Pd]$^+$, 419 [(H**L1**$_{py\text{-}nap}$)Pd(OMe)]$^+$. HRMS (TOF): *m/z* calc. for $C_{24}H_{20}N_2O_4Pd$ $[M+H]^+$: 507.8558. Found: 507.0546 $[M+H]^+$. m.p: 252-254 ^oC. Anal Calc. for ($C_{24}H_{20}N_2O_4Pd$): C, 56.87; H, 3.98; N, 5.53. Found: C, 57.01; H, 3.77; N, 5.68%.

6.3.22 Synthesis of *peri*-**[(L1**$_{py\text{-}nap}$)PdOAc]

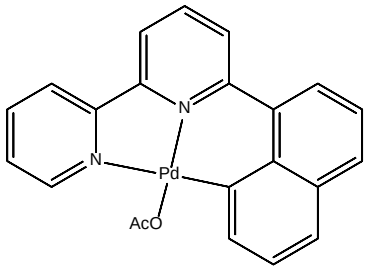

H**L1**$_{py\text{-}nap}$ (0.035 g, 0.124 mmol, 1 eq.) and palladium(II) acetate (0.030 g, 0.134 mmol, 1.1 eq were dissolved in $CHCl_3$ (8 ml) in a round bottom flask open to the air. The solution was stirred at room temperature for 24 h producing a dark yellow solution. The solution was transferred to a sample vial and layered with petroleum ether (40:60) affording *peri*-[(**L1**$_{py\text{-}nap}$)PdOAc] as dark orange crystals which could be separated by decantation and dried (0.042 g, 76%). ^1H NMR (300 MHz, $CDCl_3$): δ 1.25 (s, 3H, Pd-OC(O)CH_3), 7.47 (d, 1H, $^3J_{HH}$ = 7.6 Hz, Nap-H_{C7}), 7.60 (t, 2H, $^3J_{HH}$ = 7.6 Hz, Nap-$H_{C3,C6}$), 7.67 – 7.70 (m, 2H, Nap/Py-*H*), 7.94 – 7.87 (m, 3H, Nap/Py-*H*), 7.98 (dd, 1H, $^3J_{HH}$ = 8.1 Hz, $^4J_{HH}$ =3.0 Hz, Py-H_p), 7.98 – 8.06 (m, 2H, Py-H_m), 8.15 (d, 1H, $^3J_{HH}$ = 6.3 Hz, Nap-H_{C2}), 8.71 (d, 1H, $^3J_{HH}$ = 9.0 Hz, Py-H_o). A $^{13}C\{^1H\}$ NMR spectrum could not be obtained due to the low solubility of the material in common NMR solvents. IR (solid state): 1598 $\nu(C=N)_{pyridine}$ cm^{-1}. ESIMS (+ve, MeOH): *m/z* 387 [(**L1**$_{py\text{-}nap}$)Pd]$^+$, 421 [(**L1**$_{py\text{-}nap}$)Pd(OMe)]$^+$. m.p: 256-258 ^oC. Anal Calc. for ($C_{22}H_{16}N_2O_2Pd$): C, 59.14; H, 3.61; N, 6.27. Found: C, 59.33; H, 3.59; N, 6.01%.

6.3.23 Reaction of H**L1**$_{2,4,6\text{-Me3Ph}}$ with Pd(OAc)$_2$

A small dry Schlenk flask equipped with stir bar was evacuated and backfilled with nitrogen. The flask was then loaded with H**L1**$_{2,4,6\text{-Me3Ph}}$ (0.048 g, 0.121 mmol), Pd(OAc)$_2$ (0.037 g, 0.165 mmol), and the contents dissolved in dry toluene (10 mL). The resultant solution was stirred at 60 ^{o}C for 48 h. The reaction mixture was then filtered in the air through a thin layer of Celite and the Celite cake washed thoroughly with dichloromethane and dried under reduced pressure to give a brown solid. The ^{1}H NMR spectrum of the solid showed a mixture of species including unreacted H**L1**$_{2,4,6\text{-Me3Ph}}$. Crystallisation by layering a dichloromethane solution of the solid with petroleum ether gave after three days (**L1**$_{2,4,6\text{-Me3Ph}}$)PdOAc (0.004 g, 6%) as red crystals on the wall of the vial. (**L1**$_{2,4,6\text{-Me3Ph}}$)PdOAc was the subject of a single crystal X-ray diffraction study. ^{1}H NMR (400 MHz, $CDCl_3$): δ 1.05 (d, $^{3}J_{HH}$ 6.9 Hz, 6H, CH-(CH_3)$_2$)), 1.21 (d, $^{3}J_{HH}$ = 6.8 Hz, 6H, CH-(CH_3)$_2$)), 1.52 (s, 3H, Pd-O-C(O)CH_3), 2.18 (s, 3H, Ar-Me), 2.21 (s, 3H, N=CCH_3), 2.23 (s, 3H, Ar-Me), 3.02 (sept, $^{3}J_{HH}$ = 6.8 Hz, 2H, CH-CH_3)$_2$), 3.31 (s, 2H, Ar-CH_2), 6.81 (s, 1H, Ar-H), 7.1-7.2 (m, 4H, Ar-H), 7.51 (d, $^{3}J_{HH}$ = 7.9 Hz, 1H, Py-H), 7.82 – 7.92 (m, 2H, Py-H). IR (solid state): 1598 ν(C=N)$_{pyridine}$, 1625 ν(C=N)$_{imine}$. ESIMS (+ve, MeOH) *m/z:* 504 [M-OAc]$^{+}$. Anal. calc. for ($C_{30}H_{36}N_2O_2Pd$): C 64.00, H 6.44, N 4.98. Found C 63.79, H 6.31, N 5.03%.

6.3.24 Reaction of H**L1**$_{2,6\text{-Me2Ph}}$ with Pd(OAc)$_2$

A small dry Schlenk flask equipped with stir bar was evacuated and backfilled with nitrogen. The flask was then loaded with H**L1**$_{2,6\text{-Me2Ph}}$ (0.047 g, 0.121 mmol), Pd(OAc)$_2$ (0.037 g, 0.165 mmol), and the contents dissolved in dry toluene (10 mL). The resultant solution was stirred at 60 ^{o}C for 48 h. The reaction mixture was then filtered in the air through a thin layer of Celite and the Celite cake washed thoroughly with dichloromethane and dried under reduced pressure to give a red-brown solid. The ^{1}H NMR spectrum of the solid showed a mixture of species including unreacted H**L1**$_{2,6\text{-Me2Ph}}$. Crystallisation by layering a dichloromethane solution of the solid with petroleum ether gave after three days [(**L1**$_{2,6\text{-Me2Ph}}$)Pd(μ-OAc)]$_2$ (0.003 g, 5%) as yellow plates on the wall of the vial. [(**L1**$_{2,6\text{-Me2Ph}}$)Pd(μ-OAc)]$_2$ was the subject of a single crystal X-ray diffraction

study. ESIMS (+ve, MeCN) *m/z:* 504 $[M\text{-}OAc]^+$. 978 [M – 2OAc], 1019 $[M – (OAc)_2$ + MeCN]. FABMS *m/z:* 978 [M – 2OAc], 1037 [M – OAc], 1096 [M].

NMR scale experiments for the interconversion chemistry

(a) ortho-selectivity and peri-deuteration:

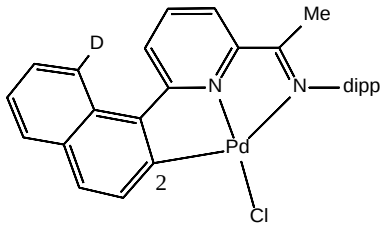

100% ortho-palladation +100% deuteration of peri-position

To a small round bottom flask, equipped with a stir bar and open to the air, was added H**L1**$_{ket\text{-}nap}$ (0.005 g, 0.012 mmol), Na_2PdCl_4 (0.004 g, 0.012 mmol) and deuterated acetic acid (3 ml). A condenser was attached and the mixture stirred and heated to 100 ^oC for 60 h. Upon cooling to room temperature, the resulting suspension was filtered to give the crude product. Recrystallization from DCM/hexane yielded peri-deuterated *ortho*-[(**L1**$_{ket\text{-}nap}$)PdCl] as an orange-yellow powder (0.006 g, 87%). ^{1}H NMR ($CDCl_3$, 400 MHz): 1.16 (d, 6H, $^3J_{HH}$ = 6.8 Hz, CH*(CH$_3$)$_2$*), 1.39 (d, 6H, $^3J_{HH}$ = 6.8 Hz, CH*(CH$_3$)$_2$*), 2.22 (s, 3H, NC*H$_3$*), 3.07 (sept, 2H, $^3J_{HH}$ = 6.8 Hz, *CH*$(CH_3)_2$), 7.25 (s, 3H, dipp-H), 7.41 (t, 1H, $^3J_{HH}$ = 7.5 Hz, ArH), 7.49-7.54 (m, 2H, Ar/Py-H), 7.60 (d, 1H, $^3J_{HH}$ = 8.6 Hz, Ar-H), 7.84 (d, 1H, $^3J_{HH}$ = 8.3 Hz, ArH), 8.02 (t, 1H, $^3J_{HH}$ = 8.3 Hz, Py-H), 8.20 (d, 1H, $^3J_{HH}$ = 8.3 Hz, Ar-H), 8.35 (d, 1H, $^3J_{HH}$ = 7.4 Hz, Ar-H).

(b) Confirmation of dichloride as intermediate

To a small round bottom flask, equipped with a stir bar and open to the air, was added (H**L1**$_{ket\text{-}nap}$)$PdCl_2$ (0.005 g, 0.009 mmol), and glacial acetic acid (3 ml). A condenser was attached and the mixture stirred and heated to 100 ^oC for 60 h. Upon cooling to room temperature, the solvent was removed under reduced pressure (firstly on a rotary

evaporator, then on a vacuum line). A 92:8 mixture of *ortho*-[(**L1**$_{ket\text{-}nap}$)PdCl] and *peri*-[(**L1**$_{ket\text{-}nap}$)PdCl] was confirmed by ^{1}H NMR spectroscopy ($CDCl_3$, 400 MHz).

(c) Solvent effect

To a small round bottom flask, equipped with a stir bar and open to the air, was added (H**L1**$_{ket\text{-}nap}$)$PdCl_2$ (0.005 g, 0.009 mmol) and toluene (3 ml). A condenser was attached and the mixture stirred and heated to 100 ^{o}C for 24 h. Upon cooling to room temperature, the solvent was removed under reduced pressure (firstly on rotary evaporator, then on a vacuum line). The product being a 50:50 mixture of *ortho*-[(**L1**$_{ket\text{-}nap}$)PdCl] and *peri*-[(**L1**$_{ket\text{-}nap}$)PdCl] was confirmed by ^{1}H NMR spectroscopy ($CDCl_3$, 400 MHz).

(d) Conversion of dichloride intermediate (H**L1**$_{ket\text{-}nap}$)$PdCl_2$ to *peri*-[(**L1**$_{ket\text{-}nap}$)PdOAc] at room temperature and acetate-chloride exchange

To a round bottom flask, equipped with a stir bar and open to the air, was added (H**L1**$_{ket\text{-}nap}$)$PdCl_2$ (0.010 g, 0.018 mmol), AgOAc (0.006 g, 0.036 mmol, 2 eq.) and chloroform (3 ml). The mixture was stirred at room temperature overnight, resulting in a white/grey precipitate. After filtration, the solvent was removed under reduced pressure to give a complex tentatively ascribed as *peri*-[(**L1**$_{ket\text{-}nap}$)Pd(OAc)]·AgCl as a yellow powder (0.011 g, 87%). ^{1}H NMR ($CDCl_3$, 400 MHz): δ 1.02 (d, 6H, $^{3}J_{HH}$ = 6.5 Hz, CH$(CH_3)_2$), 1.17 (brs, 3H, Pd-OCOCH_3), 1.22 (d, 6H, $^{3}J_{HH}$ = 6.5 Hz, CH$(CH_3)_2$), 2.32 (s, 3H, (CH_3)C=N), 2.96-3.11 (m, 2H, C$H(CH_3)_2$), 7.03-7.09 (m, 1H, Ar/PyH), 7.14-7.16 (m, 2H, Ar/Py-H) , 7.19 (s, 2H, Ar/Py-H), 7.50 (t, 1H, $^{3}J_{HH}$ = 7.8 Hz, Ar/Py-H) , 7.54 (d, 1H, $^{3}J_{HH}$ = 7.9 Hz, Ar/Py-H) , 7.89 (d, 1H, $^{3}J_{HH}$ = 7.6 Hz, Ar/Py-H), 7.95 (d, 1H, $^{3}J_{HH}$ = 7.8 Hz, Ar/Py-H), 8.18-8.23 (m, 2H, Ar/Py-H), 8.47 (d, 1H, $^{3}J_{HH}$ = 8.4 Hz, Ar/Py-H). HRMS (FAB): calculated for $C_{29}H_{29}N_2Pd$ $[M\text{-}(OAc+AgCl)]^{+}$ 511.1365, found 511.1357. The silver adduct was then dissolved in dichloromethane (5 ml) and stirred with a saturated aqueous sodium chloride solution at room temperature for 2 h. The organic layer was separated and the aqueous layer washed with dichloromethane (3 x 5 ml). The organic phases were combined, dried over $MgSO_4$ and the solvent removed under reduced pressure affording *peri*-[(**L1**$_{ket\text{-}nap}$)PdCl] as a yellow solid (0.007 g, 73%).

(e) Isomerisation of *peri*-[(**L1**$_{ket\text{-}nap}$)PdCl] to *ortho*-[(**L1**$_{ket\text{-}nap}$)PdCl] in acetic acid

To a round bottom flask, equipped with a stir bar and open to the air, was added *peri*-[(**L1**$_{ket\text{-}nap}$)PdCl] (0.005 g, 0.009 mmol) and glacial acetic acid (3 ml). A condenser was attached and the mixture stirred and heated to 100 ^{o}C for 24 and 48 h. Upon cooling to room temperature, the solvent was removed under reduced pressure (firstly on a rotary evaporator, then on a vacuum line). At 24 h, a 83:17 mixture of *ortho*-[(**L1**$_{ket\text{-}nap}$)PdCl] and *peri*-[(**L1**$_{ket\text{-}nap}$)PdCl] was confirmed by ^{1}H NMR spectroscopy ($CDCl_3$, 400 MHz). At 48 h, a 90:10 mixture of *ortho*-[(**L1**$_{ket\text{-}nap}$)PdCl] and *peri*-[(**L1**$_{ket\text{-}nap}$)PdCl] was confirmed by ^{1}H NMR spectroscopy ($CDCl_3$, 400 MHz).

(f) Thermolysis of *ortho*-[(**L1**$_{ket\text{-}nap}$)PdOAc] in toluene at 100 ^{o}C

To a 25 mL round bottom flask, equipped with stir bar and open to the air, was added *ortho*-[(**L1**$_{ket\text{-}nap}$)PdOAc] (0.005 g, 0.009 mmol) and toluene (3 mL). A condenser was attached and the mixture stirred and heated to 100 ^{o}C for 24 h. Upon cooling to room temperature, the solvent was removed under reduced pressure. No evidence for ortho-peri interconversion and some decomposition to form free ligand was confirmed by ^{1}H NMR spectroscopy ($CDCl_3$, 400 MHz).

(g) Thermolysis of *peri*-[(**L1**$_{ket\text{-}nap}$)PdOAc] in toluene at 100 ^{o}C

To a 25 mL round bottom flask, equipped with stir bar and open to the air, was added *peri*-[(**L1**$_{ket\text{-}nap}$)PdOAc] (0.005 g, 0.009 mmol) and toluene (3 mL). A condenser was attached and the mixture stirred and heated to 100 ^{o}C for 24 h. Upon cooling to room temperature, the solvent was removed under reduced pressure. No evidence for ortho-peri interconversion and some decomposition to form free ligand was confirmed by ^{1}H NMR spectroscopy ($CDCl_3$, 400 MHz).

(h) Thermolysis of *ortho*-[(**L1**$_{ket\text{-}nap}$)PdOAc] in acetic acid at 100 ^{o}C

To a 25 mL round bottom flask, equipped with a stir bar and open to the air, was added *ortho*-[(**L1**$_{ket\text{-}nap}$)PdOAc] (0.005 g, 0.009 mmol) and glacial acetic acid (3 mL). A condenser was attached and the mixture stirred and heated to 100 ^{o}C for 24 h. Upon

cooling to room temperature, the solvent was removed under reduced pressure. A 1:2 mixture of *ortho*-[(**L1**$_{ket\text{-}nap}$)PdOAc] and *peri*-[(**L1**$_{ket\text{-}nap}$)PdOAc] was confirmed by ^{1}H NMR spectroscopy ($CDCl_3$, 400 MHz).

(i) Thermolysis of *peri*-[(**L1**$_{ket\text{-}nap}$)PdOAc] in acetic acid at 100 ^{o}C

To a 25 mL round bottom flask, equipped with a stir bar and open to the air, was added *peri*-[(**L1**$_{ket\text{-}nap}$)PdOAc] (0.005 g, 0.009 mmol) and glacial acetic acid (3 mL). A condenser was attached and the mixture stirred and heated to 100 ^{o}C for 24 h. Upon cooling to room temperature, the solvent was removed under reduced pressure. A 1:2 mixture of *ortho*-[(**L1**$_{ket\text{-}nap}$)PdOAc] and *peri*-[(**L1**$_{ket\text{-}nap}$)PdOAc] was confirmed by ^{1}H NMR spectroscopy ($CDCl_3$, 400 MHz).

6.4 Experimental procedures for Chapter 4

6.4.1 Synthesis of (H**L4**$_{Et}$)Pd(OAc)$_2$

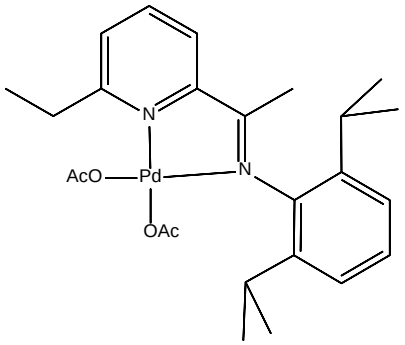

H**L4**$_{Et}$ (0.050 g, 0.162 mmol, 1 eq.) and palladium(II) acetate (0.037 g, 0.164 mmol, 1.01 eq.) were dissolved in $CHCl_3$ (10 ml) in a round bottom flask open to the air. The solution was stirred at room temperature for 16 h producing a darker yellow solution. The solvent was removed under reduced pressure affording (H**L4**$_{Et}$)Pd(OAc)$_2$ as a dark yellow solid (0.067 g, 78%). ^{1}H NMR (300 MHz, $CDCl_3$): δ 1.09 (d, 6H, $^{3}J_{HH}$ = 7.1 Hz, CH(CH_3)$_2$), 1.29 (s, 3H, Pd-OC(O)CH_3), 1.33 (t, 3H, $^{3}J_{HH}$ = 7.3 Hz, CH_2CH_3), 1.51 (d, 6H, $^{3}J_{HH}$ = 7.1 Hz, CH(CH_3)$_2$), 1.97 (s, 3H, Pd-OC(O)CH_3), 2.21 (s, 3H, Pyr-C(N)-CH_3), 3.25 (q, 2H, $^{3}J_{HH}$ = 7.3 Hz, CH_2CH$_3$), 3.35 (sept, 2H, $^{3}J_{HH}$ = 6.8 Hz, C*H*-(CH$_3$)$_2$), 7.19 (d, 2H, $^{3}J_{HH}$ = 7.6 Hz, Py/Ar-H), 7.31 (t, 1H, $^{3}J_{HH}$ = 7.7 Hz, Py/Ar-H), 7.57 (dd, 1H, $^{3}J_{HH}$ = 8.0 Hz, $^{4}J_{HH}$

= 1.3 Hz, Py/Ar-H), 7.64 (d, 1H, $^3J_{HH}$ = 7.8 Hz, Py/Ar-H), 8.02 (t, 1H, $^3J_{HH}$ = 7.9 Hz, Py/Ar-H). $^{13}C\{^1H\}$ NMR (125 MHz, $CDCl_3$): δ 13.3 (Py-CH_2*C*H_3), 18.3 (*C*H_3C=N), 20.6 (CH*Me*$_2$), 22.1 (CH*Me*$_2$), 22.7 (OCO*C*H_3), 23.4 (OCO*C*H_3), 27.8 (*C*HMe$_2$), 28.8 (Py-*C*H_2CH$_3$), 122.7 (C), 122.8 (CH), 123.1 (CH), 127.4 (CH), 128.6 (CH), 138.3 (C), 138.7 (CH), 139.8 (C), 154.5 (C), 170.3 (C=N_{imine}), 175.9 (O*C*OCH$_3$), 176.0 (O*C*OCH$_3$). IR (solid state): 1587 ν(C=N)$_{pyridine}$, 1679 ν(C=N)$_{imine}$. ESIMS (+ve, MeOH) *m/:* 473 [M-OAc]$^+$. HRMS(TOF) (MeCN): *m/z* 473 [M-OAc]$^+$, 514 [M-OAc+MeCN]$^+$. Anal. calc. for ($C_{25}H_{34}N_2O_4Pd{\cdot}CHCl_3$): C 47.87, H 5.41, N 4.29. Found C 47.09, H 6.13, N 4.62 %.

6.4.2 Synthesis of (H**L4**$_{Et}$)$PdCl_2$

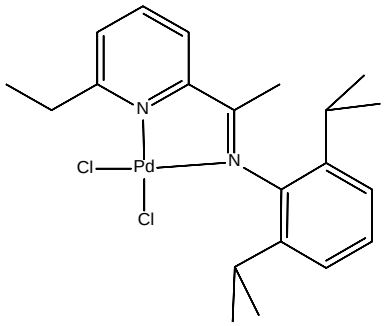

(H**L4**$_{Et}$)Pd(OAc)$_2$ (0.050 g, 0.094 mmol) was dissolved in dichloromethane (10 ml) and stirred at room temperature with a saturated aqueous sodium chloride solution (10 ml) overnight. The resultant mixture was extracted with dichloromethane (3 × 10 ml). The combined organic layers were washed with water (1 × 10 ml), dried over $MgSO_4$ and filtered. The solvent was removed under reduced pressure to give (H**L4**$_{Et}$)$PdCl_2$ as a red-brown powder (0.045 g, 99%). ^{1}H NMR (300 MHz, $CDCl_3$): δ 1.12 (d, 6H, $^3J_{HH}$ = 5.4 Hz, CH(*CH*$_3$)$_2$), 1.45 (d, 6H, $^3J_{HH}$ = 5.4 Hz, CH(*CH*$_3$)$_2$), 1.46 (t, 3H, $^3J_{HH}$ = 6.0 Hz, Py-CH$_2$C*H*$_3$), 2.20 (s, 3H, Pyr-C(N)-C*H*$_3$), 3.16 (sept, 2H, $^3J_{HH}$ = 5.4 Hz, C*H*-(CH$_3$)$_2$), 3.76 (q, 2H, $^3J_{HH}$ = 6.0 Hz, Py-CH$_2$C*H*$_3$), 7.20 (d, 2H, $^3J_{HH}$ = 6.2 Hz, Py/Ar-H), 7.34 (t, 1H, $^3J_{HH}$ = 6.2 Hz, Py/Ar-H), 7.62 (dd, 1H, $^3J_{HH}$ = 6.5 Hz, $^4J_{HH}$ = 1.0 Hz, Py/Ar-H), 7.75 (d, 1H, $^3J_{HH}$ = 6.2 Hz, $^4J_{HH}$ = 1.0 Hz, Py/Ar-H), 8.05 (t, 1H, $^3J_{HH}$ = 6.3 Hz, Py/Ar-H). $^{13}C\{^1H\}$ NMR (125 MHz, $CDCl_3$): δ 15.3 (Py-CH_2*C*H_3), 19.9 (*C*H_3C=N), 23.8 (CH*Me*$_2$), 23.9 (CH*Me*$_2$), 29.0 (*C*HMe$_2$), 32.7 (Py-*C*H_2CH$_3$), 123.8 (CH), 124.2 (CH), 128.7 (CH), 130.4 (CH), 139.5 (CH), 140.1 (C), 141.1 (C), 155.9 (C), 172.7 (C), 177.6 (C=N_{imine}). IR (solid state): 1597 ν(C=N)$_{pyridine}$, 1645 ν(C=N)$_{imime}$. ESIMS (+ve, MeOH) *m/:* 414 [M-2Cl]$^+$. HRMS (FAB): calculated for $C_{21}H_{27}N_2Pd$ [M-HCl_2]$^+$ 413.1309, found 413.1298. Anal. calc. for ($C_{21}H_{28}N_2Cl_2Pd$): C 51.92, H 5.81, N 5.77. Found C 51.85, H 5.86, N 5.91%.

6.4.3 Synthesis of (H**L4**$_{iPr}$)Pd(OAc)$_2$

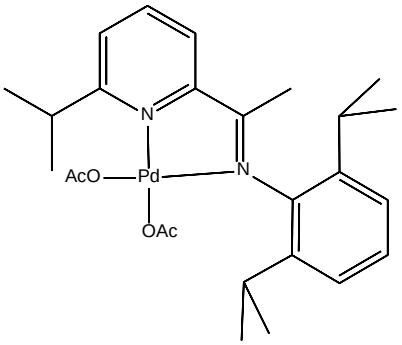

H**L4**$_{iPr}$ (0.050 g, 0.155 mmol, 1 eq.) and palladium(II) acetate (0.035 g, 0.157 mmol, 1.01 eq.) were dissolved in $CHCl_3$ (10 ml) in a round bottom flask open to the air. The solution was stirred at room temperature for 16 h producing a darker yellow solution. The solvent was removed under reduced pressure affording (H**L4**$_{iPr}$)Pd(OAc)$_2$ as a dark yellow solid (0.065 g, 77%). ^{1}H NMR (400 MHz, $CDCl_3$): δ 1.02 (d, 6H, $^3J_{HH}$ = 6.7 Hz, CH(*CH*$_3$)$_{2ar}$), 1.19 (s, 3H, Pd-OC(O)C*H*$_3$), 1.21 (s, 3H, Pd-OC(O)C*H*$_3$), 1.22 (d, 6H, $^3J_{HH}$ = 6.6 Hz, CH(*CH*$_3$)$_{2Py}$), 1.44 (d, 6H, $^3J_{HH}$ = 6.7 Hz, CH(*CH*$_3$)$_{2ar}$), 2.14 (s, 3H, Py-C(N)-C*H*$_3$), 3.27 (sept, 2H, $^3J_{HH}$ = 6.7 Hz, C*H*-(CH$_3$)$_{2ar}$), 3.98 (sept, 1H, $^3J_{HH}$ = 6.6 Hz, C*H*-(CH$_3$)$_{2Py}$), 7.13 (d, 2H, $^3J_{HH}$ = 7.7 Hz, Py/Ar-H), 7.25 (t, 1H, $^3J_{HH}$ = 7.7 Hz, Py/Ar-H), 7.55-7.58 (m, 2H, Py/Ar-H), 7.97 (t, 1H, $^3J_{HH}$ = 7.9 Hz, Py/Ar-H). ^{13}C{^{1}H} NMR (100 MHz, $CDCl_3$): δ 19.3 (*C*H$_3$C=N), 21.5 (CH*Me*$_{2ar}$), 23.5 (CH*Me*$_{2ar}$), 23.6 (OCO*C*H$_3$), 23.8 (OCO*C*H$_3$), 24.4 (CH*Me*$_{2Py}$), 28.9 (*C*HMe$_{2ar}$), 33.9 (*C*HMe$_{2Py}$), 123.3 (CH), 123.8 (CH), 124.3 (CH), 127.4 (CH), 128.4 (C), 139.7 (CH), 140.8 (C), 155.1 (C), 174.8 (C), 175.7 (C=N$_{imine}$), 176.9 (O*C*OCH$_3$), 177.2 (O*C*OCH$_3$). IR (solid state): 1576 ν(C=N)$_{pyridine}$, 1667 ν(C=N)$_{imime}$. ESIMS (+ve, MeOH) *m/:* 487 [M-OAc]$^+$. HRMS(TOF) (MeCN): *m/z* 487 [M-OAc]$^+$, 528 [M-OAc+MeCN]$^+$.

6.4.4 Synthesis of (H**L4**$_{iPr}$)PdCl$_2$

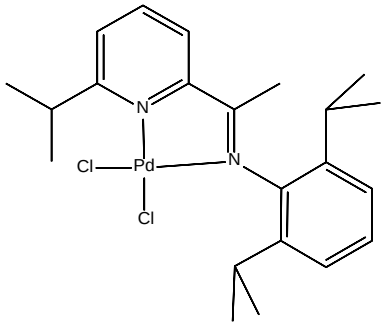

(H**L4**$_{iPr}$)Pd(OAc)$_2$ (0.050 g, 0.091 mmol) was dissolved in dichloromethane (10 ml) and stirred at room temperature with a saturated aqueous sodium chloride solution (10 ml) overnight. The resultant mixture was extracted with dichloromethane (3 × 10 ml). The combined organic layers were washed with water (1 × 10 ml), dried over $MgSO_4$ and filtered. The solvent was removed under reduced pressure to give (H**L4**$_{iPr}$)$PdCl_2$ as a red powder (0.045 g, 99%). ^{1}H NMR (400 MHz, CD_2Cl_2): δ 1.05 (d, 6H, $^3J_{HH}$ = 6.8 Hz, CH(*CH*$_3$)$_{2ar}$), 1.28 (d, 6H, $^3J_{HH}$ = 6.8 Hz, CH(*CH*$_3$)$_{2Py}$), 1.35 (d, 6H, $^3J_{HH}$ = 6.8 Hz, CH(*CH*$_3$)$_{2ar}$), 2.11 (s, 3H, Py-C(N)-C*H*$_3$), 3.07 (sept, 2H, $^3J_{HH}$ = 6.8 Hz, C*H*-(CH$_3$)$_{2ar}$), 4.76 (sept, 1H, $^3J_{HH}$ = 6.8 Hz, C*H*-(CH$_3$)$_{2Py}$), 7.14 (d, 2H, $^3J_{HH}$ = 7.8 Hz, Py/Ar-H), 7.28 (t, 1H, $^3J_{HH}$ = 7.8 Hz, Py/Ar-H), 7.62 (dd, 1H, $^3J_{HH}$ = 8.2 Hz, $^4J_{HH}$ = 1.4 Hz, Py/Ar-H), 7.65 (dd, 1H, $^3J_{HH}$ = 7.7 Hz, $^4J_{HH}$ = 1.4 Hz, Py/Ar-H), 8.00 (t, 1H, $^3J_{HH}$ = 7.9 Hz, Py/Ar-H). ^{13}C{^{1}H} NMR (100 MHz, CD_2Cl_2): δ 20.3 (*C*H$_3$C=N), 23.9 (CH*Me*$_{2Py}$), 24.0 (CH*Me*$_{2ar}$), 24.1 (CH*Me*$_{2ar}$), 29.3 (*C*HMe$_{2ar}$), 36.6 (*C*HMe$_{2Py}$), 124.0 (CH), 125.1 (CH), 128.4 (CH), 128.8 (CH), 140.3 (CH), 140.7 (C), 141.6 (C), 155.9 (C), 176.8 (C), 179.0 (C=N$_{imine}$). IR (solid state): 1567 ν(C=N)$_{pyridine}$, 1687 ν(C=N)$_{imime}$. ESIMS (+ve, MeOH) *m/:* 428 [M-2Cl]$^+$. HRMS (FAB): calculated for $C_{22}H_{29}N_2Pd$ [M-HCl$_2$]$^+$ 427.1409, found 427.1399. Anal. calc. for ($C_{22}H_{30}N_2Cl_2Pd$·0.5CH_2Cl_2): C 49.84, H 5.76, N 5.17. Found C 50.53, H 5.93, N 6.06%.

6.4.5 Synthesis of (H**L4**$_{iPr}$)$PdBr_2$

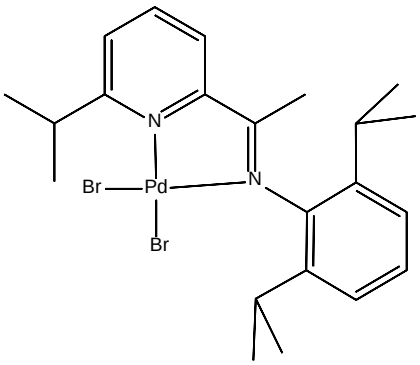

(H**L4**$_{iPr}$)Pd(OAc)$_2$ (0.050 g, 0.091 mmol) was dissolved in dichloromethane (10 ml) and stirred at room temperature with saturated aqueous sodium bromide solution (10 ml) overnight. The resultant mixture was extracted with dichloromethane (3 × 10 ml). The combined organic layers were washed with water (1 × 10 ml), dried over $MgSO_4$ and filtered. The solvent was removed under reduced pressure to give (H**L4**$_{iPr}$)$PdBr_2$ as a red powder (0.053 g, 99%). ^{1}H NMR (400 MHz, CD_2Cl_2): δ 1.04 (d, 6H, $^3J_{HH}$ = 6.7 Hz, CH(*CH*$_3$)$_{2ar}$), 1.31 (d, 6H, $^3J_{HH}$ = 6.8 Hz, CH(*CH*$_3$)$_{2Py}$), 1.39 (d, 6H, $^3J_{HH}$ = 6.7 Hz,

CH(CH_3)$_{2ar}$), 2.12 (s, 3H, Py-C(N)-CH_3), 3.09 (sept, 2H, $^3J_{HH}$ = 6.7 Hz, CH-(CH_3)$_{2ar}$), 4.87 (sept, 1H, $^3J_{HH}$ = 6.8 Hz, CH-(CH_3)$_{2Py}$), 7.14 (d, 2H, $^3J_{HH}$ = 7.9 Hz, Py/Ar-H), 7.24 (t, 1H, $^3J_{HH}$ = 7.7 Hz, Py/Ar-H), 7.64 (td, 2H, $^3J_{HH}$ = 8.1 Hz, $^4J_{HH}$ = 1.6 Hz, Py/Ar-H), 7.99 (t, 1H, $^3J_{HH}$ = 8.0 Hz, Py/Ar-H). $^{13}C\{^1H\}$ NMR (100 MHz, CD_2Cl_2): δ 19.1 (CH_3C=N), 22.7 (CHMe_{2Py}), 27.8 (CHMe_{2ar}), 28.0 (CHMe_{2ar}), 28.7 (CHMe$_{2ar}$), 37.4 (CHMe$_{2Py}$), 121.9 (CH), 122.6 (CH), 123.2 (C), 126.5 (CH), 127.5 (CH), 134.9 (C), 138.6 (CH), 138.9 (C), 154.5 (C), 175.3 (C=N$_{imine}$). IR (solid state): 1580 ν(C=N)$_{pyridine}$, 1667 ν(C=N)$_{imime}$. ESIMS (+ve, MeOH) *m/z:* 428 $[M\text{-}2Br]^+$. HRMS (FAB): calculated for $C_{22}H_{29}N_2Pd$ $[M\text{-}HBr_2]^+$ 427.1407, found 427.1398.

6.4.6 Synthesis of (**L4**$_{tBu}$)PdOAc

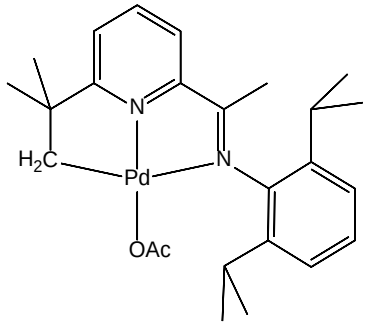

A small dry Schlenk flask equipped with stir bar was evacuated and backfilled with nitrogen. The flask was then loaded with H**L4**$_{tBu}$ (0.035 g, 0.104 mmol, 1 eq.) and $Pd(OAc)_2$ (0.024 g, 0.105 mmol, 1.01 eq.) and the contents dissolved in dry MeOH (10 mL). The resultant solution was stirred at 60 ^oC for 48 h. The reaction mixture was then filtered in the air through a thin layer of Celite and the Celite cake washed thoroughly with dichloromethane and the solvent removed under reduced pressure) to give (**L4**$_{tBu}$)PdOAc as a yellow powder (0.034 g, 66%). ^1H NMR (400 MHz, $CDCl_3$): δ 1.05 (d, 6H, $^3J_{HH}$ = 6.8 Hz, CH(CH_3)$_2$), 1.30 (d, 6H, $^3J_{HH}$ = 6.8 Hz, CH(CH_3)$_2$), 1.35 (s, 3H, Pd-OC(O)CH_3), 1.36 (s, 6H, Py-$(CH_3)_2$-CH_2), 2.08 (s, 3H, Pyr-C(N)-CH_3), 2.72 (s, 2H, (CH_3)$_2$-CH_2-Pd), 3.01 (sep, 2H, $^3J_{HH}$ = 6.8 Hz, CH-(CH_3)$_2$), 7.13 (s, 3H, Py/Ar-H), 7.27 (d, 1H, $^3J_{HH}$ = 8.0 Hz, Py/Ar-H), 7.53 (d, 1H, $^3J_{HH}$ = 7.8 Hz, Py/Ar-H), 7.88 (t, 1H, $^3J_{HH}$ = 8.1 Hz, Py/Ar-H). $^{13}C\{^1H\}$ NMR (125 MHz, $CDCl_3$): δ 16.3 (CH_3C=N), 22.2 (CHMe_2), 22.5 (CHMe_2), 22.9 (Py-C(CH_3)$_2$-CH_2), 27.5 (Py-C(CH_3)$_2$-CH_2), 29.2 (CHMe$_2$), 29.7 (OCOCH_3), 33.9 (Py-C(CH_3)$_2$-CH_2), 52.1 (Py-C(CH_3)$_2$-CH_2), 121.5 (CH), 121.9 (C), 122.3 (CH), 123.6 (CH), 125.4 (CH), 136.2 (CH), 137.4 (C), 140.8 (C), 151.5 (C), 168.3 (C=N$_{imine}$), 177.0 (OCOCH$_3$). IR (solid state): 1601 ν(C=N)$_{pyridine}$, 1654 ν(C=N)$_{imine}$.

ESIMS (+ve, MeCN): *m/z* 441 $[M\text{-}OAc]^+$. HRMS (FAB): calculated for $C_{23}H_{31}N_2Pd$ $[M\text{-}OAc]^+$ 441.1531, found 441.1528.

6.4.7 Synthesis of (**L4**$_{tBu}$)PdCl

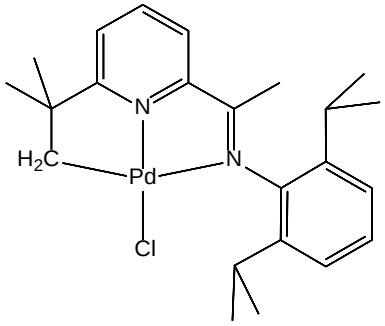

To a round bottomed flask was added H**L4**$_{tBu}$ (0.040 g, 0.119 mmol, 1 eq.) and Na_2PdCl_4 (0.035 g, 0.120 mmol, 1.01 eq.). The contents were dissolved in acetic acid (8 ml) and stirred and heated at reflux for 60 h. On cooling to room temperature, (**L4**$_{tBu}$)PdCl was obtained as a yellow solid on filtration (0.054 g , 95%). ^{1}H NMR (500 MHz, $CDCl_3$): δ 1.13 (d, 6H, $^3J_{HH}$ = 6.8 Hz, CH(*CH*$_3$)$_2$), 1.39 (d, 6H, $^3J_{HH}$ = 6.8 Hz, CH(*CH*$_3$)$_2$), 1.45 (s, 6H, Py-*(CH*$_3$*)*$_2$-CH_2), 2.18 (s, 3H, Pyr-C(N)-C*H*$_3$), 2.73 (s, 2H, $(CH_3)_2$-*CH*$_2$-Pd), 2.99 (sep, 2H, $^3J_{HH}$ = 6.8 Hz, C*H*-$(CH_3)_2$), 7.20 (s, 3H, Py/Ar-H), 7.40 (dd, 1H, $^3J_{HH}$ = 8.2 Hz, $^4J_{HH}$ = 0.9 Hz, Py/Ar-H), 7.66 (dd, 1H, $^3J_{HH}$ = 7.8 Hz, $^4J_{HH}$ = 0.9 Hz, Py/Ar-H), 7.99 (t, 1H, $^3J_{HH}$ = 8.0 Hz, Py/Ar-H). ^{13}C{^{1}H} NMR (125 MHz, $CDCl_3$): δ 17.1 (*C*H_3C=N), 23.4 (CH*Me*$_2$), 24.0 (CH*Me*$_2$), 28.6 (Py-C(*C*H_3)$_2$-CH_2), 29.7 (Py-C(*C*H_3)$_2$-CH_2), 30.9 (*C*HMe_2), 35.6 (Py-C$(CH_3)_2$-*C*H_2), 53.8 (Py-*C*$(CH_3)_2$-CH_2), 122.6 (CH), 123.4 (C), 124.7 (CH), 126.2 (CH), 126.6 (CH), 137.2 (CH), 138.0 (C), 141.7 (C), 152.5 (C), 177.3 ($C=N_{imine}$). IR (solid state): 1598 $\nu(C=N)_{pyridine}$, 1676 $\nu(C=N)_{imine}$. ESIMS (+ve, MeCN): *m/z* 441 $[M\text{-}Cl]^+$. HRMS (FAB): calculated for $C_{23}H_{31}N_2Pd$ $[M\text{-}Cl]^+$ 441.1522, found 441.1508. Anal. calc. for ($C_{23}H_{31}N_2ClPd{\cdot}2C_6H_{14}$): C 64.70, H 9.15, N 4.31. Found C 65.22, H 9.14, N 4.85%.

6.4.8 Synthesis of (**L4**$_{i\text{Pr}}$)PdOAc

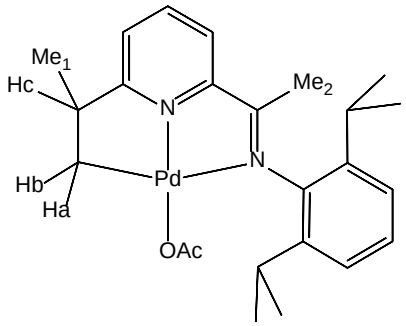

A small dry Schlenk flask equipped with stir bar was evacuated and backfilled with nitrogen. The flask was then loaded with H**L4**$_{i\text{Pr}}$ (0.060 g, 0.186 mmol, 1 eq.) and $Pd(OAc)_2$ (0.042 g, 0.188 mmol, 1.01 eq.) and the contents dissolved in dry chloroform (10 mL). The resultant solution was stirred at 60 ^{o}C for 48 h. The reaction mixture was then filtered in the air through a thin layer of Celite and the Celite cake washed thoroughly with dichloromethane and the solvent removed under reduced pressure to give a brown solid as the crude product. The ^{1}H NMR spectrum of the crude product showed (**L4**$_{i\text{Pr}}$)PdOAc along with at least two minor species. Attempts to purify the product by crystallisation were unsuccessful. ^{1}H NMR (400 MHz, $CDCl_3$): δ 1.06 (m, 6+2H, $CH(CH_3)_2$ + impurities), 1.19 (s, 3H, Pd-OC(O)CH_3), 1.32 (m, 6+1H, $CH(CH_3)_2$ + impurities), 1.36 (d, 3H, Me_1), 2.11 (s, 3H, Me_2), 2.46 (m, 1H, H_b), 2.92 (m, 4H, H_c+ $CH(CH_3)_2$), 3.45 (m, 1H, H_a), 7.20 (s, 3H, Ar-H), 7.39 (d, 1H, $^{3}J_{HH}$ = 7.8 Hz, Py-H), 7.59 (d, 1H, $^{3}J_{HH}$ = 7.8 Hz, Py-H), 7.91 (t, $^{3}J_{HH}$ = 8.0 Hz, Py-H).

6.4.9 Isolation of 'minor-1'-Cl through acetate-chloride exchange with (**L4**$_{i\text{Pr}}$)PdOAc

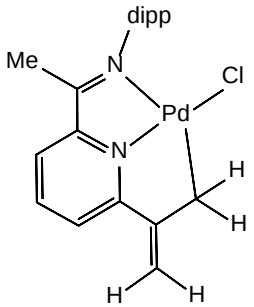

Crude (**L4**$_{i\text{Pr}}$)PdOAc (0.030 g) obtained in 6.4.8 was dissolved in dichloromethane (10 ml) and stirred at room temperature with saturated aqueous sodium chloride solution (10 ml) overnight. The resultant mixture was extracted with dichloromethane (3 × 10 ml). The combined organic layers were washed with water (1 × 10 ml), dried over $MgSO_4$ and filtered. The solvent was removed under reduced pressure to give a brown solid. Orange crystals suitable for a single crystal X-ray diffraction study were grown by layering the

dichloromethane solution of the crude mixture with petroleum ether. ESIMS (+ve) *m/z*: 425 $[M\text{-}Cl]^+$; ESIMS (-ve) *m/z*: 459 $[M]^-$. Anal. calc. for $(C_{22}H_{27}ClN_2Pd{\cdot}CH_2Cl_2)$: C 50.57, H 5.35, N 5.13 Found C 50.77, H 5.41, N 5.04%.

6.4.10 Isolation of 'minor-2'-Br through acetate-bromide exchange with (**L4**$_{i\text{Pr}}$)PdOAc

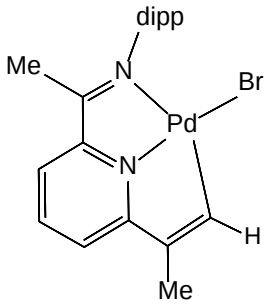

Crude (**L4**$_{i\text{Pr}}$)PdOAc (0.030 g) obtained in 6.4.8 was dissolved in dichloromethane (10 ml) and stirred at room temperature with saturated aqueous sodium bromide solution (10 ml) overnight. The resultant mixture was extracted with dichloromethane (3 × 10 ml). The combined organic layers were washed with water (1 × 10 ml), dried over $MgSO_4$ and filtered. The solvent was removed under reduced pressure to give a brown solid. Red crystals suitable for a single crystal X-ray diffraction study were grown by layering a dichloromethane solution of the crude mixture with petroleum ether. ESIMS (+ve) *m/z*: 425 $[M\text{-}Br]^+$. Anal. calc. for $(C_{22}H_{27}BrN_2Pd{\cdot}0.5H_2Cl_2)$: C 49.29, H 5.15, N 5.11. Found C 49.43, H 5.21, N 5.05%.

6.5 Experimental procedures for Chapter 5

6.5.1 Reactions with silver salts:

6.5.1.1 Synthesis of $[(\mathbf{L1}_{o\text{-tolyl}})Pd(NCMe)]^+[BF_4]^-$

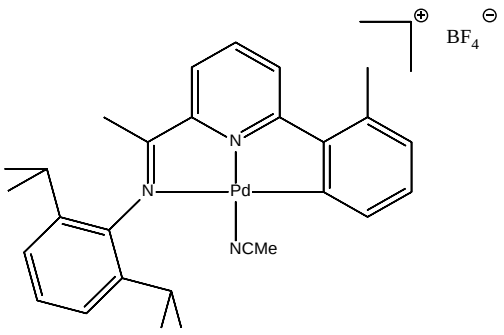

A Schlenk flask equipped with a stirrer bar was evacuated and backfilled with nitrogen. To the flask was added (**L1**$_{o\text{-}tolyl}$)PdCl (0.030 g, 0.059 mmol), $AgBF_4$ (0.017 g, 0.089 mmol, 1.5 eq,) and dry acetonitrile (10 ml). The mixture was stirred at room temperature for 16 h and then filtered by cannula into another flask to give a clear solution. The solvent was removed under reduced pressure to give [(**L1**$_{o\text{-}tolyl}$)Pd(NCMe)]$^+$[BF_4]$^-$ as a yellow solid (0.030 g, 85%). Crystals suitable for a single crystal X-ray diffraction study were grown from a acetonitrile/diethyl ether solution. ^{1}H NMR (CD_3CN, 400 MHz): δ 1.22 (d, 6H, $^3J_{HH}$ = 6.9 Hz, CH(*CH*$_3$)$_2$), 1.33 (d, 6H, $^3J_{HH}$ = 6.9 Hz, CH(*CH*$_3$)$_2$), 1.99 (s, 3H, Pd-NC*Me*), 2.30 (s, 3H, Py-C(N)-C*H*$_3$), 2.66 (s, 3H, *o*-Ar-C*H*$_3$), 3.11 (sept, 2H, $^3J_{HH}$ = 6.9 Hz, C*H*-(CH_3)$_2$), 7.04 (bs, 3H, Py/Ar-*H*), 7.37 (s, 3H, Py/Ar-*H*), 7.81 (dd, 1H, $^3J_{HH}$ = 7.8 Hz, $^4J_{HH}$ = 1.0 Hz, Py/Ar-H), 8.14 (d, 1H, $^3J_{HH}$ = 8.5 Hz, Py/Ar-H), 8.2 (t, 1H, $^3J_{HH}$ = 8.1 Hz, Py/Ar-H). ^{13}C{^{1}H} NMR (125 MHz, CD_3CN): δ 1.9 (*C*H_3CN-Pd), 18.6 (*C*H_3C=N), 23.1 (CH*Me*$_2$), 23.9 (CH*Me*$_2$), 24.2 (*Me*$_{o\text{-}tol}$), 29.4 (*C*HMe$_2$), 118.5 (CH_3*C*N-Pd under solvent peak), 125.0 (CH), 127.2 (CH), 128.7 (CH), 131.3 (CH), 131.5 (CH), 131.7 (CH), 134.1 (CH), 139.4 (C), 139.5 (C), 141.4 (C), 142.8 (CH), 147.2 (C), 155.0 (C), 156.0 (C), 166.8 (C), 178.4 (C=N$_{imine}$). IR (solid state): 1576 ν(C=N)$_{pyridine}$, 1628 ν(C=N)$_{imine}$ cm^{-1}. ^{19}F{^{1}H} NMR (375 MHz, CD_3CN): δ -152 (-BF_4). ESIMS (+ve) *m/z*: 475 [(M-NCMe)-BF_4]$^+$; ESIMS (-ve) *m/z*: 87 [BF_4]$^-$. HRMS (FAB): calculated for $C_{28}H_{32}N_3{}^{106}Pd$ [M-BF_4]$^+$ 516.1631, found 516.1653. m.p. > 270 ºC.

6.5.1.2 Synthesis of [*peri*-(**L1**$_{ket\text{-}nap}$)Pd(NCMe)]$^+$[BF_4]$^-$

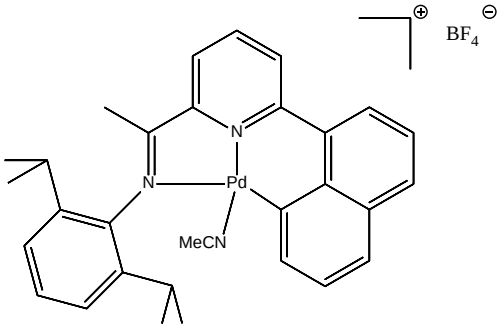

The same procedure as that described in 6.5.1.1, using *peri*-(**L1**$_{ket\text{-}nap}$)PdCl (0.030 g, 0.055 mmol), $AgBF_4$ (0.016 g, 0.082 mmol, 1.5 eq.) and dry acetonitrile (10 ml), afforded [*peri*-(**L1**$_{ket\text{-}nap}$)Pd(NCMe)]$^+$[BF_4]$^-$ as a yellow solid (0.031 g, 87%). Crystals suitable for a single crystal X-ray diffraction study were grown from an acetonitrile/diethyl ether solution. ^{1}H NMR (CD_3CN, 400 MHz): δ 1.22 (d, 6H, $^3J_{HH}$ = 6.8 Hz, CH(*CH*$_3$)$_2$), 1.37 (d, 6H, $^3J_{HH}$ = 6.8 Hz, CH(*CH*$_3$)$_2$), 1.99 (s, 3H, Pd-NC*Me*), 2.50 (s, 3H, Pyr-C(N)-C*H*$_3$), 3.16

(sept, 2H, $^{3}J_{HH}$ = 6.8 Hz, C*H*-(CH_3)$_2$), 7.39 (t, 1H, $^{3}J_{HH}$ = 7.6 Hz, Py/Ar-H), 7.45 (bs, 3H, Py/Ar-H), 7.77 (t, 1H, $^{3}J_{HH}$ = 7.8 Hz, Py/Ar-H), 7.90 (t, 2H, $^{3}J_{HH}$ = 7.8 Hz, Py/Ar-H), 8.21 (dd, 1H, $^{3}J_{HH}$ = 8.1 Hz, $^{4}J_{HH}$ = 1.0 Hz, Py/Ar-H), 8.30 (d, 1H, $^{3}J_{HH}$ = 7.6 Hz, $^{4}J_{HH}$ = 1.2 Hz, Py/Ar-H), 8.45 (t, 1H, $^{3}J_{HH}$ = 8.1 Hz, Py/Ar-H), 8.60 (d, 1H, $^{3}J_{HH}$ = 7.6 Hz, Py/Ar-H), 8.79 (d, 1H, $^{3}J_{HH}$ = 8.8 Hz, Py/Ar-H). $^{13}C\{^{1}H\}$ NMR (125 MHz, CD_3CN): δ 0.6 (*C*H_3CN-Pd), 18.1 (*C*H_3C=N), 22.6 (CH*Me*$_2$), 22.7 (CH*Me*$_2$), 28.0 (*C*HMe$_2$), 117.0 (CH_3*C*N-Pd under solvent peak), 123.3 (C), 124.0 (CH), 124.6 (CH), 125.0 (CH), 127.1 (CH), 127.4 (C), 127.7 (CH), 127.8 (CH), 129.0 (CH), 131.3 (CH), 133.3 (C), 134.7 (CH), 135.9 (C), 137.5 (C), 138.1 (CH), 139.0 (C), 139.7 (CH), 140.3 (C), 156.6 (C), 175.2 (C=Nimine). IR (solid state): 1588 $\nu(C{=}N)_{pyridine}$, 1612 $\nu(C{=}N)_{imine}$ cm^{-1}. $^{19}F\{^{1}H\}$ NMR (375 MHz, CD_3CN): δ -152 (-BF_4). ESIMS (+ve) m/z: 511 $[(M\text{-}NCMe)\text{-}BF_4]^+$; ESIMS (-ve) m/z: 87 $[BF_4]^-$. HRMS (FAB): calculated for $C_{31}H_{32}N_3{}^{106}Pd$ $[M\text{-}BF_4]^+$ 552.1630, found 552.1652. m.p. > 270 ºC.

6.5.1.3 Synthesis of [*ortho*-(**L3**$_{nap}$)Pd(NCMe)]$^+$[BF_4]$^-$

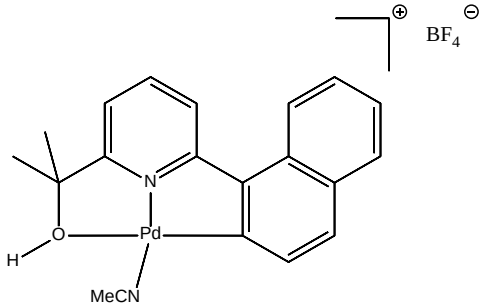

The same procedure as that described in 6.5.1.1, using *ortho*-(**L3**$_{nap}$)PdCl (0.030 g, 0.074 mmol), $AgBF_4$ (0.023 g, 0.111 mmol, 1.5 eq.) and dry acetonitrile (10 ml), afforded [*ortho*-(**L3**$_{nap}$)Pd(NCMe)]$^+$[BF_4]$^-$ as a yellow solid (0.030 g, 83%). Crystals suitable for a single crystal X-ray diffraction study were grown from an acetonitrile/diethyl ether solution. ^{1}H NMR (400 MHz, CD_3CN, $SiMe_4$): δ 1.96 (s, 6H, CH(CH_3)$_2$), 1.99 (s, 3H, Pd-NC*Me*), 7.30 (t, 1H, $^{3}J_{HH}$ = 7.6 Hz, Py/Ar-H), 7.52 (dd, 1H, $^{3}J_{HH}$ = 7.8 Hz, $^{4}J_{HH}$ = 1.3 Hz, Py/Ar-H), 7.61 (d, 1H, $^{3}J_{HH}$ = 7.8 Hz, Py/Ar-H), 7.64 (t, 1H, $^{3}J_{HH}$ = 5.6 Hz, Py/Ar-H), 7.77 (d, 1H, $^{3}J_{HH}$ = 7.8 Hz, Py/Ar-H), 8.03 (d, 1H, $^{3}J_{HH}$ = 8.0 Hz, Py/Ar-H), 8.10 (t, 1H, $^{3}J_{HH}$ = 8.0 Hz, Py/Ar-H), 8.19 (d, 1H, $^{3}J_{HH}$ = 8.3 Hz, Py/Ar-H), 8.27 (d, 1H, $^{3}J_{HH}$ = 7.5 Hz, Py/Ar-H). $^{13}C\{^{1}H\}$ NMR (125 MHz, CD_3CN): δ 1.9 (*C*H_3CN-Pd), 31.0 (Py-C-(*C*H_3)$_2$), 82.2 (Pyr-*C*-(CH_3)$_2$), 118.5 (CH_3*C*N-Pd under solvent peak), 121.6 (CH), 125.8 (CH), 126.1 (CH), 126.2 (CH), 127.7 (C), 128.0 (CH), 130.7 (CH), 133.6 (C), 134.3 (CH), 134.7 (C), 135.7 (C), 136.6 (CH), 141.3 (CH), 153.6 (C), 167.6 (C). IR (solid state): 1546

$\nu(C{=}N)_{pyridine}$ cm^{-1}. $^{19}F\{^{1}H\}$ NMR (375 MHz, CD_3CN): δ -152 (-BF_4). ESIMS (+ve) *m/z*: 368 $[(M\text{-}NCMe)\text{-}BF_4]^+$; ESIMS (-ve) *m/z*: 87 $[BF_4]^-$. HRMS (FAB): calculated for $C_{20}H_{19}N_2O^{106}Pd$ $[M\text{-}BF_4]^+$ 409.0532, found 409.0549. m.p. > 270 °C.

6.5.1.4 Synthesis of $[(\mathbf{L2}_{o\text{-tolyl}})Pd(NCMe)]^+[BF_4]^-$

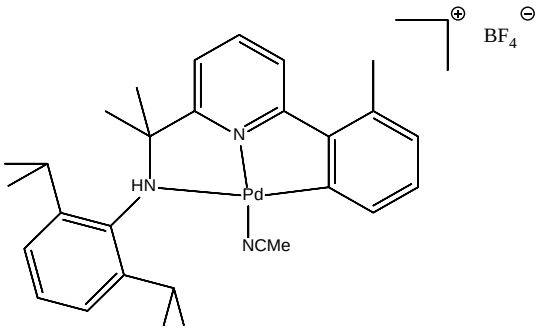

The same procedure as that described in 6.5.1.1, using $(\mathbf{L2}_{o\text{-tolyl}})PdCl$ (0.030 g, 0.057 mmol), $AgBF_4$ (0.017 g, 0.086 mmol, 1.5 eq.) and dry acetonitrile (10 ml), afforded $[(\mathbf{L2}_{o\text{-tolyl}})Pd(NCMe)]^+[BF_4]^-$ as a yellow solid (0.030 g, 85%). Crystals suitable for a single crystal X-ray diffraction study were grown from an acetonitrile/diethyl ether solution ^{1}H NMR (400 MHz, CD_3CN): δ 1.03 (d, 3H, $^{3}J_{HH}$ = 6.8 Hz, $CH(CH_3)_2$), 1.31 (d, 3H, $^{3}J_{HH}$ = 6.8 Hz, $CH(CH_3)_2$), 1.34 (d, 3H, $^{3}J_{HH}$ = 6.8 Hz, $CH(CH_3)_2$), 1.40 (d, 3H, $CH(CH_3)_2$ and s, 3H, Py-C(NH)-$(CH_3)_2$), 1.95 (s, 3H, o-Ar-CH_3), 1.99 (s, 3H, Pd-NC*Me*), 2.67 (s, 3H, Py-C(NH)-$(CH_3)_2$), 3.24 (sept, 1H, $^{3}J_{HH}$ = 6.8 Hz, C*H*-$(CH_3)_2$), 3.32 (sept, 1H, $^{3}J_{HH}$ = 6.8 Hz, C*H*-$(CH_3)_2$), 5.63 (s, 1H, N*H*), 7.04-7.09 (m, 2H, Py/Ar-*H*), 7.15 (dd, 1H, $^{3}J_{HH}$ = 7.3 Hz, $^{4}J_{HH}$ = 1.5 Hz, Py/Ar-*H*), 7.28-7.31 (m, 3H, Py/Ar-*H*), 7.37 (dd, 1H, $^{3}J_{HH}$ = 8.1 Hz, $^{4}J_{HH}$ = 0.9 Hz, Py/Ar-*H*), 8.01 (d, 1H, $^{3}J_{HH}$ = 8.3 Hz, Py/Ar-*H*), 8.12 (t, 1H, $^{3}J_{HH}$ = 8.2 Hz, Py/Ar-*H*). $^{13}C\{^{1}H\}$ NMR (125 MHz, CD_3CN): δ 1.9 (CH_3CN-Pd), 23.3 (Ar-CH-$(CH_3)_2$), 23.4 (Py-C(NH)-$(CH_3)_2$), 24.1 (Py-C(NH)-$(CH_3)_2$), 24.6 (Ar-CH-$(CH_3)_2$), 25.4 (Ar-CH-$(CH_3)_2$), 27.3 (Ar-CH-$(CH_3)_2$), 29.3 (Ar-CH-$(CH_3)_2$), 30.1 (Ar-CH-$(CH_3)_2$), 35.8 (o-Ar-CH_3), 71.5 (Py-C(NH)-$(CH_3)_2$), 118.5 (CH_3CN-Pd under solvent peak), 120.2 (CH), 123.3 (CH), 125.5 (CH), 126.5 (CH), 128.2 (CH), 130.2 (CH), 131.2 (CH), 133.1 (CH), 137.4 (C), 138.2 (C), 142.3 (CH), 143.1 (C), 144.1 (C), 146.8 (C), 153.2 (C), 165.2 (C), 170.4 (C). IR: 1498 $\nu(C\text{-}N)_{pyridine}$, 1597 $\nu(N\text{-}H)_{amine\ bend}$, 3345 $\nu(N\text{-}H)_{amine\ stretch}$ cm^{-1}. $^{19}F\{^{1}H\}$ NMR (375 MHz, CD_3CN): δ -152 (-BF_4). ESIMS (+ve) *m/z*: 491 $[M\text{-}BF_4]^+$; ESIMS (-ve) *m/z*: 87 $[BF_4]^-$. HRMS (FAB): calculated for $C_{29}H_{36}N_3{}^{106}Pd$ $[M\text{-}BF_4]^+$

532.1944, found 532.1949. m.p. > 270 °C. Anal. calc. for ($C_{29}H_{36}N_3PdBF_4 \cdot 0.5CH_2Cl_2$): C 53.50, H 5.63, N 6.34. Found C 53.73, H 5.59, N 7.21%.

6.5.1.5 Synthesis of [(**L1**$_{o\text{-tolyl}}$)Pd($NC_5H_3Cl_2$-3,5)]$^+$[BF_4]$^-$

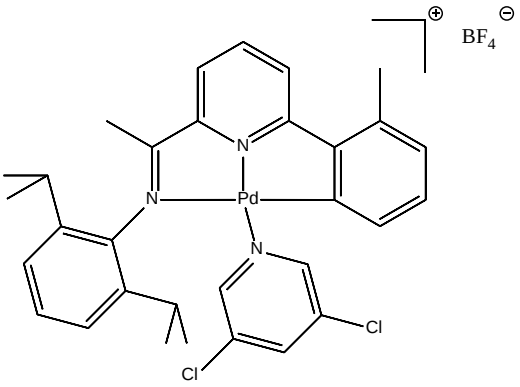

A Schlenk flask equipped with a stirrer bar was evacuated and backfilled with nitrogen. To the flask was added [(**L1**$_{o\text{-tolyl}}$)Pd(NCMe)]$^+$[BF_4]$^-$ (0.069 g, 0.098 mmol), 3,5-dichloropyridine (0.022 g, 0.147 mmol, 1.5 eq.) and dry dichloromethane (10 ml). The mixture was stirred at room temperature for 16 h before the mixture was filtered by cannula to give a clear solution. The solvent was removed under reduced pressure to give [(**L1**$_{o\text{-tolyl}}$)Pd($NC_5H_3Cl_2$-3,5)]$^+$[BF_4]$^-$ as a yellow solid (0.065 g, 93%). Crystals suitable for a single crystal X-ray diffraction study were grown from a dichloromethane/diethyl ether solution. ^{1}H NMR (400 MHz, $CDCl_3$, $SiMe_4$): δ 1.07 (d, 6H, $^3J_{HH}$ = 6.8 Hz, CH(*C*H_3)$_2$), 1.08 (d, 6H, $^3J_{HH}$ = 6.8 Hz, CH(*C*H_3)$_2$), 2.41 (s, 3H, Py-CN-C*H*$_3$), 2.61 (s, 3H, o-Ar-C*H*$_3$), 2.89 (sept, 2H, $^3J_{HH}$ = 6.8 Hz, C*H*-(CH_3)$_2$), 6.15 (dd, 1H, $^3J_{HH}$ = 7.4 Hz, $^4J_{HH}$ = 1.4 Hz, Py/Ar-*H*), 6.88 (t, 1H, $^3J_{HH}$ = 7.5 Hz, Py/Ar-*H*), 6.93 (d, 1H, $^3J_{HH}$ = 7.8 Hz, Py/Ar-*H*), 7.07 (s, 1H, Py/Ar-*H*), 7.09 (s, 1H, Py/Ar-*H*), 7.15-7.18 (m, 1H, Py/Ar-*H*), 7.83 (m, 1H, Py/Ar-*H*), 8.06 (d, 1H, $^3J_{HH}$ = 8.7 Hz, Py/Ar-*H*), 8.11-8.12 (m, 3H, Py/Ar-*H*), 8.32 (t, 1H, $^3J_{HH}$ = 8.1 Hz, Py/Ar-*H*). ^{13}C{^{1}H} NMR (100 MHz, $CDCl_3$): δ 18.1 (*C*H_3C=N), 22.2 (CH*Me*$_2$), 22.3 (CH*Me*$_2$), 23.0 (o-Ar-*C*H_3), 27.6 (*C*HMe$_2$), 123.3 (CH), 124.1 (CH), 125.3 (CH), 127.3 (CH), 129.5 (CH), 130.0 (CH), 130.1 (CH), 133.3 (C), 137.2 (C), 137.4 (C), 137.9 (CH), 138.4 (C), 142.1 (CH), 145.5 (C), 147.3 (CH), 152.8 (C), 153.9 (C), 164.6 (C), 177.0 (C=N$_{imine}$). IR (solid state): 1558 ν(C=N)$_{pyridine}$, 1645 ν(C=N)$_{imine}$ cm^{-1}. ^{19}F{^{1}H} NMR (375 MHz, $CDCl_3$): δ -151 (-BF_4). ESIMS (+ve) *m/z*: 475 [(M-Cl_2Py)-BF_4]$^+$; ESIMS (-ve) *m/z*: 87 [BF_4]$^-$. HRMS (FAB): calculated for $C_{26}H_{29}N_2{}^{106}Pd$ [(M-Cl_2Py)-BF_4]$^+$ 475.1365, found 475.1357. m.p. > 270 °C.

6.5.1.6 Synthesis of [*peri*-(**L1**$_{ket\text{-}nap}$)Pd($NC_5H_3Cl_2$-3,5)]$^+$[BF_4]$^-$

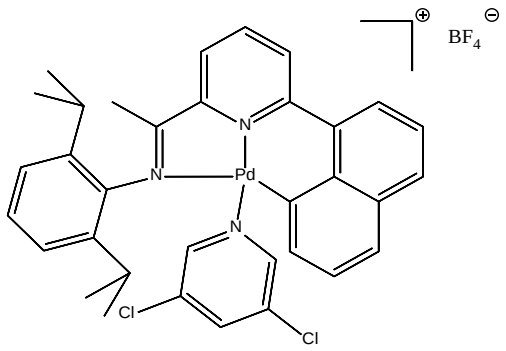

The same procedure as that described in 6.5.1.5, using [*peri*-(**L1**$_{ket\text{-}nap}$)Pd(NCMe)]$^+$[BF_4]$^-$ (0.068 g, 0.091 mmol), 3,5-dichloropyridine (0.020 g, 0.137 mmol, 1.5 eq.) and dry dichloromethane (10 ml), gave [*peri*-(**L1**$_{ket\text{-}nap}$)Pd($NC_5H_3Cl_2$-3,5)]$^+$[BF_4]$^-$ as a yellow solid (0.065 g, 96%). Crystals suitable for a single crystal X-ray diffraction study were grown from a dichloromethane/diethyl ether solution. ^{1}H NMR (400 MHz, $CDCl_3$): δ 1.03 (d, 6H, $^3J_{HH}$ = 6.8 Hz, CH(*C*H_3)$_2$), 1.15 (d, 6H, $^3J_{HH}$ = 6.8 Hz, CH(*C*H_3)$_2$), 2.56 (s, 3H, Py-CN-C*H*$_3$), 2.89 (sept, 2H, $^3J_{HH}$ = 6.8 Hz, C*H*-(CH_3)$_2$), 6.37 (d, 1H, $^3J_{HH}$ = 7.4 Hz, $^4J_{HH}$ = 1.0 Hz, Py/Ar-*H*), 7.02 (t, 1H, $^3J_{HH}$ = 7.5 Hz, Py/Ar-*H*), 7.07 (d, 2H, $^3J_{HH}$ = 7.8 Hz, Py/Ar-*H*), 7.16-7.21 (m, 1H, Py/Ar-*H*), 7.65-7.69 (m, 2H, Py/Ar-*H*), 7.74 (t, 1H, $^3J_{HH}$ = 4.0 Hz, Py/Ar-*H*), 7.99 (d, 1H, $^3J_{HH}$ = 8.0 Hz, Py/Ar-*H*), 8.02-8.03 (m, 2H, Py/Ar-*H*), 8.45 (d, 1H, $^3J_{HH}$ = 7.4 Hz, Py/Ar-*H*), 8.50-8.53 (m, 2H, Py/Ar-*H*), 8.62-8.64 (m, 1H, Py/Ar-*H*). ^{13}C{^{1}H} NMR (100 MHz, $CDCl_3$): δ 19.3 (*C*H_3C=N), 22.2 (CH*Me*$_2$), 23.4 (CH*Me*$_2$), 27.5 (*C*HMe$_2$), 123.4 (CH), 124.2 (CH), 124.5 (CH), 126.2 (C), 127.4 (CH), 127.5 (CH), 127.7 (CH), 128.6 (CH), 130.7 (CH), 132.4 (C), 132.7 (C), 133.0 (C), 133.9 (CH), 134.3 (CH), 137.7 (CH), 137.9 (C), 138.7 (C), 140.2 (CH), 146.2 (C), 147.7 (CH), 154.0 (C), 154.8 (C), 175.2 (C=N$_{imine}$). IR (solid state): 1556 ν(C=N)$_{pyridine}$, 1618 ν(C=N)$_{imine}$ cm^{-1}. ^{19}F{^{1}H} NMR (375 MHz, $CDCl_3$): δ -151 (-BF_4). ESIMS (+ve) *m/z*: 511 [(M-Cl_2Py)-BF_4]$^+$; ESIMS (-ve) *m/z*: 87 [BF_4]$^-$. HRMS (FAB): calculated for $C_{29}H_{29}N_2{}^{106}Pd$ [(M-Cl_2Py)-BF_4]$^+$ 511.1365, found 511.1357. m.p. > 270 ºC. Anal. calc. for ($C_{34}H_{32}N_3Cl_2PdBF_4{\cdot}2CH_2Cl_2$): C 47.17, H 3.95, N 4.58. Found C 47.95, H 4.36, N 5.09 %.

6.5.1.7 Synthesis of [(**L2**$_{o\text{-tolyl}}$)Pd($NC_5H_3Cl_2$-3,5)]$^+$[BF_4]$^-$

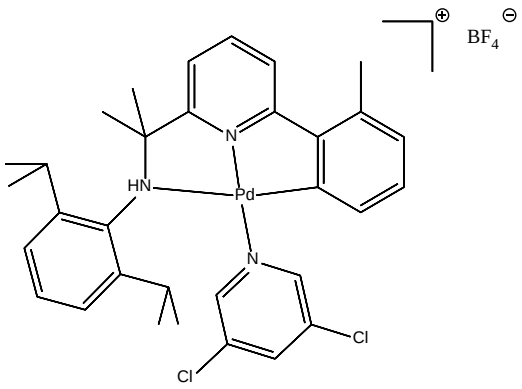

The same procedure as that described in 6.5.1.5, using [(**L2**$_{o\text{-tolyl}}$)Pd(NCMe)]$^+$[BF_4]$^-$ (0.066 g, 0.091 mmol), 3,5-dichloropyridine (0.020 g, 0.137 mmol, 1.5 eq.) and dry dichloromethane (10 ml), gave [(**L2**$_{o\text{-tolyl}}$)Pd($NC_5H_3Cl_2$-3,5)]$^+$[BF_4]$^-$ as a yellow solid (0.062 g, 95%). Crystals suitable for a single crystal X-ray diffraction study were grown from a dichloromethane/diethyl ether solution. ^{1}H NMR (400 MHz, $CDCl_3$): δ 0.60 (d, 3H, $^3J_{HH}$ = 6.6 Hz, CH(*CH*$_3$)$_2$), 1.01 (d, 3H, $^3J_{HH}$ = 6.8 Hz, CH(*CH*$_3$)$_2$), 1.12 (d, 3H, $^3J_{HH}$ = 6.6 Hz, CH(*CH*$_3$)$_2$), 1.43 (d, 3H, $^3J_{HH}$ = 6.8 Hz, CH(*CH*$_3$)$_2$), 1.47 (s, 3H, Py-C(NH)-(C*H*$_3$)$_2$), 1.99 (s, 3H, o-Ar-C*H*$_3$), 2.59 (s, 3H, Py-C(NH)-(C*H*$_3$)$_2$), 2.91 (sept, 1H, $^3J_{HH}$ = 6.6 Hz, C*H*-(CH_3)$_2$), 2.92 (sept, 1H, $^3J_{HH}$ = 6.8 Hz, C*H*-(CH_3)$_2$), 5.22 (s, 1H, N*H*), 5.76 (s, 1H, Py/Ar-*H*), 6.14 (dd, 1H, $^3J_{HH}$ = 7.3 Hz, $^4J_{HH}$ = 1.4 Hz, Py/Ar-*H*), 6.83-6.91 (m, 2H, Py/Ar-*H*), 7.02 (dd, 1H, $^3J_{HH}$ = 7.2 Hz, $^4J_{HH}$ = 2.3 Hz, Py/Ar-*H*), 7.15-7.22 (m, 2H, Py/Ar-*H*), 7.24 (d, 1H, $^3J_{HH}$ = 7.8 Hz, Py/Ar-*H*), 7.73-7.74 (m, 1H, Py/Ar-*H*), 7.88 (d, 1H, $^3J_{HH}$ = 8. Hz 4, Py/Ar-*H*), 8.07 (t, 2H, $^3J_{HH}$ = 8.2 Hz, Py/Ar-*H*). ^{13}C{^{1}H} NMR (125 MHz, $CDCl_3$): δ 22.3 (Ar-CH-(*C*H_3)$_2$), 22.5 (Py-C(NH)-(*C*H_3)$_2$), 22.7 (Py-C(NH)-(*C*H_3)$_2$), 23.5 (Ar-CH-(*C*H_3)$_2$), 23.7 (Ar-CH-(*C*H_3)$_2$), 26.2 (Ar-CH-(*C*H_3)$_2$), 26.9 (Ar-*C*H-(CH_3)$_2$), 28.1 (Ar-*C*H-(CH_3)$_2$), 34.7 (o-Ar-*C*H_3), 70.1 (Py-*C*(NH)-(CH_3)$_2$), 117.6 (CH), 121.1 (CH), 124.0 (CH), 125.1 (CH), 126.3 (CH), 128.6 (CH), 128.7 (CH), 130.0 (CH), 132.3 (C), 133.0 (C), 134.8 (C), 136.4 (C), 137.0 (CH), 137.4 (CH), 140.3 (CH), 140.9 (C), 141.5 (C), 145.4 (C), 147.8 (CH), 148.8 (C), 162.8 (C), 168.8 (C). IR: 1488 ν(C-N)$_{pyridine}$, 1594 ν(N-H)$_{amine\ bend}$, 3327 ν(N-H)$_{amine\ stretch}$ cm^{-1}. ^{19}F{^{1}H} NMR (375 MHz, $CDCl_3$): δ -151 (-BF_4). ESIMS (+ve) *m/z*: 491 [(M-Cl_2Py)-BF_4]$^+$; ESIMS (-ve) *m/z*: 87 [BF_4]$^-$. HRMS (FAB): calculated for $C_{27}H_{33}N_2{}^{106}Pd$ [(M-Cl_2Py)-BF_4]$^+$ 491.1713, found 491.1721. m.p. > 270 ^{o}C.

6.5.1.8 Synthesis of [*peri*-(**L1**$_{ket\text{-}nap}$)Pd(NC_5H_5)]$^+$[BF_4]$^-$

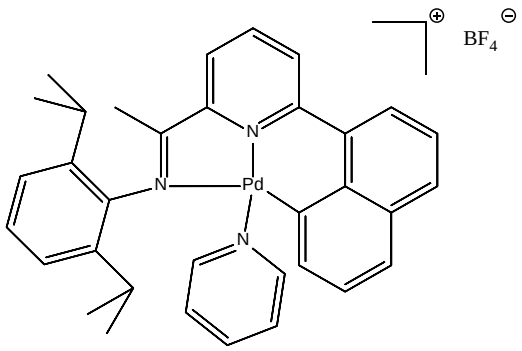

A Schlenk flask equipped with a stirrer bar was evacuated and backfilled with nitrogen. To the flask was added *peri*-[(**L1**$_{ket\text{-}nap}$)PdCl] (0.050 g, 0.091 mmol), $AgBF_4$ (0.027 g, 0.137 mmol, 1.5 eq.), pyridine (0.011 g, 0.137mmol, 1.5 eq.) and dry dichloromethane (10 ml), gave [*peri*-(**L1**$_{ket\text{-}nap}$)Pd(NC_5H_5)]$^+$[BF_4]$^-$ as a yellow solid (0.058 g, 0.085mmol, 93%). Crystals suitable for a single crystal X-ray diffraction study were grown from a dichloromethane/diethyl ether solution. ^{1}H NMR (400 MHz, $CDCl_3$, $SiMe_4$): δ 1.11 (d, 6H, $^3J_{HH}$ = 6.8 Hz, CH(*CH*$_3$)$_2$), 1.14 (d, 6H, $^3J_{HH}$ = 6.8 Hz, CH(*CH*$_3$)$_2$), 2.64 (s, 3H, *(CH*$_3$*)*C=N), 2.97 (sept, 2H, $^3J_{HH}$ = 6.8 Hz, C*H*(CH_3)$_2$), 6.37 (dd, 1H, $^3J_{HH}$ = 7.4 Hz, $^4J_{HH}$ = 1.0 Hz, Py/Ar-H), 7.04 (t, 1H, $^3J_{HH}$ = 7.7 Hz, Py/Ar-H), 7.08 (d, 1H, $^3J_{HH}$ = 7.9 Hz, Py/Ar-H), 7.16 (t, 2H, $^3J_{HH}$ = 7.1 Hz, Py/Ar-H), 7.22 (t, 1H, $^3J_{HH}$ = 7.9 Hz, Py/Ar-H), 7.43-7.46 (m, 1H, Py/Ar-H), 7.70-7.75 (m, 2H, Py/Ar-H), 7.77-7.86 (m, 2H, Py/Ar-H), 8.09 (d, 1H, $^3J_{HH}$ = 7.6 Hz, Py/Ar-H), 8.17 (d, 2H, $^3J_{HH}$ = 6.6 Hz, Py/Ar-H), 8.49 (d, 1H, $^3J_{HH}$ = 7.7 Hz, Py/Ar-H), 8.59-8.68 (m, 2H, Py/Ar-H). ^{13}C{^{1}H} NMR (100 MHz, $CDCl_3$): δ 20.2 (*C*H_3C=N), 22.4 (CH*Me*$_2$), 23.3 (CH*Me*$_2$), 24.3 (*C*HMe_2), 28.5 (Py-C(*C*H_3)$_3$), 35.1 (Py-*C*(CH_3)$_3$), 122.3 (CH), 123.2 (CH), 123.3 (C), 123.7 (CH), 126.0 (CH), 126.4 (CH), 127.1 (CH), 127.5 (CH), 128.0 (CH), 129.3 (CH), 131.7 (C), 132.4 (C), 132.9 (C), 134.3 (CH), 136.5 (CH), 137.1 (CH), 137.3 (C), 138.5 (CH), 139.2 (CH), 149.5 (C), 150.2 (C), 153.5 (C), 175.9 (C=N$_{imine}$). IR (solid state): 1561 ν(C=N)$_{pyridine}$, 1627 ν(C=N)$_{imine}$ cm^{-1}. ^{19}F{^{1}H} NMR (375 MHz, CD_3CN): δ -153 (-BF_4). ESIMS (+ve) *m/z*: 511 [(M-Cl_2Py)-BF_4]$^+$; ESIMS (-ve) *m/z*: 87 [BF_4]$^-$. HRMS (FAB): calculated for $C_{29}H_{29}N_2{}^{106}Pd$ [(M-Cl_2Py)-BF_4]$^+$ 511.1365, found 511.1369. m.p. > 270 ^{o}C. Anal. calc. for ($C_{34}H_{34}N_3PdBF_4{\cdot}2CH_2Cl_2$): C 51.01, H 4.52, N 4.96. Found C 50.64, H 4.47, N 5.93%.

6.5.1.9 Synthesis of [*peri*-(**L1**$_{ket\text{-}nap}$)Pd($NC_5H_4{}^tBu$-4)]$^+$[BF_4]$^-$

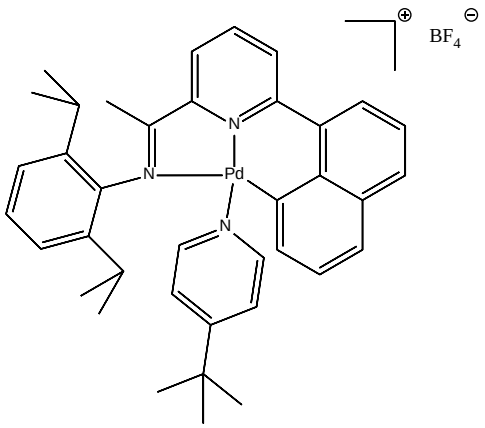

The same procedure as that described in 6.5.1.8, using *peri*-(**L1**$_{ket\text{-}nap}$)PdCl (0.050 g, 0.091mmol), $AgBF_4$ (0.027 g, 0.137mmol, 1.5 eq.), 4-*tert*-butylpyridine (0.018 g, 0.137 mmol, 1.5 eq.) and dry dichloromethane (10 ml), gave [*peri*-(**L1**$_{ket\text{-}nap}$)Pd($NC_5H_4{}^tBu$-4)]$^+$[BF_4]$^-$ as a yellow solid (0.064 g, 96%). Crystals suitable for a single crystal X-ray diffraction study were grown from a dichloromethane/diethyl ether solution. ^{1}H NMR (400 MHz, $CDCl_3$): δ 1.09 (d, 6H, $^3J_{HH}$ = 6.8 Hz, CH(*CH*$_3$)$_2$), 1.56 (d, 6H, $^3J_{HH}$ = 6.8 Hz, CH(*CH*$_3$)$_2$), 1.30 (s, 9H, Py-^{t}Bu), 2.61 (s, 3H, *(CH*$_3$*)*C=N), 2.94 (sept, 2H, $^3J_{HH}$ = 6.8 Hz, C*H*(CH_3)$_2$), 6.53 (d, 1H, $^3J_{HH}$ = 7.4 Hz, Py/Ar-H), 7.05-7.11 (m, 3H, Py/Ar-H), 7.21 (t, 1H, $^3J_{HH}$ = 7.8 Hz, Py/Ar-H), 7.47 (d, 2H, $^3J_{HH}$ = 6.0 Hz, Py/Ar-H), 7.70-7.75 (m, 2H, Py/Ar-H), 8.05 (d, 2H, $^3J_{HH}$ = 6.8 Hz, Py/Ar-H), 8.08 (d, 1H, $^3J_{HH}$ = 8.0 Hz, Py/Ar-H), 8.49 (d, 1H, $^3J_{HH}$ = 7.7 Hz, Py/Ar-H), 8.57-8.69 (m, 3H, Py/Ar-H). ^{13}C{^{1}H} NMR (100 MHz, $CDCl_3$): δ 20.3 (*C*H_3C=N), 23.2 (CH*Me*$_2$), 24.3 (CH*Me*$_2$), 28.4 (*C*HMe$_2$), 30.2 (Py-C(*C*H_3)$_3$), 35.2 (Py-*C*(CH_3)$_3$), 122.5 (CH), 124.0 (CH), 125.0 (CH), 125.2 (CH), 127.6 (C), 127.7 (CH), 128.0 (CH), 129.3 (CH), 131.3 (CH), 133.5 (C), 134.1 (C), 134.8 (CH), 136.4 (CH), 139.1 (C), 140.1 (C), 140.6 (C), 140.9 (CH), 151.1 (CH), 151.5 (CH), 155.3 (C), 155.7 (C), 163.9 (C), 175.7 (C=N$_{imine}$). IR (solid state): 1566 ν(C=N)$_{pyridine}$, 1631 ν(C=N)$_{imine}$ cm^{-1}. ^{19}F{^{1}H} NMR (375 MHz, CD_3CN): δ -153 (-BF_4). ESIMS (+ve) *m/z*: 511 [(M-Cl_2Py)-BF_4]$^+$; ESIMS (-ve) *m/z*: 87 [BF_4]$^-$. HRMS (FAB): calculated for $C_{29}H_{29}N_2{}^{106}Pd$ [(M-Cl_2Py)-BF_4]$^+$ 511.1364, found 511.1371. m.p. > 270 ^{o}C.

6.5.1.10 Synthesis of [*peri*-(**L1**$_{ket\text{-}nap}$)Pd(NC_5H_4Br-3)]$^+$[BF_4]$^-$

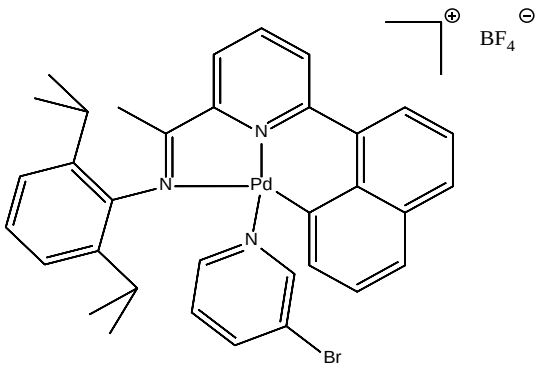

The same procedure as that described in 6.5.1.8, using *peri*-(**L1**$_{ket\text{-}nap}$)PdCl (0.050 g, 0.091 mmol), $AgBF_4$ (0.027 g, 0.137mmol, 1.5 eq.), 3-bromopyridine (0.022 g, 0.137 mmol, 1.5 eq.) and dry dichloromethane (10 ml), gave [*peri*-(**L1**$_{ket\text{-}nap}$)Pd(NC_5H_4Br-3)]$^+$[BF_4]$^-$ as a yellow solid (0.063 g, 91%). Crystals suitable for a single crystal X-Ray diffraction study were grown from a dichloromethane/diethyl ether solution. ^{1}H NMR (400 MHz, $CDCl_3$, $SiMe_4$): δ 1.09 (d, 6H, $^3J_{HH}$ = 6.7 Hz, CH(*CH*$_3$)$_2$), 1.20 (d, 6H, $^3J_{HH}$ = 6.7 Hz, CH(*CH*$_3$)$_2$), 2.60 (s, 3H, *(CH*$_3$*)*C=N), 2.97 (sept, 2H, $^3J_{HH}$ = 6.7 Hz, C*H*$(CH_3)_2$), 6.46 (dd, 1H, $^3J_{HH}$ = 7.2 Hz, $^4J_{HH}$ = 0.7 Hz, Py/Ar-H), 7.05-7.11 (m, 3H, Py/Ar-H), 7.18-7.24 (m, 2H, Py/Ar-H), 7.71-7.76 (m, 2H, Py/Ar-H), 7.90-7.95 (m, 1H, Py/Ar-H), 8.06 (d, 1H, $^3J_{HH}$ = 7.8 Hz, Py/Ar-H), 8.18 (s, 1H, Py/Ar-H), 8.21(d, 1H, $^3J_{HH}$ = 5.6 Hz, Py/Ar-H), 8.49-8.56 (m, 3H, Py/Ar-H), 8.69 (dd, 1H, $^3J_{HH}$ = 8.0 Hz, $^4J_{HH}$ = 1.2 Hz, Py/Ar-H). ^{13}C{^{1}H} NMR (100 MHz, $CDCl_3$): δ 20.2 (*C*H_3C=N), 23.3 (CH*Me*$_2$), 24.4 (CH*Me*$_2$), 28.5 (*C*HMe_2), 121.3 (C), 124.3 (CH), 125.2 (CH), 125.5 (CH), 126.8 (CH), 127.7 (C), 128.0 (CH), 128.6 (CH), 128.7 (CH), 129.4 (CH), 131.7 (CH), 133.4 (C), 134.1 (C), 135.0 (CH), 135.2 (C), 136.3 (CH), 139.0 (C), 139.9 (C), 141.0 (CH), 142.0 (CH), 150.8 (CH), 151.9 (CH), 155.1 (C), 155.9 (C), 176.0 (C=N$_{imine}$). IR (solid state): 1572 ν(C=N)$_{pyridine}$, 1647 ν(C=N)$_{imine}$ cm^{-1}. ^{19}F{^{1}H} NMR (375 MHz, CD_3CN): δ -151 (-BF_4). ESIMS (+ve) *m/z*: 511 [(M-Cl_2Py)-BF_4]$^+$; ESIMS (-ve) *m/z*: 87 [BF_4]$^-$. HRMS (FAB): calculated for $C_{29}H_{29}N_2{}^{106}Pd$ [(M-Cl_2Py)-BF_4]$^+$ 511.1359, found 511.1353. m.p. > 270 ^{o}C.

6.5.1.11 Synthesis of [*peri*-(**L1**$_{ket\text{-}nap}$)Pd($NC_5H_3Me_2$-2,5)]$^+$ [BF_4]$^-$

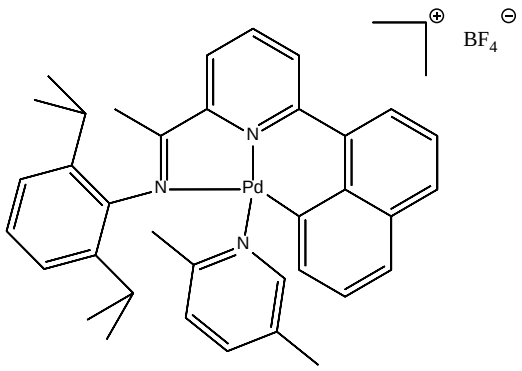

The same procedure as that described in 6.5.1.8, using (**L1**$_{ket\text{-}nap}$)PdCl (0.050 g, 0.091 mmol), $AgBF_4$ (0.027 g, 0.137 mmol, 1.5 eq.), 3,5-dimethylpyridine (0.015 g, 0.137 mmol, 1.5 eq.) and dry dichloromethane (10 ml), gave [*peri*-(**L1**$_{ket\text{-}nap}$)Pd($NC_5H_3Me_2$-2,5)]$^+$[BF_4]$^-$ as a yellow solid (0.058 g, 90%). Crystals suitable for a single crystal X-ray diffraction study were grown from a dichloromethane/diethyl ether solution. ^{1}H NMR (400 MHz, $CDCl_3$): δ 0.58 (d, 3H, $^3J_{HH}$ = 6.7 Hz, CH(*CH*$_3$)$_2$), 0.68 (d, 3H, $^3J_{HH}$ = 6.7 Hz, CH(*CH*$_3$)$_2$), 1.30 (d, 3H, $^3J_{HH}$ = 6.6 Hz, CH(*CH*$_3$)$_2$), 1.64 (d, 3H, $^3J_{HH}$ = 6.6 Hz, CH(*CH*$_3$)$_2$), 1.75 (s, 3H, Py-*CH*$_3$), 1.97 (s, 3H, Py-*CH*$_3$), 2.48 (sept, 1H, $^3J_{HH}$ = 6.7 Hz, C*H*(CH_3)$_2$), 2.52 (s, 3H, *(CH*$_3$*)*C=N), 3.11 (sept, 1H, $^3J_{HH}$ = 6.6 Hz, C*H*(CH_3)$_2$), 6.56 (d, 1H, $^3J_{HH}$ = 6.7 Hz, Py/Ar-H), 6.62 (dd, 1H, $^3J_{HH}$ = 7.8 Hz, $^4J_{HH}$ = 1.1 Hz, Py/Ar-H), 6.86 (d, 1H, $^3J_{HH}$ = 7.8 Hz, Py/Ar-H), 7.01 (t, 1H, $^3J_{HH}$ = 7.5 Hz, Py/Ar-H), 7.07 (t, 1H, $^3J_{HH}$ = 7.8 Hz, Py/Ar-H), 7.27 (d, 2H, $^3J_{HH}$ = 7.9 Hz, Py/Ar-H), 7.73-7.79 (m, 2H, Py/Ar-H), 8.00 (d, 2H, $^3J_{HH}$ = 8.5 Hz, Py/Ar-H), 8.34-8.42 (m, 2H, Py/Ar-H), 8.47 (d, 1H, $^3J_{HH}$ = 7.4 Hz, Py/Ar-H), 8.57 (d, 1H, $^3J_{HH}$ = 7.8 Hz, Py/Ar-H). ^{13}C{^{1}H} NMR (100 MHz, $CDCl_3$): δ 16.8 (Py-*C*H_3), 19.5 (Py-*C*H_3), 20.4 (*C*H_3C=N), 23.8 (CH*Me*$_2$), 23.9 (CH*Me*$_2$), 24.3 (CH*Me*$_2$), 25.9 (CH*Me*$_2$), 26.8 (*C*HMe$_2$), 27.7 (*C*HMe$_2$), 121.2 (C), 122.2 (CH), 123.5 (C), 123.7 (CH), 124.2 (CH), 124.6 (CH), 126.0 (CH), 126.9 (CH), 127.1 (CH), 127.8 (C), 128.1 (CH), 129.7 (CH), 130.1 (CH), 132.0 (CH), 132.1 (C), 133.2 (C), 133.4 (C), 134.4 (CH), 134.5 (C), 138.4 (C), 138.8 (CH), 140.5 (CH), 150.6 (CH), 152.9 (C), 154.4 (C), 155.0 (C), 175.9 (C=N$_{imine}$). IR (solid state): 1565 ν(C=N)$_{pyridine}$, 1647 ν(C=N)$_{imine}$ cm^{-1}. ^{19}F{^{1}H} NMR (375 MHz, CD_3CN): δ -151 (-BF_4). ESIMS (+ve) *m/z*: 511 [(M-Cl_2Py)-BF_4]$^+$; ESIMS (-ve) *m/z*: 87 [BF_4]$^-$. HRMS (FAB): calculated for $C_{29}H_{29}N_2{}^{106}Pd$ [(M-Cl_2Py)-BF_4]$^+$ 511.1365, found 511.1390. m.p. > 270 ^{o}C. Anal. calc. for ($C_{36}H_{38}N_3PdBF_4{\cdot}2CH_2Cl_2$): C 52.11, H 4.83, N 4.80. Found C 51.63, H 5.40, N 5.42 %.

6.5.2 Allylic arylations

All the allylic acetates (**Figure 6.1**): (*E*)-3-(4-methylphenyl)-2-propen-1-ol acetate, (*E*)-3-(4-Methoxyphenyl)-2-propen-1-ol acetate, (*E*)-3-(4-nitrophenyl)-2-propen-1-ol acetate, (*E*)-3-(2-methylphenyl)-2-propen-1-ol acetate, (*E*)-3-((2-methoxycarbonyl)-phenyl)-2-propen-1-ol acetate and (*E*)-3-(2-nitrophenyl)-2-propen-1-ol acetate were prepared by the literature methods,[16] except for cinnamyl acetate which was purchased from Santa-Cruz Ltd.

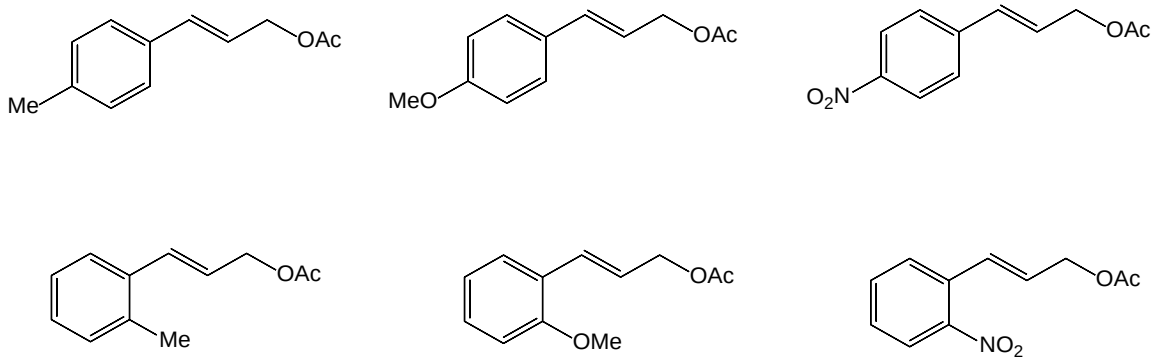

Figure 6.1 | Allylic acetates prepared by the literature methods

The following typical procedure was used for the allylic arylation of allylic acetates with sodium tetraphenylborate:

A stock solution of complex (**L1**$_{o\text{-tolyl}}$)Pd(OAc) with a concentration of 5.3×10^{-6} mg/ml was prepared in methanol. The stock solution (0.1 mL, 1.00×10^{-9} mmol), methanol (4.9 mL), and $NaBPh_4$ (0.684 g, 2.0 mmol) were added to a reaction vessel open to the air. Cinnamyl acetate (0.176 g, 1.0 mmol) was added to the solution. The reaction mixture was stirred at 50 °C for 1 h and allowed to cool to 25 °C. After removal of the solvent, water (5 mL) was added to the residue. The resulting suspension was extracted with diethyl ether (5 mL × 4). The combined organic layer was dried over $MgSO_4$. The resulting solution was concentrated under reduced pressure. The crude product was purified by column chromatography on silica gel (dichloromethane: petroleum ether = 1:15) to give 1,1'-[(1*E*)-prop-1-ene-1,3-diyl]dibenzene (0.192 g, 0.99 mmol, 99%) as colourless oil.

1,1'-[(1*E*)-Prop-1-ene-1,3-diyl]dibenzene[17] [CAS: 3412-44-0] (0.192 g, 0.99 mmol, 99%) ^{1}H NMR (400 MHz, $CDCl_3$) δ 3.54 (d, 2H, $^{3}J_{HH}$ = 6.8 Hz, -CH=CHCH$_2$-), 6.35 (dt, 1H, $^{3}J_{HH}$ = 15.5 and 6.8 Hz, -CH=CHCH$_2$-), 6.45 (d, 1H, $^{3}J_{HH}$ = 15.5 Hz, -CH=CHCH$_2$-), 7.17-7.36 (m, 10H, ArH). ^{13}C{^{1}H} NMR (100 MHz, $CDCl_3$) δ 39.3, 126.1, 126.4, 127.1, 128.4, 128.6, 129.2, 131.0, 137.3, 140.1. ESIMS (+ve) *m/z*: 194 $[M]^+$.

(*E*)-1-(4-Methoxyphenyl)-3-phenylpropene[17] [CAS: 35856-81-6] (0.177 g, 0.79 mmol, 79%) ^{1}H NMR (400 MHz, $CDCl_3$) δ 3.53 (d, 2H, $^{3}J_{HH}$ = 6.8 Hz, -CH=CHCH$_2$-), 3.80 (s, 3H, -OCH$_3$), 6.22 (dt, 1H, $^{3}J_{HH}$ = 15.7 and 6.8 Hz, -CH=CHCH$_2$-),6.40 (d, 1H, $^{3}J_{HH}$ = 15.7 Hz, -CH=CHCH$_2$-), 6.83 (d, 2H, $^{3}J_{HH}$ = 8.7 Hz, ArH), 7.20-7.33 (m, 7H, ArH). ^{13}C{^{1}H} NMR (100 MHz, $CDCl_3$) δ 39.3, 55.3, 113.9, 126.1, 127.0, 127.2, 128.4, 128.6, 130.3, 130.4, 140.4, 158.8. ESIMS (+ve) *m/z*: 224 $[M]^+$.

(*E*)-1-(4-Methylphenyl)-3-phenylpropene[17] [CAS: 134539-87-0] (0.179 g, 0.86 mmol, 86%) ^{1}H NMR (400 MHz, $CDCl_3$) δ 2.31 (s, 3H, CH_3), 3.53 (d, 2H, $^{3}J_{HH}$ = 7.0 Hz, -CH=CHCH$_2$-), 6.29 (dt, 1H, $^{3}J_{HH}$ = 15.7 and 7.1 Hz, - CH=CHCH$_2$-),6.42 (d, 1H, $^{3}J_{HH}$ = 15.7 Hz, -CH=CHCH$_2$-), 7.08 (d, 2H, $^{3}J_{HH}$ = 8.2 Hz, ArH), 7.19−7.35 (m, 7H, ArH). ^{13}C{^{1}H} NMR (100 MHz, $CDCl_3$) δ 21.2, 39.4, 125.8, 126.1, 128.2, 128.4, 128.9, 129.3, 130.9, 134.6, 136.9, 140.5. ESIMS (+ve) *m/z*: 208 $[M]^+$.

(*E*)-1-(4-Nitrophenyl)-3-phenylpropene[17] [CAS: 156904-24-4] (0.234 g, 0.98 mmol, 98%) ^{1}H NMR (400 MHz, $CDCl_3$) δ 3.60 (brd, 2H, $^{3}J_{HH}$ = 6.2 Hz, -CH=CHCH$_2$-), 6.49 (d, 1H, $^{3}J_{HH}$ = 15.4 Hz, -CH=CHCH$_2$-), 6.57 (dt, 1H, $^{3}J_{HH}$ = 15.4 and 6.2 Hz, -CH=CHCH$_2$-),7.23−7.27 (m, 3H, ArH), 7.32−7.36 (m, 2H, ArH), 7.47 (d, 2H, $^{3}J_{HH}$ = 9.0 Hz, ArH), 8.16 (d, 2H, $^{3}J_{HH}$ = 9.0 Hz, ArH). ^{13}C{^{1}H} NMR (100 MHz, $CDCl_3$) δ 39.5, 124.0, 126.5, 126.6, 128.7, 128.7, 129.2, 134.6, 139.0, 143.9, 144.9. ESIMS (+ve) *m/z*: 239 $[M]^+$.

(*E*)-1-(2-Methoxyphenyl)-3-phenylpropene[18] [CAS: 1246889-00-6] (0.211 g, 0.94 mmol, 94%) ^{1}H NMR (400 MHz, $CDCl_3$) δ 3.49 (d, 2H, $^{3}J_{HH}$ = 7.1 Hz, -CH=CHCH$_2$-), 3.75 (s, 3H, -

OCH_3), 6.27 (dt, 1H, $^3J_{HH}$ = 15.6 and 7.2 Hz, -CH=C*H*CH$_2$-), 6.74 (d, 1H, $^3J_{HH}$ = 15.6 Hz, - C*H*=CHCH$_2$-), 6.78−6.83 (m, 2H, ArH), 7.08−7.14 (m, 2H, ArH), 7.16−7.24 (m, 4H, ArH), 7.33 (d, 1H, $^3J_{HH}$ = 7.5 Hz, ArH). $^{13}C\{^1H\}$ NMR (100 MHz, $CDCl_3$) δ 39.8, 55.3, 110.7, 120.5, 125.7, 125.9, 126.4, 126.5, 128.1, 128.4, 128.6, 129.7, 140.5, 156.4. ESIMS (+ve) *m/z*: 224 $[M]^+$.

(*E*)-1-(2-Methylphenyl)-3-phenylpropene[19] [CAS: 83135-54-0] (0.177 g, 0.85 mmol, 85%) ^1H NMR (400 MHz, $CDCl_3$) δ 2.33 (s, 3H, CH_3), 3.57 (d, 2H, $^3J_{HH}$ = 7.2 Hz, -CH=CHC*H*$_2$-), 6.22 (dt, 1H, $^3J_{HH}$ = 15.7 and 7.2 Hz, -CH=C*H*CH$_2$-), 6.66 (d, 1H, $^3J_{HH}$ = 15.7 Hz, -CH=C*H*CH$_2$-), 7.11−7.14 (m, 3H, ArH), 7.19−7.32 (m, 5H, ArH), 7.40−7.42 (m, 1H, ArH). $^{13}C\{^1H\}$ NMR (100 MHz, $CDCl_3$) δ 19.9, 39.7, 125.5, 125.6, 126.2, 127.1, 128.5, 128.7, 129.1, 130.2, 130.5, 135.1, 136.7, 140.3. ESIMS (+ve) *m/z*: 208 $[M]^+$.

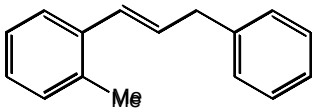

(*E*)-1-(2-Nitrophenyl)-3-phenylpropene[20] [CAS:] (0.179 g, 0.75 mmol, 75%) ^1H NMR (400 MHz, $CDCl_3$) δ 3.61 (d, 2H, $^3J_{HH}$ = 6.7 Hz, -CH=CHC*H*$_2$-), 6.34 (dt, 1H, $^3J_{HH}$ = 15.3 and 6.7 Hz, -CH=C*H*CH$_2$-), 6.95 (d, 1H, $^3J_{HH}$ = 15.3 Hz, -C*H*=CHCH$_2$-), 7.21-7.37 (m, 6H, ArH), 7.50-7.60 (m, 2H, ArH), 7.88-7.92 (m, 1H, ArH). $^{13}C\{^1H\}$ NMR (100 MHz, $CDCl_3$) δ 39.6, 124.4, 126.3, 126.4, 127.7, 128.6, 128.7, 132.9, 133.1, 134.8, 139.3, 147.8. ESIMS (+ve) *m/z*: 239 $[M]^+$.

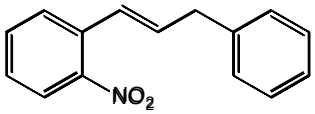

6.6 Crystallographic Studies

Data for all crystalographically characterised samples were collected on a Bruker APEX 2000 CCD diffractometer. The data were corrected for Lorentz and polarisation effects and empirical absorption corrections applied. Structure solution by direct methods and structure refinement based on full-matrix least-squares on F^2 employed SHELXTL version 6.10.[21] Hydrogen atoms were included in calculated positions (C-H = 0.96 – 1.00 Å) riding on the bonded atom with isotropic displacement parameters set to 1.5 U_{eq}(C) for methyl H atoms and 1.2 U_{eq}(C) for all other H atoms. All non-H atoms were refined with anisotropic displacement parameters.

References

1 G. Liu, Q. Ye, C. Zuo, J. Yu, J. Yang, J. Jiang, S. Shen, and W.Liu, *Guijinshu*, 2014, **35**, 59.

2 C. J. Christopher, P. J. Smith and T. Welton, *J. Mol. Catal. A Chem.*, **2003**, *206*, 77.

3 J. Parks, B. Wagner and R. Holm, *J. Organomet. Chem.*, 1973, **56**, 53.

4 C. Burstein, C. W. Lemann and F. Glorius, *Tetrahedron*, 2005, **61**, 6207.

5 Y.-H. Lin, MSc project report, 2012, University of Leicester.

6 S. Bruns, V. Sinnwell and J. Voss, *Magn. Reson. Chem*., 2003, **41**, 269.

7 T. Leermann, F. Leroux, and F. Colobert, *Org. Lett*., 2011, **13**, 4479.

8 T. Wang, X. Q. Hao, J. J. Huang, K. Wang and M. P. Song, *Organometallics*, 2014, **33**, 194.

9 Y. Zhou, T. Kijima, and T. Izumi, *J. Heterocyclic Chem*., 2009, **46**, 116.

10 A. P. Armitage, O. Boyron, Y. D. M. Champouret, M. Patel, K. Singh and G. A. Solan, *Catalysts*, 2015, **5**, 1425.

11 T.N.Y. Hoang, M. Humbert-Droz, T. Dutronc, L. Guénée, C. Besnard and C. Piguet, *Inorg. Chem*., 2013, **52**, 5570.

12 S. Kaiser, S. P. Smidt and A. Pfaltz, *Angew. Chem. Int. Ed*., 2006, **45**, 5194.

13 M. Kajino, A. Kawada, Y. Nakayama and H. Kimura, "*1,3-benzothiazinone derivitaves and use thereof*" (2004), *International Publication No.* ***2003/020719,*** p 108. Osaka: Japan.

14 K. Nienkemper, V. Kotov, G. Kehr, G. Erker and R. Fröhlich, *Eur. J. Inorg. Chem*., 2006, 366.

15 W. B. Cross, E. G. Hope, Y.-H. Lin, S. A. Macgregor, K. Singh, G. A. Solan and N. Yahyaa, *Chem. Commun*., 2013, **49**, 1918.

16 D. Pan, A. Chen, Y. Su, W. Zhou, S. Li, W. Jia, J. Xiao, Q. Liu, L. Zhang and N. Jiao, *Angew. Chem. Int. Ed.*, 2008, **47**, 4729.

17 Y. M. A. Yamada, S. M. Sarkar, Y. J. Uozumi, *J. Am. Chem. Soc*., 2012, **134**, 3190.

18 H. Yang, H. Yan, P. Sun. Y. Zhu, L. Lu, D. Liu, G. Rong and J. Mao, *Green Chem*., 2013, **15**, 976.

19 J. Barluenga, L. Florentino, F. Aznar and C. Valdés, *Org. Lett*. 2013, **13**, 510.

20 M.-B. Li, Y. Wang, and S.-K. Tian, *Angew. Chem. Int. Ed.*, 2012, **51**, 2968.

21 (a) J. Huang, E. D. Stevens, S. P. Nolan and J. L. Peterson, *J. Am. Chem. Soc*., 1999, **121**, 2674 (b) M. Scholl, T. M. Trnka, J. P. Morgan and R. H. Grubbs, *Tet. Lett*., 1999, **40**, 2247 (c) M. Scholl, S. Ding, C. W. Lee and R. H. Grubbs, *Org. Lett*., 1999, **6**, 953.

Appendix: Crystallography

Crystal data and structure refinement for HL1$_{o\text{-tolyl}}$

Identification code	13089	
Empirical formula	C26 H30 N2	
Formula weight	370.52	
Temperature	150(2) K	
Wavelength	0.71073 Å	
Crystal system	Triclinic	
Space group	P-1	
Unit cell dimensions	a = 8.203(3) Å	α= 75.438(8)°.
	b = 9.638(4) Å	β= 79.299(8)°.
	c = 13.752(5) Å	γ= 80.671(7)°.
Volume	1026.4(7) Å^3	
Z	2	
Density (calculated)	1.199 Mg/m^3	
Absorption coefficient	0.070 mm^{-1}	
F(000)	400	
Crystal size	0.26 x 0.16 x 0.09 mm^3	
Theta range for data collection	1.55 to 25.00°.	
Index ranges	-9<=h<=9, -11<=k<=11, -16<=l<=16	
Reflections collected	7562	
Independent reflections	3590 [R(int) = 0.0756]	
Completeness to theta = 25.00°	99.1 %	
Absorption correction	Empirical	
Max. and min. transmission	0.969 and 0.550	
Refinement method	Full-matrix least-squares on F^2	
Data / restraints / parameters	3590 / 0 / 259	
Goodness-of-fit on F^2	0.950	
Final R indices [I>2sigma(I)]	R1 = 0.0628, wR2 = 0.1454	
R indices (all data)	R1 = 0.0994, wR2 = 0.1685	
Largest diff. peak and hole	0.226 and -0.273 e.Å^{-3}	

Crystal data and structure refinement for H**L1**$_{2,4,6\text{-Me3Ph}}$

Identification code	14103	
Empirical formula	C28 H34 N2	
Formula weight	398.57	
Temperature	150(2) K	
Wavelength	0.71073 Å	
Crystal system	Monoclinic	
Space group	P2(1)/n	
Unit cell dimensions	a = 8.3828(15) Å	α= 90°.
	b = 19.519(3) Å	β= 94.844(3)°.
	c = 14.132(2) Å	γ= 90°.
Volume	2304.0(7) Å^3	
Z	4	
Density (calculated)	1.149 Mg/m^3	
Absorption coefficient	0.066 mm^{-1}	
F(000)	864	
Crystal size	0.45 x 0.25 x 0.22 mm^3	
Theta range for data collection	1.78 to 25.00°.	
Index ranges	-9<=h<=9, -23<=k<=23, -16<=l<=16	
Reflections collected	16450	
Independent reflections	4048 [R(int) = 0.0527]	
Completeness to theta = 25.00°	100.0 %	
Absorption correction	Empirical	
Max. and min. transmission	0.969 and 0.618	
Refinement method	Full-matrix least-squares on F^2	
Data / restraints / parameters	4048 / 0 / 279	
Goodness-of-fit on F^2	1.023	
Final R indices [I>2sigma(I)]	R1 = 0.0438, wR2 = 0.1024	
R indices (all data)	R1 = 0.0591, wR2 = 0.1084	
Largest diff. peak and hole	0.185 and -0.157 e.Å^{-3}	

Crystal data and structure refinement for H**L1**$_{ald\text{-}nap}$

Identification code	16007	
Empirical formula	C28 H28 N2	
Formula weight	392.52	
Temperature	150(2) K	
Wavelength	0.71073 Å	
Crystal system	Triclinic	
Space group	P-1	
Unit cell dimensions	a = 8.335(12) Å	α= 76.45(2)°.
	b = 10.513(14) Å	β= 83.31(3)°.
	c = 13.007(18) Å	γ = 79.73(2)°.
Volume	1087(3) Å^3	
Z	2	
Density (calculated)	1.199 Mg/m^3	
Absorption coefficient	0.070 mm^{-1}	
F(000)	420	
Crystal size	0.37 x 0.17 x 0.04 mm^3	
Theta range for data collection	1.62 to 25.00°.	
Index ranges	-9<=h<=9, -12<=k<=12, -15<=l<=15	
Reflections collected	7865	
Independent reflections	3793 [R(int) = 0.1765]	
Completeness to theta = 25.00°	98.8 %	
Absorption correction	Empirical	
Max. and min. transmission	0.969 and 0.222	
Refinement method	Full-matrix least-squares on F^2	
Data / restraints / parameters	3793 / 277 / 275	
Goodness-of-fit on F^2	0.848	
Final R indices [I>2sigma(I)]	R1 = 0.1104, wR2 = 0.2304	
R indices (all data)	R1 = 0.2845, wR2 = 0.2952	
Largest diff. peak and hole	0.496 and -0.322 e.Å^{-3}	

Crystal data and structure refinement for H**L2**$_{o\text{-tolyl}}$

Identification code	12081	
Empirical formula	C27 H34 N2	
Formula weight	386.56	
Temperature	150(2) K	
Wavelength	0.71073 Å	
Crystal system	Triclinic	
Space group	P-1	
Unit cell dimensions	a = 8.980(2) Å	α= 81.463(5)°.
	b = 11.466(3) Å	β= 74.086(4)°.
	c = 12.013(3) Å	γ = 73.187(5)°.
Volume	1135.4(5) Å^3	
Z	2	
Density (calculated)	1.131 Mg/m^3	
Absorption coefficient	0.065 mm^{-1}	
F(000)	420	
Crystal size	0.34 x 0.23 x 0.16 mm^3	
Theta range for data collection	1.77 to 25.00°.	
Index ranges	-10<=h<=10, -13<=k<=13, -14<=l<=14	
Reflections collected	8341	
Independent reflections	3982 [R(int) = 0.0598]	
Completeness to theta = 25.00°	99.2 %	
Absorption correction	Empirical	
Max. and min. transmission	0.969 and 0.482	
Refinement method	Full-matrix least-squares on F^2	
Data / restraints / parameters	3982 / 0 / 269	
Goodness-of-fit on F^2	0.956	
Final R indices [I>2sigma(I)]	R1 = 0.0549, wR2 = 0.1228	
R indices (all data)	R1 = 0.0780, wR2 = 0.1348	
Largest diff. peak and hole	0.202 and -0.213 e.Å^{-3}	

Crystal data and structure refinement for H**L1**$_{py\text{-}nap}$

Identification code	15152	
Empirical formula	C20 H14 N2	
Formula weight	282.33	
Temperature	150(2) K	
Wavelength	0.71073 Å	
Crystal system	Triclinic	
Space group	P-1	
Unit cell dimensions	a = 6.441(8) Å	α= 87.87(2)°.
	b = 10.494(13) Å	β= 78.69(3)°.
	c = 10.814(13) Å	γ= 83.58(3)°.
Volume	712.3(15) Å^3	
Z	2	
Density (calculated)	1.316 Mg/m^3	
Absorption coefficient	0.078 mm^{-1}	
F(000)	296	
Crystal size	0.11 x 0.05 x 0.03 mm^3	
Theta range for data collection	1.92 to 24.99°.	
Index ranges	-7<=h<=7, -12<=k<=12, -12<=l<=12	
Reflections collected	5154	
Independent reflections	2484 [R(int) = 0.2241]	
Completeness to theta = 24.99°	98.8 %	
Absorption correction	Empirical	
Max. and min. transmission	0.969 and 0.392	
Refinement method	Full-matrix least-squares on F^2	
Data / restraints / parameters	2484 / 209 / 199	
Goodness-of-fit on F^2	0.643	
Final R indices [I>2sigma(I)]	R1 = 0.0800, wR2 = 0.0767	
R indices (all data)	R1 = 0.3659, wR2 = 0.1184	
Largest diff. peak and hole	0.192 and -0.183 e.Å^{-3}	

Crystal data and structure refinement for (L1$_{o\text{-tolyl}}$)Pd(OAc)

Identification code	12101	
Empirical formula	C57 H66 Cl2 N4 O4 Pd2	
Formula weight	1154.84	
Temperature	150(2) K	
Wavelength	0.71073 Å	
Crystal system	Orthorhombic	
Space group	Pbcn	
Unit cell dimensions	a = 10.676(3) Å	α= 90°.
	b = 20.786(5) Å	β= 90°.
	c = 23.803(5) Å	γ= 90°.
Volume	5282(2) Å^3	
Z	4	
Density (calculated)	1.452 Mg/m^3	
Absorption coefficient	0.832 mm^{-1}	
F(000)	2376	
Crystal size	0.12 x 0.10 x 0.07 mm^3	
Theta range for data collection	1.71 to 26.00°.	
Index ranges	-13<=h<=13, -25<=k<=25, -29<=l<=29	
Reflections collected	39340	
Independent reflections	5195 [R(int) = 0.1969]	
Completeness to theta = 26.00°	100.0 %	
Absorption correction	Empirical	
Max. and min. transmission	0.831 and 0.572	
Refinement method	Full-matrix least-squares on F^2	
Data / restraints / parameters	5195 / 0 / 318	
Goodness-of-fit on F^2	0.888	
Final R indices [I>2sigma(I)]	R1 = 0.0600, wR2 = 0.0990	
R indices (all data)	R1 = 0.1375, wR2 = 0.1168	
Largest diff. peak and hole	0.778 and -0.962 e.Å^{-3}	

Crystal data and structure refinement for (L2$_{o\text{-tolyl}}$)Pd(OAc)

Identification code	12070	
Empirical formula	C29 H36 N2 O2 Pd	
Formula weight	551.00	
Temperature	150(2) K	
Wavelength	0.71073 Å	
Crystal system	Monoclinic	
Space group	P2(1)/n	
Unit cell dimensions	a = 10.0969(18) Å	α= 90°.
	b = 15.771(3) Å	β= 102.798(3)°.
	c = 16.881(3) Å	γ= 90°.
Volume	2621.3(8) Å^3	
Z	4	
Density (calculated)	1.396 Mg/m^3	
Absorption coefficient	0.736 mm^{-1}	
F(000)	1144	
Crystal size	0.26 x 0.25 x 0.04 mm^3	
Theta range for data collection	1.79 to 26.00°.	
Index ranges	-12<=h<=12, -19<=k<=19, -20<=l<=20	
Reflections collected	20200	
Independent reflections	5154 [R(int) = 0.0768]	
Completeness to theta = 26.00°	100.0 %	
Absorption correction	Empirical	
Max. and min. transmission	0.831 and 0.699	
Refinement method	Full-matrix least-squares on F^2	
Data / restraints / parameters	5154 / 0 / 315	
Goodness-of-fit on F^2	0.943	
Final R indices [I>2sigma(I)]	R1 = 0.0400, wR2 = 0.0751	
R indices (all data)	R1 = 0.0550, wR2 = 0.0793	
Largest diff. peak and hole	0.683 and -0.824 e.Å^{-3}	

Crystal data and structure refinement for (L3$_{o\text{-tolyl}}$) Pd(OAc)

Identification code	14024	
Empirical formula	C17 H22 N O4.50 Pd	
Formula weight	418.76	
Temperature	150(2) K	
Wavelength	0.71073 Å	
Crystal system	Monoclinic	
Space group	P2(1)/c	
Unit cell dimensions	a = 19.368(4) Å	α= 90°.
	b = 11.946(3) Å	β= 113.956(4)°.
	c = 16.027(3) Å	γ= 90°.
Volume	3388.9(12) Å^3	
Z	8	
Density (calculated)	1.641 Mg/m^3	
Absorption coefficient	1.118 mm^{-1}	
F(000)	1704	
Crystal size	0.45 x 0.16 x 0.05 mm^3	
Theta range for data collection	1.15 to 26.00°.	
Index ranges	-23<=h<=23, -14<=k<=14, -19<=l<=19	
Reflections collected	25850	
Independent reflections	6648 [R(int) = 0.1081]	
Completeness to theta = 26.00°	99.9 %	
Absorption correction	Empirical	
Max. and min. transmission	0.831 and 0.632	
Refinement method	Full-matrix least-squares on F^2	
Data / restraints / parameters	6648 / 0 / 405	
Goodness-of-fit on F^2	0.904	
Final R indices [I>2sigma(I)]	R1 = 0.0551, wR2 = 0.1040	
R indices (all data)	R1 = 0.0979, wR2 = 0.1149	
Largest diff. peak and hole	0.786 and -0.607 e.Å^{-3}	

Crystal data and structure refinement for (L1$_{o\text{-tolyl}}$)PdCl

Identification code	12082	
Empirical formula	C53 H60 Cl4 N4 Pd2	
Formula weight	1107.65	
Temperature	150(2) K	
Wavelength	0.71073 Å	
Crystal system	Monoclinic	
Space group	C2/c	
Unit cell dimensions	a = 22.889(4) Å	α= 90°.
	b = 9.7814(17) Å	β= 102.300(4)°.
	c = 22.312(4) Å	γ = 90°.
Volume	4880.8(15) Å^3	
Z	4	
Density (calculated)	1.507 Mg/m^3	
Absorption coefficient	0.996 mm^{-1}	
F(000)	2264	
Crystal size	0.21 x 0.11 x 0.05 mm^3	
Theta range for data collection	1.82 to 26.00°.	
Index ranges	-28<=h<=28, -12<=k<=12, -27<=l<=27	
Reflections collected	18673	
Independent reflections	4784 [R(int) = 0.1331]	
Completeness to theta = 26.00°	99.9 %	
Absorption correction	Empirical	
Max. and min. transmission	0.831 and 0.597	
Refinement method	Full-matrix least-squares on F^2	
Data / restraints / parameters	4784 / 0 / 291	
Goodness-of-fit on F^2	0.882	
Final R indices [I>2sigma(I)]	R1 = 0.0558, wR2 = 0.0910	
R indices (all data)	R1 = 0.0912, wR2 = 0.1015	
Largest diff. peak and hole	0.906 and -1.029 e.Å^{-3}	

Crystal data and structure refinement for (L2$_{o\text{-tolyl}}$)PdCl

Identification code	12077	
Empirical formula	C27.75 H34.50 Cl2.50 N2 Pd	
Formula weight	591.10	
Temperature	150(2) K	
Wavelength	0.71073 Å	
Crystal system	Triclinic	
Space group	P-1	
Unit cell dimensions	a = 9.4219(18) Å	α= 90.712(3)°.
	b = 10.957(2) Å	β= 107.959(3)°.
	c = 13.941(3) Å	γ= 95.861(3)°.
Volume	1360.5(5) Å^3	
Z	2	
Density (calculated)	1.443 Mg/m^3	
Absorption coefficient	0.946 mm^{-1}	
F(000)	607	
Crystal size	0.26 x 0.17 x 0.13 mm^3	
Theta range for data collection	1.54 to 26.00°.	
Index ranges	-11<=h<=11, -13<=k<=13, -17<=l<=17	
Reflections collected	10723	
Independent reflections	5286 [R(int) = 0.0386]	
Completeness to theta = 26.00°	98.8 %	
Absorption correction	Empirical	
Max. and min. transmission	0.831 and 0.706	
Refinement method	Full-matrix least-squares on F^2	
Data / restraints / parameters	5286 / 0 / 314	
Goodness-of-fit on F^2	1.055	
Final R indices [I>2sigma(I)]	R1 = 0.0444, wR2 = 0.1159	
R indices (all data)	R1 = 0.0522, wR2 = 0.1210	
Largest diff. peak and hole	1.970 and -1.129 e.Å^{-3}	

Crystal data and structure refinement for (L3$_{o\text{-tolyl}}$)PdCl

Identification code	14045	
Empirical formula	C15 H16 Cl N O Pd	
Formula weight	368.14	
Temperature	150(2) K	
Wavelength	0.71073 Å	
Crystal system	Orthorhombic	
Space group	Pca2(1)	
Unit cell dimensions	a = 12.471(3) Å	α= 90°.
	b = 12.978(3) Å	β= 90°.
	c = 17.840(4) Å	γ= 90°.
Volume	2887.4(11) Å^3	
Z	8	
Density (calculated)	1.694 Mg/m^3	
Absorption coefficient	1.461 mm^{-1}	
F(000)	1472	
Crystal size	0.43 x 0.21 x 0.19 mm^3	
Theta range for data collection	1.57 to 27.00°.	
Index ranges	-15<=h<=15, -16<=k<=16, -22<=l<=22	
Reflections collected	23015	
Independent reflections	6252 [R(int) = 0.0445]	
Completeness to theta = 27.00°	99.8 %	
Absorption correction	Empirical	
Max. and min. transmission	0.831 and 0.635	
Refinement method	Full-matrix least-squares on F^2	
Data / restraints / parameters	6252 / 1 / 349	
Goodness-of-fit on F^2	0.988	
Final R indices [I>2sigma(I)]	R1 = 0.0318, wR2 = 0.0624	
R indices (all data)	R1 = 0.0367, wR2 = 0.0639	
Largest diff. peak and hole	0.826 and -0.374 e.Å^{-3}	

Crystal data and structure refinement for (H**L1**$_{2,6\text{-Me2Ph}}$)Pd(OAc)$_2$

Identification code	15108	
Empirical formula	C31 H42 N2 O6 Pd	
Formula weight	645.07	
Temperature	150(2) K	
Wavelength	0.71073 Å	
Crystal system	Monoclinic	
Space group	C2/c	
Unit cell dimensions	a = 10.833(2) Å	α= 90°.
	b = 13.905(3) Å	β= 92.329(4)°.
	c = 41.269(9) Å	γ= 90°.
Volume	6211(2) Å^3	
Z	8	
Density (calculated)	1.380 Mg/m^3	
Absorption coefficient	0.641 mm^{-1}	
F(000)	2688	
Crystal size	0.34 x 0.11 x 0.06 mm^3	
Theta range for data collection	0.99 to 26.00°.	
Index ranges	-13<=h<=12, -17<=k<=17, -50<=l<=50	
Reflections collected	23784	
Independent reflections	6098 [R(int) = 0.0611]	
Completeness to theta = 26.00°	99.9 %	
Absorption correction	Empirical	
Max. and min. transmission	0.831 and 0.692	
Refinement method	Full-matrix least-squares on F^2	
Data / restraints / parameters	6098 / 6 / 370	
Goodness-of-fit on F^2	1.037	
Final R indices [I>2sigma(I)]	R1 = 0.0423, wR2 = 0.0910	
R indices (all data)	R1 = 0.0572, wR2 = 0.0957	
Largest diff. peak and hole	0.752 and -0.470 e.Å^{-3}	

Crystal data and structure refinement for the pyridine activated palladium complex of H$\mathbf{L1}_{2,6\text{-}Me2Ph}$

Identification code	12058	
Empirical formula	C65.50 H86 N4 O4 Pd2	
Formula weight	1206.18	
Temperature	150(2) K	
Wavelength	0.71073 Å	
Crystal system	Monoclinic	
Space group	C2/c	
Unit cell dimensions	a = 30.291(6) Å	α= 90°.
	b = 27.350(6) Å	β= 109.650(6)°.
	c = 28.663(6) Å	γ= 90°.
Volume	22364(8) $Å^3$	
Z	16	
Density (calculated)	1.433 Mg/m^3	
Absorption coefficient	0.697 mm^{-1}	
F(000)	10096	
Crystal size	0.21 x 0.15 x 0.06 mm^3	
Theta range for data collection	1.49 to 26.00°.	
Index ranges	-37<=h<=37, -33<=k<=33, -35<=l<=35	
Reflections collected	87659	
Independent reflections	21966 [R(int) = 0.2255]	
Completeness to theta = 26.00°	99.9 %	
Absorption correction	Empirical	
Max. and min. transmission	0.862 and 0.651	
Refinement method	Full-matrix least-squares on F^2	
Data / restraints / parameters	21966 / 0 / 1257	
Goodness-of-fit on F^2	0.784	
Final R indices [I>2sigma(I)]	R1 = 0.0732, wR2 = 0.1298	
R indices (all data)	R1 = 0.1939, wR2 = 0.1580	
Largest diff. peak and hole	0.613 and -0.735 $e.Å^{-3}$	

Crystal data and structure refinement for (L1$_{2,4,6\text{-}Me3Ph}$)Pd(OAc)

Identification code	14123	
Empirical formula	C30 H36 N2 O2 Pd	
Formula weight	563.01	
Temperature	150(2) K	
Wavelength	0.71073 Å	
Crystal system	Triclinic	
Space group	P-1	
Unit cell dimensions	a = 9.0902(17) Å	α= 71.811(4)°.
	b = 10.5026(19) Å	β= 75.867(4)°.
	c = 15.370(3) Å	γ = 69.220(4)°.
Volume	1288.6(4) Å^3	
Z	2	
Density (calculated)	1.451 Mg/m^3	
Absorption coefficient	0.750 mm^{-1}	
F(000)	584	
Crystal size	0.28 x 0.16 x 0.11 mm^3	
Theta range for data collection	2.14 to 25.99°.	
Index ranges	-11<=h<=11, -12<=k<=12, -18<=l<=18	
Reflections collected	10149	
Independent reflections	4994 [R(int) = 0.0949]	
Completeness to theta = 25.99°	98.7 %	
Absorption correction	Empirical	
Max. and min. transmission	0.831 and 0.573	
Refinement method	Full-matrix least-squares on F^2	
Data / restraints / parameters	4994 / 0 / 324	
Goodness-of-fit on F^2	0.869	
Final R indices [I>2sigma(I)]	R1 = 0.0656, wR2 = 0.1056	
R indices (all data)	R1 = 0.1111, wR2 = 0.1189	
Largest diff. peak and hole	0.788 and -1.021 e.Å^{-3}	

Crystal data and structure refinement for *peri*-[(**L1**$_{ket\text{-}nap}$)OAc]

Identification code	12007	
Empirical formula	C33 H36 Cl4 N2 O2 Pd	
Formula weight	740.84	
Temperature	150(2) K	
Wavelength	0.71073 Å	
Crystal system	Monoclinic	
Space group	P2(1)/c	
Unit cell dimensions	a = 16.649(10) Å	α= 90°.
	b = 11.043(6) Å	β= 114.617(10)°.
	c = 18.579(11) Å	γ = 90°.
Volume	3106(3) Å^3	
Z	4	
Density (calculated)	1.585 Mg/m^3	
Absorption coefficient	0.976 mm^{-1}	
F(000)	1512	
Crystal size	0.43 x 0.38 x 0.12 mm^3	
Theta range for data collection	1.35 to 26.00°.	
Index ranges	-20<=h<=20, -13<=k<=13, -22<=l<=22	
Reflections collected	23875	
Independent reflections	6107 [R(int) = 0.1476]	
Completeness to theta = 26.00°	99.9 %	
Absorption correction	Empirical	
Max. and min. transmission	0.831 and 0.474	
Refinement method	Full-matrix least-squares on F^2	
Data / restraints / parameters	6107 / 0 / 331	
Goodness-of-fit on F^2	0.906	
Final R indices [I>2sigma(I)]	R1 = 0.0627, wR2 = 0.1406	
R indices (all data)	R1 = 0.0969, wR2 = 0.1514	
Largest diff. peak and hole	0.651 and -0.914 e.Å^{-3}	

Crystal data and structure refinement for (H**L1**$_{py\text{-}nap}$)Pd(OAc)$_2$

Identification code	15148	
Empirical formula	C25 H21 Cl3 N2 O4 Pd	
Formula weight	626.19	
Temperature	150(2) K	
Wavelength	0.71073 Å	
Crystal system	Triclinic	
Space group	P-1	
Unit cell dimensions	a = 7.399(4) Å	α= 91.876(10)°.
	b = 12.054(6) Å	β= 99.664(10)°.
	c = 14.644(7) Å	γ = 103.524(9)°.
Volume	1248.3(11) Å^3	
Z	2	
Density (calculated)	1.666 Mg/m^3	
Absorption coefficient	1.100 mm^{-1}	
F(000)	628	
Crystal size	0.18 x 0.09 x 0.04 mm^3	
Theta range for data collection	1.41 to 26.00°.	
Index ranges	-9<=h<=9, -14<=k<=14, -18<=l<=18	
Reflections collected	9847	
Independent reflections	4840 [R(int) = 0.1293]	
Completeness to theta = 26.00°	98.8 %	
Absorption correction	Empirical	
Max. and min. transmission	0.831 and 0.201	
Refinement method	Full-matrix least-squares on F^2	
Data / restraints / parameters	4840 / 18 / 318	
Goodness-of-fit on F^2	0.985	
Final R indices [I>2sigma(I)]	R1 = 0.1047, wR2 = 0.2447	
R indices (all data)	R1 = 0.1434, wR2 = 0.2627	
Largest diff. peak and hole	1.965 and -2.856 e.Å^{-3}	

Crystal data and structure refinement for *peri*-**[(L1**$_{py\text{-}nap}$)PdOAc]

Identification code	15140	
Empirical formula	C23 H17 Cl3 N2 O2 Pd	
Formula weight	566.14	
Temperature	150(2) K	
Wavelength	0.71073 Å	
Crystal system	Orthorhombic	
Space group	Pca2(1)	
Unit cell dimensions	a = 16.588(5) Å	α= 90°.
	b = 16.098(4) Å	β= 90°.
	c = 8.261(2) Å	γ= 90°.
Volume	2206.2(11) Å^3	
Z	4	
Density (calculated)	1.704 Mg/m^3	
Absorption coefficient	1.228 mm^{-1}	
F(000)	1128	
Crystal size	0.31 x 0.10 x 0.02 mm^3	
Theta range for data collection	1.76 to 26.00°.	
Index ranges	-20<=h<=20, -19<=k<=19, -10<=l<=10	
Reflections collected	16703	
Independent reflections	4321 [R(int) = 0.1369]	
Completeness to theta = 26.00°	100.0 %	
Absorption correction	Empirical	
Max. and min. transmission	0.831 and 0.577	
Refinement method	Full-matrix least-squares on F^2	
Data / restraints / parameters	4321 / 1 / 281	
Goodness-of-fit on F^2	0.792	
Final R indices [I>2sigma(I)]	R1 = 0.0507, wR2 = 0.0776	
R indices (all data)	R1 = 0.0937, wR2 = 0.0860	
Largest diff. peak and hole	0.640 and -0.490 e.Å^{-3}	

Crystal data and structure refinement for *peri*-[(**L2**$_{nap}$)PdOAc]

Identification code	12069	
Empirical formula	C32 H39 N2 O3.50 Pd	
Formula weight	614.05	
Temperature	150(2) K	
Wavelength	0.71073 Å	
Crystal system	Monoclinic	
Space group	P2(1)/c	
Unit cell dimensions	a = 8.965(3) Å	α= 90°.
	b = 15.135(5) Å	β= 90.929(6)°.
	c = 20.959(7) Å	γ = 90°.
Volume	2843.6(16) Å^3	
Z	4	
Density (calculated)	1.434 Mg/m^3	
Absorption coefficient	0.690 mm^{-1}	
F(000)	1276	
Crystal size	0.26 x 0.17 x 0.05 mm^3	
Theta range for data collection	1.66 to 26.00°.	
Index ranges	-11<=h<=11, -18<=k<=18, -25<=l<=25	
Reflections collected	21814	
Independent reflections	5568 [R(int) = 0.1215]	
Completeness to theta = 26.00°	99.9 %	
Absorption correction	Empirical	
Max. and min. transmission	0.831 and 0.641	
Refinement method	Full-matrix least-squares on F^2	
Data / restraints / parameters	5568 / 0 / 341	
Goodness-of-fit on F^2	1.028	
Final R indices [I>2sigma(I)]	R1 = 0.0608, wR2 = 0.1316	
R indices (all data)	R1 = 0.0895, wR2 = 0.1406	
Largest diff. peak and hole	1.575 and -0.899 e.Å^{-3}	

Crystal data and structure refinement for *ortho*-[(**L3**$_{nap}$)PdOAc]

Identification code	14016	
Empirical formula	C20 H19 N O3 Pd	
Formula weight	427.76	
Temperature	150(2) K	
Wavelength	0.71073 Å	
Crystal system	Orthorhombic	
Space group	Pccn	
Unit cell dimensions	a = 17.522(4) Å	α= 90°.
	b = 17.716(4) Å	β= 90°.
	c = 22.070(5) Å	γ = 90°.
Volume	6851(3) Å^3	
Z	16	
Density (calculated)	1.659 Mg/m^3	
Absorption coefficient	1.102 mm^{-1}	
F(000)	3456	
Crystal size	0.40 x 0.23 x 0.07 mm^3	
Theta range for data collection	1.63 to 26.00°.	
Index ranges	-21<=h<=21, -21<=k<=21, -27<=l<=26	
Reflections collected	51555	
Independent reflections	6741 [R(int) = 0.1117]	
Completeness to theta = 26.00°	100.0 %	
Absorption correction	Empirical	
Max. and min. transmission	0.831 and 0.566	
Refinement method	Full-matrix least-squares on F^2	
Data / restraints / parameters	6741 / 0 / 457	
Goodness-of-fit on F^2	0.960	
Final R indices [I>2sigma(I)]	R1 = 0.0475, wR2 = 0.0983	
R indices (all data)	R1 = 0.0728, wR2 = 0.1066	
Largest diff. peak and hole	1.731 and -0.851 e.Å^{-3}	

Crystal data and structure refinement for *peri*-[(**L1**$_{ket\text{-}nap}$)PdCl]

Identification code	12067	
Empirical formula	C29 H29 Cl N2 Pd	
Formula weight	547.39	
Temperature	150(2) K	
Wavelength	0.71073 Å	
Crystal system	Monoclinic	
Space group	P2(1)/c	
Unit cell dimensions	a = 9.763(2) Å	α= 90°.
	b = 14.505(3) Å	β= 97.290(4)°.
	c = 16.773(4) Å	γ= 90°.
Volume	2356.1(9) Å^3	
Z	4	
Density (calculated)	1.543 Mg/m^3	
Absorption coefficient	0.922 mm^{-1}	
F(000)	1120	
Crystal size	0.25 x 0.21 x 0.11 mm^3	
Theta range for data collection	1.86 to 26.00°.	
Index ranges	-12<=h<=12, -17<=k<=17, -20<=l<=20	
Reflections collected	17994	
Independent reflections	4623 [R(int) = 0.0578]	
Completeness to theta = 26.00°	100.0 %	
Absorption correction	Empirical	
Max. and min. transmission	0.831 and 0.719	
Refinement method	Full-matrix least-squares on F^2	
Data / restraints / parameters	4623 / 0 / 303	
Goodness-of-fit on F^2	0.996	
Final R indices [I>2sigma(I)]	R1 = 0.0355, wR2 = 0.0724	
R indices (all data)	R1 = 0.0457, wR2 = 0.0758	
Largest diff. peak and hole	0.605 and -0.501 e.Å^{-3}	

Crystal data and structure refinement for *peri*-[(**L2**$_{nap}$)PdCl]

Identification code	12076	
Empirical formula	C30 H33 Cl N2 Pd	
Formula weight	563.43	
Temperature	150(2) K	
Wavelength	0.71073 Å	
Crystal system	Orthorhombic	
Space group	Pca2(1)	
Unit cell dimensions	a = 19.610(4) Å	α= 90°.
	b = 11.581(2) Å	β= 90°.
	c = 23.058(4) Å	γ= 90°.
Volume	5236.4(18) Å^3	
Z	8	
Density (calculated)	1.429 Mg/m^3	
Absorption coefficient	0.832 mm^{-1}	
F(000)	2320	
Crystal size	0.26 x 0.25 x 0.18 mm^3	
Theta range for data collection	1.76 to 27.00°.	
Index ranges	-24<=h<=24, -14<=k<=14, -29<=l<=29	
Reflections collected	42115	
Independent reflections	11323 [R(int) = 0.0620]	
Completeness to theta = 27.00°	99.9 %	
Absorption correction	Empirical	
Max. and min. transmission	0.831 and 0.627	
Refinement method	Full-matrix least-squares on F^2	
Data / restraints / parameters	11323 / 1 / 626	
Goodness-of-fit on F^2	1.001	
Final R indices [I>2sigma(I)]	R1 = 0.0378, wR2 = 0.0712	
R indices (all data)	R1 = 0.0435, wR2 = 0.0730	
Absolute structure parameter	-0.040(18)	
Largest diff. peak and hole	0.754 and -0.390 e.Å^{-3}	

Crystal data and structure refinement for *ortho*-[(**L3**$_{naph}$)PdCl]

Identification code	14055	
Empirical formula	C147 H134 Cl14 N8 O8 Pd8	
Formula weight	3488.12	
Temperature	150(2) K	
Wavelength	0.71073 Å	
Crystal system	Orthorhombic	
Space group	Pna2(1)	
Unit cell dimensions	a = 15.295(4) Å	α= 90°.
	b = 19.586(5) Å	β= 90°.
	c = 11.679(3) Å	γ = 90°.
Volume	3498.9(15) Å^3	
Z	1	
Density (calculated)	1.655 Mg/m^3	
Absorption coefficient	1.331 mm^{-1}	
F(000)	1742	
Crystal size	0.26 x 0.16 x 0.13 mm^3	
Theta range for data collection	1.69 to 25.99°.	
Index ranges	-18<=h<=18, -24<=k<=24, -14<=l<=14	
Reflections collected	26422	
Independent reflections	6864 [R(int) = 0.1891]	
Completeness to theta = 25.99°	100.0 %	
Absorption correction	Empirical	
Max. and min. transmission	0.831 and 0.496	
Refinement method	Full-matrix least-squares on F^2	
Data / restraints / parameters	6864 / 422 / 372	
Goodness-of-fit on F^2	0.918	
Final R indices [I>2sigma(I)]	R1 = 0.0878, wR2 = 0.1721	
R indices (all data)	R1 = 0.2232, wR2 = 0.2161	
Largest diff. peak and hole	0.937 and -0.487 e.Å^{-3}	

Crystal data and structure refinement for *ortho*-[(**L1**$_{ket\text{-}nap}$)PdCl]

Identification code	16014	
Empirical formula	C29 H29 Cl N2 Pd	
Formula weight	547.39	
Temperature	150(2) K	
Wavelength	0.71073 Å	
Crystal system	Monoclinic	
Space group	P2(1)/c	
Unit cell dimensions	a = 10.3807(19) Å	α= 90°.
	b = 14.917(3) Å	β= 100.696(4)°.
	c = 15.894(3) Å	γ= 90°.
Volume	2418.5(8) Å^3	
Z	4	
Density (calculated)	1.503 Mg/m^3	
Absorption coefficient	0.898 mm^{-1}	
F(000)	1120	
Crystal size	0.25 x 0.06 x 0.04 mm^3	
Theta range for data collection	1.89 to 26.00°.	
Index ranges	-12<=h<=12, -17<=k<=18, -19<=l<=19	
Reflections collected	18756	
Independent reflections	4753 [R(int) = 0.1703]	
Completeness to theta = 26.00°	99.7 %	
Absorption correction	Empirical	
Max. and min. transmission	0.831 and 0.585	
Refinement method	Full-matrix least-squares on F^2	
Data / restraints / parameters	4753 / 18 / 302	
Goodness-of-fit on F^2	0.766	
Final R indices [I>2sigma(I)]	R1 = 0.0596, wR2 = 0.0760	
R indices (all data)	R1 = 0.1342, wR2 = 0.0914	
Largest diff. peak and hole	0.850 and -1.090 e.Å^{-3}	

Crystal data and structure refinement for (H**L1**$_{ald\text{-}nap}$)$PdCl_2$

Identification code	16043	
Empirical formula	C29 H30 Cl4 N2 Pd	
Formula weight	654.75	
Temperature	150(2) K	
Wavelength	0.71073 Å	
Crystal system	Monoclinic	
Space group	P2(1)/n	
Unit cell dimensions	a = 10.060(2) Å	α= 90°.
	b = 11.775(2) Å	β= 90.37(3)°.
	c = 23.032(5) Å	γ= 90°.
Volume	2728.2(9) $Å^3$	
Z	4	
Density (calculated)	1.594 Mg/m^3	
Absorption coefficient	1.094 mm^{-1}	
F(000)	1328	
Crystal size	0.14 x 0.11 x 0.05 mm^3	
Theta range for data collection	2.20 to 26.00°.	
Index ranges	-12<=h<=12, 0<=k<=14, 0<=l<=28	
Reflections collected	5363	
Independent reflections	5363 [R(int) = 0.0000]	
Completeness to theta = 26.00°	99.9 %	
Absorption correction	Empirical	
Max. and min. transmission	0.831 and 0.549	
Refinement method	Full-matrix least-squares on F^2	
Data / restraints / parameters	5363 / 12 / 302	
Goodness-of-fit on F^2	0.715	
Final R indices [I>2sigma(I)]	R1 = 0.0677, wR2 = 0.1102	
R indices (all data)	R1 = 0.1777, wR2 = 0.1278	
Largest diff. peak and hole	0.583 and -0.713 e.$Å^{-3}$	

Crystal data and structure refinement for (H**L1**$_{ket\text{-}nap}$)$PdCl_2$

Identification code	16046	
Empirical formula	C31 H32 Cl8 N2 Pd	
Formula weight	822.59	
Temperature	150(2) K	
Wavelength	0.71073 Å	
Crystal system	Triclinic	
Space group	P-1	
Unit cell dimensions	a = 8.8725(12) Å	α= 88.721(3)°.
	b = 12.8984(18) Å	β= 77.111(3)°.
	c = 15.781(2) Å	γ= 76.355(3)°.
Volume	1709.9(4) $Å^3$	
Z	2	
Density (calculated)	1.598 Mg/m^3	
Absorption coefficient	1.193 mm^{-1}	
F(000)	828	
Crystal size	0.21 x 0.13 x 0.11 mm^3	
Theta range for data collection	1.32 to 26.00°.	
Index ranges	-10<=h<=10, -15<=k<=15, -19<=l<=19	
Reflections collected	13501	
Independent reflections	6628 [R(int) = 0.1296]	
Completeness to theta = 26.00°	98.9 %	
Absorption correction	Empirical	
Max. and min. transmission	0.831 and 0.514	
Refinement method	Full-matrix least-squares on F^2	
Data / restraints / parameters	6628 / 0 / 384	
Goodness-of-fit on F^2	0.834	
Final R indices [I>2sigma(I)]	R1 = 0.0769, wR2 = 0.1324	
R indices (all data)	R1 = 0.1480, wR2 = 0.1516	
Largest diff. peak and hole	1.080 and -0.917 e.$Å^{-3}$	

Crystal data and structure refinement for *ortho*-[(**L1**$_{ket\text{-}nap}$)PdOAc]

Identification code	16028	
Empirical formula	C32 H34 Cl2 N2 O2 Pd	
Formula weight	655.91	
Temperature	150(2) K	
Wavelength	0.71073 Å	
Crystal system	Monoclinic	
Space group	P2(1)/n	
Unit cell dimensions	a = 11.223(3) Å	α= 90°.
	b = 12.782(4) Å	β= 97.778(6)°.
	c = 20.785(6) Å	γ = 90°.
Volume	2954.1(15) Å^3	
Z	4	
Density (calculated)	1.475 Mg/m^3	
Absorption coefficient	0.841 mm^{-1}	
F(000)	1344	
Crystal size	0.34 x 0.10 x 0.04 mm^3	
Theta range for data collection	1.88 to 26.00°.	
Index ranges	-13<=h<=13, -15<=k<=15, -25<=l<=25	
Reflections collected	22759	
Independent reflections	5798 [R(int) = 0.1946]	
Completeness to theta = 26.00°	100.0 %	
Absorption correction	Empirical	
Max. and min. transmission	0.831 and 0.552	
Refinement method	Full-matrix least-squares on F^2	
Data / restraints / parameters	5798 / 12 / 375	
Goodness-of-fit on F^2	0.795	
Final R indices [I>2sigma(I)]	R1 = 0.0652, wR2 = 0.1010	
R indices (all data)	R1 = 0.1643, wR2 = 0.1252	
Largest diff. peak and hole	0.502 and -0.833 e.Å^{-3}	

Crystal data and structure refinement for *ortho*-[(**L2**$_{nap}$)PtCl]

Identification code	15136	
Empirical formula	C32 H37 Cl N2 O2 Pt	
Formula weight	712.18	
Temperature	150(2) K	
Wavelength	0.71073 Å	
Crystal system	Monoclinic	
Space group	P2(1)/c	
Unit cell dimensions	a = 8.8091(15) Å	α= 90°.
	b = 20.812(3) Å	β= 94.301(3)°.
	c = 15.843(3) Å	γ = 90°.
Volume	2896.5(8) Å^3	
Z	4	
Density (calculated)	1.633 Mg/m^3	
Absorption coefficient	4.968 mm^{-1}	
F(000)	1416	
Crystal size	0.21 x 0.10 x 0.08 mm^3	
Theta range for data collection	1.62 to 27.00°.	
Index ranges	-11<=h<=11, -26<=k<=26, -20<=l<=20	
Reflections collected	24193	
Independent reflections	6324 [R(int) = 0.0601]	
Completeness to theta = 27.00°	100.0 %	
Absorption correction	Empirical	
Max. and min. transmission	0.831 and 0.572	
Refinement method	Full-matrix least-squares on F^2	
Data / restraints / parameters	6324 / 16 / 351	
Goodness-of-fit on F^2	0.904	
Final R indices [I>2sigma(I)]	R1 = 0.0316, wR2 = 0.0568	
R indices (all data)	R1 = 0.0425, wR2 = 0.0589	
Largest diff. peak and hole	0.951 and -0.892 e.Å^{-3}	

Crystal data and structure refinement for (H**L4**$_{Et}$)Pd(OAc)$_2$

Identification code	16010	
Empirical formula	C25 H38 N2 O6 Pd	
Formula weight	568.97	
Temperature	150(2) K	
Wavelength	0.71073 Å	
Crystal system	Triclinic	
Space group	P-1	
Unit cell dimensions	a = 9.596(2) Å	α= 77.755(5)°.
	b = 10.052(2) Å	β= 84.915(5)°.
	c = 15.568(4) Å	γ= 68.004(7)°.
Volume	1360.6(5) Å^3	
Z	2	
Density (calculated)	1.389 Mg/m^3	
Absorption coefficient	0.721 mm^{-1}	
F(000)	592	
Crystal size	0.27 x 0.09 x 0.03 mm^3	
Theta range for data collection	2.23 to 26.00°.	
Index ranges	-11<=h<=11, -12<=k<=12, -19<=l<=19	
Reflections collected	10826	
Independent reflections	5290 [R(int) = 0.1567]	
Completeness to theta = 26.00°	99.0 %	
Absorption correction	Empirical	
Max. and min. transmission	0.831 and 0.576	
Refinement method	Full-matrix least-squares on F^2	
Data / restraints / parameters	5290 / 0 / 297	
Goodness-of-fit on F^2	0.764	
Final R indices [I>2sigma(I)]	R1 = 0.0756, wR2 = 0.1219	
R indices (all data)	R1 = 0.1530, wR2 = 0.1465	
Largest diff. peak and hole	0.671 and -1.416 e.Å^{-3}	

Crystal data and structure refinement for (H**L4**$_{i\text{Pr}}$)$PdCl_2$

Identification code	15122	
Empirical formula	C24 H34 Cl6 N2 Pd	
Formula weight	669.63	
Temperature	150(2) K	
Wavelength	0.71073 Å	
Crystal system	Monoclinic	
Space group	P2(1)/n	
Unit cell dimensions	a = 18.176(4) Å	α= 90°.
	b = 8.888(2) Å	β= 97.977(4)°.
	c = 18.815(4) Å	γ= 90°.
Volume	3010.1(11) $Å^3$	
Z	4	
Density (calculated)	1.478 Mg/m^3	
Absorption coefficient	1.165 mm^{-1}	
F(000)	1360	
Crystal size	0.28 x 0.12 x 0.06 mm^3	
Theta range for data collection	1.46 to 26.00°.	
Index ranges	-22<=h<=21, -10<=k<=10, -23<=l<=22	
Reflections collected	22776	
Independent reflections	5904 [R(int) = 0.0819]	
Completeness to theta = 26.00°	99.9 %	
Absorption correction	Empirical	
Max. and min. transmission	0.831 and 0.603	
Refinement method	Full-matrix least-squares on F^2	
Data / restraints / parameters	5904 / 0 / 305	
Goodness-of-fit on F^2	0.912	
Final R indices [I>2sigma(I)]	R1 = 0.0454, wR2 = 0.0877	
R indices (all data)	R1 = 0.0687, wR2 = 0.0936	
Largest diff. peak and hole	0.912 and -0.757 e.$Å^{-3}$	

Crystal data and structure refinement for (H**L4**$_{i\text{Pr}}$)$PdBr_2$

Identification code	15129	
Empirical formula	C23 H32 Br2 Cl2 N2 Pd	
Formula weight	673.63	
Temperature	150(2) K	
Wavelength	0.71073 Å	
Crystal system	Monoclinic	
Space group	P2(1)/c	
Unit cell dimensions	a = 16.973(3) Å	α= 90°.
	b = 12.025(2) Å	β= 109.352(3)°.
	c = 13.914(3) Å	γ = 90°.
Volume	2679.5(9) $Å^3$	
Z	4	
Density (calculated)	1.670 Mg/m^3	
Absorption coefficient	3.887 mm^{-1}	
F(000)	1336	
Crystal size	0.28 x 0.10 x 0.03 mm^3	
Theta range for data collection	2.12 to 27.00°.	
Index ranges	-21<=h<=21, -15<=k<=15, -17<=l<=17	
Reflections collected	22003	
Independent reflections	5855 [R(int) = 0.0679]	
Completeness to theta = 27.00°	99.9 %	
Absorption correction	Empirical	
Max. and min. transmission	0.831 and 0.588	
Refinement method	Full-matrix least-squares on F^2	
Data / restraints / parameters	5855 / 0 / 278	
Goodness-of-fit on F^2	0.869	
Final R indices [I>2sigma(I)]	R1 = 0.0367, wR2 = 0.0658	
R indices (all data)	R1 = 0.0565, wR2 = 0.0697	
Largest diff. peak and hole	0.872 and -0.607 e.$Å^{-3}$	

Crystal data and structure refinement for 'minor-1'-Cl

Identification code	15102	
Empirical formula	C23 H28 Cl4 N2 Pd	
Formula weight	580.67	
Temperature	150(2) K	
Wavelength	0.71073 Å	
Crystal system	Monoclinic	
Space group	P2(1)/c	
Unit cell dimensions	a = 9.807(4) Å	α= 90°.
	b = 12.736(5) Å	β= 97.373(9)°.
	c = 20.718(9) Å	γ= 90°.
Volume	2566.3(19) $Å^3$	
Z	4	
Density (calculated)	1.503 Mg/m^3	
Absorption coefficient	1.152 mm^{-1}	
F(000)	1176	
Crystal size	0.15 x 0.11 x 0.04 mm^3	
Theta range for data collection	1.88 to 26.00°.	
Index ranges	-12<=h<=12, -15<=k<=15, -25<=l<=25	
Reflections collected	19738	
Independent reflections	5036 [R(int) = 0.2496]	
Completeness to theta = 26.00°	99.8 %	
Absorption correction	Empirical	
Max. and min. transmission	0.831 and 0.335	
Refinement method	Full-matrix least-squares on F^2	
Data / restraints / parameters	5036 / 36 / 276	
Goodness-of-fit on F^2	0.889	
Final R indices [I>2sigma(I)]	R1 = 0.0852, wR2 = 0.1595	
R indices (all data)	R1 = 0.2122, wR2 = 0.1922	
Largest diff. peak and hole	1.414 and -0.786 e.$Å^{-3}$	

Crystal data and structure refinement for 'minor-2'-Br

Identification code	15112	
Empirical formula	C23 H28 Br Cl3 N2 Pd	
Formula weight	625.13	
Temperature	150(2) K	
Wavelength	0.71073 Å	
Crystal system	Monoclinic	
Space group	P2(1)/c	
Unit cell dimensions	a = 9.9812(18) Å	α= 90°.
	b = 12.535(2) Å	β= 98.254(3)°.
	c = 20.683(4) Å	γ = 90°.
Volume	2560.9(8) $Å^3$	
Z	4	
Density (calculated)	1.621 Mg/m^3	
Absorption coefficient	2.611 mm^{-1}	
F(000)	1248	
Crystal size	0.25 x 0.21 x 0.10 mm^3	
Theta range for data collection	1.91 to 27.00°.	
Index ranges	-12<=h<=12, -16<=k<=15, -26<=l<=26	
Reflections collected	20962	
Independent reflections	5575 [R(int) = 0.0464]	
Completeness to theta = 27.00°	99.8 %	
Absorption correction	Empirical	
Max. and min. transmission	0.831 and 0.633	
Refinement method	Full-matrix least-squares on F^2	
Data / restraints / parameters	5575 / 0 / 277	
Goodness-of-fit on F^2	0.976	
Final R indices [I>2sigma(I)]	R1 = 0.0486, wR2 = 0.1165	
R indices (all data)	R1 = 0.0686, wR2 = 0.1234	
Largest diff. peak and hole	2.111 and -0.603 e.$Å^{-3}$	

Crystal data and structure refinement for ($L4_{tBu}$)PdCl

Identification code	16060	
Empirical formula	C95 H127 Cl13 N8 Pd4	
Formula weight	2267.50	
Temperature	150(2) K	
Wavelength	0.71073 Å	
Crystal system	Orthorhombic	
Space group	P2(1)2(1)2(1)	
Unit cell dimensions	a = 9.656(5) Å	α= 90°.
	b = 13.002(7) Å	β= 90°.
	c = 21.755(12) Å	γ = 90°.
Volume	2731(3) $Å^3$	
Z	1	
Density (calculated)	1.378 Mg/m^3	
Absorption coefficient	1.010 mm^{-1}	
F(000)	1158	
Crystal size	0.43 x 0.16 x 0.04 mm^3	
Theta range for data collection	1.82 to 26.00°.	
Index ranges	-11<=h<=11, -16<=k<=15, -26<=l<=26	
Reflections collected	21447	
Independent reflections	5353 [R(int) = 0.1678]	
Completeness to theta = 26.00°	100.0 %	
Absorption correction	Empirical	
Max. and min. transmission	0.831 and 0.371	
Refinement method	Full-matrix least-squares on F^2	
Data / restraints / parameters	5353 / 253 / 288	
Goodness-of-fit on F^2	0.865	
Final R indices [I>2sigma(I)]	R1 = 0.0760, wR2 = 0.1659	
R indices (all data)	R1 = 0.1418, wR2 = 0.1862	
Largest diff. peak and hole	1.935 and -1.606 e.$Å^{-3}$	

Crystal data and structure refinement for {*peri*-[(**L1**$_{ket\text{-}nap}$)Pd(NCMe)]}$^{+}$[BF_4]$^{-}$

Identification code	14099	
Empirical formula	C31 H32 B F4 N3 Pd	
Formula weight	639.81	
Temperature	150(2) K	
Wavelength	0.71073 Å	
Crystal system	Monoclinic	
Space group	P2(1)/n	
Unit cell dimensions	a = 11.856(2) Å	α= 90°.
	b = 10.943(2) Å	β= 92.856(4)°.
	c = 21.728(4) Å	γ = 90°.
Volume	2815.4(9) Å^3	
Z	4	
Density (calculated)	1.509 Mg/m^3	
Absorption coefficient	0.711 mm^{-1}	
F(000)	1304	
Crystal size	0.28 x 0.14 x 0.05 mm^3	
Theta range for data collection	1.88 to 26.00°.	
Index ranges	-14<=h<=14, -13<=k<=13, -26<=l<=26	
Reflections collected	21659	
Independent reflections	5525 [R(int) = 0.1340]	
Completeness to theta = 26.00°	99.9 %	
Absorption correction	Empirical	
Max. and min. transmission	0.831 and 0.678	
Refinement method	Full-matrix least-squares on F^2	
Data / restraints / parameters	5525 / 0 / 367	
Goodness-of-fit on F^2	0.860	
Final R indices [I>2sigma(I)]	R1 = 0.0612, wR2 = 0.1058	
R indices (all data)	R1 = 0.1120, wR2 = 0.1207	
Largest diff. peak and hole	1.060 and -0.736 e.Å^{-3}	

Crystal data and structure refinement for {*ortho*-[(**L3**$_{nap}$)Pd(NCMe)]}$^{+}$[BF_4]$^{-}$

Identification code	14120	
Empirical formula	C20 H19 B F4 N2 O Pd	
Formula weight	496.58	
Temperature	150(2) K	
Wavelength	0.71073 Å	
Crystal system	Orthorhombic	
Space group	Pca2(1)	
Unit cell dimensions	a = 25.416(4) Å	α= 90°.
	b = 7.0008(11) Å	β= 90°.
	c = 22.645(3) Å	γ = 90°.
Volume	4029.3(10) Å^3	
Z	8	
Density (calculated)	1.637 Mg/m^3	
Absorption coefficient	0.970 mm^{-1}	
F(000)	1984	
Crystal size	0.36 x 0.15 x 0.10 mm^3	
Theta range for data collection	1.60 to 27.00°.	
Index ranges	-31<=h<=32, -8<=k<=8, -28<=l<=28	
Reflections collected	32466	
Independent reflections	8761 [R(int) = 0.1148]	
Completeness to theta = 27.00°	100.0 %	
Absorption correction	Empirical	
Max. and min. transmission	0.831 and 0.504	
Refinement method	Full-matrix least-squares on F^2	
Data / restraints / parameters	8761 / 1 / 529	
Goodness-of-fit on F^2	0.892	
Final R indices [I>2sigma(I)]	R1 = 0.0540, wR2 = 0.0786	
R indices (all data)	R1 = 0.0863, wR2 = 0.0877	
Largest diff. peak and hole	0.862 and -0.810 e.Å^{-3}	

Crystal data and structure refinement for [(**L1**$_{o\text{-tolyl}}$)Pd(NCMe)]$^{+}$[PF_6]$^{-}$

Identification code	15011	
Empirical formula	C29.50 H35 Cl3 F6 N P Pd	
Formula weight	761.30	
Temperature	150(2) K	
Wavelength	0.71073 Å	
Crystal system	Triclinic	
Space group	P-1	
Unit cell dimensions	a = 11.028(3) Å	α= 71.724(5)°.
	b = 12.133(3) Å	β= 84.480(6)°.
	c = 14.729(4) Å	γ= 64.221(5)°.
Volume	1683.3(8) Å^3	
Z	2	
Density (calculated)	1.502 Mg/m^3	
Absorption coefficient	0.890 mm^{-1}	
F(000)	770	
Crystal size	0.44 x 0.17 x 0.05 mm^3	
Theta range for data collection	1.46 to 26.00°.	
Index ranges	-13<=h<=13, -14<=k<=14, -18<=l<=18	
Reflections collected	13413	
Independent reflections	6550 [R(int) = 0.1334]	
Completeness to theta = 26.00°	98.9 %	
Absorption correction	Empirical	
Max. and min. transmission	0.831 and 0.435	
Refinement method	Full-matrix least-squares on F^2	
Data / restraints / parameters	6550 / 0 / 362	
Goodness-of-fit on F^2	0.874	
Final R indices [I>2sigma(I)]	R1 = 0.0834, wR2 = 0.1787	
R indices (all data)	R1 = 0.1483, wR2 = 0.2071	
Largest diff. peak and hole	1.107 and -1.118 e.Å^{-3}	

Crystal data and structure refinement for [(**L1**$_{o\text{-tolyl}}$)(NCMe)Pd$^{\cdots}$Ag-(NCMe)$_2$][BF$_4$]$_2$

Identification code	14078	
Empirical formula	C65 H77 Ag2 B4 Cl3 F16 N10 Pd2	
Formula weight	1880.50	
Temperature	150(2) K	
Wavelength	0.71073 Å	
Crystal system	Triclinic	
Space group	P-1	
Unit cell dimensions	a = 10.311(4) Å	α= 102.351(7)°.
	b = 12.889(5) Å	β= 100.835(7)°.
	c = 16.224(6) Å	γ = 108.068(7)°.
Volume	1925.9(12) Å^3	
Z	1	
Density (calculated)	1.621 Mg/m^3	
Absorption coefficient	1.148 mm^{-1}	
F(000)	938	
Crystal size	0.24 x 0.23 x 0.20 mm^3	
Theta range for data collection	1.74 to 26.00°.	
Index ranges	-12<=h<=12, -15<=k<=15, -19<=l<=19	
Reflections collected	15289	
Independent reflections	7491 [R(int) = 0.0765]	
Completeness to theta = 26.00°	98.9 %	
Absorption correction	Empirical	
Max. and min. transmission	0.831 and 0.586	
Refinement method	Full-matrix least-squares on F^2	
Data / restraints / parameters	7491 / 603 / 558	
Goodness-of-fit on F^2	0.934	
Final R indices [I>2sigma(I)]	R1 = 0.0667, wR2 = 0.1515	
R indices (all data)	R1 = 0.1035, wR2 = 0.1696	
Largest diff. peak and hole	1.191 and -0.734 e.Å^{-3}	

Crystal data and structure refinement for [(**L2**$_{o\text{-}tolyl}$) (NCMe)Pd···$AgBF_4$···Pd(**L2**$_{o\text{-}tolyl}$)(NCMe)][BF_4]$_2$

Identification code	14082	
Empirical formula	C62 H82 Ag B3 F12 N6 O Pd2	
Formula weight	1508.44	
Temperature	150(2) K	
Wavelength	0.71073 Å	
Crystal system	Triclinic	
Space group	P-1	
Unit cell dimensions	a = 11.046(2) Å	α= 78.800(4)°.
	b = 12.139(2) Å	β= 83.020(4)°.
	c = 24.459(5) Å	γ = 88.589(5)°.
Volume	3193.4(11) Å^3	
Z	2	
Density (calculated)	1.569 Mg/m^3	
Absorption coefficient	0.941 mm^{-1}	
F(000)	1532	
Crystal size	0.15 x 0.13 x 0.11 mm^3	
Theta range for data collection	1.71 to 26.00°.	
Index ranges	-13<=h<=13, -14<=k<=14, -29<=l<=30	
Reflections collected	25285	
Independent reflections	12404 [R(int) = 0.1111]	
Completeness to theta = 26.00°	98.9 %	
Absorption correction	Empirical	
Max. and min. transmission	0.831 and 0.652	
Refinement method	Full-matrix least-squares on F^2	
Data / restraints / parameters	12404 / 1 / 755	
Goodness-of-fit on F^2	0.776	
Final R indices [I>2sigma(I)]	R1 = 0.0639, wR2 = 0.1059	
R indices (all data)	R1 = 0.1412, wR2 = 0.1224	
Largest diff. peak and hole	0.856 and -0.752 e.Å^{-3}	

Crystal data and structure refinement for {[*peri*-(**L2**$_{ket\text{-}nap}$) (NCMe)Pd]$\cdots$Ag(OH_2)$\cdots$[*peri*-(**L2**$_{ket\text{-}nap}$)Pd(NCMe)]}[BF_4]$_3$

Identification code	14094	
Empirical formula	C64 H70 Ag B3 Cl4 F12 N6 O Pd2	
Formula weight	1662.16	
Temperature	150(2) K	
Wavelength	0.71073 Å	
Crystal system	Monoclinic	
Space group	P2(1)/c	
Unit cell dimensions	a = 16.306(3) Å	α= 90°.
	b = 15.292(3) Å	β= 100.494(4)°.
	c = 28.325(5) Å	γ= 90°.
Volume	6944(2) $Å^3$	
Z	4	
Density (calculated)	1.590 Mg/m^3	
Absorption coefficient	1.023 mm^{-1}	
F(000)	3336	
Crystal size	0.25 x 0.17 x 0.03 mm^3	
Theta range for data collection	1.46 to 26.00°.	
Index ranges	-20<=h<=20, -18<=k<=18, -34<=l<=34	
Reflections collected	53804	
Independent reflections	13642 [R(int) = 0.2242]	
Completeness to theta = 26.00°	99.9 %	
Absorption correction	Empirical	
Max. and min. transmission	0.831 and 0.626	
Refinement method	Full-matrix least-squares on F^2	
Data / restraints / parameters	13642 / 827 / 850	
Goodness-of-fit on F^2	0.775	
Final R indices [I>2sigma(I)]	R1 = 0.0702, wR2 = 0.0990	
R indices (all data)	R1 = 0.1882, wR2 = 0.1251	
Largest diff. peak and hole	1.038 and -0.858 e.$Å^{-3}$	

Crystal data and structure refinement for [(**L1**$_{o\text{-}tolyl}$)Pd($NC_5H_3Cl_2$-3,5)]$^+$[BF_4]$^-$

Identification code	14089	
Empirical formula	C31 H32 B Cl2 F4 N3 Pd	
Formula weight	710.71	
Temperature	150(2) K	
Wavelength	0.71073 Å	
Crystal system	Monoclinic	
Space group	P2(1)/n	
Unit cell dimensions	a = 10.976(2) Å	α= 90°.
	b = 19.372(4) Å	β= 98.218(3)°.
	c = 14.446(3) Å	γ = 90°.
Volume	3040.2(10) Å^3	
Z	4	
Density (calculated)	1.553 Mg/m^3	
Absorption coefficient	0.837 mm^{-1}	
F(000)	1440	
Crystal size	0.36 x 0.30 x 0.19 mm^3	
Theta range for data collection	1.77 to 27.00°.	
Index ranges	-14<=h<=14, -24<=k<=24, -18<=l<=18	
Reflections collected	25255	
Independent reflections	6633 [R(int) = 0.0616]	
Completeness to theta = 27.00°	99.9 %	
Absorption correction	Empirical	
Max. and min. transmission	0.831 and 0.718	
Refinement method	Full-matrix least-squares on F^2	
Data / restraints / parameters	6633 / 0 / 385	
Goodness-of-fit on F^2	0.997	
Final R indices [I>2sigma(I)]	R1 = 0.0425, wR2 = 0.0914	
R indices (all data)	R1 = 0.0588, wR2 = 0.0965	
Largest diff. peak and hole	1.897 and -0.438 e.Å^{-3}	

Crystal data and structure refinement for {*peri*-[(**L1**$_{ket\text{-}nap}$)Pd($NC_5H_3Cl_2$-3,5)]}$^+$[BF_4]$^-$

Identification code	14091	
Empirical formula	C69 H66 B2 Cl6 F8 N6 Pd2	
Formula weight	1578.40	
Temperature	150(2) K	
Wavelength	0.71073 Å	
Crystal system	Monoclinic	
Space group	P2(1)/c	
Unit cell dimensions	a = 12.027(3) Å	α= 90°.
	b = 15.698(4) Å	β= 98.229(5)°.
	c = 19.226(5) Å	γ= 90°.
Volume	3592.6(17) Å^3	
Z	2	
Density (calculated)	1.459 Mg/m^3	
Absorption coefficient	0.789 mm^{-1}	
F(000)	1596	
Crystal size	0.34 x 0.32 x 0.29 mm^3	
Theta range for data collection	1.68 to 26.00°.	
Index ranges	-14<=h<=14, -19<=k<=19, -23<=l<=23	
Reflections collected	27516	
Independent reflections	7065 [R(int) = 0.1051]	
Completeness to theta = 26.00°	100.0 %	
Absorption correction	Empirical	
Max. and min. transmission	0.831 and 0.471	
Refinement method	Full-matrix least-squares on F^2	
Data / restraints / parameters	7065 / 1 / 438	
Goodness-of-fit on F^2	1.005	
Final R indices [I>2sigma(I)]	R1 = 0.0705, wR2 = 0.1785	
R indices (all data)	R1 = 0.1048, wR2 = 0.1954	
Largest diff. peak and hole	2.204 and -1.241 e.Å^{-3}	

Crystal data and structure refinement for [(**L2**$_{o\text{-}tolyl}$)Pd($NC_5H_3Cl_2$-3,5)]$^+$[BF_4]$^-$

Identification code	14127	
Empirical formula	C40 H56 B Cl2 F4 N3 O2 Pd	
Formula weight	874.99	
Temperature	150(2) K	
Wavelength	0.71073 Å	
Crystal system	Triclinic	
Space group	P-1	
Unit cell dimensions	a = 11.425(4) Å	α= 90.894(7)°.
	b = 11.522(4) Å	β= 92.443(7)°.
	c = 28.143(11) Å	γ= 90.402(7)°.
Volume	3700(2) Å^3	
Z	4	
Density (calculated)	1.571 Mg/m^3	
Absorption coefficient	0.708 mm^{-1}	
F(000)	1816	
Crystal size	0.31 x 0.27 x 0.11 mm^3	
Theta range for data collection	0.72 to 26.00°.	
Index ranges	-14<=h<=14, -14<=k<=14, -34<=l<=34	
Reflections collected	28933	
Independent reflections	14327 [R(int) = 0.1221]	
Completeness to theta = 26.00°	98.6 %	
Absorption correction	Empirical	
Max. and min. transmission	0.831 and 0.515	
Refinement method	Full-matrix least-squares on F^2	
Data / restraints / parameters	14327 / 0 / 789	
Goodness-of-fit on F^2	0.893	
Final R indices [I>2sigma(I)]	R1 = 0.0790, wR2 = 0.1701	
R indices (all data)	R1 = 0.1423, wR2 = 0.1887	
Largest diff. peak and hole	1.189 and -1.413 e.Å^{-3}	

Crystal data and structure refinement for {*peri*-[(**L1**$_{ket\text{-}nap}$)Pd(NC_5H_5)]}$^+$[BF_4]$^-$

Identification code	15064	
Empirical formula	C35 H36 B Cl2 F4 N3 Pd	
Formula weight	762.78	
Temperature	150(2) K	
Wavelength	0.71073 Å	
Crystal system	Monoclinic	
Space group	P2(1)/c	
Unit cell dimensions	a = 11.070(2) Å	α= 90°.
	b = 15.847(3) Å	β= 100.148(4)°.
	c = 19.313(4) Å	γ= 90°.
Volume	3334.8(12) Å^3	
Z	4	
Density (calculated)	1.519 Mg/m^3	
Absorption coefficient	0.769 mm^{-1}	
F(000)	1552	
Crystal size	0.20 x 0.14 x 0.03 mm^3	
Theta range for data collection	1.67 to 26.00°.	
Index ranges	-13<=h<=13, -19<=k<=19, -23<=l<=23	
Reflections collected	25633	
Independent reflections	6552 [R(int) = 0.1315]	
Completeness to theta = 26.00°	99.9 %	
Absorption correction	Empirical	
Max. and min. transmission	0.831 and 0.636	
Refinement method	Full-matrix least-squares on F^2	
Data / restraints / parameters	6552 / 0 / 393	
Goodness-of-fit on F^2	0.861	
Final R indices [I>2sigma(I)]	R1 = 0.0583, wR2 = 0.1039	
R indices (all data)	R1 = 0.1066, wR2 = 0.1152	
Largest diff. peak and hole	0.970 and -0.821 e.Å^{-3}	

Crystal data and structure refinement for {*peri*-[(**L1**$_{ket\text{-}nap}$)Pd(NC_5H_4Br-3)]}$^+$[BF_4]$^-$

Identification code	15081	
Empirical formula	C35 H35 B Br Cl2 F4 N3 Pd	
Formula weight	841.68	
Temperature	150(2) K	
Wavelength	0.71073 Å	
Crystal system	Monoclinic	
Space group	P2(1)/c	
Unit cell dimensions	a = 12.608(2) Å	α= 90°.
	b = 13.186(2) Å	β= 96.197(4)°.
	c = 20.717(4) Å	γ= 90°.
Volume	3424.1(10) Å^3	
Z	4	
Density (calculated)	1.633 Mg/m^3	
Absorption coefficient	1.917 mm^{-1}	
F(000)	1688	
Crystal size	0.44 x 0.05 x 0.03 mm^3	
Theta range for data collection	1.62 to 26.00°.	
Index ranges	-15<=h<=15, -16<=k<=16, -25<=l<=25	
Reflections collected	26394	
Independent reflections	6737 [R(int) = 0.1426]	
Completeness to theta = 26.00°	99.9 %	
Absorption correction	Empirical	
Max. and min. transmission	0.831 and 0.635	
Refinement method	Full-matrix least-squares on F^2	
Data / restraints / parameters	6737 / 16 / 438	
Goodness-of-fit on F^2	0.800	
Final R indices [I>2sigma(I)]	R1 = 0.0569, wR2 = 0.0868	
R indices (all data)	R1 = 0.1300, wR2 = 0.1019	
Largest diff. peak and hole	0.604 and -0.646 e.Å^{-3}	

Crystal data and structure refinement for {*peri*-[(**L1**$_{ket\text{-}nap}$)Pd($NC_5H_4{}^tBu$-4)]}$^+[BF_4]^-$

Identification code	15062	
Empirical formula	C38 H42 B F4 N3 Pd	
Formula weight	733.96	
Temperature	150(2) K	
Wavelength	0.71073 Å	
Crystal system	Monoclinic	
Space group	P2(1)/c	
Unit cell dimensions	a = 12.040(2) Å	α= 90°.
	b = 21.835(4) Å	β= 108.947(4)°.
	c = 13.402(3) Å	γ = 90°.
Volume	3332.6(11) Å^3	
Z	4	
Density (calculated)	1.463 Mg/m^3	
Absorption coefficient	0.611 mm^{-1}	
F(000)	1512	
Crystal size	0.33 x 0.13 x 0.05 mm^3	
Theta range for data collection	1.79 to 27.00°.	
Index ranges	-15<=h<=15, -26<=k<=27, -17<=l<=17	
Reflections collected	27732	
Independent reflections	7265 [R(int) = 0.0746]	
Completeness to theta = 27.00°	99.9 %	
Absorption correction	Empirical	
Max. and min. transmission	0.831 and 0.719	
Refinement method	Full-matrix least-squares on F^2	
Data / restraints / parameters	7265 / 0 / 432	
Goodness-of-fit on F^2	0.949	
Final R indices [I>2sigma(I)]	R1 = 0.0459, wR2 = 0.0856	
R indices (all data)	R1 = 0.0698, wR2 = 0.0920	
Largest diff. peak and hole	0.849 and -0.571 e.Å^{-3}	

Crystal data and structure refinement for {*peri*-[(**L1**$_{ket\text{-}nap}$)Pd($NC_5H_3Me_2$-2,5)]}$^+$[BF_4]$^-$

Identification code	15096	
Empirical formula	C37 H40 B Cl2 F4 N3 Pd	
Formula weight	790.83	
Temperature	150(2) K	
Wavelength	0.71073 Å	
Crystal system	Triclinic	
Space group	P-1	
Unit cell dimensions	a = 11.3562(19) Å	α= 61.810(2)°.
	b = 13.169(2) Å	β= 89.305(3)°.
	c = 13.414(2) Å	γ = 86.488(3)°.
Volume	1764.4(5) Å^3	
Z	2	
Density (calculated)	1.489 Mg/m^3	
Absorption coefficient	0.730 mm^{-1}	
F(000)	808	
Crystal size	0.22 x 0.18 x 0.17 mm^3	
Theta range for data collection	1.72 to 27.00°.	
Index ranges	-14<=h<=14, -16<=k<=16, -17<=l<=17	
Reflections collected	14866	
Independent reflections	7564 [R(int) = 0.0365]	
Completeness to theta = 27.00°	98.2 %	
Absorption correction	Empirical	
Max. and min. transmission	0.831 and 0.716	
Refinement method	Full-matrix least-squares on F^2	
Data / restraints / parameters	7564 / 0 / 440	
Goodness-of-fit on F^2	1.021	
Final R indices [I>2sigma(I)]	R1 = 0.0422, wR2 = 0.1034	
R indices (all data)	R1 = 0.0493, wR2 = 0.1068	
Largest diff. peak and hole	1.250 and -0.804 e.Å^{-3}	